UCRL-ID-145167

Hydrologic Resources Management Program and underground Test Area Project FY 2000 Progress Report

M. L. Davisson, G. F. Eaton, N. L. Hakem, G. B. Hudson, I. D. Hutcheon, C. A. Laue, A. B. Kersting, J. M. Kenneally, J. E. Moran, D. L. Phinney, T. P. Rose, D. K. Smith, E. R. Slywester, L. Wang, R. Williams, M. Zavarin

July 1, 2001

U.S. Department of Energy

Lawrence Livermore National Laboratory

DISCLAIMER

This work was performed under the auspices of the U. S. Department of Energy by the University of California, Lawrence Livermore National Laboratory under Contract No. W-7405-Eng-48.

Hydrologic Resources Management Program and Underground Test Area Project FY 2000 Progress Report

Editors

Timothy P. Rose
Rosa I. Yamamoto
Gail F. Eaton

Contributors

M. Lee Davisson
Gail F. Eaton
Nadia L Hakem
G. Bryant Hudson
Ian D. Hutcheon
Carola A. Laue
Annie B. Kersting
Jacqueline M. Kenneally
Jean E. Moran
Douglas L. Phinney
Timothy P. Rose
David K. Smith
Eric R. Sylwester
Lumin Wang
Ross Williams
Mavrik Zavarin

July 2001

Table of Contents

Hydrologic Resources Management Program and Underground Test Area Project – FY 2000 Progress Report

Introduction

This report highlights the results of FY 2000 technical studies conducted by the Analytical and Nuclear Chemistry Division (ANCD) at Lawrence Livermore National Laboratory (LLNL) in support of the Hydrology and Radionuclide Migration Program (HRMP) and Underground Test Area (UGTA) Project. This is the latest in a series of annual reports published by LLNL-ANCD to document recent investigations of radionuclide migration and transport processes at the Nevada Test Site (NTS). The HRMP is sponsored by Defense Programs (DP) at the U.S. Department of Energy, Nevada Operations Office (DOE/NV), and supports DP operations at the NTS through studies of radiochemical and hydrologic processes that are relevant to the DP mission. Other organizations that support the HRMP include Los Alamos National Laboratory (LANL), the U.S. Geological Survey (USGS), the Desert Research Institute (DRI) of the University of Nevada, the U.S. Environmental Protection Agency (EPS), and Bechtel Nevada (BN). The UGTA Project is sponsored by the Environmental Management (EM) program at DOE/NV; its goal is to determine the extent of radionuclide contamination in groundwater resulting from underground nuclear testing at the NTS. The project strategy follows guidelines set forth in a Federal Facilities Agreement and Consent Order between the U.S. Department of Energy, the U.S. Department of Defense, and the State of Nevada. Participating contractors include LLNL (both ANCD and the Energy and Environmental Sciences Directorate), LANL, USGS, DRI, BN, and IT Corporation (with subcontract support from Geotrans Inc.).

The FY 2000 HRMP and UGTA progress report follows the organization and format of our FY 1999 report (Smith and Eaton, 2000), and includes results from technical studies related to radionuclide migration and isotope hydrology at the NTS. LLNL-ANCD continues in its efforts under the HRMP to pursue a technical agenda relevant to the science-based stockpile stewardship program at DOE/NV. Support to the UGTA project is strongly driven by data acquistion and analysis efforts that assist the development of numerical models of the hydrologic source term for underground nuclear tests. FY 2000 studies highlighted in this report include the following:

(1) Chapter 1 describes the unclassified radiologic source term for 76 underground nuclear tests detonated below or within 100 m of the water table in areas 19 and 20 of the Nevada Test Site (central and western Pahute Mesa). Included are summed totals and mean values for 47 radionuclides, reported as molar concentrations and activities. These data have been used to define an unclassified radiologic source term for the 1976 Cheshire test in support of hydrologic source term modeling (Pawloski et al., 2001). Effort continues in FY 2001 to publish an unclassified radiologic source term for the six principal underground testing areas at the NTS – Area 19, Area 20, Rainier Mesa/Shoshone Mountain, Frenchman Flat, Yucca Flat (above the water table), and Yucca Flat (below the water table).

(2) Chapter 2 presents the results of FY 1999-2000 "hot well" sampling efforts at the NTS, and discusses geochemical and radiochemical results for water samples collected from six different near-field wells. The "hot well" program represents a long-term investment by DOE/NV to understand the evolution of the hydrologic source term over time. The resulting data have become increasingly important as an empirical basis for validating hydrologic source term models.

(3) Over the past several years, ANCD has worked to develop radiography techniques for resolving the spatial distribution of radionuclides in geologic materials containing test-derived radionuclides. Chapter 3 describes the development of a new β-radiography technique, and discusses the application of α- and β-radiography measurements to characterize nuclear melt glass samples from the 1957 Rainier (U12B) underground nuclear test.

(4) Recent studies suggest that bacteria can strongly affect the mobility of radionuclides in the environment. Chapter 4 discusses work-in-progress to characterize microbial communities present in NTS soils and groundwater, and outlines plans for laboratory studies to address how these microbes may impact radionuclide fate and transport. This work examines the issue of radionuclide migration at the NTS from an innovative perspective that has previously received little attention. Seed funding from HRMP was critical to the initiation of this project.

(5) Chapter 5 summarizes recent field, laboratory, and modeling investigations to determine the conditions under which plutonium is transported on mineral colloids. The recognition that mineral colloids can transport actinides considerable distances in groundwater raised many questions regarding the mechanisms controlling this process. This report discusses significant results from on-going efforts to address these questions, and outlines some of the unresolved issues that are presently under investigation.

(6) Chapter 6 describes the preparation and testing of reference standards for the quantitative analysis of tritium by Secondary Ion Mass Spectrometery (SIMS). This effort resulted in the development of a unique microanalytical capability for determining tritium sorption effects in minerals.

(7) Chapter 7 presents the results of a chlorine-36 study of regional groundwater flow in southern Nevada. This study represents the first comprehensive analysis of a ^{36}Cl database that was assembled by LLNL-ANCD over the past decade. Included are data from more than 50 locations, including a number of wells at the NTS. The data are used to define the range in ^{36}Cl compositions for both groundwater recharge and for chemically evolved waters present in major hydrostratigraphic units. Data variations are evaluated in the context of regional flow models.

(8) Lastly, Chapter 8 is a detailed analysis of a chemical and isotopic database developed during groundwater sampling in the region north of the NTS between 1997 and 1999. This study critically evaluates the possibility that regional groundwater flow through the Pahute Mesa underground testing area is derived mainly from recharge centers in central Nevada, up to 300 km north of the NTS. Isotopic data and mass balance calculations suggest that most of the groundwater in this regional flow system is

Holocene in age (<10,000 years old). This paper will appear in a special volume on the paleohydrology of the Mojave Desert to be published by the Geological Society of America in 2001.

In addition to the topical investigations described above, LLNL-ANCD contributed to several other technical products and collaborations during the past year.

A paper titled "Secondary Ion Mass Spectrometry Measurements of Volcanic Tuffs Containing Radionuclides from Underground Nuclear Tests" was published in the journal *Radiochimica Acta* (Rose et al., 2000). This work was previously presented in the FY 1999 HRMP and UGTA Progress Report (Smith and Eaton, 2000).

A paper titled "Aged Nuclear Explosive Melt Glass: Radiography and Scanning Electron Microscope Analyses Documenting Radionuclide Distribution and Glass Alteration," was recently published in the *Journal of Radioanalytical and Nuclear Chemistry* (Eaton and Smith, 2001). This work was initially outlined in the FY 1998 HRMP and UGTA report (Smith and Eaton, 1999) and was presented at the Methods and Applications of Radioanalytical Chemistry (MARC V) conference in April of 2000.

D.K. Smith presented a paper on "Insights to Repository Performance Through Study of a Nuclear Test Site" at the 24th International Symposium on the Scientific Basis for Nuclear Waste Management, held in Sydney, Australia in August 2000 (Smith et al., 2000).

UGTA staff presented a poster entitled "Environmental Isotopes in the Pahute Mesa-Oasis Valley Groundwater Flow System" at the Annual Fall Meeting of the American Geophysical Union in San Francisco in December 1999 (Rose et al., 1999). The session topic was on the interdisciplinary assessment of the Oasis Valley groundwater flow system in southern Nevada, and it included presentations from a number of UGTA contract organizations.

A.B. Kersting was invited to serve on the Actinide Migration Evaluation (AME) group for the DOE facility at Rocky Flats, near Denver, Colorado. The committee consists of experts in the fields of actinide chemistry, geochemistry, hydrology, soil erosion, and contaminant transport processes. This committee meets quarterly, and provides guidance on the integration of remediation, decontamination and decommissioning, and monitoring projects designed to help obtain closure of the site.

References Cited

Eaton, G.F. and Smith, D.K., (2001) Aged nuclear explosive melt glass: radiography and scanning electron microscope analyses documenting radionuclide distribution and glass alteration. Journal of Radioanalytical and Nuclear Chemistry, 248 (3): 543-547.

Pawloski, G.A., Tompson, A.F.B., and Carle, S.F., eds. (2001) Evaluation of the hydrologic source term from underground nuclear tests of Pahute Mesa at the Nevada Test Site: the CHESHIRE test. Lawrence Livermore National Laboratory, report in review.

Rose, T.P., Hershey, R.L., Thomas, J.M., Benedict, F.C., Hudson, G.B., Eaton, G.F., and Kenneally, J.M. (1999) Environmental isotopes in the Pahute Mesa-Oasis Valley groundwater flow system. EOS, Transactions, American Geophysical Union 1999 Fall Meeting, vol. 80, no. 46, p. 328.

Rose, T.P., Smith, D.K., and Phinney, D.L. (2000) Secondary ion mass spectrometry measurements of volcanic tuffs containing radionuclides from underground nuclear tests. Radiochimica Acta, 88: 465-473.

Smith, D.K., Kersting, A.B., Thompson, J.L., and Finnegan, D.L. (2000) Insights to repository performance through study of a nuclear test site. Lawrence Livermore National Laboratory, UCRL-JC-137194.

Smith, D.K., and Eaton, G.F., eds. (1999) Hydrologic Resources Management Program and Underground Test Area – FY 1998 Progress Report. Lawrence Livermore National Laboratory UCRL-ID-135170, July 1999, 76 p.

Smith, D.K., and Eaton, G.F., eds. (2000) Hydrologic Resources Management Program and Underground Test Area – FY 1999 Progress Report. Lawrence Livermore National Laboratory UCRL-ID-139226, July 2000, 110 p.

Chapter 1

Unclassified Radiologic Source Term for Nevada Test Site Areas 19 and 20

David K. Smith

Analytical and Nuclear Chemistry Division, Lawrence Livermore National Laboratory

This report was previously published as LLNL UCRL-ID-141706 (January, 2001)

Introduction

The radiologic source term for underground nuclear tests conducted in Areas 19 and 20 of the Nevada Test Site consists of all residual radioactivity including tritium, fission products, activation products, unburned nuclear fuels, and actinides produced by neutron reactions. In the context of a dose assessment, the radiologic source term represents the total radionuclide inventory potentially accessible to the environment. An accurate assessment of the radiologic source term is necessary in order to quantify radionuclides with sufficiently long half-lives to be transported to downgradient receptors, determine the proportion of volatile and mobile radionuclides relative to refractory and immobile radionuclides, and evaluate the toxicity of the source term.

Underground Nuclear Tests Conducted on Pahute Mesa

Figure 1 is a histogram plotting the annual frequency of 76 underground nuclear tests conducted between 1965 and 1992 in Areas 19 and Area 20 of the Nevada Test Site. The histogram includes all tests that were fired below or within 100 meters of the water table. These tests comprise the radiologic source term for Pahute Mesa. The mean firing date of the tests conducted on Pahute Mesa is April, 1979. Unlike many other sites with radioactive contamination, the radiologic source term from underground nuclear tests conducted at Nevada Test Site has been accurately quantified. However, by its nature, the source term is also diagnostic of nuclear weapons performance and design. Because the production of radionuclides depends on the performance of the device, which is in turn indicative of nuclear weapons design, the radionuclide inventory for a single test is always classified. For groups of tests where individual test data is combined, inventory totals can be summed by testing areas.

The Unclassified Radionuclide Inventory for Pahute Mesa

In June, 1994, the Department of Energy issued classification bulletin WNP-87 which provides current classification policy regarding public release of source term data for underground nuclear tests conducted at the Nevada Test Site (U.S. DOE, 1994; U.S. DOE, 2001). Current guidance permits unlimited distribution of the sum of estimated fission yields, activities of tritium, activities of unfissioned fissile materials by isotope, fission products by isotope with a half-life in excess of one year, and neutron-activated radionuclides by isotope with a half-life in excess of one year for tests conducted below or within 100 meters of the water table on Pahute Mesa. The classification guidance for Pahute Mesa applies to all tests conducted there through 1992. The effective reporting date of the inventory summed by isotope is January 1, 1994.

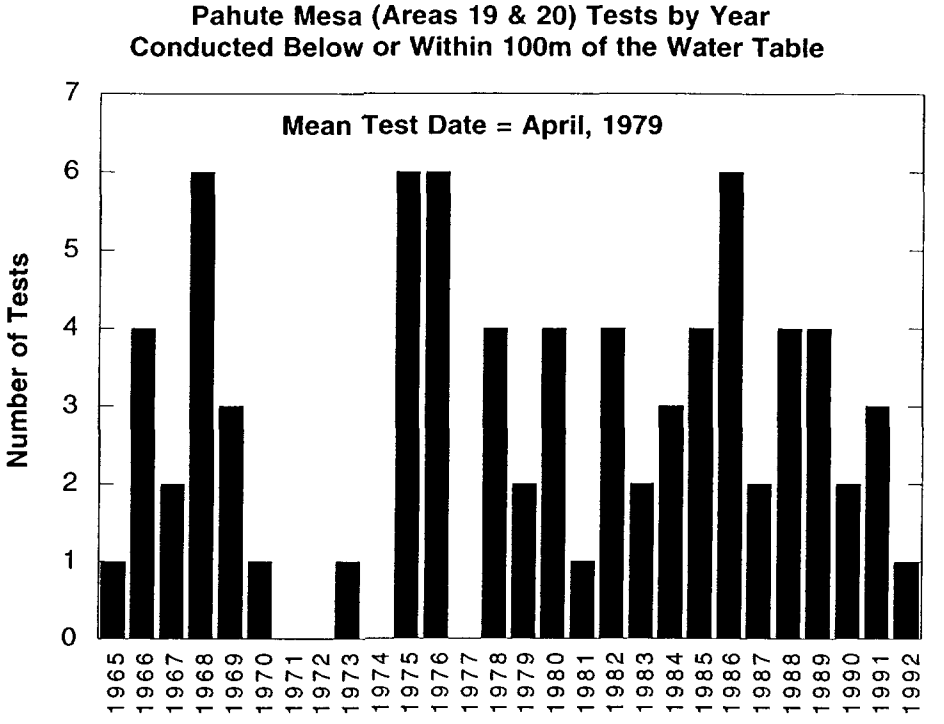

Figure 1

Using data derived from the nuclear testing program, a radionuclide inventory for each of the 828 underground nuclear tests conducted at the Nevada Test Site was produced by Lawrence Livermore National Laboratory and Los Alamos National Laboratory. A description of the methods used for selecting radionuclides for the inventory as well as the methodology for estimating post-shot radionuclide content is provided by Wild et al. (1998). All water levels and device depth of burials (corrected to as-built configuration) used in organizing the inventory were obtained from nuclear test program data archives.

Table I provides totals for 47 radionuclides summed by isotope for 76 tests conducted below or within 100 meters of the water table in Areas 19 and 20. All radionuclides are reported in moles and curies, decay corrected to January 1, 1994. Table II reports the Table I moles and curies for each radionuclide divided by 76 and represents a mean value for these tests. Half-lives were obtained from the GE Chart of Nuclides, Fourteenth Edition (Walker et al., 1989).

References

U.S. Department of Energy, 1994, Classification Bulletin – WNP-87, Washington, DC, 2p.

U.S. Department of Energy, 2001, Restricted Data Declassification Decisions 1946 to the Present (RDD-7), Office of Nuclear and National Security Information, Washington, DC, 131p., with appendices, http://www.osti.gov/opennet/rdd-7.pdf.

Walker, F.W., J.R. Parrington, and F. Feiner, 1989, Nuclides and Isotopes, Fourteenth Edition – Chart of the Nuclides, GE Nuclear Energy, General Electric Company, Nuclear Energy Operations, San Jose, California

Wild, J.F., Goishi, W., Meadows, J.W., Namboodiri, M. N., and Smith, D.K., 1998, *in* Atmospheric Nuclear Tests – Environmental and Human Consequences, C.S. Shapiro (ed.), Berlin, Springer – Verlag in Cooperation with NATO Scientific Affairs Division, p. 69 – 77.

Table I

Summed Unclassified Radionuclide Inventory for 76 Nuclear Tests Detonated Below or Within 100m of the Water Table in Areas 19 and 20*

Reported in Curies; Decay Corrected to January 1, 1994

Radionuclide	Half-Life (years)	Sum (Ci)	Moles
3H	12.3	6.99E+7	2.40E+03
14C	5730	5.55E+2	8.89E+00
26Al	7.3E+5	8.94E-3	1.82E-02
36Cl	3.01E+5	2.14E+2	1.80E+02
39Ar	269	1.85E+3	1.39E+00
40K	1.28E+9	4.69E+2	1.68E+06
41Ca	1.03E+5	1.64E+3	4.72E+02
59Ni	7.6E+4	3.99E+1	8.48E+00
63Ni	100	4.21E+3	1.18E+00
85Kr	10.73	9.54E+4	2.86E+00
90Sr	29.1	1.19E+6	9.68E+01
93Zr	1.5E+6	4.17E+1	1.75E+02
93mNb	16.1	7.59E+3	3.42E-01
94Nb	2.0E+4	1.73E+2	9.67E+00
99Tc	2.13E+5	3.07E+2	1.83E+02
107Pd	6.5E+6	1.57E+0	2.85E+01
113mCd	14.1	1.16E+3	4.57E-02
121mSn	~55	4.31E+3	6.63E-01
126Sn	~1E+5	4.92E+1	1.38E+01
129I	1.57E+7	9.45E-1	4.15E+01
135Cs	2.3E+6	3.17E+1	2.04E+02
137Cs	30.17	1.51E+6	1.27E+02
151Sm	90	5.71E+4	1.44E+01
150Eu	36	1.11E+3	1.12E-01
152Eu	13.48	3.29E+4	1.24E+00
154Eu	8.59	1.55E+4	3.72E-01
166mHo	1.2E+3	4.48E+1	1.50E-01
232Th (device)	1.4E+10	5.84E-2	2.29E+03
232Th (soil)	1.4E+10	3.38E+1	1.32E+06
232U	70	2.55E+2	4.99E-02
233U	1.592E+5	1.71E+2	7.61E+01
234U (device)	2.46E+5	1.23E+2	8.46E+01
234U (soil)	2.46E+5	1.67E+1	1.15E+01
235U (device)	7.04E+8	1.66E+0	3.27E+03
235U (soil)	7.04E+8	7.94E-1	1.56E+03
236U	2.342E+7	4.73E+0	3.10E+02
238U (device)	4.47E+9	2.19E+0	2.74E+04
238U (soil)	4.47E+9	1.67E+1	2.09E+05
237Np	2.14E+6	3.65E+1	2.18E+02
238Pu	87.7	7.16E+3	1.76E+00
239Pu	2.41E+4	1.93E+4	1.30E+03
240Pu	6.56E+3	6.20E+3	1.14E+02
241Pu	14.4	9.00E+4	3.62E+00
242Pu	3.75E+5	3.36E+0	3.52E+00
241Am	432.7	4.67E+3	5.65E+00
243Am	7.37E+3	1.79E-1	3.69E-03
244Cm	18.1	2.97E+3	1.50E-01

*^{150}Gd (1.8E+6 year half-life) was not included in the original radiologic source term for Areas 19 and 20 but was considered important due to its decay properties; the summed inventory for ^{150}Gd is 3.81E-7 Ci and 1.92E-6 moles.

Table II

Mean Unclassified Radionuclide Inventory for 76 Nuclear Tests Detonated Below or Within 100m of the Water Table in Areas 19 and 20**

Reported in Curies; Decay Corrected to January 1, 1994

Radionuclide	Half-Life (years)	Mean (Ci)	Moles
3H	12.3	9.20E+05	3.16E+01
14C	5730	7.30E+00	1.17E-01
26Al	7.3E+5	1.18E-04	2.41E-04
36Cl	3.01E+5	2.82E+00	2.37E+00
39Ar	269	2.43E+01	1.83E-02
40K	1.28E+9	6.17E+00	2.21E+04
41Ca	1.03E+5	2.16E+01	6.22E+00
59Ni	7.6E+4	5.25E-01	1.12E-01
63Ni	100	5.54E+01	1.55E-02
85Kr	10.73	1.26E+03	3.78E-02
90Sr	29.1	1.57E+04	1.28E+00
93Zr	1.5E+6	5.49E-01	2.30E+00
93mNb	16.1	9.99E+01	4.50E-03
94Nb	2.0E+4	2.28E+00	1.27E-01
99Tc	2.13E+5	4.04E+00	2.41E+00
107Pd	6.5E+6	2.07E-02	3.76E-01
113mCd	14.1	1.53E+01	6.03E-04
121mSn	~55	5.67E+01	8.72E-03
126Sn	~1E+5	6.47E-01	1.81E-01
129I	1.57E+7	1.24E-02	5.44E-01
135Cs	2.3E+6	4.17E-01	2.68E+00
137Cs	30.17	1.99E+04	1.68E+00
151Sm	90	7.51E+02	1.89E-01
150Eu	36	1.46E+01	1.47E-03
152Eu	13.48	4.33E+02	1.63E-02
154Eu	8.59	2.04E+02	4.90E-03
166mHo	1.2E+3	5.89E-01	1.98E-03
232Th (device)	1.4E+10	7.68E-04	3.01E+01
232Th (soil)	1.4E+10	4.45E-01	1.74E+04
232U	70	3.36E+00	6.57E-04
233U	1.592E+5	2.25E+00	1.00E+00
234U (device)	2.46E+5	1.62E+00	1.11E+00
234U (soil)	2.46E+5	2.20E-01	1.51E-01
235U (device)	7.04E+8	2.18E-02	4.29E+01
235U (soil)	7.04E+8	1.04E-02	2.05E+01
236U	2.342E+7	6.22E-02	4.07E+00
238U (device)	4.47E+9	2.88E-02	3.60E+02
238U (soil)	4.47E+9	2.20E-01	2.75E+03
237Np	2.14E+6	4.80E-01	2.87E+00
238Pu	87.7	9.42E+01	2.31E-02
239Pu	2.41E+4	2.54E+02	1.71E+01
240Pu	6.56E+3	8.16E+01	1.50E+00
241Pu	14.4	1.18E+03	4.75E-02
242Pu	3.75E+5	4.42E-02	4.63E-02
241Am	432.7	6.14E+01	7.43E-02
243Am	7.37E+3	2.36E-03	4.86E-05
244Cm	18.1	3.91E+01	1.98E-03

**^{150}Gd (1.8E+6 year half-life) was not included in the original radiologic source term for Areas 19 and 20 but was considered important due to its decay properties; the mean inventory for ^{150}Gd is 5.01E-9 Ci and 2.52E-8 moles.

Chapter 2

FY1999-2000 Hot Well Data Summary

Timothy P. Rose and Jacqueline M. Kenneally

Analytical and Nuclear Chemistry Division, Lawrence Livermore National Laboratory

Introduction

This report summarizes FY1999 and 2000 "hot" well sampling efforts at the Nevada Test Site (NTS), and documents analytical results for near-field groundwater samples that were collected during this time period (see Table 1). Multi-year sampling from specific near-field well sites provides a long-term perspective on how the hydrologic source term (HST) varies with time. These data constitute the only field-based empirical baseline for validating HST models at the NTS, and are a necessary element in the assessment of contaminant dose boundaries.

LLNL has participated in programs to evaluate radionuclide transport from underground nuclear test cavities since the 1970s. This effort continues today as a multi-agency project coordinated by DOE/NV and supported by LLNL, Los Alamos National Laboratory (LANL), the U.S. Geological Survey (USGS), the Desert Research Institute (DRI), Bechtel Nevada (BN), and IT Corporation (IT). During FY 1999 and 2000, hot well samples were collected at six different NTS well locations. These included pumped groundwater samples from U20n PS1-DDh (Cheshire), U4u PS2a (Dalhart), UE5n, RNM-1 and RNM-2S (all near the Cambric site); and bailed samples from U19v PS1ds (Almendro). Hot well samples are analyzed in accordance with laboratory protocols found in the Underground Test Area Project Standard Operating Procedures Manual (LLNL, 1995). Additional details regarding the FY1999 and 2000 hot well sampling effort are found in reports published by LANL (Thompson, 2000; Finnegan and Thompson, 2001).

Well U20n PS1 DDh (Cheshire)

Groundwater samples were collected from well U20n PS1 DDh on 12 October 1999. This well was recompleted from a post-shot re-entry hole for the Cheshire underground nuclear test, which was detonated on 14 February 1976 at a depth of 3,829 ft (1,167 m) below the surface of Pahute Mesa. A recent summary of the hydrogeology and the history of radionuclide migration studies at the Cheshire site is found in Sawyer et al. (1999). Additional data are found in Buddemeier et al. (1988), Smith et al. (1998), and Eaton et al. (1999).

Samples collected in 1999 were pumped from the lower perforation interval (1,250-1,253 m depth) of U20n PS1 DDh, inside the Cheshire test cavity. Analytical results are reported in Table 1. The tritium activity measured in the field at the time of sampling was 5.76×10^7 pCi/L. Subsequent re-analysis at LLNL yielded a slightly lower tritium

activity of 5.1 x 10^7 pCi/L (corrected to the October 1999 sample date). Groundwater previously collected from the same depth interval in September 1998 had a field-measured ^3H activity of 7.0 x 10^7 pCi/L. Laboratory analysis of this sample yielded a ^3H activity of 6.5 x 10^7 pCi/L (corrected to the Sept. 1998 sample date). Comparison of results for the 1998 and 1999 samples indicates the ^3H concentration in the cavity is apparently decreasing faster than the ^3H-decay rate. This suggests ^3H may be migrating in groundwater, or that groundwater pumping is gradually diluting the cavity fluid.

The $^3He/^4He$ ratio measured in 1999 was five orders of magnitude above atmospheric levels, reflecting the in-growth of ^3He derived from tritium decay ($^3H \rightarrow {}^3He + \beta^-$, $t_{½}$ = 12.3 y). The calculated ^3H-^3He age (19.7 years) is younger than the actual age of the nuclear test (25 years on 02/14/01) and may reflect the partial loss of helium gas from solution. The Cheshire cavity fluid also contains high concentrations of the gaseous fission product ^{85}Kr (2.77 x 10^4 pCi/L in the 1999 sample). The ^{85}Kr concentration decreased slightly since 1998 (3.39 x 10^4 pCi/L), and like ^3H, the rate of decrease is more rapid than the ^{85}Kr-decay rate ($t_{½}$ = 10.7 y).

The ^{14}C value of dissolved inorganic carbon (DIC) is 1.54 x 10^5 percent modern, or about 1500 times greater than pre-nuclear testing atmospheric levels. The measured ^{14}C activity is slightly lower than the 1998 value of 1.6 x 10^5 percent modern (Eaton et al., 1999), and is consistent with the observed decreases in ^3H and ^{85}Kr concentrations. It is notable that the Cheshire groundwater DIC concentration (108 mg/L as HCO_3^-) and $\delta^{13}C$ value (-6.0 ‰ PDB) is similar to uncontaminated environmental wells on Pahute Mesa. For comparison, groundwater from the U-20WW has a DIC concentration of 109 mg/L (as HCO_3^-) and a $\delta^{13}C$ value of -6.2 ‰ (Thomas et al., 1999). U-20WW is located <1 mile northwest of U20n PS1 DDh, and produces water from the same hydrostratigraphic unit (Calico Hills Fm), but at a slightly shallower depth interval (692 - 996 m; data from DOE/NV, 1997). In test cavities that remain open to exchange with the surrounding environment, there is evidently no long-term impact on groundwater DIC concentrations and stable carbon isotope ratios due to nuclear testing.

The $^{36}Cl/Cl$ ratio for Cheshire groundwater is 1.15 x 10^{-9}, and is approximately four orders of magnitude above natural environmental levels (~1 x 10^{-13}). The $^{36}Cl/Cl$ ratio is identical to the value obtained for a sample from the same depth interval in 1998 (Eaton et al., 1999). The ^{99}Tc activity measured in the 1999 Cheshire sample was 22 pCi/L, compared with a value of 31 pCi/L measured in 1998 from the same depth interval. Hence, ^{99}Tc appears to be decreasing over time at a proportionally greater rate than is observed for ^3H, ^{14}C, or ^{85}Kr.

The uranium concentration in Cheshire groundwater (2.3 µg/L) falls within the range of previously reported values for volcanic aquifer groundwaters in this region (Thomas et al., 1999). The $^{235}U/^{238}U$ ratio (0.007) indicates the uranium is of natural origin. Enrichment in the $^{234}U/^{238}U$-activity ratio (3.44) reflects the preferential leaching of ^{234}U from uranium-bearing minerals in the host rock following α-decay of ^{238}U.

Finally, it is notable that plutonium concentrations and isotopic ratios were measured for the 1999 Cheshire sample on a multi-collector magnetic sector ICP-MS. Isotopic ratios are not reported here due to classification issues. The blank-corrected total Pu concentration measured on an acidified (pH = 2) sample was 7.03 ± 1.27 pg/L. Thompson (2000) reported a ^{239,240}Pu activity of 2.1 x 10^{-2} Bq/L for water collected from the same depth interval at Cheshire in 1998. If we make the simplifying assumption that all of the Pu is present as ^{239}Pu, we calculate a concentration of 9.1 pg/L for the Thompson (2000) sample. This is comparable to our analytical result for the 1999 sample.

Well U19v PS1ds (Almendro)

The Almendro test was conducted on 06 June 1973 at a depth of 1,063 m (3,487 ft) below the surface of Pahute Mesa. Groundwater samples were collected from the post-shot re-entry hole (U19v PS1ds) on 18 August 1999 at a depth of 914 m (2999 ft), and again on 26 September 2000 at a depth of 942 m (3090 ft). Samples were also collected in September 1998 at a depth of 1,021 m (3350 ft). In each case, grab samples were collected at the specified depth interval using a wireline bailer. All reported depths are corrected for borehole slant. Analytical results for the 1999 and 2000 samples are reported in Table 1.

The groundwater temperature inside the Almendro cavity remains anomalously high nearly three decades after the test was detonated. A temperature log of the well bore last taken in 1996 recorded a maximum value of 157°C at 1,073 m vertical depth. Rose et al. (2000) noted that the observed temperatures, coupled with unusual groundwater δ^{18}O and δ^{13}C results, imply the Almendro cavity is effectively isolated from the surrounding groundwater environment. Oxygen isotope values measured for fluids within the Almendro cavity-chimney system are consistently +1.5 permil enriched in ^{18}O relative to the ambient flow system beneath Pahute Mesa. The lack of a correlated enrichment in δD implies the oxygen isotope shift is related to high temperature water-rock exchange, as observed in natural geothermal waters.

Dissolved inorganic carbon (DIC) in water taken inside the test cavity in 1998 had a δ^{13}C value of +27 permil. In 1999, a sample collected above the cavity had a δ^{13}C value of +45 permil. In comparison, δ^{13}C values of groundwater from nearby environmental wells range from -1 to -11 permil. The strong ^{13}C enrichments are generally consistent with a methanogenic process such as CO_2 reduction (e.g. $CO_2 + 8H^+ + 8e^- \rightarrow CH_4 + 2H_2O$) which tends to enrich the residual DIC in ^{13}C (e.g. Whiticar, 1999). Work is in progress to determine whether this process is bacterially mediated or abiotic.

Tritium activities at Almendro are relatively consistent over the past three years, as would be expected in a quasi-isolated system. Measured values corrected to the sample dates in 1998, 1999, and 2000 are 1.6 x 10^8, 1.6 x 10^8, and 1.5 x 10^8 pCi/L, respectively. When corrected to the Almendro zero time, the measured tritium activities are 6.7 x 10^8, 6.8 x 10^8, and 7.1 x 10^8 pCi/L, respectively.

The ^{14}C value of dissolved inorganic carbon measured on the 1999 sample is 2.47 x 10^4 percent modern, compared with a value of 2.79 x 10^4 percent modern obtained in 1998 (Kenneally, 1999). Results are not yet available for the sample collected in 2000. It is notable that the ^{14}C concentrations at Almendro are lower than expected for the observed tritium levels. For example, whereas tritium activities at Cheshire and Dalhart are lower than at Almendro, their ^{14}C values are approximately an order of magnitude greater (see Table 1). This may imply that ^{14}C is somehow being removed from solution at Almendro, possibly during the methanogenic process discussed above.

Plutonium concentrations and isotopic ratios were measured by magnetic sector ICP-MS on an acidified (pH = 2) groundwater sample collected from Almendro in 1999. Isotope ratios are not reported due to classification issues. However, the blank-corrected total Pu concentration was determined to be 58.2 ± 3.9 pg/L. This value is surprising for two reasons. First, it is approximately a factor of 3 greater than previously reported Pu concentrations in groundwater samples from the Nevada Test Site. Second, the concentrations of other sorptive ionic species (e.g. ^{137}Cs) in Almendro fluid samples have historically been quite low (e.g. Smith, 1998; Kenneally, 1999). Efforts are underway to verify the plutonium results.

Well U4u PS2a (Dalhart)

The Dalhart test was conducted on 13 October 1988 at a depth of 640 m (2,100 ft) below the surface of Yucca Flat. A post-shot re-entry hole (U4u PS2a) was completed in 1990, and a 7.3-cm OD tube was later inserted into the hole with a slotted interval between 472 and 501 m depth (Thompson, 2000). Water sampling has been problematic due to high concentrations of particulate matter in the groundwater. In FY98, BN deployed tandem Bennett pumps in U4u PS2a with the pump intake set at ~500 m depth (Kenneally, 1999), permitting limited purging of the well. Samples were subsequently collected on 23 September 1998. The site was revisited in 1999, but only a small additional amount of water was purged from the well prior to sampling on 16 August 1999. Analytical results for the 1999 samples are reported in Table 1. LLNL results from the 1998 sampling effort are found in Kenneally (1999).

The tritium activity measured for the Dalhart sample collected in 1999 was 1.6 x 10^7 pCi/L. Within analytical error, this is identical to the 1998 value reported by Kenneally (1999). Corrected to the Dalhart zero time, the measured tritium activities in 1998 and 1999 are 2.8 x 10^7 and 3.0 x 10^7 pCi/L, respectively. The ^{14}C value of dissolved inorganic carbon measured on the 1999 sample is 1.19 x 10^5 percent modern, compared with a value of 1.18 x 10^5 percent modern in 1998. These values are remarkably consistent. The lack of evidence for dilution with ambient groundwater suggests that flow rates through the chimney region are extremely slow.

Plutonium concentrations and isotopic ratios were measured by magnetic sector ICP-MS on an acidified (pH = 2) sample collected from Dalhart in August 1999. Once again, the isotope ratios are not reported due to classification issues. The blank-corrected total Pu concentration was determined to be 8.75 ± 1.7 pg/L. This concentration is similar to that

observed in the Cheshire cavity sample, but was measured on a sample taken 140 m above the working point. This result suggests that relatively refractory species may have been mobilized into the Dalhart chimney. The presence of abundant particulate matter in the groundwater may implicate colloidal transport, although there is presently no data from Dalhart to support this hypothesis.

Wells RNM-1, RNM-2S, and UE-5n (Cambric)

The Cambric test was conducted on 14 May 1965 at a depth of 294 m (965 ft) below the surface of Frenchman Flat. The RNM-1 re-entry hole was slant drilled into the cavity in 1974, and a satellite well (RNM-2S) was drilled 91 m south of the Cambric test cavity that same year. In 1975, a long-term pumping experiment was initiated at RNM-2S to study the migration of radionuclides from the Cambric test cavity under induced flow conditions (Bryant, 1992). This experiment ran until 1991, and provided important insight into the variations in mobility of different radionuclides.

Well UE-5n is located 500 m southeast of the Cambric emplacement hole, and has shown gradual increases in tritium concentration since 1989. The likely source of contaminants in UE-5n is from the infiltration of water pumped from RNM-2S, which was allowed to percolate through the unsaturated zone along a kilometer-long ditch extending from the Cambric site to the Frenchman Lake playa (Smith, 2001). Groundwater samples were collected at RNM-2S and UE-5n in 1999, and from RNM-2S and RNM-1 in 2000. Analytical results are summarized in Table 1. Details regarding sampling and analytical data for each well are discussed below.

RNM-1

Water samples were collected from well RNM-1 on 28 June 2000. The well was purged at a pump rate of ~45 gpm for 3 hours prior to sampling. Tritium was measured by the helium accumulation method (Surano et al., 1992) yielding a value of 2.84×10^4 pCi/L (corrected to the sample date). When corrected to the Cambric zero time, the measured tritium activity is 2.05×10^5 pCi/L. We note that LANL reports tritium activities for samples collected the same day that are an order of magnitude lower than our values (Finnegan and Thompson, 2001). This discrepancy may be related to the different analytical methods employed by the two labs (i.e. helium accumulation vs. liquid scintillation counting).

The helium isotope ratio measured in RNM-1 groundwater is more than two orders of magnitude above atmospheric levels ($R/R_a = 5 \times 10^2$) indicating the presence of excess ^3He from tritium decay. However, the calculated ^3H-^3He age (21.9 years) is considerably younger than the actual age of the nuclear test (35 years in 2000), implying that some of the helium was lost from the system. A possible mechanism for helium loss is discussed in the next section.

The $^{36}Cl/Cl$ ratio in RNM-1 groundwater is 1.06×10^{-12}. In comparison, environmental $^{36}Cl/Cl$ ratios measured at 8 wells in Frenchman Flat (alluvial and volcanic aquifers) range from 5.3×10^{-13} to 8.4×10^{-13} (data from Rose et al., 1997; and LLNL unpublished results). Given that RNM-1 groundwater is only slightly enriched in ^{36}Cl relative to environmental samples from the same area, it would appear that most of the ^{36}Cl originally present in the Cambric test cavity was mobilized during pumping at RNM-2S.

Uranium isotopic values measured in RNM-1 groundwater are consistent with natural abundances (i.e. $^{235}U/^{238}U = 0.007$).

RNM-2S

Groundwater samples were collected from RNM-2S on 11 October 1999, and again on 14 June 2000. In 1999, the well was pumped at nearly 600 gpm for 5 days prior to sampling, allowing time for the system to reach a steady-state. Thompson (2000) reports a tritium activity of 1.9×10^5 pCi/L for samples collected on 11 October 1999 (1.3×10^6 pCi/L at t_o = 14 May 65), and notes this value is the same as the concentration observed when continuous pumping was ended in 1991. Well RNM-2S was re-sampled eight months later in June 2000. The tritium activity of this sample, measured by the helium accumulation method, was 5.84×10^5 pCi/L (corrected to the 14 June 2000 sample date). This is equivalent to an activity of 4.21×10^6 pCi/L at the Cambric zero time.

Helium isotopic abundances were measured for RNM-2S groundwaters collected in both 1999 and 2000. The two sets of analyses are fairly consistent and indicate a strong enrichment in ^3He derived from tritium decay ($R/R_a \sim 2.5 \times 10^3$). Calculated ^3H-^3He ages are 19.2 and 19.9 years for the 1999 and 2000 samples, respectively. As observed for the RNM-1 sample, these ages are substantially younger than the age of the Cambric test, implying helium loss from the system. A possible explanation for the loss of helium is that some of the water pumped from RNM-2S during the 1975-1991 radionuclide migration experiment has been recycled back into the system. Partial degassing of helium would likely occur at the surface, and during re-infiltration of the water through the vadose zone. Observed variations in δD and $\delta^{18}O$ values at RNM-1 and RNM-2S tend to support this recycling hypothesis.

Groundwater samples from eight different wells perforating the alluvial and volcanic aquifers in central Frenchman Flat have a composite average δD and $\delta^{18}O$ value of -107 ‰ and -13.8‰, respectively (Rose et al., 1997; and LLNL unpublished data). This average does not include RNM-1 and RNM-2S, which show comparative enrichments in δD (-104 to -105‰) and $\delta^{18}O$ (-12.7 to -13.0‰). On a plot of δD versus $\delta^{18}O$ (Figure 1), the RNM-1 and RNM-2S data plot along a line projected from the Frenchman Flat average value, with a slope of 2.8. This variation indicates the RNM-1 and RNM-2S groundwaters have undergone enrichment in heavy isotopes (^2H and ^{18}O) due to evaporation, as would occur if water were brought to the surface for a period of time. Note that the data point for UE-5n also plots along the same evaporation trajectory. These data suggest that some of the groundwater now present at RNM-1 and RNM-2S was recycled from Cambric ditch.

The $^{36}Cl/Cl$ ratios measured for RNM-2S groundwaters collected in 1999 and 2000 are 1.64×10^{-10} and 1.62×10^{-10}, respectively. These ratios are approximately two orders of magnitude greater than observed at RNM-1, implying that ^{36}Cl tended to move conservatively with groundwater during pumping. It is notable that low level abundances of the fission products ^{99}Tc and ^{129}I were also detected (by Accelerator Mass Spectrometry) in the RNM-2S samples taken in 1999. As with ^{36}Cl, these species tend to move as conservative anions in groundwater.

Uranium isotopes were analyzed for the RNM-2S sample collected in June 2000. The data are similar to that of the RNM-1 sample taken the same year, and indicate natural isotopic abundances.

UE-5n

Water samples were collected at UE-5n on 09 September 1999 at a depth of 222 m (730 ft) below the surface. Water was withdrawn using a Bennett pump with a pumping rate of 1.9 L/min. The purge volume at the start of sampling was ~5300 L. Finnegan and Thompson (2001) report tritium activities in the range of 1.32×10^5 to 1.48×10^5 pCi/L for these samples. The $^3He/^4He$ ratio measured for UE-5n groundwater is more than two orders of magnitude above atmospheric levels ($R/R_a = 4.5 \times 10^2$) reflecting the in-growth of ^3He from tritium decay. Assuming a tritium activity of 1.32×10^5 pCi/L, the ^3H-^3He age of the groundwater is calculated to be 9.5 years. This is significantly younger than the ages measured at RNM-1 and RNM-2S, but approximately coincides with the first appearance of tritium at UE-5n in 1989. This tends to support the idea that the source of contamination in UE-5n originated from water that infiltrated from Cambric ditch. The fact that UE-5n groundwater has a δD-$\delta^{18}O$ pair that plots along the evaporation trend in Figure 1 further strengthens this argument.

The $^{36}Cl/Cl$ ratio measured at UE-5n (6.10×10^{-10}) is actually higher than the values found in RNM-2S. This observation provides further evidence that ^{36}Cl moves conservatively with tritium in groundwater. Very low levels of ^{99}Tc and ^{129}I were also observed in UE-5n groundwater (Table 1). Lastly, it is notable that the ^{14}C concentration in UE-5n is quite low (18.8 percent modern) given the amount of tritium present in the water. In comparison, the ^{14}C concentration at RNM-2S is 413 percent modern. Assuming that UE-5n contains recycled water originating from RNM-2S, the difference in ^{14}C values at these two wells implies radiocarbon has been removed from solution. A possible explanation is that the ^{14}C (which is transported dominantly as HCO_3^-) was removed by isotopic exchange with calcite during re-infiltration from Cambric ditch. Calcite is a common trace mineral in the unsaturated alluvium at the Nevada Test Site, and is known to readily exchange carbon isotopes with bicarbonate groundwaters.

References

Bryant, E.A. (1992) The Cambric Migration Experiment – A Summary Report. Los Alamos National Laboratory, LA-12335, September 1992.

Buddemeier, R.W., Hunt, J.R., Rego, J.H. (1988) Radionuclide migration at the Cheshire event site. In: R.W. Buddemeier (ed.), Hydrology and Radionuclide Migration Program 1985-1986 Progress Report. Lawrence Livermore National Laboratory, UCRL-53779, p. 3-18.

DOE/NV (1997) Regional groundwater flow and tritium transport modeling and risk assessment of the underground test area, Nevada Test Site, Nevada. U.S. Department of Energy, Nevada Operations Office, Environmental Restoration Division, Las Vegas, NV, DOE/NV-477.

Eaton, G.F., Rose, T.P., Smith, D.K., Kenneally, J.M. and Hudson, G.B. (1999) FY 1998 sampling and analysis at CHESHIRE (U20n PS1 DDH). In: D.K. Smith and G.F. Eaton (eds.), Hydrologic Resources Management Program and Underground Test Area FY 1998 Progress Report, Lawrence Livermore National Laboratory, UCRL-ID-135170, p. 1-5.

Finnegan, D.L., and Thompson, J.L. (2001) Laboratory and Field Studies Related to Radionuclide Migration at the Nevada Test Site in Support of the Underground Test Area Program and Hydrologic Resources Management Project, October 1, 1999 – September 30, 2000. Los Alamos National Laboratory, LA-13787-PR, 19 p.

Kenneally, J.M. (1999) FY 1998 Hot Well Report. In: D.K. Smith and G.F. Eaton (eds.), Hydrologic Resources Management Program and Underground Test Area FY 1998 Progress Report, Lawrence Livermore National Laboratory, UCRL-ID-135170, p. 15-27.

LLNL (1995) Analytical Measurements: Standard Operating Procedures for the Underground Test Area. Isotope Sciences Division, Lawrence Livermore National Laboratory, unpublished report.

Rose, T.P., Kenneally, J.M., Smith, D.K., Davisson, M.L., Hudson, G.B., and Rego, J.H. (1997) Chemical and isotopic data for groundwater in southern Nevada. Lawrence Livermore National Laboratory, UCRL-ID-128000, 35 p.

Rose, T.P., Pawloski, G.A., and Smith, D.K. (2000) Environmentally closed nuclear test cavity-chimney systems: evidence and controlling factors. Lawrence Livermore National Laboratory report prepared for the U.S. Department of Energy, Nevada Operations Office, Environmental Restoration Division, 31 p.

Sawyer, D.A., Thompson, J.L., and Smith, D.K. (1999) The Cheshire migration experiment: A summary report. Los Alamos National Laboratory, LA-13555-MS, 32 p.

Smith, D.K. (2001) Evaluation of the radiochemistry of near-field water samples at the Nevada Test Site applied to the definition of a Hydrologic Source Term. Lawrence Livermore National Laboratory report prepared for the National Nuclear Security Agency, Nevada Operations Office, Environmental Restoration Division, July 2001.

Smith, D.K., Kersting, A.B., Rose, T.P., Kenneally, J.M., Hudson, G.B., Eaton, G.F., and Davisson, M.L. (1998) Hydrologic Resources Management Program and Underground Test Area Operable Unit FY 1997 Progress Report. Lawrence Livermore National Laboratory, UCRL-ID-130792, 92 p.

Surano, K.A., Hudson, G.B., Failor, R.A., Sims, J.M., Holland, R.C., MacLean, S.C., and Garrison, J.C. (1992) Helium-3 mass spectrometry for low-level tritium analysis of environmental samples. Jour. Radioanal. Nuclear Chem. Articles, 161: 443-453.

Thomas, J.M., Benedict, F.C., Jr., Rose, T.P., Hershey, R.L., Paces, J.B., Peterman, Z.E., Farnham, I.M., Johannesson, K.H., Singh, A.K., Stetzenbach, K.J., Hudson, G.B., Kenneally, J.M., Eaton, G.F., and Smith, D.K. (1999) Geochemical and isotopic interpretations of groundwater flow in the Oasis Valley flow system, southern Nevada. Preliminary report prepared for U.S. Department of Energy, Nevada Operations Office, June 1999.

Thompson, J.L. (2000) Laboratory and Field Studies Related to Radionuclide Migration at the Nevada Test Site, October 1, 1998 – September 30, 1999. Los Alamos National Laboratory, LA-13701-PR, 23 p.

Whiticar, M.J. (1999) Carbon and hydrogen isotope systematics of bacterial formation and oxidation of methane. Chemical Geology, 161: 291-314.

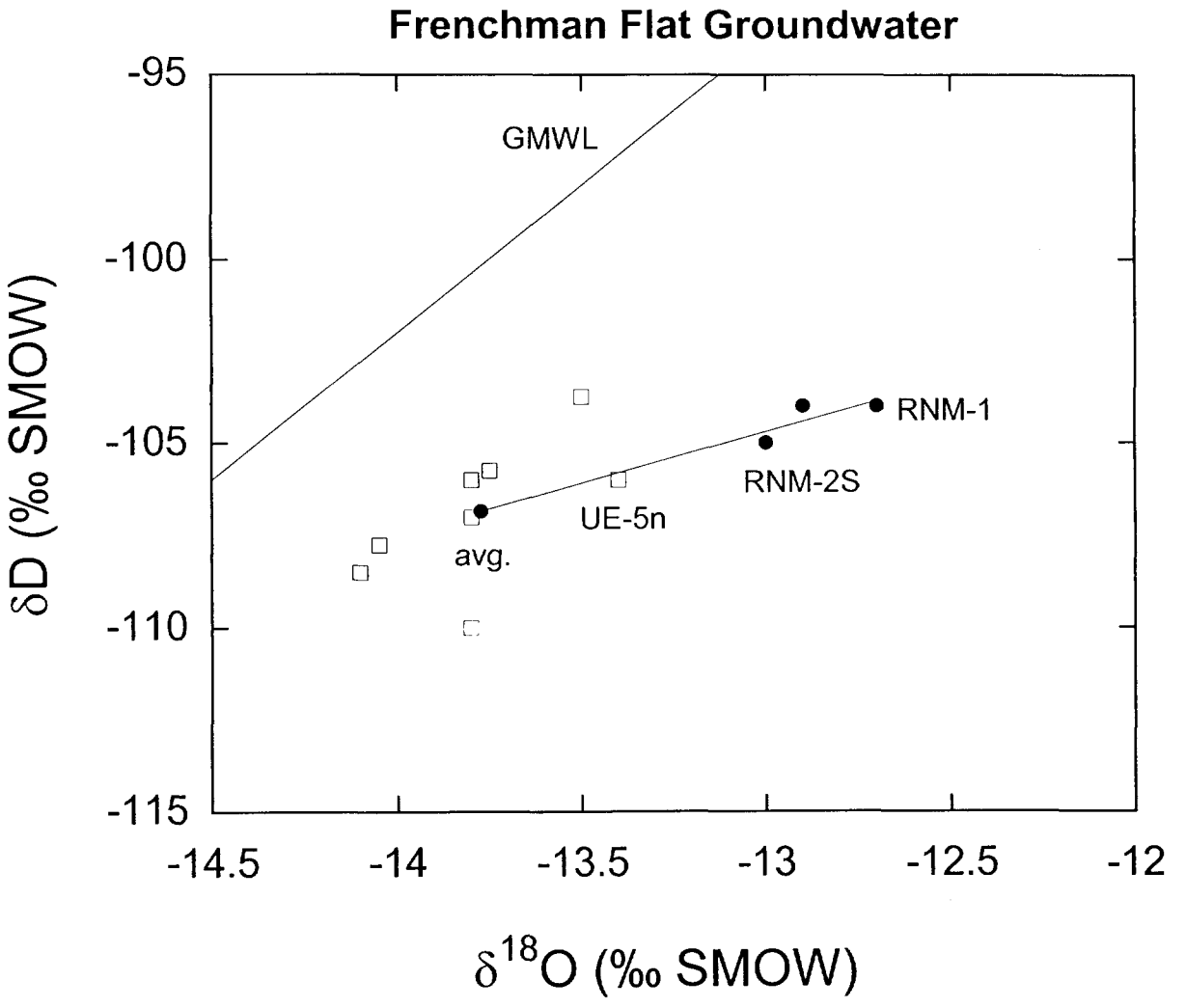

Figure 1. Plot of δD versus $\delta^{18}O$ values of groundwater samples from alluvial and volcanic aquifers in central Frenchman Flat. The solid circle labeled "avg." denotes the composite average δD-$\delta^{18}O$ value of samples from eight wells (shown as open boxes). Samples collected from wells RNM-1, RNM-2S, and UE-5n plot along a low slope evaporation trajectory (m = 2.8) projected from the composite average value. This evaporation signature suggests a component of recycled water from Cambric ditch is present at RNM-1, RNM-2S, and UE-5n. GMWL is the global meteoric water line ($\delta D = 8\delta^{18}O + 10$).

Table 1. Cavity or Near-Cavity Hot Well Analyses, FY1999-2000
Well Data

Well name	Test	Test Date	Latitude	Longitude	Surface Elevation	Well Depth	EOI	Water Depth	Sample Method	Sample Depth	Sample date
Units			*(d m s)*	*(d m s)*	*(ft)*	*(ft bgs)*	*(ft bgs)*	*(ft bgs)*		*(ft bgs)*	*date collected in field*
U20n PS1 DDh	Cheshire	14-Feb-76	37 14 25	116 25 24	6468	4253	4100-4110	2051	pump	4100	12-Oct-99
U19v PS1ds	Almendro	06-Jun-73	37 14 53	116 20 57	6842	3837	---	2026	bailer	3090	26-Sep-00
U19v PS1ds	Almendro	06-Jun-73	37 14 53	116 20 57	6842	3837	---	2026	bailer	2999	18-Aug-99
U4u PS2a	Dalhart	13-Oct-88	37 05 13	116 02 51	4117	2280	1548-1644	1636	pump	1640	16-Aug-99
UE5n	Cambric	14-May-65	36 49 34	116 06 59	3112	1690	720-1687	705	pump	730	09-Sep-99
RNM-1	Cambric	14-May-65	36 49 28	115 58 01	3135	1302	1063-1075	789*	pump	---	28-Jun-00
RNM-2S	Cambric	14-May-65	36 49 21	115 58 01	3133	1120	1038-1119	723	pump	---	14-Jun-00
RNM-2S	Cambric	14-May-65	36 49 21	115 58 01	3133	1120	1038-1119	723	pump	800	11-Oct-99

* water depth not corrected for borehole slant
EOI = effective open interval

Table 1. Cavity or Near-Cavity Hot Well Analyses, FY1999-2000 (continued)
Water Quality and Anion Data

Well name	Test	Sample date	pH	T	TDIC as HCO_3	Cond.	Br	Cl	F	NO_3	SO_4
Units		*date collected in field*		*(°C)*	*(mg/L)*	*(μS/cm)*	*(mg/L)*	*(mg/L)*	*(mg/L)*	*(mg/L)*	*(mg/L)*
U20n PS1 DDh	Cheshire	12-Oct-99	8.2	38.2	108	324	<0.03	11.1	3.6	2.3	28.2
U19v PS1ds	Almendro	26-Sep-00	9.3*	---	---	742*	<0.1	48.2	9.5	<0.09	3.8
U19v PS1ds	Almendro	18-Aug-99	8.2*	---	120	728*	<0.03	40.5	9.9	<0.02	3.9
U4u PS2a	Dalhart	16-Aug-99	8.2*	---	160	352*	<0.03	5.8	0.7	18.5	12.0
UE5n	Cambric	09-Sep-99	8.4	26.5	183	453	<0.03	12.0	0.8	8.1	31.8
RNM-1	Cambric	28-Jun-00	8.0	26.0	---	416	0.2	12.3	0.3	16.2	36.5
RNM-2S	Cambric	14-Jun-00	7.8*	---	---	429*	0.2	14.8	0.4	14.3	36.8
RNM-2S	Cambric	11-Oct-99	8.2	24.6	168	440	<0.03	13.7	0.6	13.9	37.0

* values measured in the laboratory

Table 1. Cavity or Near-Cavity Hot Well Analyses, FY1999-2000 (continued)
Cation and Trace Element Data

Well name	Test	Sample date	Al	As	B	Ba	Ca	Fe	I	K	Li	Mg	Mn	Mo	Na	Pb	Pu	Se	Si	Sr	U
Unit		*date collected in field*	*(mg/L)*	*(µg/L)*	*(mg/L)*	*(mg/L)*	*(mg/L)*	*(µg/L)*	*(µg/L)*	*(mg/L)*	*(mg/L)*	*(mg/L)*	*(µg/L)*	*(µg/L)*	*(mg/L)*	*(µg/L)*	*(pg/L)*	*(µg/L)*	*(mg/L)*	*(µg/L)*	*(µg/L)*
U20n PS1 DDh	Cheshire	12-Oct-99	0.07	3	0.14	<0.005	4.7	1420	13	2.2	<0.05	0.1	110	10	65	0.67	7.03	<2	24	10	2.3
U19v PS1ds	Almendro	26-Sep-00	0.29	---	---	---	0.8	260	---	11.9	---	0.1	---	---	---	---	---	---	---	---	---
U19v PS1ds	Almendro	18-Aug-99	0.52	1716	1.54	0.07	0.9	12000	2	9.8	0.42	0.2	250	1226	162	63	58.2	8	11	40	nd
U4u PS2a	Dalhart	16-Aug-99	12.0	4	0.12	0.03	13.1	1270	3	14.0	0.14	2.7	90	nd	72	8.6	8.75	nd	37	30	4.2
UE5n	Cambric	09-Sep-99	<0.02	9	0.34	<0.005	7.5	60	30	8.0	<0.05	2.0	10	5	86	0.37	---	<2	---	50	4.0
RNM-1	Cambric	28-Jun-00	0.37	---	---	---	26.0	180	---	8.0	0.03	9.4	---	---	44	---	---	---	20	300	4.0
RNM-2S	Cambric	14-Jun-00	0.38	---	---	---	18.0	180	---	9.70	0.02	5.2	---	---	62	---	---	---	35	140	5.0
RNM-2S	Cambric	11-Oct-99	<0.02	5	0.24	<0.005	17.0	10	11	9.2	<0.05	5.6	<2	3	63	0.24	---	<2	---	110	4.0

Table 1. Cavity or Near-Cavity Hot Well Analyses, FY1999-2000 (continued)
Stable Isotope Data

Well name	Test	Sample date	δD_{SMOW}	$\delta^{18}O_{SMOW}$	$\delta^{13}C_{PDB}$	^3He	^4He	R/R_a
Unit		*date*	*‰*	*‰*	*‰*	*atoms/g*	*atoms/g*	*$^3He/^4He$*
Half-life (a)		*collected*	*stable*	*stable*	*stable*	*stable*	*stable*	*ratio*
Ref. date		*in field*						*sample/air*
U20n PS1 DDh	Cheshire	12-Oct-99	-113	-15.0	-6.0	2.01e+12	1.01e+13	1.44e+5
U19v PS1ds	Almendro	26-Sep-00	-111	-13.4	---	---	---	---
U19v PS1ds	Almendro	18-Aug-99	-111	-13.4	+45.0	---	---	---
U4u PS2a	Dalhart	16-Aug-99	-100	-12.8	-8.7	---	---	---
UE5n	Cambric	09-Sep-99	-106	-13.4	-8.3	1.95e+9	3.16e+12	4.48e+2
RNM-1	Cambric	28-Jun-00	-104	-12.7	---	1.43e+9	2.05e+12	5.05e+2
RNM-2S	Cambric	14-Jun-00	-105	-13.0	---	2.50e+10	6.43e+12	2.84e+3
RNM-2S	Cambric	11-Oct-99	-104	-12.9	-9.3	2.35e+10	6.40e+12	2.65e+3

Table 1. Cavity or Near-Cavity Hot Well Analyses, FY1999-2000 (continued)
Radiochemical Data

Well name	Test	Sample date	^{3}H	^{3}H	^{14}C	$^{36}Cl/Cl$	^{36}Cl	^{85}Kr	^{99}Tc	$^{129}I/^{127}I$	$^{234}U/^{238}U$	$^{234}U/^{238}U$ activity ratio	$^{234}U/^{235}U$	$^{235}U/^{238}U$	^{234}U	^{235}U	^{238}U
Unit		*date*	*(pCi/L)*	*(pCi/L)*	*pmc*	*ratio*	*(pCi/L)*	*(pCi/L)*	*(pCi/L)*	*ratio*	*ratio*	*ratio*	*ratio*	*ratio*	*(pCi/L)*	*(pCi/L)*	*(pCi/L)*
Half-life (a)		*collected*	*12.3*	*12.3*	*5730*		*3.01E+05*	*10.73*	*2.13E+05*						*2.46E+05*	*7.04E+08*	*4.47E+09*
Ref. date		*in field*	*collect.*	*time zero*	*collect.*		*collect.*	*collect.*	*collect.*						*collect.*	*collect.*	*collect.*
U20n PS1 DDh	Cheshire	12-Oct-99	5.1e+7	1.9e+8	1.54e+5	1.15e-9	4.20e-1	2.77e+4	2.20e+1	---	1.888e-4	3.44	2.633e-2	7.171e-3	3.00	0.04	0.86
U19v PS1ds	Almendro	26-Sep-00	1.5e+8	7.1e+8	---	---	---	---	---	---	---	---	---	---	---	---	---
U19v PS1ds	Almendro	18-Aug-99	1.6e+8	6.8e+8	2.47e+4	1.60e-9	2.14e+0	---	---	---	---	---	---	---	---	---	---
U4u PS2a	Dalhart	16-Aug-99	1.6e+7	3.1e+7	1.19e+5	4.45e-8	8.52e+0	---	---	---	---	---	---	---	---	---	---
UE5n	Cambric	09-Sep-99	---	---	1.88e+1	6.01e-10	2.38e-1	<40	2.29e-3	3.51e-9	---	---	---	---	---	---	---
RNM-1	Cambric	28-Jun-00	2.84e+4	2.05e+5	---	1.06e-12	4.30e-4	---	---	---	1.363e-4	2.48	1.869e-2	7.292e-3	3.33	0.06	1.33
RNM-2S	Cambric	14-Jun-00	5.84e+5	4.21e+6	---	1.62e-10	7.92e-2	---	---	---	1.233e-4	2.24	1.693e-2	7.285e-3	3.77	0.08	1.66
RNM-2S	Cambric	11-Oct-99	---	---	4.13e+2	1.64e-10	7.40e-2	<40	9.72e-4	2.12e-7	---	---	---	---	---	---	---

Chapter 3

Alpha and Beta Radiography Results from Nuclear Melt Glass of the Rainier U12B Test, Nevada Test Site

Gail F. Eaton

Analytical and Nuclear Chemistry Division, Lawrence Livermore National Laboratory

Introduction

During FY1998 and FY1999, an alpha (α) radiography technique was developed for application to geologic and nuclear melt glass samples (Smith et al., 1999; Eaton and Smith, 2001). The results of this work showed that by modifying an existing α–radiography technique, it was possible to spatially resolve areas of high α–activity in melt glasses. The ability to determine where radionuclides are distributed in nuclear melt glass has implications for understanding how radionuclides are released into the environment. On going research includes determining the source of colloidal plutonium, which has been documented to be mobile in fractured volcanic rock aquifers (Kersting et al., 1999). Eaton and Smith (2001) showed that a secondary alteration layer of clay (probably smectite) forms on melt glass surfaces, which may be a source of the colloidal material. Radiography techniques that are discussed in this paper may be subsequently used as an imaging technique to elucidate the association of plutonium and colloids.

The success in accurately siting areas of α–activity in thin sections of nuclear melt glass prompted additional research into developing a companion beta (β) radiography application. The majority of β–emission studies on geologic samples have relied on counting techniques, which do not yield spatial information. In this study, we have adapted a β-radiography technique originally developed for biomedical research for use with geologic samples, providing a clear and literal image of the distribution of both high and low level β–emitters. We subsequently applied both α– and β–radiography techniques to nuclear melt glass and geologic samples from the Rainier Test (RT). The RT was chosen for this study because: 1) there is a relatively large amount of nuclear melt glass available from this test, and 2) the geology and melt glass from the RT has been extensively characterized (e.g. Schwartz et al., 1984; Thompson and Misz, 1959).

Sample Descriptions

The RT was detonated in the U12B tunnel at the Nevada Test Site (NTS) on September 19, 1957. The U12B tunnel was mined laterally into the granular tuff of the Oak Springs Formation on Rainier Mesa (Fig. 1). Samples were taken from three core lines drilled from the U12B complex following the detonation (Fig. 2). Three of these samples are from the melt glass puddle, and the fourth is a volcanic tuff sample from approximately 50-ft directly below the detonation cavity. The tuff sample served as a 'background' sample devoid of any non-natural radioactivity. Two of the melt glass samples (H and T-11 #2) have distinctly banded layers of light to dark gray glass, and sample T-11 #2 has clearly recognizable pieces of pink volcanic tuff layered throughout the sample. Sample

I-36 has no obvious inclusions of tuff, and consists of slightly laminated, rough textured, light gray glass. The volcanic tuff is a fine-grained, welded rhyolite tuff that is pink in color. The sample is slightly laminated and contains very small, light colored inclusions that are probably pumice fragments (Warner and Violet, 1959). Brief sample descriptions are given in Table 1.

Table 1: Description of melt glass and geologic samples taken from U12B core lines.

Sample	Core Line	α–activity (cpm)*	Description
(1) T-11 #1	T-11	---	Welded rhyolitic tuff: light pink and slightly laminated, with light pumiceous inclusions.
(2) T-11 #2	T-11	400	Melt Glass: banded dark glass with pink inclusions of volcanic tuff. Not vesicular.
(3) H	H	800	Melt Glass: banded dark and light glass. Banded in an oval manner. Not vesicular.
(4) I-36	K-1	200	Melt Glass: light gray, slightly laminated glass. Not vesicular.

*cpm = counts per minute. Readings taken using a Blue Alpha hand-held meter placed in direct contact with the thin sections.

Methods: Alpha and Beta Radiography

Polished thin sections were made from each of the three glass samples and the volcanic tuff sample. Samples were mounted in epoxy plugs and cut with a precision wafer saw to expose their cross-sectional area before being mounted on circular slides, ground to ~30 μm thickness, and then finished to a high polish. The α–radiography analyses were made using TASTRAK CR-39 detectors placed directly onto the thin section surface, which was then etched using a sodium hydroxide solution. Refer to Smith et al. (1999) for details of this method.

The β–radiography method applied in this study was originally developed for use in the biomedical field, where β–radiography is commonly used determine the location of β–emitting isotopes in tissue samples. We found that Kodak BioMax™ MS film for high-energy β– and γ–particles (e.g. ^{32}P, ^{125}I), and BioMax™ MR film for low-energy β–particles (e.g. ^{3}H, ^{14}C, ^{32}P, ^{35}S, ^{45}Ca, ^{59}Fe) produced images when exposed to thin sections made from nuclear melt glass samples. These images were produced by placing the thin sections directly onto a sheet of BioMax™ film that was loaded into a cassette under darkroom conditions (Fig. 3). The cassette was necessary to ensure that there was no light exposure to the film. The tightly closed cassette was then placed into a freezer (-20°C) during the period of the exposure. Exposure times varied according to the level of β–activity initially measured in each sample by placing an Eberline™ E-120 hand-held meter in direct contact with the thin sections. Accordingly, high-activity samples were exposed for only a very short time (~1-4 hours for the melt glass samples). The films

were then developed in a darkroom under a safe light outfitted with a Kodak GBX-2 filter. Kodak GBX developer and fixer solutions were used to develop the images, and the films were then allowed to dry for 1-2 hours under normal light conditions.

Results

α-radiography

The α–radiography analyses of the RT melt glass samples produced distinct tracks in the CR-39 detectors after an exposure time of 24 to 26 hours (Figs. 4 - 6). It was evident from the density of the tracks that this exposure time could be greatly reduced (Fig. 4). As in previous studies (Smith et al., 1999; Eaton and Smith, 2001), the α–activity seems to be most strongly associated with areas of dark colored glass. Areas of smooth, non-vesicular light and dark gray glass produced the highest density of α–tracks in the detectors (Fig 4 – 6). Within these regions, the α–track density was relatively uniform, with only minor clusters of α–tracks and no α–track stars.

The volcanic tuff sample was exposed for a much longer time period of 4 months since tracks were not observed in the α–detector over a 24-hour period. Following this 4-month exposure, α–tracks with a track density similar to the melt glass samples were clearly visible in the detector (Fig. 7).

β-radiography

Both the high- and low-energy β-films produced images. The BioMax™ MR film imaged both the high and low-energy β–emissions, but the resultant images were very over-exposed, even after short exposure times. The BioMax™ MS film, employed almost exclusively in this study, produced the clearest images – but only for high-energy β–emissions (Figs. 4 and 5). For all three melt glass samples, the images showed that the high-energy β–emissions follow similar distribution pattern to that of the α–tracks. This is especially well illustrated in Figure 4. In samples H and T-11 #2, the β–activity consistently correlates with the darker melt glass (Fig 4 and 5). It should be noted that although sample I-36 produced β–emission images (Fig. 6), they are too faint to reproduce here.

The volcanic tuff sample failed to produce β–emission images in the BioMax ™ MS film, even after a 14-day exposure time. This suggests that β–emitters are present only at very low (natural) abundances in this sample.

Discussion

The results of this study indicate that the distribution of α and β–emitters in the melt glass samples from the RT is relatively uniform. This uniformity in distribution suggests that the radionuclides are well mixed in the glass despite the chaotic textures formed during melt glass condensation and cooling of the cavity following the detonation. In addition, the radionuclides appear to be volumetrically incorporated into the melt glass, and not randomly distributed onto glass surfaces. The lack of α–track stars and significant clustering of α–activity indicate that there are no distinct radionuclide sinks or

mineralogical controls on siting of α–emitting isotopes. These results are in keeping with α-radiography of other Nevada Test Site nuclear melt glasses (Smith et al., 1999; Eaton and Smith, 2001). Although the β–emitters are also relatively uniform in distribution, areas of increased β–activity are evident in sample H. Toward the center of this melt glass sample, regions of increased activity are apparent in the β–emission image (Fig. 4). This concentration does not correlate with any textural feature and may be the result of bulk compositional differences in the melt glass.

The volcanic tuff sample was analyzed as a background sample to determine whether the contribution from decay of naturally occurring α–emitting isotopes of uranium (U) and thorium (Th) in volcanic rock is large enough to bias α–activity mapped in the melt glass. It took 4-months to produce roughly the same track density in the volcanic tuff detector as seen after only a 1-hour exposure for the melt glass detectors. This implies that the contribution of natural U+Th decay to the bulk α–activity in the melt glass is minimal. The presence of volcanic tuff inclusions in the melt glass explains areas in the α– and β–images that exhibit no perceptible radionuclide activity over short exposure times.

Future Work

This study demonstrates that β–radiography techniques can be successfully used to generate images of radionuclide distributions in samples of nuclear melt glass or debris. The ability to site β–emitting isotopes in geologic media provides another tool for elucidating radionuclide distributions in underground nuclear test environments. On going studies that can be enhanced by this new technique may include colloid studies and matrix diffusion experiments. For example, radiography techniques can be used to pinpoint areas of high α and β–activity as a precursor to microbeam analyses in colloid studies. In matrix diffusion experiments, the β–radiography technique may be useful in mapping the extent of diffusion of conservative radionuclides (e.g. ^{3}H, ^{14}C, ^{36}Cl, ^{129}I) into geologic media. For tracer flow-through experiments, a "spike" of β–emitting isotopes can now be added and tracked alongside α–emitting isotopes.

References Cited

Eaton, G.F, and Smith, D.K. (2001) Aged Nuclear Explosive Melt Glass: Radiography and Scanning Electron Microscope Analyses Documenting Radionuclide Distribution and Glass Alteration. Journal of Radioanalytical and Nuclear Chemistry, v. 248, n. 3., 543-547.

Kersting, A.B., Efurd, D.W., Finnegan, D.L., Rohop, D.J., Smith, D.K. and Thompson, J. L. (1999) Migration of plutonium in groundwater at the Nevada Test Site. Nature, v. 397, n. 6714, pp. 56–59.

Smith. D.K., Eaton, G.F., Rose T.P., Kenneally, J.M., Hudson, G.B., Davisson, M.L., Benedict, F.C., and Criss, R.E., (1999) Hydrologic Resources Management Program and Underground Test Area FY 1998 Progress Report, Lawrence Livermore National Laboratory, UCRL-ID-135170, 76 p.

Schwartz, L., Piwinskii, A., Ryerson, F., Tewes, H., and Beiriger, W. (1984) Glass produced by underground nuclear explosions, *in:* Natural Glasses, North Holland, L.D. Pye, J.A. O'Keefe, and V.D., Frechette (eds.), pp. 559-591.

Thompson, T.L. and Misz, J.B. (1959) Geologic studies of underground nuclear explosions Rainier and Neptune: Final Report. Lawrence Livermore National Laboratory Internal Report, UCRL-5757, 59 p.

Warner, S.E. and Violet, C.E. (1959) Properties of the environment of underground nuclear detonations at the Nevada Test Site: Rainier Event. Lawrence Livermore National Laboratory, UCRL-5542 - Rev., 127 p.

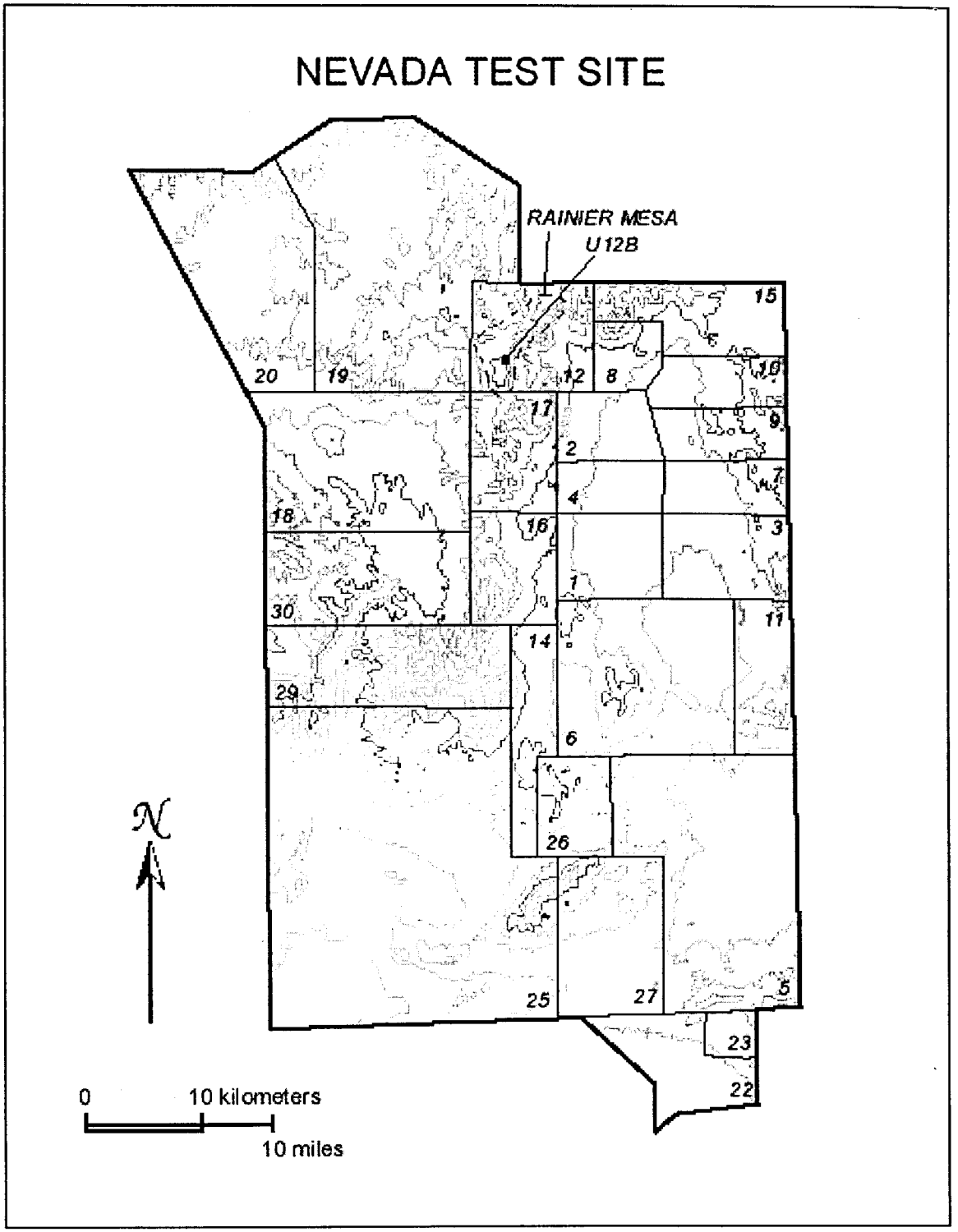

Figure 1: Map of the Nevada Test Site showing the location of Rainier Mesa, and the U12B Tunnel.

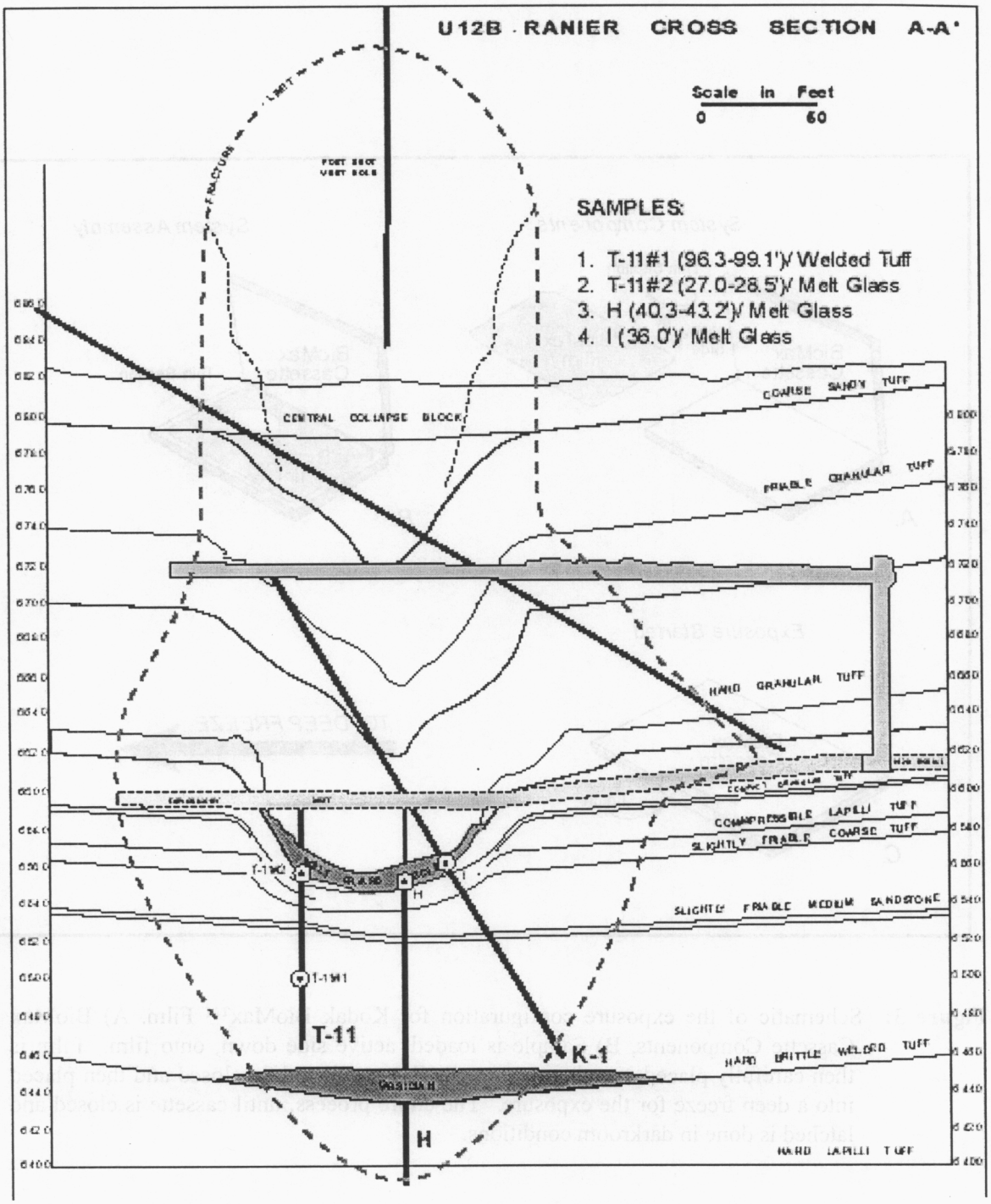

Figure 2: Cross-section through the U12B cavity showing the location of the 3 melt glass samples and the volcanic tuff sample.

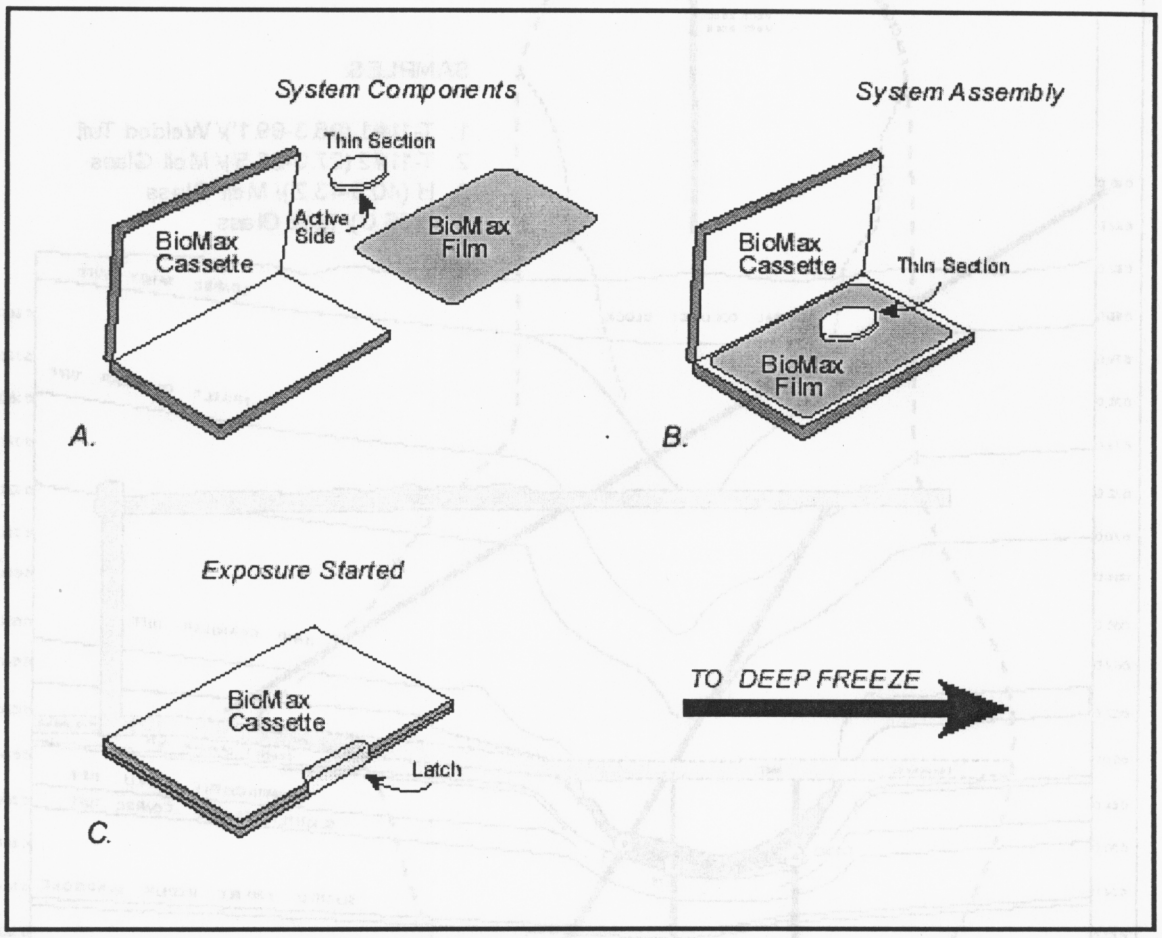

Figure 3: Schematic of the exposure configuration for Kodak BioMax™ Film. A) BioMax Cassette Components, B) Sample is loaded, active side down, onto film. Film is then carefully placed into the cassette. C) Cassette is tightly closed and then placed into a deep freeze for the exposure. The entire process, until cassette is closed and latched is done in darkroom conditions.

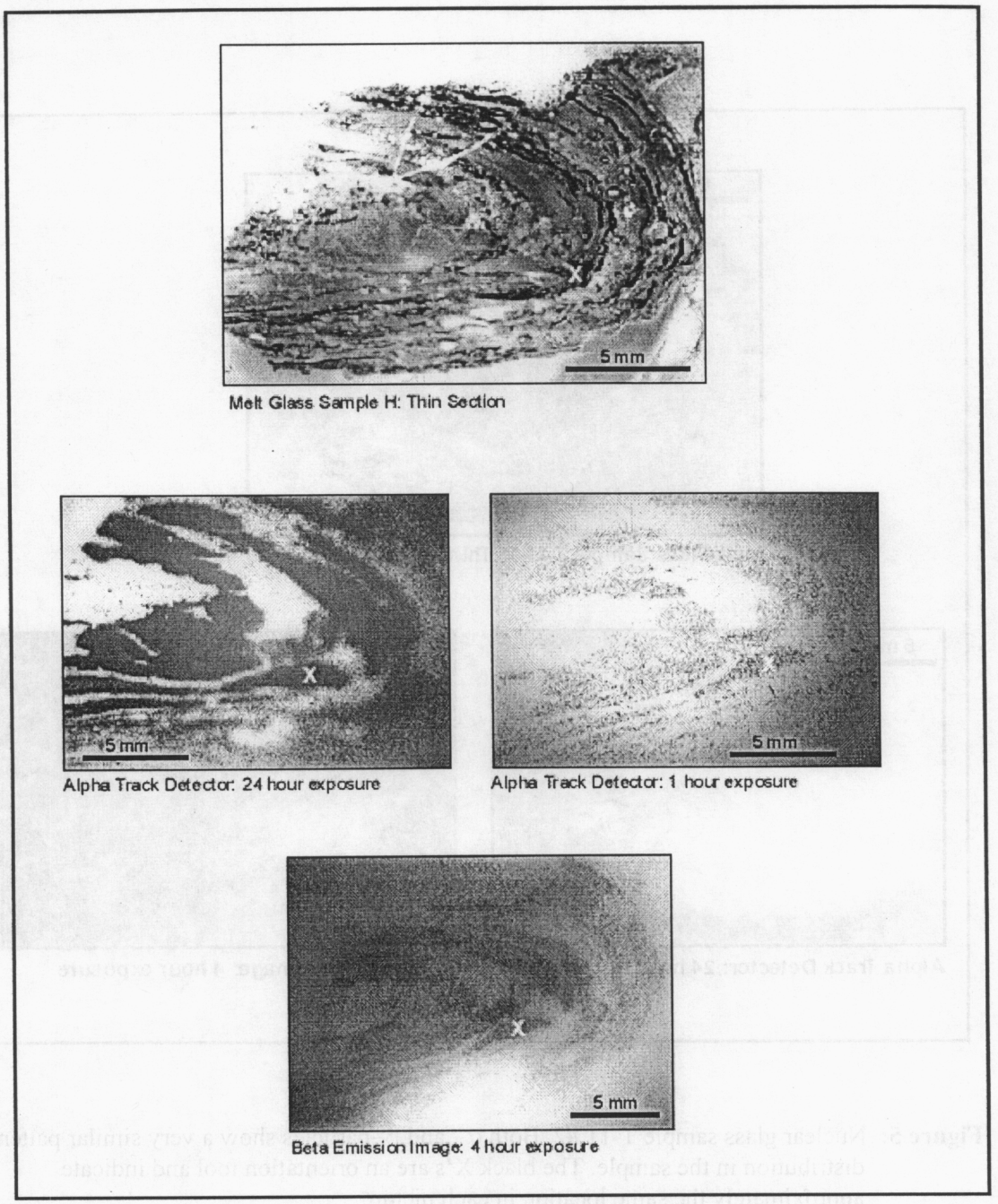

Figure 4: Nuclear melt glass sample H. Both α– and β–particles show a very similar pattern of distribution in the sample. The white X's are an orientation tool and indicate approximately the same location in each picture.

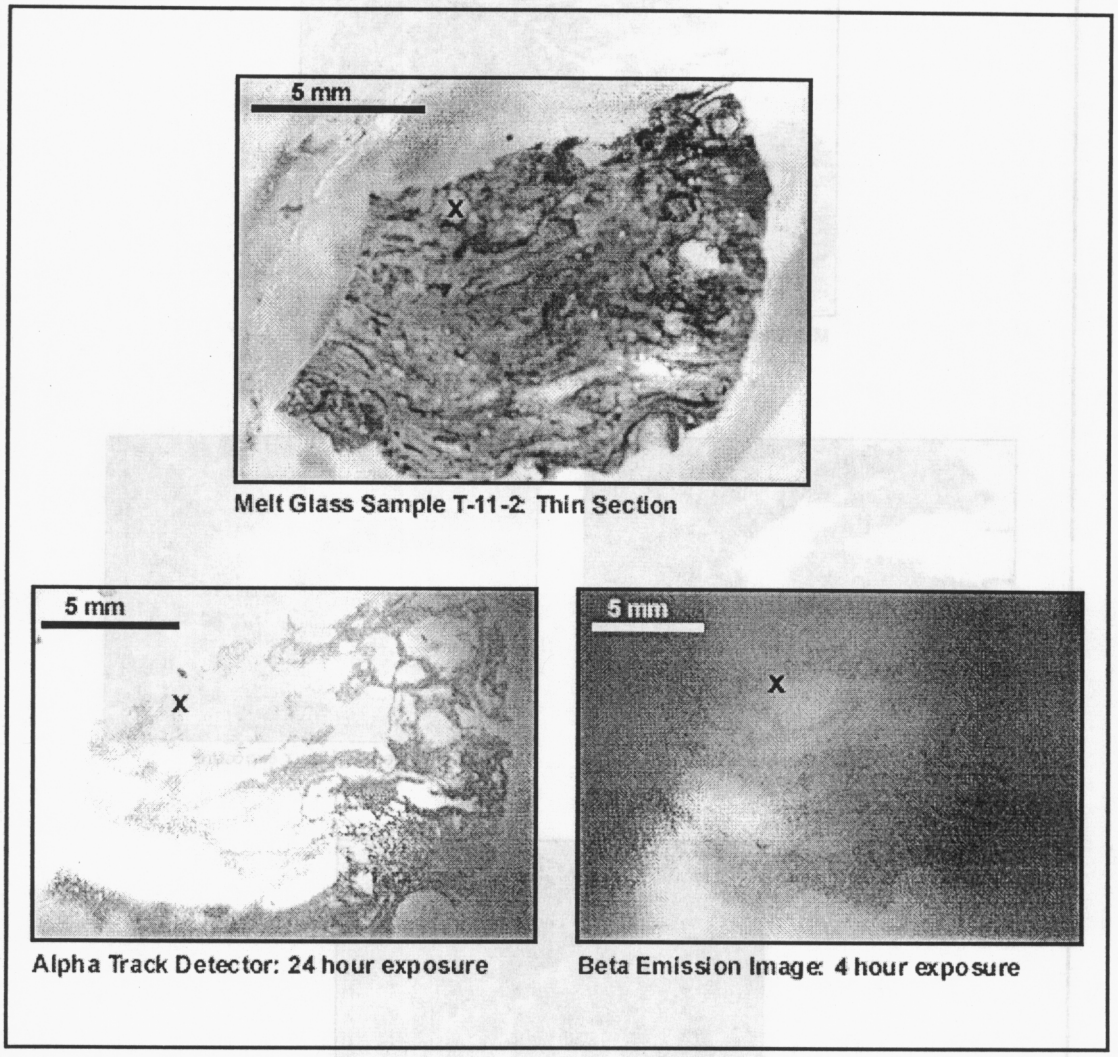

Figure 5: Nuclear glass sample T-11 #2. Both α– and β–particles show a very similar pattern of distribution in the sample. The black X's are an orientation tool and indicate approximately the same location in each picture.

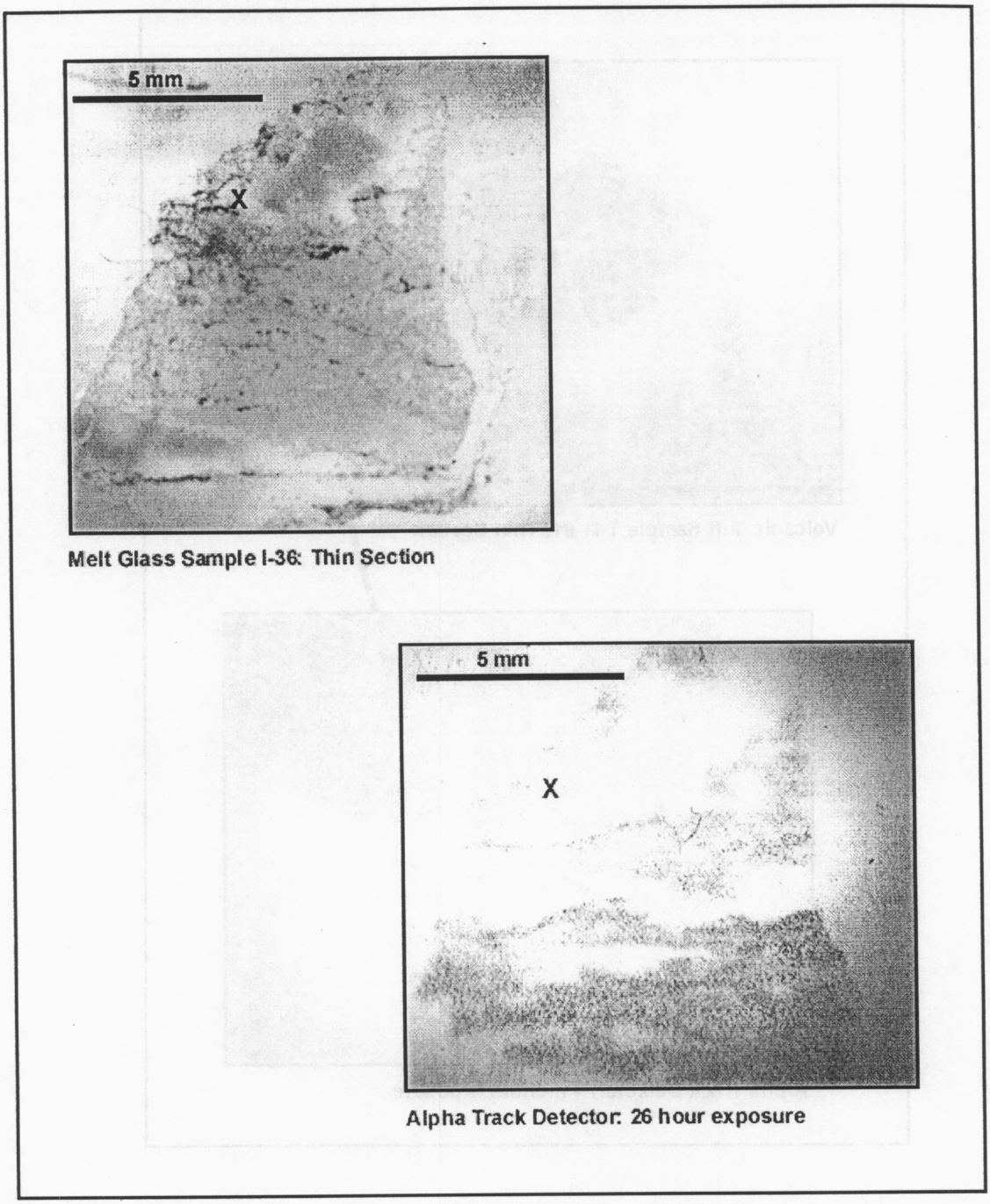

Figure 6: Nuclear melt glass sample I-36. Although β–emission images were produced for this sample, they were too faint to produce clear photographs. The black X's are an orientation tool and indicate approximately the same location in each picture.

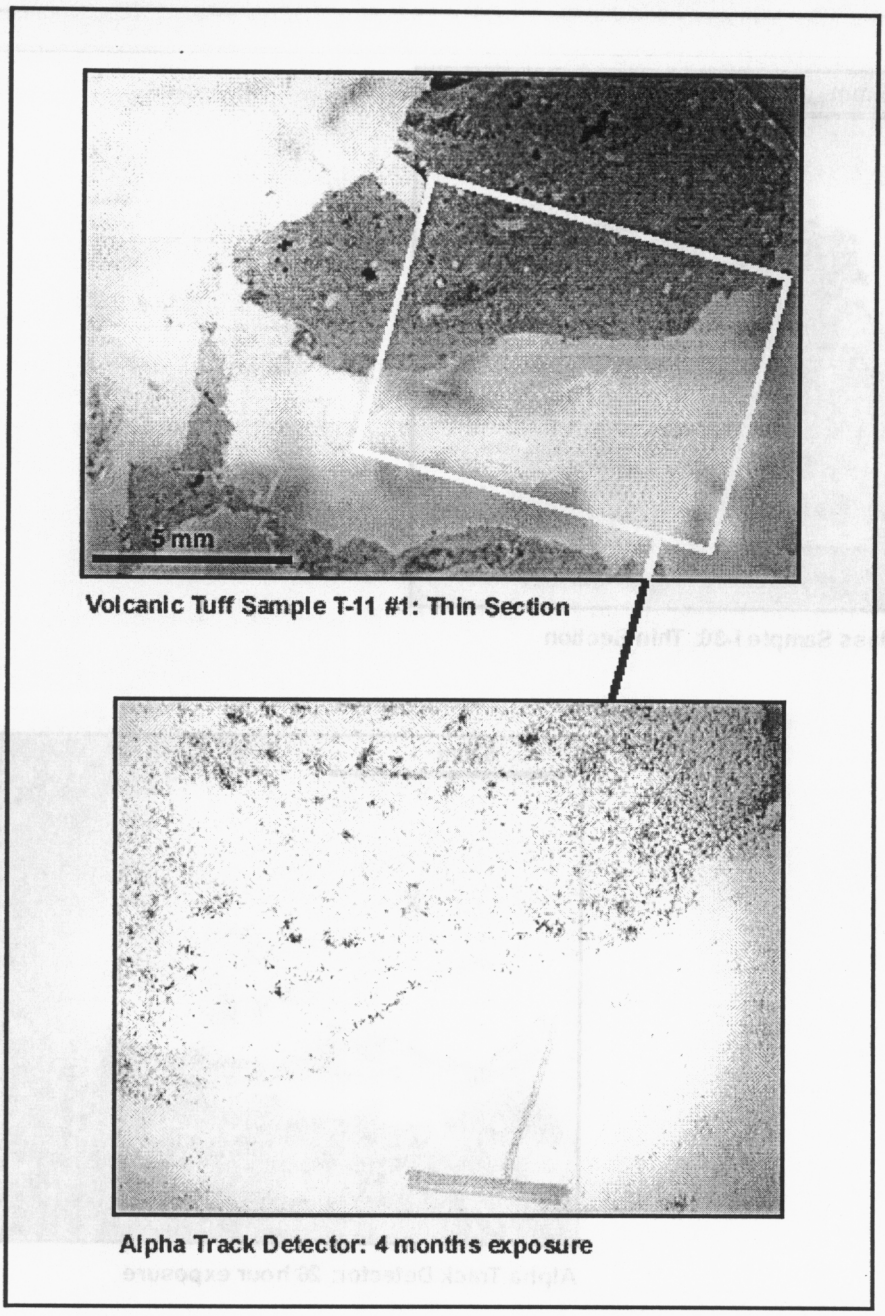

Figure 7: Volcanic Tuff sample T-11 #1. The lower image is the enlarged area outlined by the white box in the upper image.

Chapter 4

Microbial Impact on Radionuclide Mobility: Preliminary Investigations at the NTS

Carola A. Laue

Analytical and Nuclear Chemistry Division, Lawrence Livermore National Laboratory

Research in recent years [1-6] suggests that one of the most diverse groups of living organisms - the bacteria - may strongly affect the fate and transport of metals and radionuclides in the environment. Most of the research on biochemical interactions of microbes with contaminants has been performed in the laboratory, utilizing well-characterized microbes under idealized conditions that barely resemble the natural environment. Less emphasis has been placed on the actual identification of bacteria in contaminated natural systems. Studies of natural systems are important both in terms of identifying strains of bacteria that are effective in remediation, and in avoiding possible negative impacts on remediation efforts by introducing foreign organisms into otherwise "balanced" environments.

The long-range goal of this project is to investigate the impact of native microbes on the fate and transport of radionuclides at the Nevada Test Site (NTS). This assessment is the first step toward determining whether naturally-occurring microorganisms at the NTS can be effectively utilized in remediation strategies. Our effort builds upon previous microbial characterization work at the NTS, largely in support of the Yucca Mountain Project [e.g. 7-9], but differs in its emphasis and in some of the laboratory methods that are utilized.

We will investigate microbial communities in samples taken from two distinct environments: groundwater and near-surface soils. In both cases, our research is focused on identifying the microorganisms found in representative samples, and on characterizing the geochemistry of the microbial environment. Following these initial steps, we plan to explore how these microbes interact with their environment by closely simulating NTS conditions and tracking microbial activities under certain directed stresses.

In January 2001, we collected soil samples at different depths (up to 75 cm below the surface) from the following NTS locations: Massachusetts Mountains, Frenchman Lake (east and west side; Area 5), Yucca Lake (Area 6), and near Hood crater (Area 2). In addition, we collected groundwater from Water Well 5b, and surface waters from Yucca Lake and from ponds at Water Well 5b and Water Well C. In May 2001, an additional groundwater sample was obtained from the U-19v PS1ds (Almendro) borehole on Pahute Mesa. This sample is of interest both because of the presence of radionuclides in the groundwater (~10^8 pCi/L ^{3}H), and because the water temperature within the Almendro nuclear test cavity is significantly elevated (~150°C). This raises the question as to what kind of microbial community (if any) has developed in such an extreme environment?

During our initial microbial characterization work, we have focused on samples from Frenchman Lake due to its varying contamination levels. The west side of the playa contains relatively low levels of fallout-derived contamination, while the east side has radiological restrictions. Since the geological conditions are identical at both sites, we are interested to see if an increased exposure to radionuclides resulted in the development of different microbial community structures. We assume that the community structures were identical prior to atmospheric nuclear testing.

Two parallel methods to determine the native microbial diversity in the NTS samples are in progress.

- Total microbial DNA was extracted from soil samples and a hypervariable region from the Small Subunit (SSU) ribosomal DNA genes (rDNA) was amplified using sets of universal primers, which amplify the SSU rDNA of all organisms (Polymerase Chain Reaction [10]). The amplified products were uniformly fragmented, biotin-labeled, and hybridized to our custom SSU GeneChip microarray (Affymetrix, Inc.) that identifies 120 subdivisions of prokaryotes, eukaryotes and archaea. The SSU GeneChip arrays can also be used to determine the relative abundance of different organisms derived from the samples.

- Microbial organisms are identified by classical culturing techniques. Given the preliminary data from the GeneChip analyses, we were able to choose different media appropriate for culturing observed microbes. In addition, a nutrient poor media was chosen to simulate environmental conditions at the NTS. Defined amounts of soil are inoculated into the chosen media (R2B, Frankia, and Mycobacterium broth). Small samples from these soil-media slurries were drawn at the time of inoculation and than repeatedly after certain time intervals for a total of two weeks. Slurry aliquots were then spread onto appropriate media plates (R2A, Frankia, and Mycobacterium agar) and incubated until individual colonies were sufficiently grown (Figure 1). The colonies are then separated, striked, and incubated in order to obtain pure cultures for subsequent identification. The experiments described above are performed at two different temperatures, simulating the seasonal temperature fluctuations at the NTS.

Gaining knowledge of the microbial communities encountered in the environment at the NTS is crucial for future investigations of microbial-actinide interactions. Once we have isolated native NTS bacterial strains, we will be able to assess the ability of individual microorganisms and microbial communities to alter the chemical behavior of actinides in the environment and/or utilize actinides in metabolic processes.

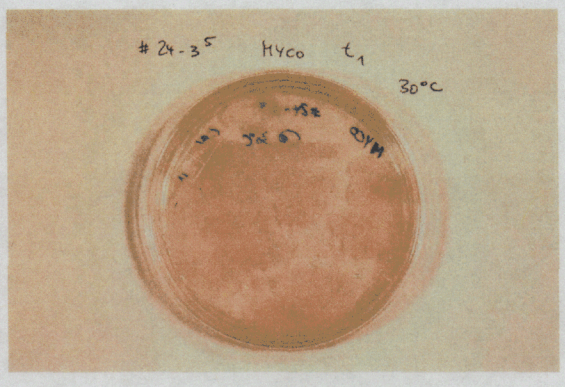

Figure 1. Microbial culturing plate (Mycobacterium agar) with bacteria grown from a slurry aliquot of NTS soil from Frenchman Lake. This image was taken 6 hours after inoculation and incubation at 30°C in the liquid media. Bacteria grew across most of the surface of the media within 24 hours after spreading onto the agar. From these types of culture plates, we are isolating and identifying the bacteria that are native to the NTS.

References

(1) Pace, N. R., *A Molecular View of Microbial Diversity and the Biosphere*, Science **276** (1997) 734-740.

(2) *Metal Ions and Bacteria*, Beveridge, T. J. and Doyle, R. J., Ed's, John Wiley & Sons, New York, 1989.

(3) Panak, PJ; Raff, J; Selenska-Pobell, S; Geipel, G; Bernhard, G; Nitsche, H. *Complex formation of U(VI) with Bacillus-isolates from a uranium mining waste pile*, Radiochim. Acta, **88** (2000) 71-76.

(4) Fowle, D. A., Fein, J. B., Martin, A. M., *Experimental Study of Uranyl Adsorption onto Bacillus subtilis*, Environ. Sci. Technol. **34** (2000) 3737-3741.

(5) John, S.G., Ruggiero, Hersman, L. E., Neu, M. P., *Siderophore-mediated plutonium uptake by the common soil aerobe Aureobacterium flavescens (JG-9)*, Proceeding of 220th National Meeting of the American Chemical Society, Washington, D. C., Aug 2000.

(6) A NABIR Primer, McCullough, J., Hazen, T. C., Benson, S. M., Metting F. B., Palmisano, A.C., *Bioremediation of Metals and Radionuclides ... What it is and How it works*, http://www.lbl.gov/NABIR/primer/primer.html

(7) Haldeman, D.L., Amy, P.S., *Bacterial heterogeneity in deep subsurface tunnels at Rainier Mesa, Nevada Test Site*, Microbial Ecology **25** (1993) 183-194.

(8) Haldeman, D.L., Amy, P.S., Ringelberg, D., White, D.C., *Characterization of the microbiology within a 21-m^3 section of rock from the deep subsurface*, Microbial Ecology **26** (1993) 145-159.

(9) Kieft, T.L., Kovacik, W.P., Ringelberg, D.B., White, D.C., Haldeman, D.L., Amy, P.S., Hersman, L.E., *Factors limiting microbial growth and activity at a proposed high-level nuclear repository, Yucca Mountain, Nevada*, Appl. Environ. Microbiol. **63** (1997) 3128-3133.

(10) Relman, D.A., *The Identification of Uncultured Microbial Pathogens*, J. Infect. Diseases **168** (1993) 1-8.

Chapter 5

Report on Field, Laboratory and Modeling Results on Mineral Colloids

Annie B. Kersting, Nadia L. Hakem, Mavrik Zavarin, Eric R. Sylwester, Lumin Wang and Ross Williams

Lawrence Livermore National Laboratory

Executive Summary

This report summarizes our results to date and outlines the work for FY01. This project integrates field, experimental and modeling work to determine under what conditions colloid-facilitated transport of Pu may be important. The field portion of our project involved entering the tunnel system at Rainier Mesa, NTS and collecting groundwaters from the unsaturated environment. We determined what radionuclides and colloids were present in an unsaturated groundwater system, flowing away from underground nuclear tests. Results of our experimental and geochemical modeling efforts to date are also summarized in this report and were undertaken to help determine the long term transport behavior of Pu in groundwater.

From the water samples collected from the tunnels on Rainier Mesa, NTS we can conclude:

- The colloids consist of clays (illite), zeolites (clinoptilolite), and calcite. This is similar to the minerals identified in groundwater from ER20-5 and Cheshire.
- The groundwaters are impacted by radionuclides that include: ^{3}H, ^{90}Sr, ^{106}Ru, ^{125}Sb, ^{137}Cs, Pu and Am.
- The majority of the activity is associated with the colloidal fraction of the groundwater.

This work in conjunction with our previous colloid characterization work at ER20-5 and Cheshire, supports the hypothesis that the important mineral colloids at the NTS are clays, zeolites and calcite. In addition, the radionuclides are always associated with the colloidal fraction and not the dissolved phase. These result are critical for future modeling efforts to determine the long term behavior of actinides.

From our sorption experiments we can conclude that Pu (IV) sorbs strongly to clinoptilolite colloids under groundwater conditions observed at the NTS. We have also determined that Pu(IV) did not change oxidation states during experiment.

Sorption of Pu(IV) to clinoptilolite colloids is equivalent to a Kd value of $\sim 10^5$ mL/g at pH ~8. In this intermediate pH (and lower pHs), sorption seems to be suppressed to some degree as a result of aqueous Pu-carbonate complexation. Although we are able to fit these data to both NEM and DLM surface complexation, the consistent overestimation of sorption at intermediate pHs suggests that our aqueous speciation database is incomplete for Pu(IV) solutions under these conditions. Additional sorption data that span a larger range of pH and pCO_2 should allow for a more complete analysis of factors affecting Pu(IV) and Pu(V) sorption to both clinoptilolite and calcite.

1. Introduction

In 1997 and 1998, very low concentrations of plutonium (Pu) were detected in NTS groundwater collected from ER20-5 wells located on Pahute Mesa. It was determined that the Pu was originally deposited from an underground nuclear test 1.3 km north of ER20-5 well locations (Kersting et al., 1999). Greater than 90% of the Pu and other radionuclides were associated with the colloidal fraction (< 1 micron particles) in the groundwater. The colloids consisted mainly of zeolite (mordenite, clinoptilolite/heulandite), clays (illite, smectite) and cristobalite (SiO_2).

These field observations raised a number of questions regarding the dominant mechanisms that may control the Pu migration. Kersting et al., (1999) suggested that the Pu may sorb to mineral colloids present in NTS groundwaters and be transported away from test cavities. If colloid-facilitated transport of Pu and other insoluble radionuclides is a viable mode of transport, then current models that are based solely on solubility of these species in groundwater may severely underestimate transport distances. For this reason, we have pursued a field, laboratory, and modeling approach to determine:

- if the actinides are associated with colloid minerals in groundwater at other locations at the NTS,
- the size, composition and concentration of naturally occurring colloids in NTS waters,
- which mineral colloids are the strongest sorbers of actinides, and
- what is the maximum amount of Pu that is likely to be transported in groundwater and under what conditions.

This report summarizes our results to date and outlines the work for FY01. The field portion of our project involved entering the tunnel system at Rainier Mesa, NTS and collecting groundwaters from the unsaturated environment. We wanted to determine what radionuclides were present in unsaturated groundwater system, flowing away from underground nuclear tests and if they were associated with the mineral colloids. We report the major results from analysis of groundwater samples collected from the tunnel system, at Rainier Mesa. A separate memo report is being compiled for Defense Threat Reduction Agency (DTRA), summarizing the results of our fieldwork in the tunnels. Results from our field sampling are not for distribution until they have been reviewed and released by DTRA, DOD.

Results of our experimental and geochemical modeling efforts to date will be summarized in this report. Experiments initiated in FY00 and continuing through FY01 focus on Pu (1V and V oxidation states) sorption/desorption on the different mineral colloids identified in the groundwater at NTS. This work will help to determine which mineral colloids sorb actinides.

2. Fieldwork in the Rainier Mesa Tunnels, NTS

In August of 1998, scientists from ANCD at LLNL in conjunction with Defense Threat Reduction Agency (DTRA), spent four days collecting water samples from the tunnels on Rainier Mesa, NTS. The tunnel system provides unprecedented access to impacted waters resulting from underground nuclear testing.

2.1. Sample Collection

Our field sampling was very successful. Samples were collected from three tunnels; U12E, U12T and U12N. The majority of the water samples were collected from pipes sampling vadose zone water collected behind cement portals (Figure 1A). In tunnel U12T, we were able to collect water that was dripping off the tunnel walls unencumbered by the engineered cement barriers (Figure 1B). This water represents the most representative natural vadose zone water. Therefore, all colloid characterization work was carried out using these samples (U12T-A, U12T-B, U12T-C, U12T-D, and U12T-E).

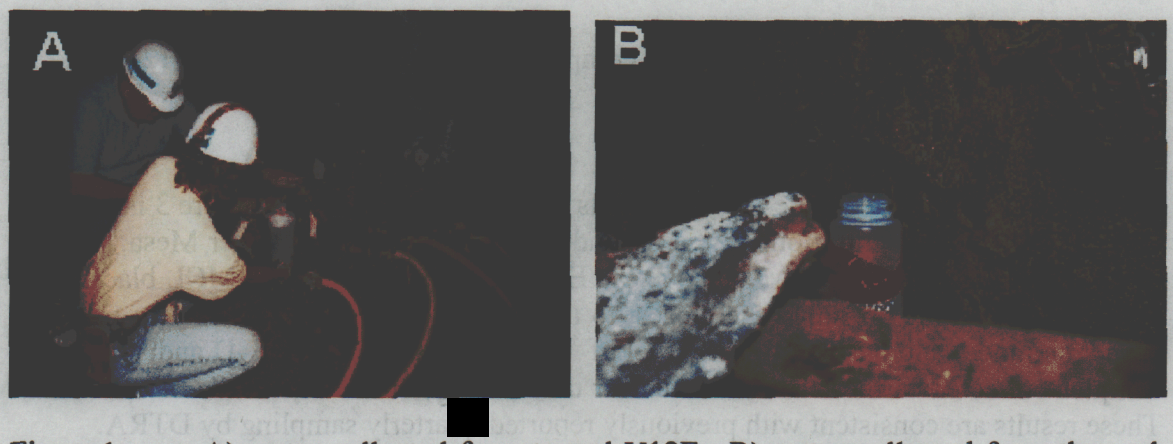

Figure 1. A) water collected from tunnel U12E. B) water collected from the rock wall of tunnel U12T

2.2. Groundwater Composition

To date, these groundwater samples have been analyzed for groundwater composition, colloid content, gamma-emitting radionuclides, and Pu, Am and ^{90}Sr. Figure 2 is a comparison of the cation composition of water collected in U12T, J-13, WW-20,and ER20-5, NTS. WW-20 and ER20-5 are wells located in volcanic rocks similar to those on Rainier Mesa. J-13 is groundwater from the proposed Yucca Mountain Repository. The water in the tunnels is similar to water on Pahute Mesa, although the Na concentration is much higher.

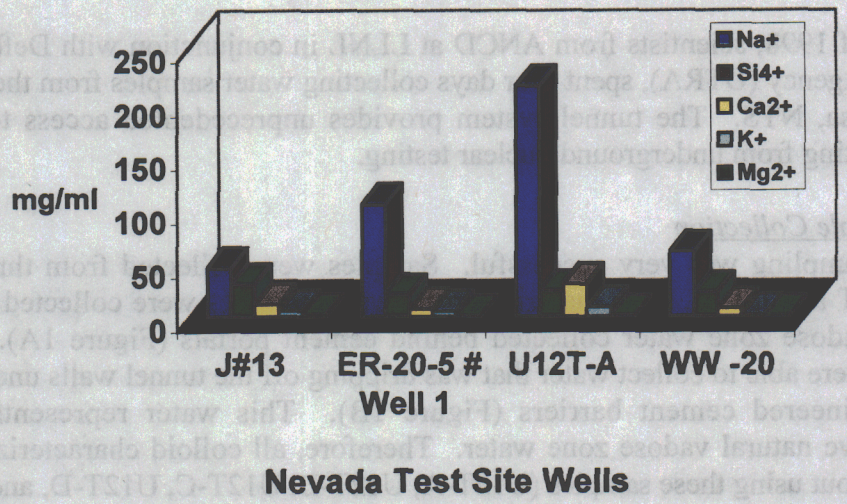

Figure 2. Comparison of the cation composition of groundwater from U12T rock wall samples.

2.3. Radiochemical Analysis

All the water samples collected in the tunnels contained tritium (^3H). Figure 3 is a plot of the tritium (^3H) concentrations in the groundwater samples from Rainier Mesa. All the samples collected have ^3H levels above the EPA drinking water limit (MCL black line). In T-tunnel, sampleT-2100 is the closest to the nuclear detonations (2100 feet from the tunnel entrance) and has the highest level of ^3H. Samples T-A, T-B, T-D and T-E are all samples collected farthest from the nuclear detonations, on the rockwalls of the tunnel. These results are consistent with previously reported quarterly sampling by DTRA.

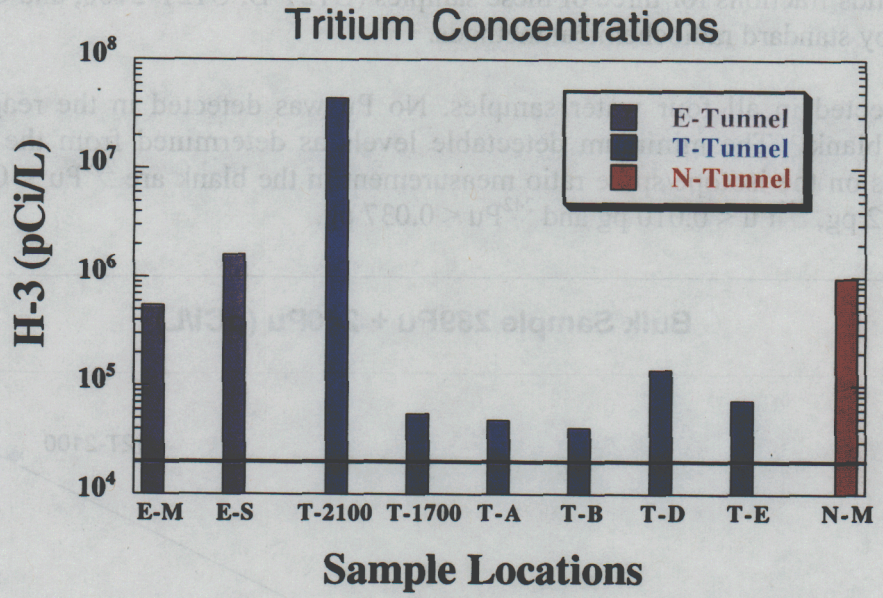

Figure 3. Tritium concentrations of Rainier Mesa water samples (concentrations corrected to 9/99).

Representative water samples were selected for radiochemical analysis. ^{137}Cs, ^{125}Sb and ^{106}Ru were the only gamma-emitting radionuclides detected in the water samples. Pu, Am and ^{90}Sr were detected in the samples. The overwhelming majority of the Pu, Am, and ^{90}Sr was detected on the filterable, or colloidal fraction. These results mimic those found in ER20-5 groundwaters.

Table 1. Radionuclides detected in water samples from Rainier Mesa Tunnels. X = detected, ND = non detect, NA = not analyzed, * = near reporting limit

Sample ID	^{137}Cs	^{125}Sb	^{106}Ru	Pu	Am	^{90}Sr
U12E-M	X	ND	ND	X	X	X
U12E-S	X	ND	ND	NA	NA	NA
U12T-2100	X	X	X	X	X*	X
U12T-1700	ND	ND	ND	X	ND*	NA
U12T-B	ND	ND	ND	X	X	ND
U12T-E	ND	ND	ND	NA	NA	NA
U12N-M	X	ND	ND	X	X	X

2.4. Mass Spectrometry Results

Four of the tunnel water samples (U12T-A, U12T-B, U12T-2100, and U12E-M) were analyzed for plutonium concentration and isotopic composition by thermal ionization mass spectrometry (TIMS). This is a much more sensitive technique than standard alpha counting. These samples were shaken vigorously for two minutes to suspend and homogenize the solids prior to drawing aliquots. As such, the mass spectrometric

analyses are for the bulk sample, i.e., the dissolved and solid fractions. The analytical procedure is described in more detail below. Separate analyses of the dissolved and the filterable solids fractions for three of these samples (U12T-B, U12T-2100, and U12E-M) were made by standard radiochemical methods.

Pu was detected in all four water samples. No Pu was detected in the reagent and processing blank. The minimum detectable levels as determined from the 2-sigma uncertainties on the isotope/spike ratio measurement in the blank are $^{239}Pu < 0.010$ pg, $^{240}Pu < 0.022$ pg, $^{241}Pu < 0.010$ pg and $^{242}Pu < 0.037$ pg.

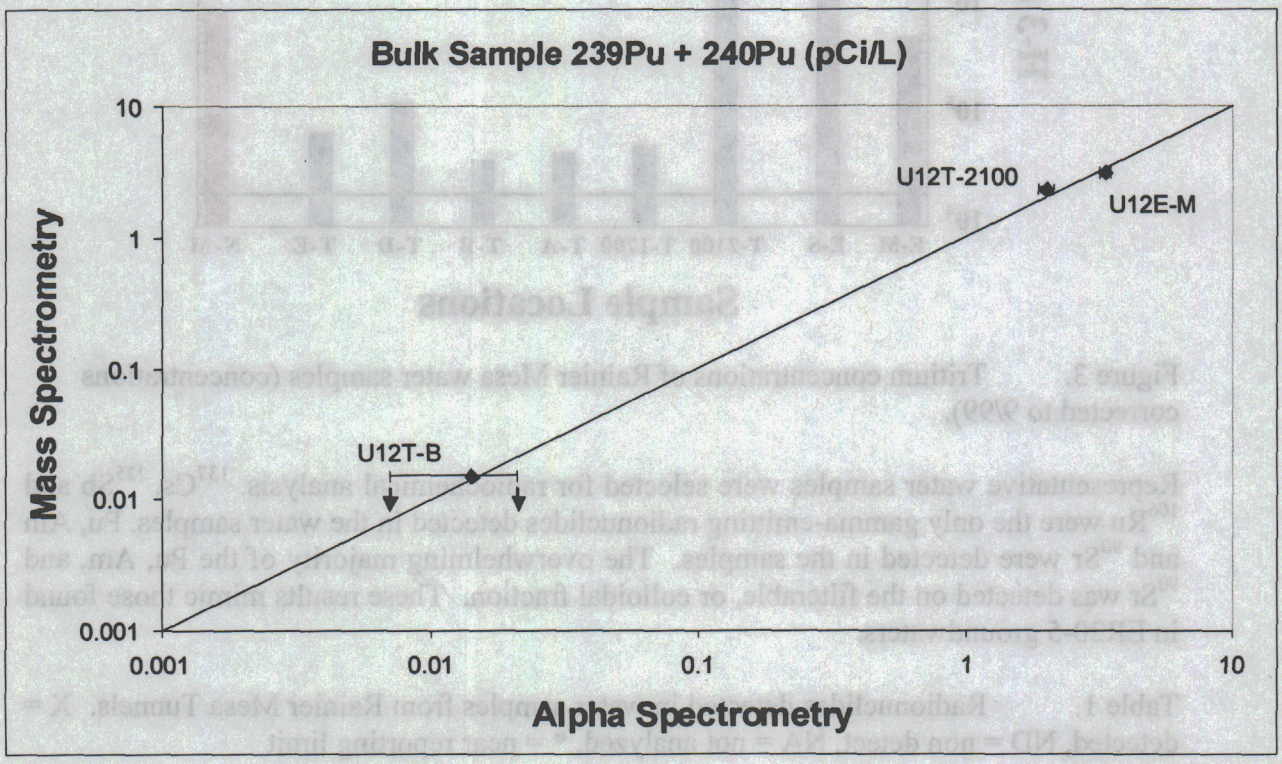

Figure 4. Comparison of concentrations of 239Pu +240Pu using 2 different analytical methods. Agreement is excellent.

2.5. SEM Characterization of Mineral Colloids

Water sample U12T-A was filtered and the colloidal fraction characterized by Scanning Electron Microscope (SEM), X-ray diffraction (XRD), and Transmission Electron Microscopy (TEM). Each of these state-of-the-art micro analytical techniques offer either quantitative or qualitative chemical or morphological information, that when used together helps to positively identify the mineral colloids. Figure 5 shows three SEM images of the colloids. The colloidal fraction was small and a new technique had to be developed to successfully analyze the sample by XRD. Calcite and a clay, possibly illite were identified by XRD. To date, TEM analysis confirmed the presence of the clay being illite, a zeolite-clinoptilolite and calcite.

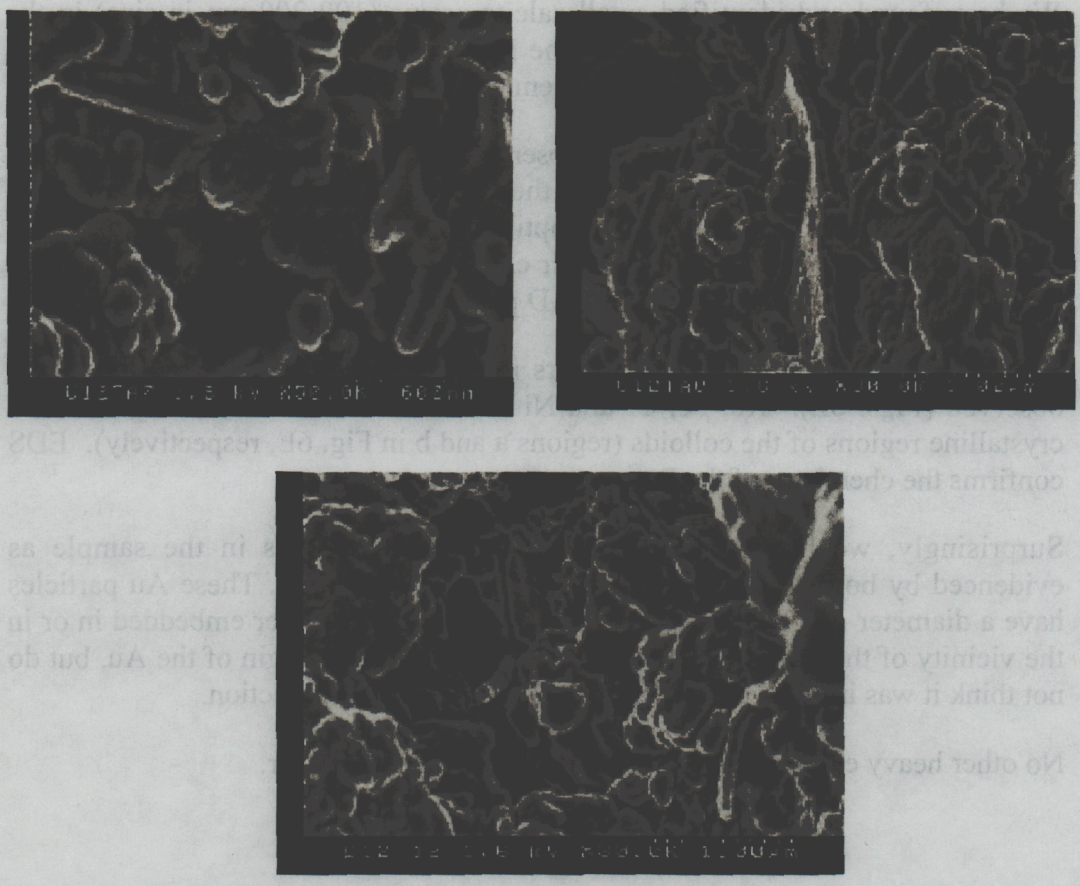

Figure 5. SEM images of U12T-A colloids. The flat platy minerals are most likely clays and the rod shaped minerals are probably zeolite.

2.6. TEM Characterization of Mineral Colloids

Detailed transmission electron microscopy (TEM) analysis has been conducted on sample U12TA at the University of Michigan using the newly acquired field emission gun (FEG) TEM. Bright-field (BF) and high resolution (HR) TEM imaging, selected area electron diffraction (SAD) as well as nano-beam energy dispersive x-ray spectroscopy (EDS) analysis were conducted for the characterization of the sample. A 200 keV electron beam was used for the analysis. In order to create electron transparent thin areas for the analysis, the original colloid clusters in the sample were crushed and suspended on a holey-carbon film supported by Cu grid, so the original morphology observed in the SEM analysis has been destroyed. Although extensive effort has been devoted to the analysis, we have only analyzed a small fraction (~10%) of the colloids collected on one grid due to the complexity of the sample.

The major results of the analysis are:

- We have found and identified small illite grains (several hundred nanometers in size) (Figs. 6A and B). The most convincing evidence is from the direct observation of 2 nm spacing of the (001) basal planes (Fig. 6B). Energy Dispersive Spectrum (EDS) confirms the chemistry of the illite.

- We have found and identified small calcite grains (100-200 nm in size) in the sample (Fig. 6C). The evidence for the identification include an indexed SAD pattern in Fig. 6C. EDS confirms the chemistry of the calcite.

- Micro sized zeolite grains have been observed (Fig. 6D). However, at present, we have not been able to further identify the phase within the zeolite group. Two possible phases are chabazite and clinoptilolite. EDS analysis could not be used to distinguish the phases based on their chemistry. We will further identify the phase after a detailed analysis of the SAD pattern.

- A Ru-rich colloid (several micrometers in size) containing Fe, Cr and Ni was observed (Figs. 6E). Ru, Fe, Cr and Ni were detected in both amorphous and crystalline regions of the colloids (regions a and b in Fig. 6E, respectively). EDS confirms the chemistry of the Ru.

- Surprisingly, we have observed many Au nano-particles in the sample as evidenced by both TEM images and EDS spectra (Fig. 6F). These Au particles have a diameter range between 2-10 nm and seem to be either embedded in or in the vicinity of the Ru-rich phases. We do not know the origin of the Au, but do not think it was introduced during sample preparation or collection.

- No other heavy elements have been found in the sample so far.

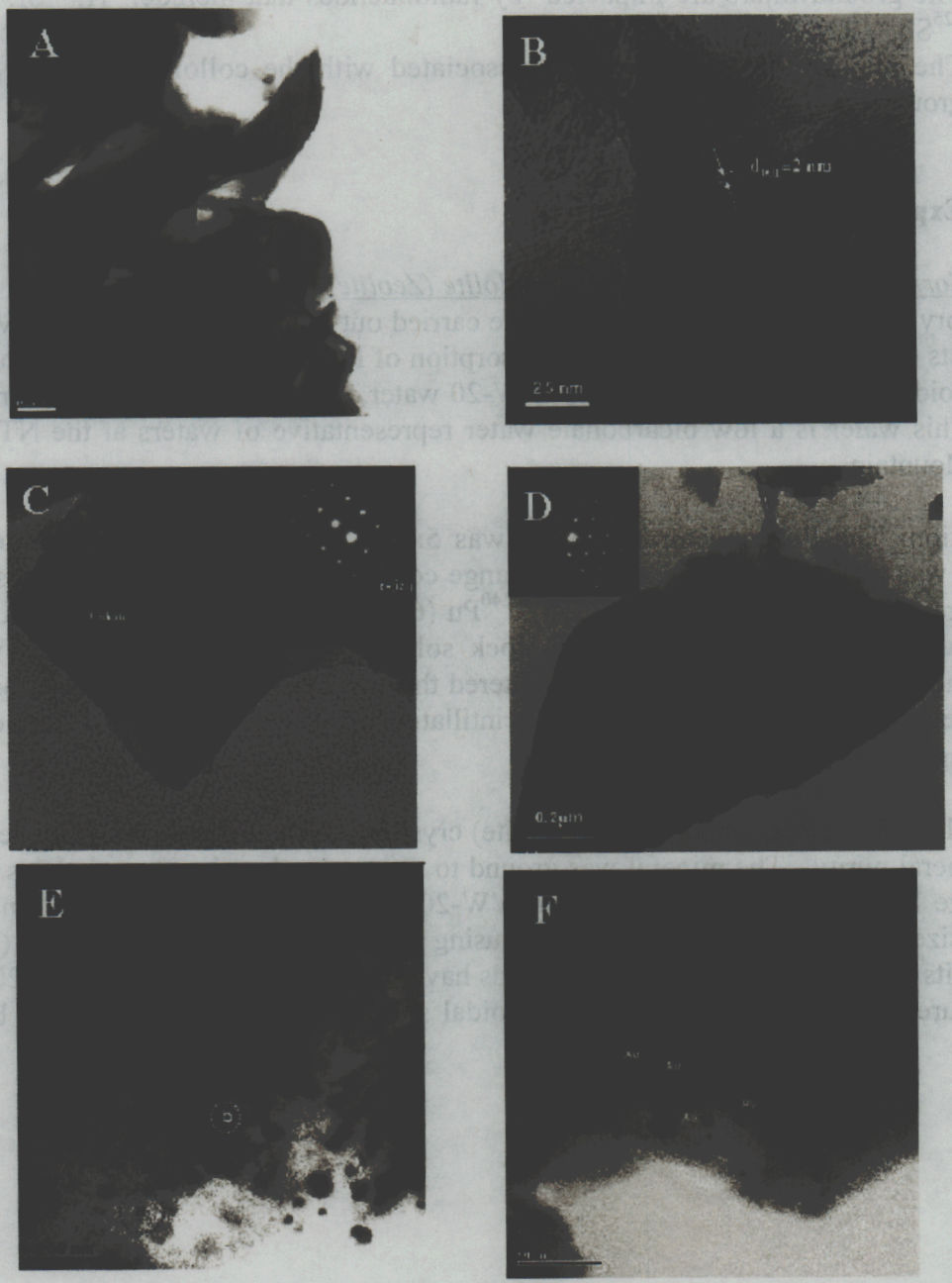

Figure 6. TEM images of A: BF TEM image of illite grains, B: HRTEM image of illite grains, C: BF-TEM image and SAD pattern of calcite, D: BF-TEM image and SAD pattern from a zeolite grain, E: BF-TEM image of a Ru-rich colloid, F: BF-TEM image showing Au nano-particles.

2.7. Summary of Results from the Field Study of Colloids

From our water samples collected from the tunnels on Rainier Mesa, NTS we can conclude:

- The colloids consist of clays (illite), zeolites (clinoptiolite), and calcite. This is similar to the minerals identified in groundwater from ER20-5 and Cheshire.

- The groundwaters are impacted by radionuclides that include: ^{3}H, ^{90}Sr, ^{106}Ru, ^{125}Sb, ^{137}Cs, Pu and Am.
- The majority of the activity is associated with the colloidal fraction of the groundwater.

3. Experimental

3.1. Sorption of Plutonium onto Clinoptilolite (Zeolite) Colloids

Laboratory batch sorption experiments were carried out at room temperature to evaluate the effects of time and solution pH on the sorption of Pu(IV) onto clinoptilolite colloids. The colloidal solution was prepared in WW-20 water, collected from a well in Area 20, NTS. This water is a low bicarbonate water representative of waters at the NTS and Yucca Mountain.

Pu solution: The Pu concentration used was $5x10^{-9}$ M. Weapons grade plutonium solution was purified using an anion exchange column. The Pu isotopic compositions (wt%) are ^{238}Pu (0.09%), ^{239}Pu (92.555), ^{240}Pu (6.58%), ^{241}Pu (0.48%), ^{242}Pu (0.30%). The oxidation state of Pu(IV) in the stock solution was confirmed using UV/VIS spectrometry. The Pu(IV) solution was filtered through a 20 nm pore size filter prior to use in the sorption experiments. A liquid scintillation analyzer was used for Pu α-activity measurements.

Colloidal solution: Pure clinoptilolite (zeolite) crystals were hand picked for greater than 99% mineral purity. The mineral was ground to a fine powder, then the particles in the size range 100-200 nm were separated in WW-20 water using ultra-centrifugation. The particle sizes of the colloids were measured using photon correlation spectroscopy (PCS). The results indicate that >90% of the colloids have particle sizes between 100 to 200 nm (see Figure 7). The concentration of colloidal solution used was measured to be 0.3 mg/mL.

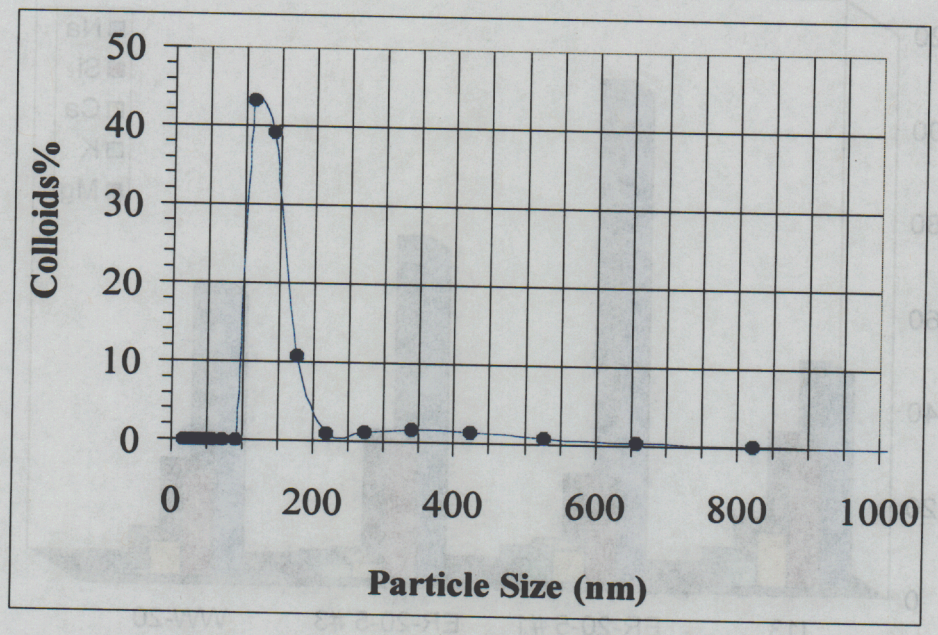

Figure 7. PCS Measurement of Colloidal Size Distribution

WW-20 water: The water was collected from a well (WW-20) located at the NTS, so that it represents the water hosted in the volcanic aquifers at the NTS. The water was filtered through a membrane with pore size of 100,000 NMW (~ 7nm) prior to use. The chemical analysis of the water indicated the presence of HCO_3^- (110ppm), Na (60 ppm), SO_4^{2-} (32 ppm) and Si (21.9 ppm) in the water (Figure 8.). The pH of WW-20 water was ~ pH 8.

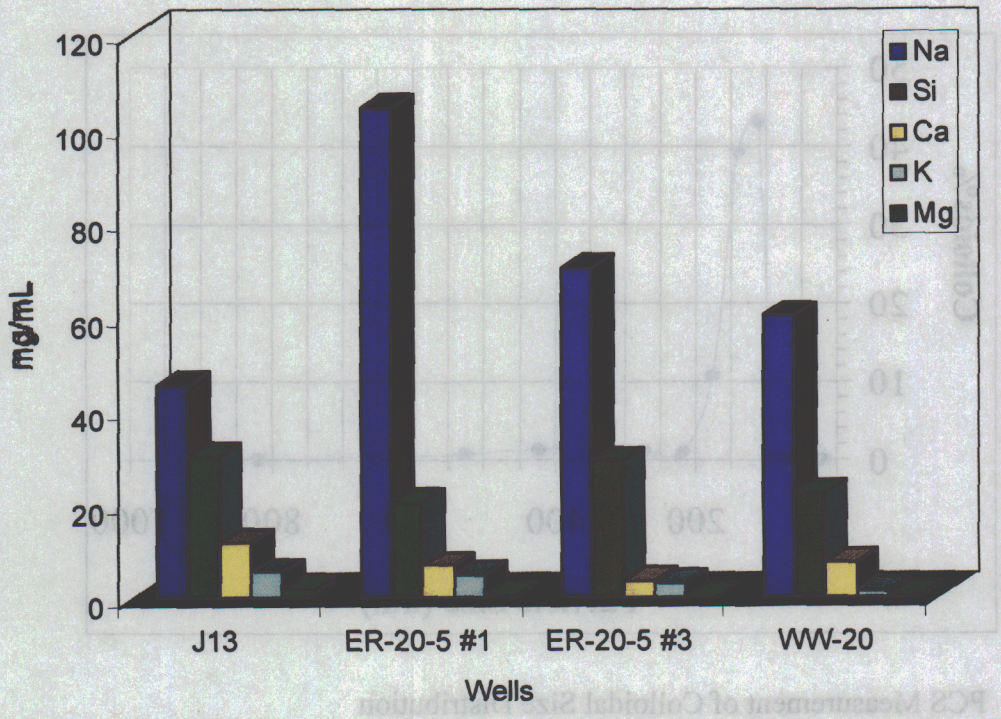

Figure 8. Comparison of WW-20 cation chemistry with water from ER20-5 (area 20,) and J-13, NTS

Batch sorption experiments: Three series of experiments were carried out to determine the effect of time, pH and Pu(IV) concentrations, respectively. For each set of sorption experiments, a second series of "control" solutions were prepared under the exact same conditions but in the absence of the colloids. The "controls" were used to monitor any precipitation or sorption of Pu onto the container and filters during the experiments. If applicable, the pH adjustment was made by adding 0.1 M HCL or NaOH. Samples and "controls" were kept in closed polyethylene containers and were gently shaken on an Environ-Shaker (Lab-Line Instrument, Inc.) with a slow and stable shaking speed (300 rpm), until the equilibrium was reached.

After sorption occurred, a separation of the colloidal phase from the liquid phase was performed by ultrafiltration using Centricon-30 filters, 4.1 nm pore size (Amicon). Special attention was made during this step to avoid the presence of any colloids or small particles in the supernatant that may result in erroneous sorption ratio calculations. The sorption ratios were calculated using the following equation:

$$Sorption\% = \frac{A_{unf} - A_f}{A_{unf}} x100$$

Where A_{unf} and A_f are the α-activity (cpm/mL) in the unfiltered and filtered samples, respectively.

3.2. Experimental Results and Discussion

The sorption of Pu(IV) on clinoptilolite colloids as a function of time at pH 6 and 8 is plotted in Figure 9. The Pu(IV) sorption reached 65% level in just several days and remained in that level for up to 18 days. Then the Pu partition onto the filterable materials (presumable colloids) started increasing slowly to reach ~100% in 150 days.

The Pu(IV) strongly sorbed to the clinoptilolite at both pH 6 and pH 8. We think that the first plateau in the plot may present Pu(IV) sorption onto some strong sorption sites of clinoptilolite. The latter may be due to any one or all of the following: Pu(IV) sorption onto some weak sorption sites of clinoptilolite, formation of Pu(IV) colloids, and surface precipitation of Pu(IV) on clinoptilolite. We are using EXAFS techniques to try and determine what is happening to the solution after approximately 20 days.

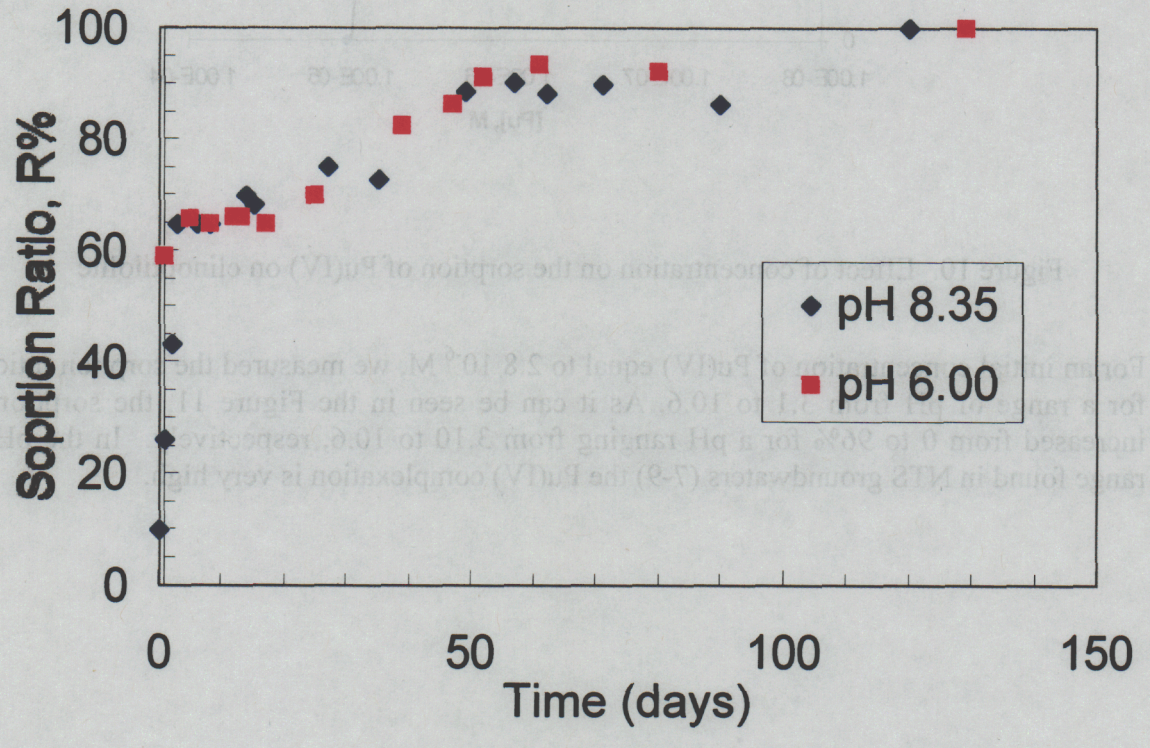

Figure 9. Pu Sorption as a Function of Time at pH 6 and 8

The effect of Pu (IV) concentration on sorption was investigated from 10^{-8} M up to 10^{-5} M Pu(IV) concentrations, pH was equal to 7.5± 0.1. The sorption ratio reached up to 90% for an initial concentration of Pu(IV) equal or lower than 10^{-6} M (Figure 10). For concentration higher than 10^{-5} M, the sorption decreased significantly most likely due to the fact that all colloid sites were already sorbed by Pu(IV) ions.

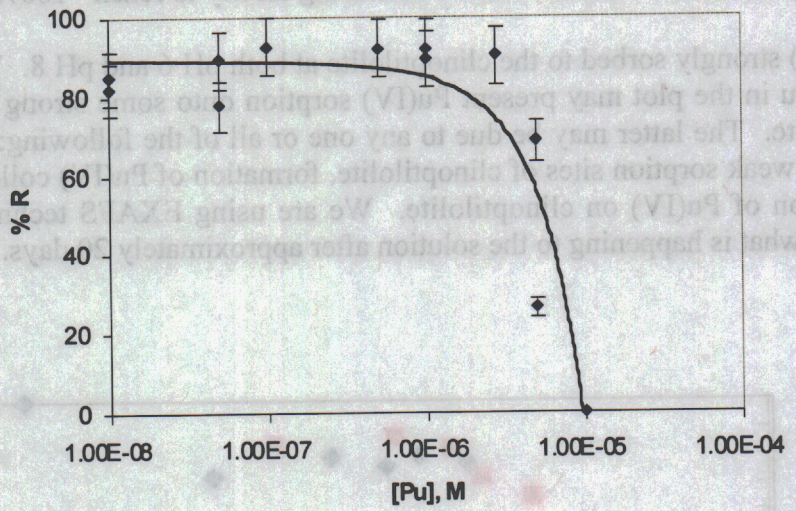

Figure 10. Effect of concentration on the sorption of Pu(IV) on clinoptilolite

For an initial concentration of Pu(IV) equal to 2.8 10^{-6} M, we measured the sorption ratio for a range of pH from 3.1 to 10.6. As it can be seen in the Figure 11, the sorption increased from 0 to 96% for a pH ranging from 3.10 to 10.6, respectively. In the pH range found in NTS groundwaters (7-9) the Pu(IV) complexation is very high.

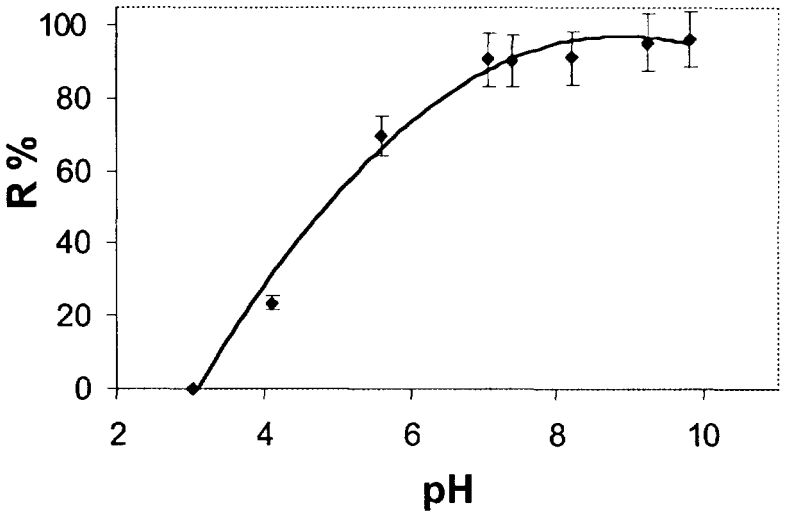

Figure 11. Effect of the pH on Pu(IV) sorption

3.3. Determination of oxidation state and structure of Pu sorbed on clinoptiolite

After the sorption experiments were completed, X-ray atomic structure (XAS) was used to determine the oxidation and structure of the Pu. This information is important for modeling. XAS determines whether reduction or oxidation processes took place during sorption of Pu on clinoptiolite colloids. For Pu(IV) the short-range structural information we collected was used to identify whether sorption occurred via ion-exchange or covalent bonding with surface sites.

XAS provides information on sorption *mechanisms* that increase our fundamental understanding of the chemical processes involved at the molecular level. Identifying specific sorption mechanisms will allow us to design experiments targeting the most important chemical processes in sorption, identify environmental systems where these processes occur, and ideally lead to better predictive capability through modeling.

The information gained from XAS includes the oxidation state of the element targeted as well as average local structure around that element. Structural details include the identity, coordination number and radial distances (i.e. bond lengths) for atoms within ~4-5 Å of the absorbing atom. Detection limits generally range from 1-10 ppm for oxidation state determination to 10-100 ppm or greater for detailed structural analysis. Analysis is non-destructive; this allows us to track kinetic changes in a sample over time or to repeat measurements of a stable sample in order to improve resolution.

After the sorption experiments, samples were centrifuged and the solution drawn off to leave a wet paste consisting of the actinides sorbed to the colloidal material as the final sample form. The wet paste samples were studied directly using X-ray absorption

spectroscopy. For the concentrations given above, 100% sorption of the actinides to the colloids would result in calculated actinide concentrations of 3300 (for most Pu) ppm.

In all samples investigated, the Pu(IV) remained the $Pu^{4+}(aq)$ oxidation state (see Fig. 12). The Pu(V) samples all reduced to Pu(IV). Reference standards for Pu(IV) [$Pu^{4+}(aq)$] and Pu(V) plutonyl [$PuO_2^{+}(aq)$] are shown for comparison.

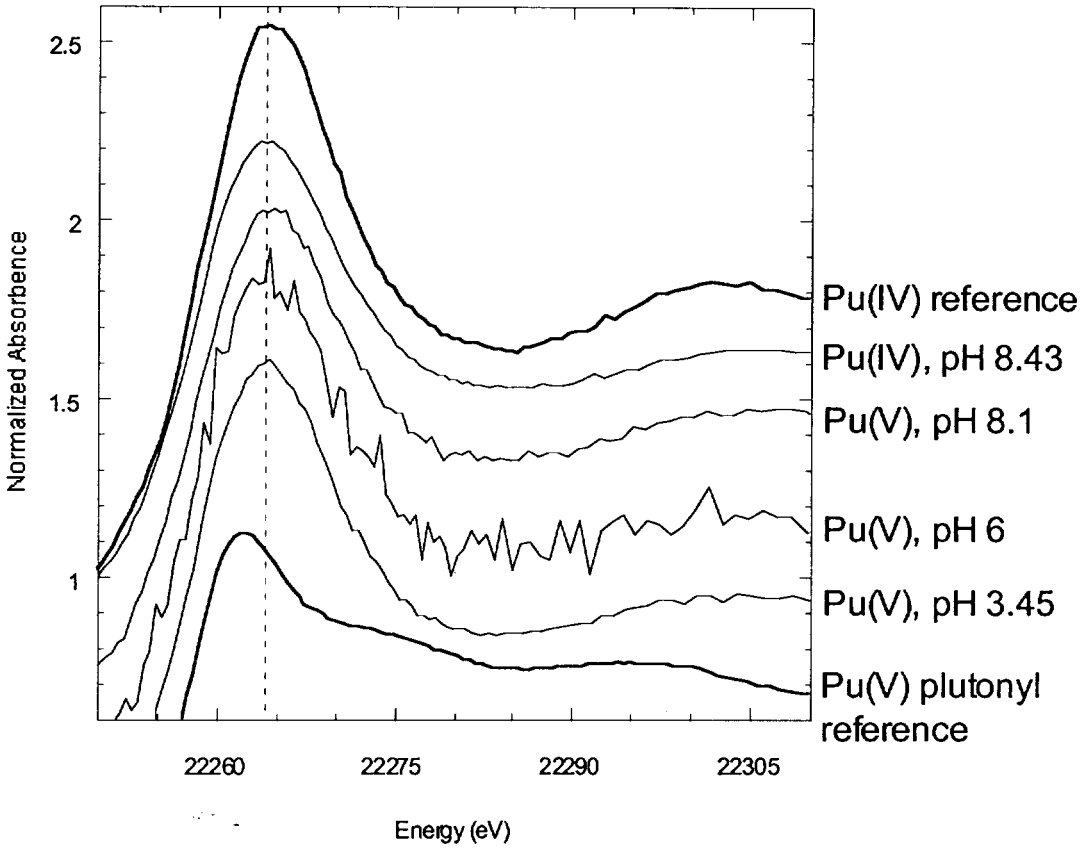

Figure 12: XANES of NTS samples (identified by initial oxidation state), with Pu^{4+} and PuO_2^{+} spectra shown for reference. Note especially (1) the absorption peak of the samples has the position of Pu(IV) and (2) the samples have lost the high energy shoulder that identifies the plutonyl structure.

All of the spectral features we observe are consistent with inner-sphere, bidentate complexation of Pu(IV) to the silica tetrahedra of the clinoptilolite. The bond lengths observed for the first three shells (consisting of oxygen, oxygen, and silicon) are similar to bond lengths for shells in coffinite, which has the formula $U^{IV}SiO_4$. Preliminary results also indicate that the third peak in the FT spectrum may be the result of a monodentate silicon shell (with a similar shell also found in coffinite) and not the result

of Pu-Pu interactions. If this is the case, then plutonium is sorbing to the colloid as monomeric units.

4. Modeling Plutonium Sorption to Clinoptilolite Colloids

From our experimental results, Pu(IV) interaction with clinoptilolite colloids is modeled. Clinoptilolite sorption was modeled using both the non-electrostatic and the diffuse layer surface complexation models. A description of these models is presented below and justification for their use is discussed in the methods section of this report.

Minerals that can exhibit surface charge (e.g. goethite, calcite, aluminosilicates etc.) can significantly reduce radionuclide (RN) mobility in the environment. The reduced mobility is a result of surface complexation (SC) and ion exchange (IE) reactions. Surface complexation (SC) and ion exchange (IE) reactions provide a mechanistic approach to modeling sorption and can account for the effect of changing environmental conditions on sorption.

In modeling radionuclide (RN) migration in the environment, partitioning Kd constants are often used to model sorption. Kd constants are typically reported as a ratio of total sorbed concentration (mol/g) to total aqueous concentration (mol/mL). Although the Kd approach can adequately describe the sorptive behavior of a particular sediment at a particular pH and solution composition, the many factors that affect RN sorption in dynamic geologic environments cannot be accounted for.

4.1 Surface Complexation

Surface complexation (SC) reactions involve mineral surface functional groups and aqueous species. Factors that influence surface complexation on a particular mineral include:

- Surface area
- pH
- Aqueous complexation
- Ionic strength, and
- Surface charge

There are many models that have been used to describe SC reactions (non-electrostatic, constant capacitance, diffuse layer, triple layer, and others) Here, we fit Pu surface complexation using two of the simpler models: the non-electrostatic model (NEM) and the diffuse layer model (DLM). Unlike all other SC models, the NEM (Kurbatov et al., 1951) assumes that surface electrical charge does not affect equilibrium SC reactions. Although the NEM approach over-simplifies the factors affecting SC, several investigators have used this model approach to describe sorption reactions (Bradbury and Baeyens, 1997; Davis et al., 1998; Zachara et al., 1994). Davis et al. (1998) argued that the NEM approach may be the most appropriate for complex environmental applications since the surface charging behavior of non-ideal natural mineral phases is not well known. The electrostatic models typically contain one or more parameters that account

for surface charge effects. The DLM is one of the simplest electrostatic models and relies on a modified Gouy-Chapman theory to describe the effect of electrostatics on sorption.

4.2 Ion Exchange

The permanent charge on some clay minerals is the result of non-charge-balanced ion substitution When other cations such as Pu^{4+} are present, they may also become associated with the negatively charged surface via IE.

4.3 Data Fitting Routine and Aqueous Speciation Data

Sorption data were fit using a modified version of the fitting program FITEQL (Herbelin and Westall, 1994). The code was modified to allow for:

- Automated activity correction using the extended Debye Huckel model
- Automated retrieval of aqueous speciation data from a database
- An ion exchange capability
- Code stability in cases of large species matrices.

Aqueous speciation constants were based on the GEMBOCHS thermodynamic data base version data.com.V8.R6 (Johnson and Lundeen, 1997) with revisions as noted in Tompson et al. (1999) and in the text below.

Table 2 contains the complexation constants used for Pu speciation. Two sets of aqueous speciation constants were used for Pu(IV). The first was taken from Rai et al. (1999). The second was taken from Triay et al. (1997). Fitting was accomplished using the newer data of Rai et al. (1999). A comparison of the two Pu(IV) speciation constants reveals that the difference in reaction constant K for $Pu(CO_3)_5^{6-}$ differs by 11 orders of magnitude. This extremely large inconsistency illustrates the potential uncertainty in published speciation constants for Pu(IV) in particular. This uncertainty is, in large part, due to the extremely low solubility of PuO_2, which makes aqueous speciation measurements difficult to perform. In addition, it is highly likely that all aqueous species and their related speciation constants of importance under the condition of our sorption experiments are not known. For example, it is likely that a Pu(IV)-monocarbonate species exists even though the data of Rai et al. (1999) did not detect it under the conditions of their experiments. The uncertainty in speciation constants and dominant species adds additional complexity when attempting to fit sorption data because aqueous speciation can greatly affect fitting results. Nevertheless, we attempt to address these uncertainties in the sorption fitting results discussed below.

4.4. Clinoptilolite Sorption Data and Modeling

Figures 13 and 14 present the speciation of Pu(IV) under the conditions of the clinoptilolite sorption experiments for the two sets of speciation constants listed in Table 2. Although there is a large difference between the two sets of constants, some similarities in the behavior of Pu(IV) are visible. In effect, for both sets of speciation constants, positively charged hydroxide species dominate speciation at low pH, negatively charged carbonate (or hydroxycarbonate) species dominate at intermediate pH, and the neutral $Pu(OH)_4(aq)$ species dominates at high pH. Given that sorption often

decreases under conditions where negatively charged aqueous species dominate, the speciation data suggests that sorption at intermediate pHs will be suppressed by the formation of Pu-carbonate species in solution.

Table 2. Species used in surface complexation fits.

species	log K	#	component	#	component	#	component	#	component
$PuOH^{+3}$	-0.5	-1	H^+	1	H_2O	1	Pu^{+4}		
$Pu(OH)_2^{+2}$	-1.66	-2	H^+	1	Pu^{+4}	2	H_2O		
$Pu(OH)_3^+$	-4.62	-3	H^+	1	Pu^{+4}	3	H_2O		
$Pu(OH)_4(aq)$	-8.85	-4	H^+	1	Pu^{+4}	4	H_2O		
$Pu(OH)_2(CO_3)_2^{-2}$	-2.76	-4	H^+	2	HCO_3^-	1	Pu^{+4}	2	H_2O
$Pu(CO_3)_5^{-6}$	-16.31	-5	H^+	5	HCO_3^-	1	Pu^{+4}		
$PuO_2CO_3^-$	-5.21	-1	H^+	1	HCO_3^-	1	PuO_2^+		
$PuO_2OH(aq)$	-9.73	-1	H^+	1	H_2O	1	PuO_2^+		
		old aqueous Pu(IV)-carbonate species†							
$PuCO_3^{+2}$	6.67	-1	H^+	1	HCO_3^-	1	Pu^{+4}		
$Pu(CO_3)_2(aq)$	9.24	-2	H^+	2	HCO_3^-	1	Pu^{+4}		
$Pu(CO_3)_3^{-2}$	8.11	-3	H^+	3	HCO_3^-	1	Pu^{+4}		
$Pu(CO_3)_4^{-4}$	1.58	-4	H^+	4	HCO_3^-	1	Pu^{+4}		
$Pu(CO_3)_5^{-6}$	-7.15	-5	H^+	5	HCO_3^-	1	Pu^{+4}		

† Data from Triay et al. (1997).

Table 3. Composition of the WW-20 water used in simulations surface complexation.†

species	mg/L	mol/L
H		pH = 8
HCO3	110	1.82E-3
Na	60	2.61E-3
SO4	32	3.30E-4
Si	21.9	1.01E-3
Cl	11.6	3.30E-4
Ca	7.18	1.80E-4
F	2.6	1.40E-4
NO3	1.48	2.00E-5
K	1.3	3.30E-5
Mg	0.28	1.20E-5

† We assume in the following modeling experiments that Pu only complexes with OH^- and CO_3^{2-} species.

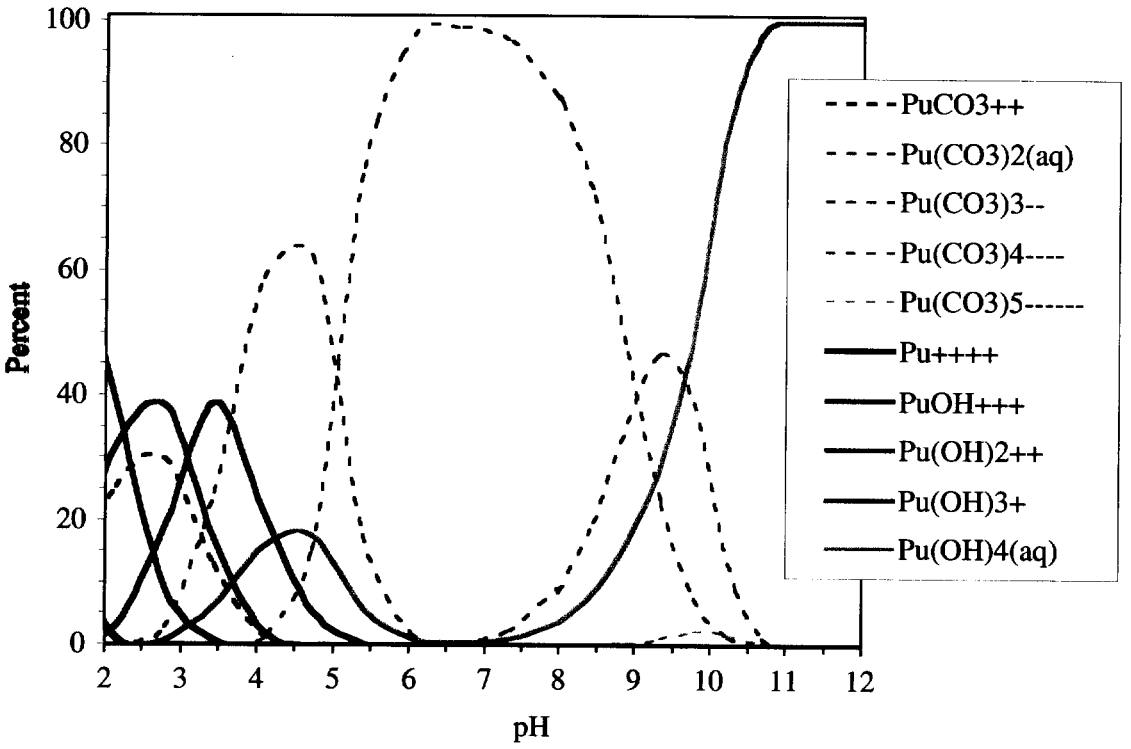

Figure 13. Speciation of Pu(IV) under conditions of clinoptilolite sorption experiments using the speciation constants from Triay et al. (1997).

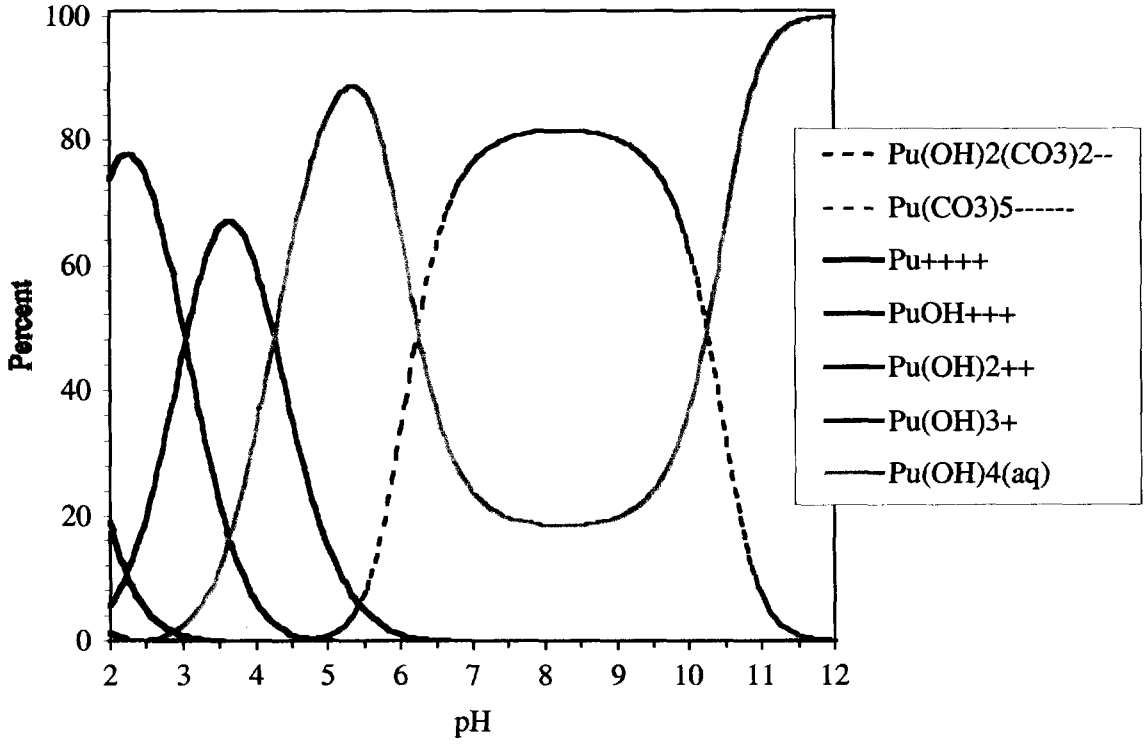

Figure 14. Speciation of Pu(IV) under conditions of clinoptilolite sorption experiments using the speciation constants of Rai et al. (1999).

Modeling the interaction of Pu with clinoptilolite was accomplished by fitting the sorption data to a non-electrostatic (NEM) and diffuse layer (DLM) surface complexation models.[1] Several authors have recently shown that sorption of RNs on aluminosilicate minerals can be related to SC on alumina and silica surfaces since surface functional groups are comparable (McKinley et al., 1995; Turner et al., 1996). This generalized aluminosilicate model is used to fit our Pu-clinoptilolite sorption data here. Thus, aluminol and silanol protonation and deprotonation reactions are assumed to be equivalent to those of silica and alumina, as described in Turner (1995) (log K's for $>AlOH_2^+$, $>AlO^-$, and $>SiO^-$ are 8.33, -9.73, and -7.20, respectively). For simplicity, the DLM acidity constants for SiO_2 and _-Al_2O_3 reported by Turner (1995) were used both in the NEM fits and the DLM fits.

In order to retain the most simplified approach to describing the reactive sites on aluminosilicate minerals, several additional simplifying assumption were made. A single type of silanol and aluminol reactive site was used to fit the data. A total site density of 2.31 sites/nm^2 was assumed. This value was taken from Dzombak and Morel (1990) who used this site density for SC modeling of hydrous ferric oxide surfaces. This site density

[1] Although it is possible that Pu(IV) or Pu(V) exchanges onto permanently charged sites in clinoptilolite (IE sites) the bound or complexed oxygen atoms that surround them make ion exchange into zeolite channels sterically difficult. Additional experiments at very low ionic strengths could help elucidate whether ion exchange reaction may be of importance in some cases.

was also used by Turner (1995) for a variety of minerals to minimize the number of fitting parameters and arrive at a uniform set of surface complexation reactions.

4.5 Results and Discussion of Pu Sorption to Clinoptilolite Colloids

Table 4 contains the best fit log K values for the various surface complexation and ion exchange models used to fit the sorption data.

Table 4. Best fit parameters for modeling Pu sorption to clinoptilolite and calcite.

Model	Species	log K	Species	log K	Species	log K
	---------- Pu(IV) on clinoptilolite ----------					
NEM‡	$SiOPu(OH)_2^+$	0.47	$AlOPu(OH)_2^+$	5.92	$AlOPu(OH)_4^-$	-10.67
DLM	$SiOPu(OH)_2^+$	2.59	$AlOPu(OH)_3$	-6.58	*$AlOPu(OH)_4^-$†*	*-7.36†*
	---------- Pu(V) on clinoptilolite ----------					
NEM§	$SiOPuO_2$	-3.05	$SiOPuO_2OH^-$	-11.61	$AlOPuO_2$	-3.09
DLM	$SiOPuO_2$	-3.65	*$SiOHPuO_2$¶*	*3.18¶*		
	---------- Pu(IV) on calcite ----------					
NEM	$Pu(OH)_3^+$ --> Ca^{2+}			2.61		
	---------- Pu(V) on calcite ----------					
NEM¡	PuO_2^+ --> Ca^{2+}			1.63		
NEM	PuO_2^+ --> Ca^{2+}			1.73	$PuO_2(CO_3)_3^{5-}$	-24.1*

‡ Compared to values of 2.32±0.89, 5.95±0.47, and -11.93, respectively, reported in Zavarin and Bruton (1999b).

§ Compared to values of -6.43, -14.80, and -3.09, respectively, reported in Zavarin and Bruton (1999b). Note the $AlOPuO_2$ log K was not fit here because sorption was too weak to attempt a complete fit.

† The fit using the $AlOPu(OH)_4^-$ species **instead** of $AlOPu(OH)_3$ results in a better goodness of fit but a much less conservative estimate of sorption at high pH.

¶ The fit of $SiOPuO_2$ **or** $SiOHPuO_2$ results in an equivalent goodness of fit.

¡ Compared to 1.85±0.35 reported by Zavarin and Bruton (1999a).

* Compared to -20.99 listed in Triay et al. (1997).

Figure 15 is a log scale plot of aqueous Pu(IV) in solution as a function of pH in equilibrium with the clinoptilolite colloids. The dashed line at the top of the figure indicates the initial Pu concentration in solution prior to sorption. Sorption data is more typically presented as % sorbed as a function of pH. Here, we present the aqueous concentration data and on a log scale to better resolve the trace aqueous concentration of Pu at high pH. The suppression of Pu sorption at the intermediate pH range coincides with the dominance of Pu-carbonate species in solution. This would suggest that Pu-carbonate aqueous species can effectively reduce the sorption of Pu to these colloids.

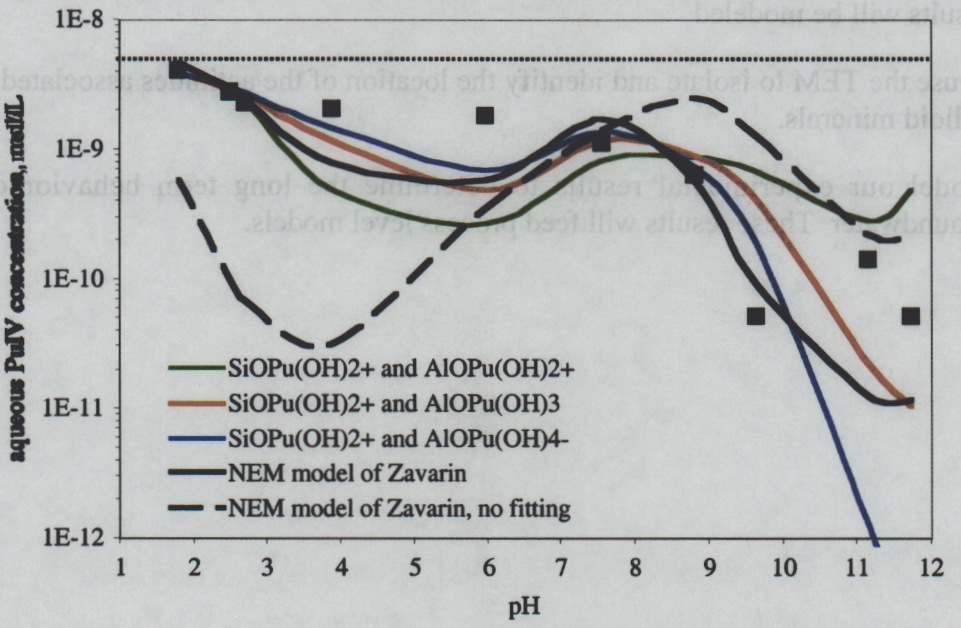

Figure 15. Sorption data for Pu(IV) on clinoptilolite colloids. Dashed line represents the initial aqueous concentration in solution. Each curve represents an individual attempt to fit the sorption data using the surface species listed in the figure. Note: log scale.

4.6. Modeling Conclusions

Sorption of Pu(IV) to clinoptilolite colloids is equivalent to a Kd value of ~10^5 mL/g at pH ~8. In this intermediate pH (and lower pHs), sorption seems to be suppressed to some degree as a result of aqueous Pu-carbonate complexation. Although we are able to fit these data to both NEM and DLM surface complexation, the consistent overestimation of sorption at intermediate pHs suggests that our aqueous speciation database is incomplete for Pu(IV) solutions under these conditions. Additional sorption data that span a larger range of pH and pCO_2 should allow for a more complete analysis of factors affecting Pu(IV) and Pu(V) sorption to both clinoptilolite and calcite.

5. Future Work FY01

In FY01 we will continue to:

- conduct desorption experiments of Pu(IV) on clinoptiolite to determine if sorption onto colloids is an irreversible process. This is important in our understanding of the long term behavior of Pu in groundwater.

- our experimental program using Pu(V). Pu(V) is the predominant form of plutonium in the natural environment, so we will study its sorption and desorption onto the clinoptilolite zeolite colloids following the same method as Pu(IV).

- use XAFS to determine the oxidation state of the Pu(V) after the experiment. These results will be modeled

- to use the TEM to isolate and identify the location of the actinides associated with the colloid minerals.

- model our experimental results to determine the long term behavior of Pu in groundwater These results will feed process level models.

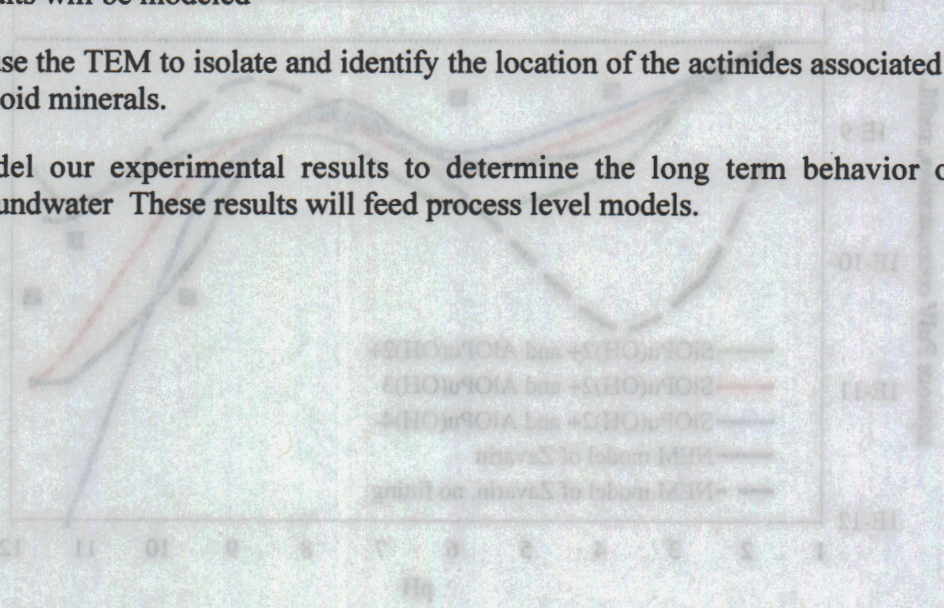

6. References

Bradbury M. H. and Baeyens B. (1997) A mechanistic description of Ni and Zn sorption on Na- montmorillonite .2. Modeling. *Journal of Contaminant Hydrology* **27**(3-4), 223-248.

Davis J. A., Coston J. A., Kent D. B., and Fuller C. C. (1998) Application of the surface complexation concept to complex mineral assemblages. *Environmental Science & Technology* **32**(19), 2820-2828.

Doner H. E. and Zavarin M. (1997) The role of carbonates in trace and minor element chemistry. In *Soils and environment : soil processes from mineral to landscape scale*, Vol. Advances in geoecology 30 (ed. K. Auerswald, J. M. Bigham, and H. Stanjek), pp. 422. Catena Verlag.

Duff M. C. and Amrhein C. (1996) Uranium(VI) adsorption on goethite and soil in carbonate solutions. *Soil Science Society of America Journal* **60**(5), 1393-1400.

Dzombak D. A. and Morel F. M. M. (1990) *Surface complexation modeling : hydrous ferric oxide*. Wiley.

Herbelin A. L. and Westall J. C. (1994) FITEQL, A computer program for determination of chemical equilibrium constants from experimental data. Department of Chemistry, Oregon State University.

Johnson J. W. and Lundeen S. R. (1997) Gembochs thermodynamic datafiles for use with the Eq3/6 modeling package. Lawrence Livermore National Laboratory.

Kersting, A.B., Efurd, D.W., Finnegan, D.L., Rokop, D.J., Smith, D.K. and Thompson, J.L. (1999) Migration of Plutonium in Groundwater at the Nevada Test Site. *Nature*, 397:56-59.

Kurbatov M. H., Wood G. B., and Kurbatov J. D. (1951) Isothermal adsorption of cobalt from dilute solutions. *Journal of Physical Chemistry* **55**, 1170-1182.

McKinley J. P., Zachara J. M., Smith S. C., and Turner G. D. (1995) The influence of uranyl-hydrolysis and multiple site-binding reaction on adsorption of U(VI) to montmorillonite. *Clays and Clay Minerals* **45**(5), 586-598.

Rai, D., Hess, N.J., Felmy, A.R., Moore, D.A., Yui, M., Vitorge, P. (1999) A thermodynamic model for the solubility of PuO_2(am) in the aqueous K^+-HCO_3^--CO_3^{2-}-OH^--H_2O system. *Readiochimica Acta* **86**:89-99.

Rose, T.P., Kenneally, J.M., Smith, D.K., Davidson, M.L, Hudson, G.B., and Rego J.H., (1997) Chemical and Isotopic Data for Groundwater in Southern Nevada, Lawrence Livermore National Laboratory report, UCRL-ID-128000.

Triay I. R., Meijer A., Conca J. L., Kung K. S., Rundberg R. S., Streitelmeier b. A., Tait C. D., Clark D. L., Neu M. P., and Hobart D. E. (1997) Summary and synthesis report on radionuclide retardation for the yucca mountain site characterization project, pp. 274. Los Alamos National Laboratory, LA-13262-MS.

Tompson A. F. B., Bruton C. J., and Pawloski G. A. (1999) Evaluation of the hydrologic source term from the underground nuclear tests in Frenchman Flat and the Nevada Test Site: The CAMBRIC test. Lawrence Livermore National Laboratory, UCRL-ID-132300.

Turner D. R. (1995) A uniform approach to surface complexation modeling of radionuclide sorption, pp. 103. Center for Nuclear Waste Regulatory Analyses, CNWRA 95-001.

Van Cappellen P., Charlet L., Stumm W., and Wersin P. (1993) A surface complexation model of the carbonate mineral-aqueous solution interface. *Geochimica et Cosmochimica Acta* **57**, 3505-3518.

Zachara J. M., Cowan C. E., and Resch C. T. (1991) Sorption of divalent metals on calcite. *Geochimica et Cosmochimica Acta* **55**(6), 1549-1562

Zachara J. M., Resch C. T., and Smith S. C. (1994) Influence of humic substances on Co2+ sorption by a subsurface mineral separate and its mineralogic components. *Geochimica et Cosmochimica Acta* **58**(2), 553-566.

Zavarin, M., and Bruton, C. J. 1999a. Non-electrostatic surface complexation approach to modeling radionuclide migration at the Nevada Test Site: The role of iron oxides and carbonates. Migration '99, Lake Tahoe, NV, September 26-October 1 (UCRL-JC-133474-ABS).

Zavarin, M., and Bruton, C. J. 1999b. Non-electrostatic surface complexation approach to modeling radionuclide migration at the Nevada Test Site: The role of aluminosilicates. American Geophysical Union 1999 Fall Meeting, San Francisco, CA, December 13-17 (UCRL-JC-135644-ABS)

Chapter 6

Development and Testing of Tritium Reference Standards for the Secondary Ion Mass Spectrometer

Timothy P. Rose, Douglas L. Phinney, Ian D. Hutcheon, G. Bryant Hudson, and David K. Smith

Analytical and Nuclear Chemistry Division, Lawrence Livermore National Laboratory

Executive Summary

Tritium reference standards were prepared for the ion microprobe by irradiating ^3He atoms with thermal neutrons to induce the reaction $^3He(n,p)^3H$. The resultant tritium was implanted into high purity Si and SiO_2 target materials. Given the total neutron fluence and the ^3He concentration in the sample capsule, the quantity of tritium produced is readily determined. Tritium depth profiles were measured on the ^3H-implanted Si and SiO_2 targets using the ion microprobe. A Cs^+ primary ion beam was utilized to enhance the abundance sensitivity for tritium. However, for the SiO_2 target this approach requires the concurrent application of an electron flood gun to alleviate surface charging during secondary ion sputtering. The depth profiling results were used to calculate sensitivity factors (SFs) for ^3H in the Si and SiO_2 substrates. The SF is an empirical conversion factor that permits the determination of concentrations from measured secondary ion intensity ratios. Ion microprobe measurements of zeolitized volcanic tuff samples from the Nevada Test Site were used to establish an approximate ^3H-detection limit for natural, hydrous rock samples. The newly developed reference standards provide a unique capability for directly measuring ^3H sorption effects in natural materials.

Introduction

Tritium is widely considered to behave as a non-reactive, non-sorbing species in the natural environment. Contaminant dose boundary models developed for the Underground Test Area (UGTA) project at the Nevada Test Site (NTS) are calibrated assuming conservative tritium transport in groundwater (U.S. Department of Energy, 1997). However, limited experimental data suggest that tritium is preferentially adsorbed to certain types of solids, particularly zeolite minerals. Zeolites are characterized by an ability to lose and gain water molecules reversibly without changing their structure (Mumpton, 1977). Data for the equilibrium isotopic partitioning of tritium between water and synthetic zeolites suggests tritium is slightly enriched in the solid phase, with $\alpha_{H_2O\text{-}HTO}$ near 1.1 at 25°C (Andreev and Polevoi, 1996). This has important implications for tritium migration in groundwater at the NTS, where zeolitized volcanic rocks are widespread in occurrence. Tritium sorption has been proposed as a mechanism to explain differences between observed and simulated breakthrough curves during the induced migration of radionuclides from an underground nuclear test cavity (Burbey and Wheatcraft, 1986).

Previous tritium sorption studies were dependent on mass balance relationships to determine partition coefficients (e.g., Tanaka and Yamamoto, 1976; Ono et al., 1980; Bindal et al., 1984). However, there are sizable discrepancies in the results of these different studies. An alternative approach is to measure tritium sorption in the solid matrix using secondary ion mass spectrometry (SIMS, or ion microprobe). An advantage of this method over bulk analytical methods is the ability to detect all elements and their isotopes at trace concentrations with high spatial resolution (e.g., Wilson et al., 1989). In principle, SIMS is well suited for tritium determination because of the high sensitivity of the instrument for hydrogen analyses, and because interferences at mass-3 are related only to molecular hydrogen species (Ottolini et al., 1995). Moreover, the ability to produce high-resolution depth profiles using the ion microprobe is particularly beneficial for investigating diffusional isotopic exchange processes (e.g., Chacko et al., 1999).

Quantitative SIMS analysis of tritium sorption and exchange requires the development of a reference standard containing a known amount of tritium implanted in a matrix with a major element composition similar to the tritium-bearing "unknowns". This report describes a novel method for producing tritium-implanted reference standards, and discusses the methods used to develop and test these standards for use on the ion microprobe. To our knowledge, reference standards of this type did not exist prior to the current study.

Method of Reference Standard Development

Tritium reference standards were prepared by irradiating high purity Si and SiO_2 targets with thermal neutrons in a ^3He atmosphere. Tritium is produced by the reaction

$$^3He\ (n,p)\ ^3H$$

and virtually all of the resultant ^3H is implanted within the target, or in the walls of the sample container. By using pre-polished wafers of Si and SiO_2, the ^3H implanted materials were essentially ready-to-use following the irradiation. Details of the preparation method are as follows.

High purity wafers of semiconductor-grade silicon or low-OH SiO_2 (Suprasil 300, Heraeus-Amersil) were individually flame-sealed inside silica tubes (0.9 cm i.d., 0.1 cm wall thickness, ~7 cm length) containing 555 torr (0.73 atm) of ^3He gas. A total of five individual target capsules were prepared, two containing Si, and three containing SiO_2. The capsules were sent to the Oregon State University Radiation Center where they were irradiated in a Triga Research Reactor for 3 hours 40 minutes at 1 MW power to deliver a total thermal neutron fluence of $\sim 10^{15}$ n/cm^2 to the samples.

Approximately 4.13 x 10^{14} atoms of tritium were produced in each target capsule, with an activity of 2 x 10^{-5} Ci. Assuming the implanted tritium is uniformly distributed, the estimated surface concentration is 1.5 x 10^{13} atoms/cm^2 in the Si targets, and 1.8 x 10^{13} atoms/cm^2 in the SiO_2 targets (due to differences in surface area). Details of this calculation are found in Appendix A.

SIMS Analytical Procedure

The tritium-implanted reference standards and volcanic tuff samples from the Nevada Test Site were analyzed using a modified Cameca ims-3f secondary ion mass spectrometer at Lawrence Livermore National Laboratory. Negatively charged secondary ions were generated by sputtering the samples with a 10 to 70 nA $^{133}Cs^+$ primary ion beam with an impact energy of 14.5 keV, rastered over either a 225 x 225 μm (Si samples) or 120 x 120 μm (SiO_2 and tuff samples) area. The combination of a Cs^+ primary ion beam and negative secondary ions, instead of an $^{16}O^-$ primary ion beam and positive secondary ions, produced a higher sputtering rate and suppressed the formation of molecular species (e.g., H_2, HD and H_3), thereby increasing the overall detection efficiency for tritium. Negative secondary ions were accelerated to a nominal energy of 4500 eV and focused into the mass spectrometer tuned to a mass resolving power (m/Δm) of ~350. An aperture inserted in the sample image plane allowed only secondary ions arising from a circular, 62 μm diameter region in the center of the rastered area to enter the mass spectrometer. Secondary ion intensities were measured over the mass sequence 0.95, ^1H, ^2H, ^3H, ^{16}O, 29.8, ^{30}Si; integration times were 1 second, except for ^3H (20 seconds). Due to the very large range of secondary ion intensities, a dual, Faraday cup – electron multiplier collector was used and secondary ion species with intensity exceeding 10^6 sec^{-1} were measured on the Faraday cup.

Concentrations in unknowns are calculated from ion intensity ratios using the approach described in Zinner and Crozaz (1986). For a Si or SiO_2 sample matrix, the concentration [X] of the trace isotope (e.g., ^3H) can be determined from the following expression:

$$[X] = \left(\frac{I(X)}{I(^{30}Si)} \right) \times [^{30}Si] \times SF \qquad (1)$$

where I(X) is the trace isotope secondary ion intensity; I(^{30}Si) is the matrix isotope secondary ion intensity; [^{30}Si] is the ^{30}Si concentration in the matrix, measured in the same units as [X]; and SF is the sensitivity factor (an empirical conversion factor from the measured secondary ion intensity ratio to the concentration of the trace isotope of interest). In practice, the ^{30}Si concentration is determined by measuring the Si or SiO_2 concentration (using an electron microprobe) and assuming that ^{30}Si is present in its natural isotopic abundance. The SF for ^3H is not known *a priori*, but will be determined from the ion intensity ratio of $^3H/^{30}Si$ measured on the reference standards, and from the tritium implant fluence in atoms/cm^2 (found in Appendix A).

Two different matrix compositions were used to prepare the tritium reference standards: Si and SiO_2. Since Si is a conductor, there are no significant issues with surface charging during ion beam analysis. For SiO_2, however, surface charge buildup is problematic, especially with a Cs^+ beam. To alleviate this problem, a normal incidence electron flood gun was used on these samples. The flood gun creates a uniform cloud of electrons directly above the sample surface that act to neutralize charge buildup from the primary ion beam. In addition, all materials were coated with a thin layer of gold to enhance surface conductivity.

Results

SIMS Analysis of Tritium Reference Standards

Ion microprobe depth profiles were run at five different locations on an individual tritium-implanted silicon wafer. Tritium depth profiles and $^3H^-/^{30}Si^-$ ion intensity ratios were similar for each of the five silicon matrix runs. This suggests the tritium was relatively uniform in its surface distribution. Depth profiles were measured at two locations on a tritium-implanted SiO_2 wafer. The measured depth profiles were similar for both SiO_2 matrix runs. A Dektak IIA profilometer was used to measure the depths of the sputter craters in both the Si and SiO_2 substrates. Accurate determinations of crater depths are necessary for determining sensitivity factors.

Figure 1 is a plot of the $^3H^-/^{30}Si^-$ ion intensity ratio as a function of depth in the silicon matrix. The plot is representative of the tritium depth profiles measured at five different points in this sample. The tritium was implanted to a maximum depth of about 2 μm, and has a peak atom density at a depth of ~0.5 and 1 μm.

Figure 2 shows a similar plot for the SiO_2 matrix. In this case, the maximum implantation depth for tritium (~2.5 μm) is slightly greater than in the silicon matrix. Moreover, the peak ^3H atom density occurs at a shallower depth interval than in the silicon matrix. Differences in the tritium distributions in Si and SiO_2 *may* reflect diffusional effects (for example, if the samples were relatively warm during implantation). Note also that the maximum $^3H^-/^{30}Si^-$ ion intensity ratio is approximately an order of magnitude higher in SiO_2 than in silicon metal (compare Figures 1 and 2). Given that the ^3H concentrations are similar for both materials (Appendix A), this implies that the relative useful yield of $^3H^-$ is greater in SiO_2 than in a silicon matrix.

Sensitivity factors (SFs) were calculated for $^3H^-$ in Si metal and SiO_2 substrates using equation (1). The ^3H concentrations were obtained from the tritium implant fluence (1.52×10^{13} atoms/cm^2 in Si, and 1.78×10^{13} atoms/cm^2 in SiO_2) assuming that all of the ^3H is quantitatively implanted and retained in the substrate. The $^3H^-/^{30}Si^-$ ion intensity ratios used in the SF calculations were determined by integrating the area under each

depth profile curve. The SF values are reported in Table 1, and were determined from five analyses of Si and two analyses of SiO_2. These newly established values now permit the quantitative determination of ^3H concentrations in Si-bearing substrates, including natural silicate minerals. An example calculation is given in the following section.

Table 1. Sensitivity Factors for $^3H^-$

Substrate	SF value
Si metal	27.5 ± 1.9
SiO_2	350 ± 18

SIMS Analysis of ER-20-6 Core Samples

Rose et al. (2000) reported the results of SIMS measurements of anthropogenic radionuclides in volcanic tuff samples from the Nevada Test Site. The tuff samples were obtained from the ER-20-6 #1 borehole, located 166 m southwest of surface ground zero for the Bullion underground nuclear test. Given that the ER-20-6 samples contain abundant zeolite minerals, the possibility exists that ^3H may have been adsorbed to the sample matrix concurrently with the deposition of other radionuclides. The new tritium reference standards permit the quantitative evaluation of this problem.

Preliminary SIMS measurements on an ER-20-6 #1 sample (669 m depth) revealed a $^1H^-$ intensity ~100 times that observed in the Si and SiO_2 reference standards. This is due to the high water content of the natural sample, and results in a mass-tail at the ^3H mass position. To overcome this mass-tail problem, a series of steps were taken to determine the background level of the ion microprobe at mass-3. The key step was the comparison of a lawsonite reference standard with the tuffaceous volcanic rocks. Lawsonite is a hydrous calcium aluminum silicate that contains ~11 wt.% H_2O (Deer et al., 1962), but contains no tritium. Hence, the lawsonite standard could be used to establish a procedure for measuring the mass-3 baseline value for a "wet" sample. Once this procedure was established, the ER-20-6 #1 samples were examined for the presence of tritium. Preliminary measurements at five spots in two different ER-20-6 #1 samples (581 and 669 m depth) failed to reveal the presence of ^3H above the background level (see discussion below). However, these measurements do provide a SIMS detection limit for ^3H in natural zeolitized tuffs.

The mean $^3H^-/^{30}Si^-$ ion intensity ratios measured on the ER-20-6 #1 samples ranged from $(0.93 \pm 0.62) \times 10^{-7}$ to $(4.66 \pm 1.84) \times 10^{-7}$. Reported errors are 1σ values. These ion ratios can be converted to atom densities using the SF value determined in the previous section. Since the natural substrates are not pure SiO_2, it is necessary to multiply by the weight percent of SiO_2 in the sample. The measured SiO_2 concentration in the zeolitized matrix varied from 59.7 to 67.8 wt.% (Rose et al., 2000). Hence, the *approximate* ^3H detection limit is on the order of:

$$[I(^3H^-)/I(^{30}Si^-)]*(SF)*[SiO_2]*[^{30}Si]*(\rho_m) \cong (10^{-7})(350)(0.6)(2.9 \times 10^{20})(2.16) = 10^{16} \text{ atoms/cm}^3$$

where the $[^{30}Si]$ value is given in units of atoms/g SiO_2, and ρ_m is the density of the sample matrix (2.16 g/cm^3). This value is limited by the water content of the sample (which increases the background) and by the abundance sensitivity of the mass spectrometer. The detection limit would be significantly lower in anhydrous samples.

Discussion and Future Work

Although tritium was not detected in the ER-20-6 #1 core samples by SIMS analysis, an earlier study by Thompson et al. (1997) indicates that tritium is present in these samples. The implication is that the tritium may be uniformly distributed throughout the zeolite-rich matrix of these samples, rather than being concentrated at "hot spots". If we assume a uniform distribution, the data in Thompson et al. (1997) provide a means of quantifying the number of ^3H atoms sputtered by the incident ion beam at any given point in the sample matrix. This value can then be compared to the detection limit for SIMS measurements of ^3H established above.

Thompson et al. (1997) measured the bulk tritium concentrations of seven sidewall cores collected between 576 and 756 m depth in the ER-20-6 #1 borehole. These include a split of the 581 m sample that was analyzed during this study, and two additional samples collected within ±3 m of the 669 m sample. Water was extracted by heating whole core samples under vacuum at 105°C for eight hours. The liberated water was then analyzed for tritium by liquid scintillation counting. Tritium activities corrected to the zero time for the Bullion test (13 June 1990) ranged from 4.9×10^5 to 2.5×10^7 pCi/L.

Zeolite minerals (principally clinoptilolite) comprise between 44 and 93% of the core samples collected from the 550-675 m interval in the Bullion emplacement hole (U-20bd) with an average value near ~75% (Warren et al., 2000). Clinoptilolite in samples from 581 and 669 m in ER-20-6 #1 has an average water content of ~16% (from electron microprobe analyses, H_2O by difference; Rose et al., 2000). Hence, the *expected* yield from a fully dehydrated core sample would range from ~7 to 15% H_2O. The amount of water actually extracted from the cores varied from 2.1 to 14 wt.% (Thompson et al., 1997). However, samples from the unsaturated zone all had values <3.3 wt.% whereas

saturated zone samples had values >6.8 wt.% (Thompson et al., 1997). This implies that (1) the saturated zone samples (below 618 m depth) may have contained interstitial water that was not bound to the zeolite mineral structure, and (2) the zeolitic water was probably not fully extracted from any of the samples.

The sample that contained the greatest amount of ^3H in the Thompson et al. (1997) study was from 672 m depth (2.5×10^7 pCi/L ^3H at zero time; 14 wt.% H_2O). Although it is likely that some of this ^3H is derived from pore water, the sample provides an upper bound on the amount of tritium observed in the natural zeolitized tuffs. The number of tritium atoms in the sample at t = 0 is approximately:

$$2.5 \times 10^7 \frac{\text{pCi}}{\text{L H}_2\text{O}} \left(\frac{3.7 \times 10^{-2}\ \text{s}^{-1}}{1\ \text{pCi}} \right) \left(\frac{\text{atom } ^3\text{H}}{1.784 \times 10^{-9}\ \text{s}^{-1}} \right) \left(\frac{1\ \text{L H}_2\text{O}}{1000\ \text{g H}_2\text{O}} \right) \left(\frac{0.14\ \text{g H}_2\text{O}}{\text{g rock}} \right) = 7.3 \times 10^{10} \frac{\text{atoms } ^3\text{H}}{\text{g rock}}$$

Applying the radioactive decay equation, the amount of tritium present in September 2000 would be ~4.1×10^{10} atoms ^3H per gram of rock.

To determine the quantity of material actually sputtered by the incident primary ion beam, we will assume a ~60 μm diameter point-of-analysis that was sampled to a depth of 2.5 μm. The sputtered volume is therefore ~7.1×10^3 μm^3. Given that the density of clinoptilolite is 2.16 g/cm^3, the mass of material sputtered is on the order of 15 ng. Hence, the amount of tritium contained in the sputtered volume is estimated at only ~615 atoms ^3H. In comparison, the estimated amount of tritium in the sputter volume of the SiO_2 tritium standard is ~5.0×10^8 atoms, or nearly a factor of 10^6 greater than the ER-20-6 #1 sample.

To summarize, we have prepared tritium reference standards for the ion microprobe using two types of substrates: Si metal and SiO_2. The approach that was utilized ([n,p] reactions on ^3He atoms) can easily be duplicated, and the amount of tritium implanted depends simply on the total thermal neutron fluence delivered to the samples, and on the initial ^3He concentration. Ion microprobe depth profiles were measured on the tritium standards and used to determine sensitivity factors. These values permit the determination of ^3H concentrations in a sample from SIMS ion intensity ratios. Ion microprobe measurements on volcanic tuff samples from the Nevada Test Site were used to establish ^3H detection limits in natural, water-bearing samples.

In natural systems where the volumetric ratio of sorptive rock to tritiated water is large, even relatively small sorption effects could impact the total amount of tritium in solution. This may have important implications for the hydrologic source term at the Nevada Test Site. The newly developed reference standards can be used to quantify tritium sorption coefficients. This would basically involve performing laboratory sorption experiments on appropriate geologic materials, followed by quantitative analysis for ^3H on the ion microprobe. By measuring the sorption coefficients over a range in concentrations, it is

theoretically possible to scale the results to levels that are relevant to the natural environment. In addition, tritium depth profiling would be useful for investigating whether matrix diffusion is a viable mechanism for attenuating tritium fluxes in fractured volcanic aquifers. These results could subsequently be used to develop quantitative models for tritium retardation in groundwater at the Nevada Test Site.

References Cited

Andreev, B.M., and Polevoi, A.S. (1996) Isotopic equilibrium of hydrogen in sorption of water by synthetic zeolites, silica gel, and alumina gel. Radiochemistry, 38: 160-165.

Bindal, R.C., Prabhakar, S., Jayaraman, A.P. (1984) Sorptive behavior of tritiated water on molecular sieves. Radiochim. Acta, 36: 215-218.

Burbey, T.J., and Wheatcraft, S.W. (1986) Tritium and chlorine-36 migration from a nuclear explosion cavity. Desert Research Institute, Water Resources Center Publication 45050, Las Vegas, NV, 136 p.

Chacko, T., Riciputi, L.R., Cole, D.R., and Horita, J. (1999) A new technique for determining equilibrium hydrogen isotope fractionation factors using the ion microprobe: application to the epidote-water system. Geochim. Cosmochim. Acta, 63: 1-10.

Deer, W.A., Howie, R.A., and Zussman, J. (1962) *Rock-Forming Minerals. Vol. 1 Ortho- and Ring Silicates.* Longman, London, 333 p.

Mumpton, F.A. (1977) Natural zeolites. In: F.A. Mumpton (ed.), *Mineralogy and Geology of Natural Zeolites.* Mineral. Soc. of Am., Rev. Mineral., v. 4: 1-17.

Ono, F., Nakazawa, M., Takahashi, Y., and Kanno, M. (1980) Distribution equilibrium of tritium between adsorbed water on molecular sieve 5A and environmental water. J. Nucl. Sci. Technol., 17: 721-723.

Ottolini, L., Bottazzi, P., Zanetti, A., and Vannucci, R. (1995) Determination of hydrogen in silicates by secondary ion mass spectrometry. Analyst, 120: 1309-1313.

Rose, T.P., Smith, D.K., and Phinney, D.L. (2000) Secondary ion mass spectrometry measurements of volcanic tuffs containing radionuclides from underground nuclear tests. Radiochim. Acta, in press.

Tanaka, S., and Yamamoto, Y. (1976) Removal of tritiated water vapor by adsorption. J. Nucl. Sci. Technol., 13: 251-259.

Thompson, J.L., Efurd, D.W., Rokop, D.J., Finnegan, D.L., Guell, M.A., Kersting, A.B., Martinez, B.A., and Smith, D.K. (1997) Laboratory and Field Studies Related to the Hydrologic Resources Management Program, October 1, 1995 – September 30, 1996. Los Alamos National Laboratory, LA-13270-PR, 24 p.

U.S. Department of Energy (1997) Regional Groundwater Flow and Tritium Transport Monitoring and Risk Assessment of the Underground Test Area, Nevada Test Site, Nevada. U.S. Department of Energy, Nevada Operations Office, Environmental Restoration Division, DOE/NV-477, Las Vegas, NV.

Warren, R.G., Sawyer, D.A., Byers, F.M., Jr., and Cole, G.L. (2000) A petrographic/geochemical database and stratigraphic framework for the southwestern Nevada volcanic field. Los Alamos National Laboratory, LA-UR-00-3791.

Wilson, R.G., Stevie, F.A., and Magee, C.W. (1989) Secondary Ion Mass Spectrometry: A Practical Handbook for Depth Profiling and Bulk Impurity Analysis. John Wiley and Sons, New York.

Zinner, E., and Crozaz, G. (1986) A method for the quantitative measurement of rare earth elements in the ion microprobe. International Journal of Mass Spectrometry and Ion Processes, 69: 17-38.

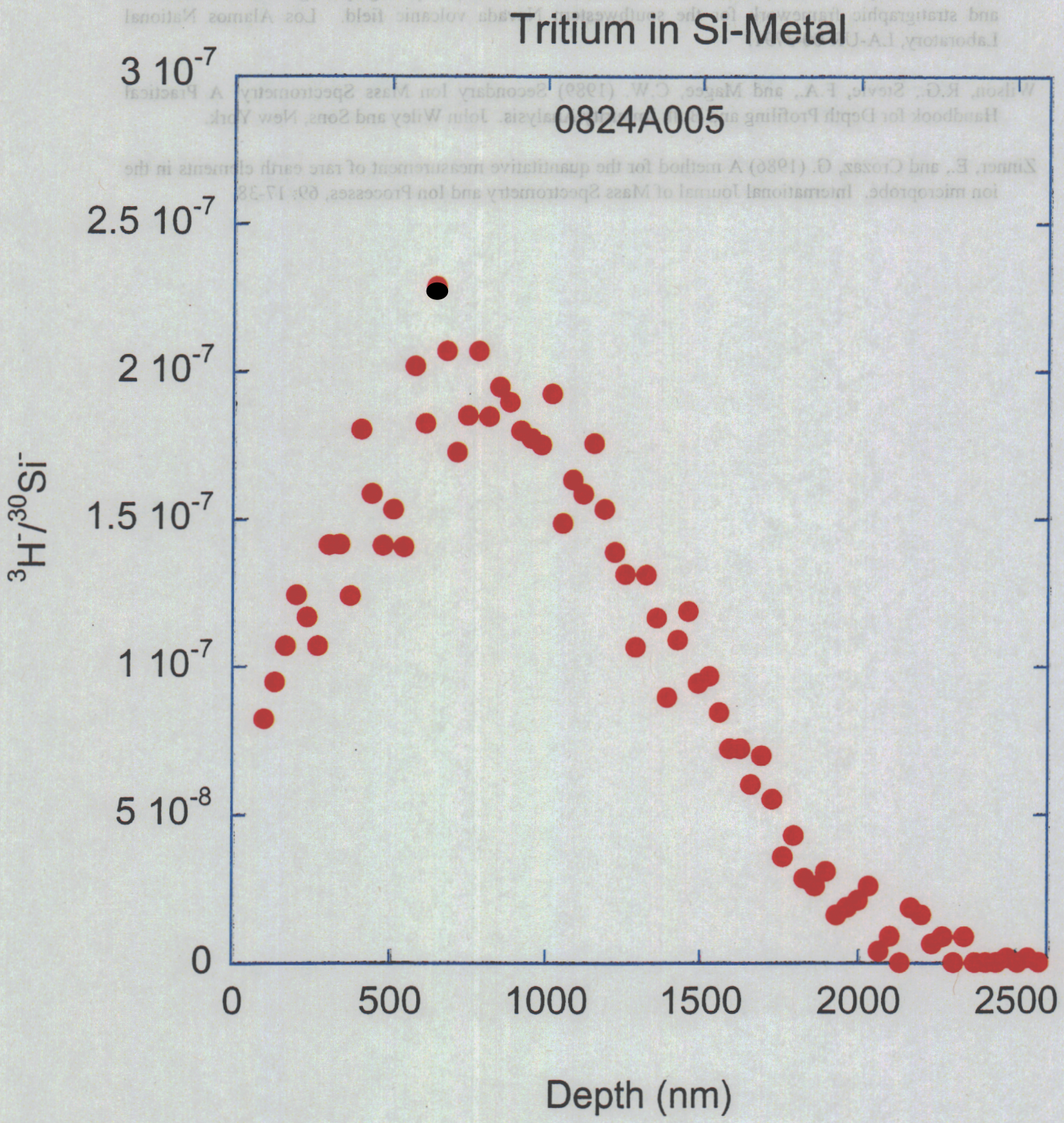

Figure 1. Depth profile of the $^{3}H^{-}/^{30}Si^{-}$ ion intensity ratio in a tritium-implanted silicon matrix.

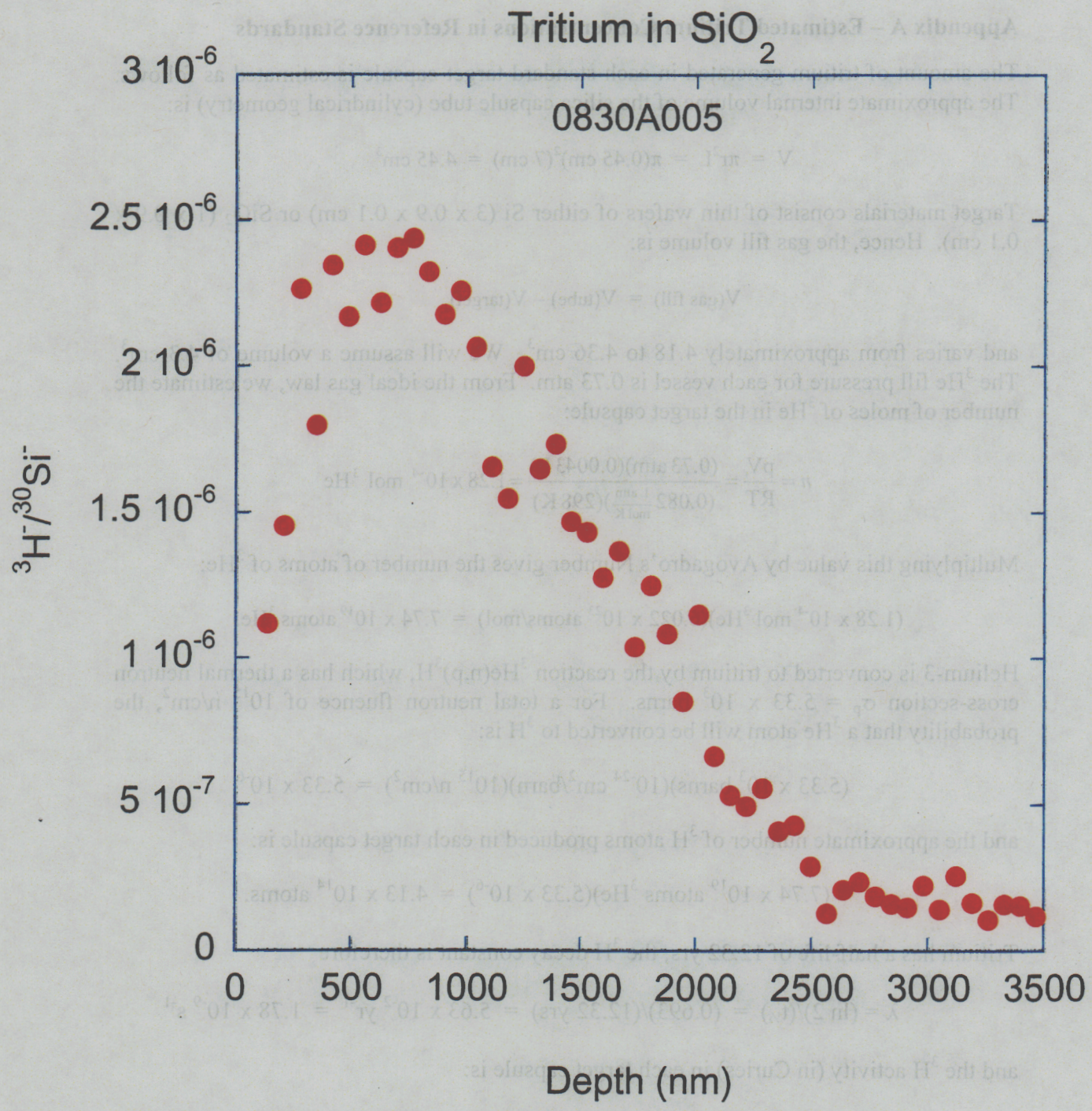

Figure 2. Depth profile of the $^{3}H^{-}/^{30}Si^{-}$ ion intensity ratio in a tritium-implanted SiO_2 matrix.

Appendix A – Estimated Tritium Concentrations in Reference Standards

The amount of tritium generated in each standard target capsule is estimated as follows. The approximate internal volume of the silica capsule tube (cylindrical geometry) is:

$$V = \pi r^2 L = \pi(0.45\ \text{cm})^2(7\ \text{cm}) = 4.45\ \text{cm}^3$$

Target materials consist of thin wafers of either Si (3 x 0.9 x 0.1 cm) or SiO_2 (1 x 0.9 x 0.1 cm). Hence, the gas fill volume is:

$$V(\text{gas fill}) = V(\text{tube}) - V(\text{target})$$

and varies from approximately 4.18 to 4.36 cm^3. We will assume a volume of 4.3 cm^3. The ^3He fill pressure for each vessel is 0.73 atm. From the ideal gas law, we estimate the number of moles of ^3He in the target capsule:

$$n = \frac{pV}{RT} = \frac{(0.73\ \text{atm})(0.0043\ \text{L})}{(0.082\ \frac{\text{L atm}}{\text{mol K}})(298\ \text{K})} = 1.28 \times 10^{-4}\ \text{mol}\ ^3\text{He}$$

Multiplying this value by Avogadro's Number gives the number of atoms of ^3He:

$$(1.28 \times 10^{-4}\ \text{mol}\ ^3\text{He})(6.022 \times 10^{23}\ \text{atoms/mol}) = 7.74 \times 10^{19}\ \text{atoms}\ ^3\text{He}.$$

Helium-3 is converted to tritium by the reaction $^3He(n,p)^3H$, which has a thermal neutron cross-section $\sigma_p = 5.33 \times 10^3$ barns. For a total neutron fluence of 10^{15} n/cm^2, the probability that a ^3He atom will be converted to ^3H is:

$$(5.33 \times 10^3\ \text{barns})(10^{-24}\ \text{cm}^2/\text{barn})(10^{15}\ \text{n/cm}^2) = 5.33 \times 10^{-6}$$

and the approximate number of ^3H atoms produced in each target capsule is:

$$(7.74 \times 10^{19}\ \text{atoms}\ ^3\text{He})(5.33 \times 10^{-6}) = 4.13 \times 10^{14}\ \text{atoms}.$$

Tritium has a half-life of 12.32 yrs; the ^3H decay constant is therefore

$$\lambda = (\ln 2)/(t_{½}) = (0.693)/(12.32\ \text{yrs}) = 5.63 \times 10^{-2}\ \text{yr}^{-1} = 1.78 \times 10^{-9}\ \text{s}^{-1}$$

and the ^3H activity (in Curies) in each target capsule is:

$$(4.13 \times 10^{14}\ \text{atoms}\ ^3\text{H})(1.78 \times 10^{-9}\ \text{s}^{-1})[(1\ \text{Ci})/(3.7 \times 10^{10}\ \text{s}^{-1})] = 2 \times 10^{-5}\ \text{Ci}.$$

Tritium concentration in the target materials

Virtually all of the ^3H produced in each target capsule is implanted in the target material, or in the walls of the capsule. Assuming a uniform neutron flux, it is anticipated that the ^3H will be evenly distributed on all surfaces.

The surface area of the interior of each capsule is approximately equal to the combined surface areas of a right circular cylinder + a rectangular solid. There are slight variations between each capsule. In addition, the total surface area is somewhat greater in capsules containing Si because the silicon targets were ~3x the length of the SiO_2 targets.

The surface area of the cylindrical capsules is approximately:

$$2\pi rL + (2)\pi r^2 = 2\pi(0.45\text{ cm})(7\text{ cm}) + (2)\pi(0.45\text{ cm})^2 = 21.06\text{ cm}^2$$

and that of the target materials is:

$$\text{Si target: } 2(3.0\text{ cm})(0.9\text{ cm}) + 2(3.0\text{ cm})(0.1\text{ cm}) + 2(0.9\text{ cm})(0.1\text{ cm}) = 6.18\text{ cm}^2$$

$$SiO_2\text{ target: } 2(1.0\text{ cm})(0.9\text{ cm}) + 2(1.0\text{ cm})(0.1\text{ cm}) + 2(0.9\text{ cm})(0.1\text{ cm}) = 2.18\text{ cm}^2.$$

The total surface area inside the capsules is:

$$\text{Si target capsules: } \sim 27.24\text{ cm}^2$$

$$SiO_2\text{ target capsules: } \sim 23.24\text{ cm}^2.$$

Assuming the implanted tritium is uniformly distributed, the approximate concentration per unit area in the reference standards is:

$$\text{Si target: } (4.13 \times 10^{14}\ ^3H\text{ atoms})/(27.24\text{ cm}^2) = 1.52 \times 10^{13}\text{ atoms/cm}^2$$

$$SiO_2\text{ target: } (4.13 \times 10^{14}\ ^3H\text{ atoms})/(23.24\text{ cm}^2) = 1.78 \times 10^{13}\text{ atoms/cm}^2$$

Chapter 7

A Chlorine-36 Study of Regional Groundwater Flow in Southern Nevada

Jean E. Moran and Timothy P. Rose

Analytical and Nuclear Chemistry Division, Lawrence Livermore National Laboratory

Executive Summary

Chlorine-36 data for groundwater samples from southern Nevada were evaluated as a means of constraining hydrogeologic processes in regional flow systems in the vicinity of the Nevada Test Site (NTS). Data from more than 50 locations were used to investigate the $^{36}Cl/Cl$ systematics in two settings: (1) the Death Valley regional carbonate aquifer system, including the Pahranagat Valley, Yucca and Frenchman Flats, Ash Meadows, and the Spring Mountains, and (2) the carbonate, volcanic, and alluvial aquifers in Yucca and Frenchman Flat.

End-member $^{36}Cl/Cl$ compositions were identified for both the initial (recharge) and chemically evolved components in the carbonate aquifer. The initial cosmogenic component during recharge is characterized by high $^{36}Cl/Cl$ and low Cl values, whereas more chemically-evolved carbonate aquifer groundwaters are typically low in $^{36}Cl/Cl$ and high in Cl. Laboratory studies were performed to determine the characteristics of leachable chloride in carbonate and volcanic tuff samples from Nevada. Leachable chloride concentrations were high in limestone from Army Well #1 (up to ~75 mg/L). In contrast, less than 1 mg/L of chloride was leached from a zeolitized volcanic tuff from well UE-7f in Yucca Flat. The measured $^{36}Cl/Cl$ ratios for both rock types were low.

Groundwater $^{36}Cl/Cl$ values are observed to evolve along flow paths in the Death Valley regional carbonate aquifer due to water-rock interaction processes. Initial $^{36}Cl/Cl$ ratios in Pahranagat Valley samples are similar to that of modern recharge waters in southern Nevada. In contrast, carbonate aquifer groundwaters beneath Yucca Flat exhibit highly evolved compositions with comparatively low $^{36}Cl/Cl$ ratios and high Cl concentrations. Groundwater from Army Well #1 and Ash Meadows springs have higher $^{36}Cl/Cl$ ratios than most Yucca Flat carbonate groundwaters, possibly reflecting mixing with less evolved groundwater originating in the Spring Mountains. Waters from different hydrostratigraphic units at the NTS fall into dissimilar groups based on $^{36}Cl/Cl$ and Cl values. Most significantly, water from Tertiary Volcanic Aquifers has a ^{36}Cl signature that is distinct from water from the Lower Carbonate Aquifer, providing a means of examining vertical transport between these units. In combination with other geochemical and hydrogeologic data sets, the ^{36}Cl end members defined here provide a means of constraining aquifer residence times. This study develops the necessary framework for future interpretive studies of ^{36}Cl in southern Nevada groundwaters. A study of vertical interactions between hydrostratigraphic units in Frenchman Flat is planned for FY01.

1.0 Introduction

Over the past decade, geochemists at Lawrence Livermore National Laboratory (LLNL) have measured $^{36}Cl/Cl$ values on groundwater samples from more than 50 locations in southern Nevada, many of which are from wells located on the Nevada Test Site (NTS). These data were collected in support of U.S. Department of Energy funded projects aimed at delineating groundwater resources that may be impacted by radionuclide contamination from underground nuclear tests. Prior to this report, the comprehensive LLNL ^{36}Cl dataset had not been analyzed in the context of groundwater flow and contaminant transport issues at the NTS. However, other studies have shown the value of ^{36}Cl measurements for identifying chloride sources, determining groundwater flow paths and mixing processes, constraining subsurface residence times, and discriminating between waters of different age and origin (e.g. Andrews et al., 1986; Bentley et al., 1986b; Paul et al., 1986; Torgersen et al., 1991; Fehn et al., 1992).

The objective of this study is to evaluate the benefit of ^{36}Cl data as an independent tool for constraining hydrogeologic interpretations in the NTS region (U.S. Department of Energy, 1997). In particular, the ^{36}Cl data will be used in concert with other chemical and isotopic parameters to assess: (1) the chemical evolution of groundwater along defined flowpaths, and (2) the extent of groundwater interaction between major hydrostratigraphic units (HSUs). The latter is a particularly important issue in Frenchman and Yucca Flats, where vertical flow from the tuff aquitard downward into the regional carbonate aquifer is likely to be the rate-limiting step governing radionuclide transport from the many tests conducted above this contact.

The interpretation of ^{36}Cl data requires the identification of end-member compositions and their approximate input functions. Prior to this study, end-members were poorly defined for southern Nevada groundwater systems. Hence, a small number of $^{36}Cl/Cl$ analyses were performed specifically for this study on meteoric water samples, mountain spring waters, and rock leachates. These data assist in delineating mixing end members, and help to establish limits on potential water-rock interaction.

2.0 Background

2.1 Hydrogeologic framework

The NTS is located within the Death Valley regional groundwater flow system, which encompasses a 15,800 mi^2 area in the southern Great Basin (Harrill et al., 1988; Laczniak et al., 1996). The principal aquifers in the region occur in fractured carbonate rocks and basin-fill deposits, although fractured volcanic rocks comprise locally important aquifers (Thomas et al., 1996). Much of the eastern half of the Great Basin is underlain by thick, laterally continuous sections of Paleozoic carbonate rock with depositional thicknesses as great as 9,000 m (Dettinger et al., 1995). Within this carbonate province, groundwater is transported southward along deep regional flowpaths that transcend local topographic

boundaries. Recharge occurs in high altitude areas in central Nevada, and in the Spring Mountains and Sheep Range in southern Nevada (Winograd et al., 1998; Davisson et al., 1999). Major discharge areas occur at Ash Meadows and the Death Valley playa.

For the present study, we will focus on regional flowpaths through Yucca and Frenchman Flats, in the eastern half of the NTS, and interactions between aquifers in these basins. Major hydrostratigraphic units for this area include Paleozoic carbonate rocks, Cenozoic volcanic rocks, and alluvial basin fill deposits (Winograd and Thordarson, 1975), although regional flow is transmitted only through the carbonate aquifer. The volcanic rocks consist mainly of rhyolitic tuffs that are subdivided into an upper tuff aquifer and a lower tuff aquitard. The tuff aquitard effectively separates the carbonate aquifer from the tuff aquifer and alluvial deposits throughout most of Yucca Flat, and part of Frenchman Flat (Winograd and Thordarson, 1975; Laczniak et al., 1996). The difference in hydraulic head between the volcanic and carbonate units indicates the Cenozoic aquifers are semi-perched relative to the Paleozoic carbonate aquifer. The only pathway by which this semi-perched water exits Yucca and Frenchman Flats is by downward leakage into the underlying carbonate aquifer. The annual downward flux is inferred to be small (2 to 2000 ac-ft/yr) due to the relatively impermeable nature of the tuff aquitard (Winograd and Thordarson, 1975). However, a key question regarding radionuclide transport in Yucca and Frenchman Flats is the extent to which the shallow alluvial and volcanic aquifers are in hydrologic communication with the underlying carbonate aquifer.

Regional flow through Frenchman and Yucca Flats is commonly inferred to originate from the Pahranagat Valley in eastern Nevada (Winograd and Friedman, 1972; Thomas et al., 1996), although Pahranagat Valley is actually a *discharge* area for the White River flow system (Eakin, 1966). The source of regional flow through the eastern NTS is probably best described as a west-verging component of the White River flow system (cf. Thomas et al., 1996). For this report, we will assume that the end-member composition for the White River Valley flow component can be described by non-evaporated springs in the Pahranagat Valley (see discussion below). Regional flow from Pahranagat Valley passes beneath Frenchman Flat, and continues to the southwest toward discharge areas at Ash Meadows and Death Valley (Winograd and Thordarson, 1975; Laczniak et al., 1996). Regional flow from Pahranagat Valley also enters southern Yucca Flat, but is then diverted southward into Frenchman Flat by the low permeability Belted Range thrust system (Winograd and Thordarson, 1975). The relatively flat hydraulic gradient between Yucca Flat and Ash Meadows (<1 ft/mile) suggests a high degree of hydraulic continuity within the aquifer, and probably reflects a high fracture permeability (Laczniak et al., 1996).

2.2 Chlorine-36 as a Tracer in Groundwater Systems

Chlorine has one long-lived isotope, ^{36}Cl, with a half-life of 301,000 years. Natural production of ^{36}Cl occurs in three ways: (1) cosmic-ray spallation of ^{40}Ar and neutron activation of ^{36}Ar in the atmosphere; (2) cosmic-ray spallation of K and Ca on and near

the earth's surface; and (3) neutron activation of ^{35}Cl (from U-Th series decay) at depth over long periods of time. Typical $^{36}Cl/Cl$ ratios of common rocks range from $4x10^{-15}$ for limestone to $50x10^{-15}$ for granite. In addition, neutron activation of ^{35}Cl in seawater during atmospheric nuclear testing raised $^{36}Cl/Cl$ ratios in the atmosphere by >2 orders of magnitude in the 1950s and early 1960s (Bentley et al., 1982). However, the high concentration of Cl in seawater effectively dilutes the $^{36}Cl/Cl$ ratios in the ocean to below the detection limit ($1x10^{-15}$) of accelerator mass spectrometry (AMS).

Seaspray-derived chloride in meteoric water causes $^{36}Cl/Cl$ ratios in precipitation to vary with distance from the ocean. The lowest ratios are recorded along coastal regions ($15x10^{-15}$) and the highest ratios are found in the continental interior (up to $1000x10^{-15}$ for the continental U.S.; Bentley et al., 1986). Recent studies suggest that the 'initial value' for the decay of ^{36}Cl in hydrologic systems is ambiguously determined in various hydrologic settings (Davis et al., 1998). This is in part because ^{36}Cl from nuclear weapons testing still may be cycling in the atmosphere (Cornett et al., 1997). Furthermore, chloride sources in groundwater may be mixed even near the recharge area, and seasonal recharge may not reflect average annual ^{36}Cl concentrations. For the study area, published estimates of the initial $^{36}Cl/Cl$ ratio are 400 to 500 x 10^{-15} (Hainsworth et al., 1994, Bentley and Davis, 1982). However, measured values in recently recharged groundwater and soils throughout the southwestern U.S. are between 500 and 880 x 10^{-15} (Davis et al., 1998).

Chloride is a relatively conservative (i.e., non-reactive) anion in groundwater. Changes to the $^{36}Cl/Cl$ ratio in groundwater along a flowpath are due to decay of ^{36}Cl, subsurface production of ^{36}Cl from ^{35}Cl in water, and water-rock interaction. Evapotranspiration at the earth's surface and ion filtration in the subsurface change the Cl concentration without changing the $^{36}Cl/Cl$ ratio. Mixing with water of a different $^{36}Cl/Cl$ ratio will yield intermediate compositions that can be delineated on a plot of $^{36}Cl/Cl$ vs. 1/Cl (see discussion).

Groundwater flow studies using ^{36}Cl from the western United States are limited in number, but include a regional hydrology study of the Dixie Valley (NV) geothermal field (Nimz et al., 1999), studies of sources of chloride in hydrothermal fluids from the Valles Caldera, New Mexico (Phillips et al., 1984; Rao et al., 1996) and a study of the movement of anthropogenic ^{36}Cl in the Snake River Plain Aquifer (Beasley et al., 1993). These projects document significant addition of Cl to groundwater in geothermal areas due to water-rock interaction. Several other studies use ^{36}Cl to address recharge rates in arid western soils (Phillips, 1994; Phillips et al., 1988; Scanlon et al., 1990; Liu et al., 1995; Tyler et al., 1996; Fabryka-Martin et al., 1993). In general, these studies show that chloride is concentrated in soil zones due to evaporation. High $^{36}Cl/Cl$ ratios in the soil zone reflect modern "bomb pulse" inputs.

3.0 Sampling and Analytical Methods

Water samples were collected for environmental level $^{36}Cl/Cl$ analysis from more than 50 wells and springs on and near the NTS, between 1992 and 1997 (Rose et al., 1997). A small number of additional samples were collected during FY 2000. This included two groundwater samples from the Spring Mountains (Cold Creek Spring and Deer Creek Spring), three integrated precipitation samples from recharge areas in central Nevada, and three rock samples that were selected for chloride leaching. All water samples were collected in plastic bottles with no preservative. Waters were processed using the standard technique for preparation of AgCl targets for AMS analysis. The meteoric and mountain spring samples have very low Cl concentrations (Table 1), and a pre-concentration step was necessary, using a relatively large volume of water (approximately 1500 ml each). These samples were concentrated using rotary vacuum distillation, which does not volatilize chloride. Sulfur species (which have an isobar at mass 36) were removed by precipitation of $BaSO_4$ with $Ba(NO_3)_2$. AgCl precipitation was then carried out using $AgNO_3$. Procedural and reagent blanks were processed using halite from a Silurian formation in Michigan, which has ^{36}Cl levels below the AMS detection limit.

Winter precipitation samples were collected at three locations in central Nevada (Austin, Little Antelope, and Currant Summits) at elevations between 2130 and 2280 m. Winter snowfall accounts for >50% of the annual precipitation, and ~90% of the annual recharge in Nevada (Winograd et al., 1998; Rose et al., 1999). Samples were accumulated in 6" diameter PVC pipe collectors with mineral oil at the bottom to minimize evaporation effects. Chloride concentrations were measured on all three samples, but only the samples from Austin and Currant Summits were analyzed for ^{36}Cl.

Rock samples selected for chloride leaching and analysis consisted of two carbonate samples and one volcanic tuff sample. These included drill core samples of limestone from Army Well #1 (Cambrian Bonanza King Fm., 1134' depth) and volcanic tuff from UE-7f in Yucca Flat (Tunnel Fm., Tunnel 3 member, 2063' depth). An additional sample of Devonian Devils Gate Limestone (from the type locale near Eureka, NV) was analyzed for its leachable Cl concentration, but not for ^{36}Cl. Samples were crushed using a mortar and pestle. The two limestones were first sieved at 14-100 mesh, 100-150 mesh (.15mm to .10mm) and >150 mesh. Small amounts of rock (approximately 10 g total) were leached using de-ionized water, and Cl concentrations were measured by ion chromatography. Based on those results, a larger sample (90 g) of the Army Well #1 limestone was chosen for ^{36}Cl analysis, which was crushed and sieved at >70 mesh (.21mm) and <70 mesh. A 250 g sample from UE-7f was crushed and sieved at <70 mesh, and 70-250 mesh. These size fractions were later combined during processing in order to make a sufficiently large carrier-free target for $^{36}Cl/Cl$ measurement by AMS (1 mg Cl is required). Approximately equal masses of de-ionized water and rock powder were combined in glass containers, and tumbled at a slow speed for 24 hours for the leaching. The Army Well #1 sample was filtered at 0.45 μm, and AgCl precipitation was

carried out on the filtrate. The UE-7f sample would not pass through the filter paper, and the liquid component was separated using a centrifuge.

Total chloride was measured by ion chromatography, with a detection limit of 0.1 mg/L and a typical relative standard deviation of 1 to 4%. $^{36}Cl/Cl$ ratios were measured at Purdue University's PRIME Lab, with a detection limit of $5x10^{-15}$, and a typical relative standard deviation of 5%. PRIME Lab's techniques for measuring low level $^{36}Cl/Cl$ are described in Sharma et al. (1997). The meteoric water samples and low Cl concentration spring water samples presented some analytical difficulty, because of incomplete removal of sulfate. The target material from Currant Summit precipitation had ^{36}S that interfered with the ^{36}Cl signal, and no ratio is reported. While PRIME Lab uses a gas filled magnet to provide separation of ^{36}S from ^{36}Cl, 1σ errors for these samples are higher than usual due to unresolved interference from ^{36}S. Likewise, the UE-7f sample extracted less than 1 mg Cl, and had a greater error due to fewer analytical repetitions.

4.0 Results and Discussion

The $^{36}Cl/Cl$ results for environmental samples collected between 1992 and 1997 are reported in Table 1, along with sample locations, water levels, hydrostratigraphic units, and field parameters. Ancillary chemical and isotopic data for these samples are found in Rose et al. (1997). Sample locations are shown in Figures 1 and 2. Analytical results for new samples collected during FY 2000 are summarized in Table 2, and sample locations are shown in Figure 1. A wide range in both Cl concentration and $^{36}Cl/Cl$ is observed in the combined data sets, indicating multiple sources for Cl and/or ^{36}Cl. The highest ratios are slightly greater than the predicted value for the initial, cosmogenic ratio, but close to values measured in recently recharged groundwater and in soils in previous studies (Davis et al., 1998). Relative to other deep groundwater basins, these waters have very low Cl concentrations (< 50 mg/L compared to hundreds of mg/L in many sedimentary basins), indicating a lack of influence from deep-seated brines or interaction with evaporite minerals.

4.1 $^{36}Cl/Cl$ end-member compositions

Two principal end-member compositions exist for the $^{36}Cl/Cl$ system in southern Nevada: (1) the initial cosmogenic component that is introduced during groundwater recharge, characterized by high $^{36}Cl/Cl$ ratios and low Cl concentrations; and (2) the component derived from water-rock interaction, characterized by decreasing $^{36}Cl/Cl$ ratios and increasing Cl concentrations along a flow path. Preliminary constraints on end-member compositions were obtained from measurements on precipitation samples, groundwater samples from the Spring Mountains, groundwater samples from Pahranagat Valley, and rock leaching experiments.

The Cl concentrations measured in the precipitation samples from Austin Summit and Little Antelope Summit are typical for inland meteoric water. Stable Cl concentrations in

precipitation vary depending on the frequency, intensity, and origin of the storm events in a given area. However, the comparatively high Cl concentration in the precipitation sample from Currant Summit (7.4 mg/L) may reflect the proximity of this sample site to a large playa. Windblown dust originating from salt deposits on the playa can readily account for the observed Cl value. This sample also had high sulfur, typical of terrigenous material. The low Cl concentrations measured in the Spring Mountain samples suggest that these waters are not evaporated, that they have a short subsurface residence time, and that they are representative of the meteoric component for that area. The measured $^{36}Cl/Cl$ ratios for recharge waters are consistent with previous values reported for the area (Hainsworth et al., 1994, Tyler et al., 1996, Davis et al., 1998).

During rock leaching experiments, the limestone samples yielded considerably more leachable Cl than did the volcanic tuff samples (Table 1). In general, both the bulk Cl concentrations and water-leachable Cl are much greater for carbonates than for volcanic rocks. Kenneally (1995) also found that carbonate rocks are higher (22 to 93 ppm) in leachable Cl than volcanic rocks (0.5 to 24 ppm) for 10 core samples from the Nevada Test Site. The low U and Th concentration in carbonate rocks results in decreased secular equilibrium $^{36}Cl/Cl$ ratios relative to volcanic rocks. Hence, the carbonate rock leachate sample had a $^{36}Cl/Cl$ ratio of approximately 10×10^{-15} while the tuff leachate had a ratio of 48×10^{-15} (Table 1).

Figure 3 is a plot of $^{36}Cl/Cl$ ratios versus 1/Cl for samples from the lower carbonate aquifer (LCA) illustrating the two end-member compositions. Simple mixing processes are linear on this plot. As we note, the recharge end-member has an initial $^{36}Cl/Cl$ ratio in the range of approximately 600 to 800×10^{-15}, with a relatively dilute initial Cl concentration. In contrast, the carbonate rock leachate end-member is a chemically evolved water with an estimated Cl concentration of 80 mg/L and a $^{36}Cl/Cl$ ratio of 10×10^{-15} (Figure 3). Hence, dissolution of Cl from the carbonate rock results in progressively lower $^{36}Cl/Cl$ ratios and higher Cl concentrations along a given flowpath in the LCA. Note that most of the LCA samples from the NTS (yellow triangles in Figure 3) evidently lie on a mixing line between a "high" Cl recharge end member (1/Cl = 0.15 is equivalent to 6.7 mg/L Cl) and the carbonate rock end-member (lower left-hand corner of the Figure 3).

4.2 Variations along carbonate aquifer flowpaths in southern Nevada

Previous deuterium-calibrated models for regional groundwater flow through the carbonate aquifer indicate that 35-40% of the discharge at Ash Meadows originates from the Pahranagat Valley area (northeast of the NTS), and passes beneath Frenchman Flat in route to Ash Meadows (Winograd and Friedman, 1972; Thomas et al., 1996). The remaining 60-65% of the Ash Meadows spring discharge is attributed to groundwater originating from the Spring Mountains. This general model establishes a framework for examining the evolution of $^{36}Cl/Cl$ compositions along a regional flow path.

Stable isotope data indicates that groundwater in the Pahranagat Valley originates from recharge in the mountains that border the White River Valley in east-central Nevada. The White River flow system evidently bifurcates in the Pahranagat Valley area, with some of the flow moving southward toward the Colorado River, and the remainder of the flow moving toward the NTS, and ultimately Ash Meadows (e.g. Thomas et al., 1996). The $^{36}Cl/Cl$ ratios in Pahranagat Valley waters are among the highest of those measured in southern Nevada and reflect the exclusively cosmogenic ^{36}Cl component found in meteoric waters – even in the large carbonate springs in Pahranagat Valley. This observation implies relatively short carbonate aquifer residence times in this area, despite the fact that Pahranagat Valley is >100 km south of the "headwaters" of the White River flow system (see also Davisson et al., 1999).

The range in $^{36}Cl/Cl$ values (600-750 x 10^{-15}) for the Pahranagat Valley samples is likely due to spatial and temporal variability in the $^{36}Cl/Cl$ ratio in meteoric water falling in the area, together with local groundwater mixing processes. While the $^{36}Cl/Cl$ ratios have a rather small range in values, Cl concentrations vary between 3 and 83 mg/L. An examination of the $\delta^{18}O$ and δD values for these samples (Figure 4), reveals that the low concentration samples plot along the Global Meteoric Water Line ($\delta D = 8\delta^{18}O + 10$; Craig, 1961) while samples with higher Cl concentration fall on an evaporative trend with a slope of 4.8. Pahranagat Valley is an agricultural area, and the high-Cl waters are likely evaporated during irrigation. All of the evaporated waters are from relatively shallow wells that penetrate alluvial aquifers. Concentrating Cl in the water by evaporation does not change the $^{36}Cl/Cl$ ratio. The mixing end-member for this area therefore has a "cosmogenic" or "meteoric" ratio of approximately $700x10^{-15}$, while the Cl value for this end-member ranges from a meteoric (<7 mg/L Cl) to an evaporated meteoric water signature (10's of mg/L Cl).

A plot of the $^{36}Cl/Cl$ ratio versus ^{36}Cl concentration (Figure 5) illustrates the reactions taking place for the Cl system. The initial value on this plot represents the predicted *and* measured range in $^{36}Cl/Cl$ and ^{36}Cl concentrations for groundwater recharge in Nevada (Davis et al., 1998; Hainsworth et al., 1994; Knies, 1994; Bentley and Davis, 1982; and this work). LCA waters all plot to the left of the initial value, indicating that addition of low ratio chlorine (water-rock interaction) is the dominant process for these waters. In contrast, non-evaporated Pahranagat Valley groundwaters all plot within the initial value field. Waters with ratios higher than the initial value may be affected by mixing with young water containing bomb pulse ^{36}Cl. These waters have a component of water that is less than 50 years old. It is clear from these data that the processes of radioactive decay and subsurface production are not important for the Cl system in these waters.

Aside from evaporated waters from Pahranagat Valley, the highest Cl concentrations are observed in LCA groundwater samples fromYucca Flat (Water Well C, Water Well C-1, UE-1h and ER-3-1). These waters have the lowest observed $^{36}Cl/Cl$ ratios and are probably closest to being in chemical equilibrium (with respect to Cl) with the carbonate

host formation. Other wells in the Yucca Flat LCA (e.g., U-3cn#5, UE-10j, and ER-6-1) have comparatively lower Cl concentrations and higher $^{36}Cl/Cl$ ratios. These samples may contain a component of younger groundwater, possibly derived from downward leakage from one of the shallower aquifer units in Yucca Flat, although this idea is currently speculative. Alternatively, these waters may have been transported along shorter flowpaths, with shorter residence times in the carbonate aquifer. The $^{36}Cl/Cl$ ratio in Army Well #1 water can be interpreted as a mixture of LCA groundwater from Yucca Flat and groundwater originating from the Spring Mountains. This interpretation is consistent with previous geochemical models for regional flow in this area. Our samples from the Spring Mountains have significantly higher $^{36}Cl/Cl$ ratios than LCA water from NTS wells, which accounts for the increase in the $^{36}Cl/Cl$ ratio in Army Well #1. The ^{36}Cl signature of Army Well #1 water is very close to that measured in the Ash Meadows spring samples, and there is likely little change in the ^{36}Cl content of the water between Mercury Valley and Ash Meadows.

4.3 Aquifer residence times

It is notable that groundwater samples with low $^{36}Cl/Cl$ ratios commonly show high ^{4}He abundances (Figure 6), suggesting a correlation related to aquifer residence times. Detectable buildup of ^{4}He in groundwater occurs over 1,000- to 10,000-year time scales due to decay of U and Th in the aquifer matrix. We observe that *some* of the samples that have resided in the LCA long enough for their $^{36}Cl/Cl$ ratios to decrease to values less than $\sim 5 \times 10^{-13}$ (due to water-rock interaction) also exhibit significant buildup of ^{4}He.

In general, low $^{36}Cl/Cl$ ratios and high Cl concentrations characterize groundwaters with long residence times, as observed for groundwaters from the LCA. For example, the UE-10j well is screened over three discrete intervals in the LCA, and the $^{36}Cl/Cl$ ratio decreases with depth while the Cl concentration increases over the same interval (see Table 1). The UE-10j samples also show an increase in ^{4}He with depth. This trend may be the result of longer flowpaths for the deeper section of the LCA, allowing more interaction with the aquifer material.

Several independent pieces of geochemical evidence suggest that groundwater ages in the regional carbonate aquifer are generally less than 10,000 years (e.g. Thomas et al., 1996; Davisson et al., 1999; Rose and Davisson, 2001). However, a residence time of 10,000 years is insufficient for radioactive decay of ^{36}Cl to have an effect on the $^{36}Cl/Cl$ ratio. Furthermore, buildup of ^{36}Cl due to neutron capture on ^{35}Cl in the groundwater is also negligible over 10,000 years unless U concentrations are extremely high. Hence, the primary "aging" effect we expect to see in LCA groundwaters from southern Nevada is a progressive enrichment in Cl coupled with decreasing $^{36}Cl/Cl$ ratios. More careful consideration of the relationships between ^{4}He and $^{36}Cl/Cl$ sources and processes are needed before these observed correlations can be used to measure quantitative residence times.

4.4 Variations in $^{36}Cl/Cl$ ratios in different hydrostratigraphic units

On a plot of $^{36}Cl/Cl$ ratios versus Cl concentrations (Figure 7), groupings are evident for well water samples from the various hydrostratigraphic units of Southern Nevada. Most significantly, waters derived from the regional Lower Carbonate Aquifer (LCA) fall into a group that is distinct from waters sampled from Tertiary Volcanic Aquifers (TVA). While LCA waters have uniformly low ratios, and concentrations greater than 10 mg/L Cl, TVA waters have high ratios and are strikingly uniform in their Cl concentrations, between 5 and 8 mg/L.

Waters from alluvial aquifers (AA) are characterized by relatively high ratios and highly variable Cl. These waters may be evaporated to some degree, resulting in increased Cl concentrations, while the $^{36}Cl/Cl$ ratio is likely to be dominated by the meteoric (cosmogenic) component. The highest ratios measured in AA waters may have a component of bomb pulse ^{36}Cl, indicating the presence of recharge water <50 years in age. Waters from the Upper Clastic Confining Unit (UCCU) in Yucca Flat have a Cl concentration range similar to waters from alluvial aquifers, and $^{36}Cl/Cl$ ratios that are somewhat lower. Water in confined aquifers may take longer flowpaths and therefore have a greater ^{36}Cl component derived from water-rock interaction. For the same reason, these waters are less likely to have a bomb pulse component.

The ^{36}Cl results suggest that LCA groundwaters in the NTS area are affected by interaction (leaching of Cl) with the carbonate aquifer, but that mixing with waters from Tertiary volcanic aquifers does not affect the Cl system. TVA waters have distinct ^{36}Cl signatures and do not fall on mixing trends with LCA waters (Figures 3 and 5). These results are consistent with hydrogeologic data that suggests slow interaction between these different aquifers due to low permeability in the volcanic units.

5.0 Summary and Future Work

This study provides a preliminary interpretation of the LLNL ^{36}Cl data that has been collected over the past decade. By adding several carefully chosen samples from the regional flow system, end members for the Cl system have been identified. These data provide an independent test of regional flow models, and allow us to better distinguish the extent to which groundwater from different hydrostratigraphic units is interacting.

$^{36}Cl/Cl$ ratios in waters from southern Nevada are interpreted in the hydrogeologic framework put forth by Winograd and Thordarson (1975). More recent geochemical studies suggest that groundwater ages in the Death Valley regional carbonate aquifer may be less than 10,000 years (e.g. Thomas et al., 1996; Davisson et al., 1999). The relatively young ages, low Cl concentrations, and short subsurface residence times of groundwater in the study area suggest that ^{36}Cl decay and subsurface production on ^{35}Cl negligibly small. Hence, the dominant factors controlling the observed $^{36}Cl/Cl$ ratios and Cl

concentrations are: (1) the initial values inherited during recharge, and (2) the progressive dissolution of ^{36}Cl-absent chloride along groundwater flow paths. The ^{36}Cl signature of LCA water is distinct from TVA and AA waters, which provides the basis for using ^{36}Cl as an independent tool for constraining hydrogeologic interpretations of mixing and vertical flow.

This study provides the foundation for future work, which will include a ^{36}Cl study of vertical interactions between hydrostratigraphic units in Frenchman Flat. The development of new wells that penetrate the LCA in Frenchman Flat will provide the opportunity to carefully evaluate vertical transport processes in this area. The results of these studies are likely to be of direct application in Yucca Flat, where a similar hydrostratigraphic sequence exists. In addition, Cl leaching studies of solid material from Frenchman Flat wells will provide a means of constraining aquifer residence times, and will help to better elucidate the controls on Cl dissolution rates in groundwater systems.

References

Andrews JN; Fontes JCh; Michelot JL; Elmore D. (1986) In-situ neutron flux, ^{36}Cl production and groundwater evolution in crystalline rocks at Stripa, Sweden. Earth Planet. Sci. Lett., 77: 49-59.

Beasley TM; Cecil LD; Sharma P; Kubik PW; Fehn U; Mann LJ; Gove HE. (1993) Chlorine-36 in the Snake River Plain aquifer at the Idaho-National-Engineering-Laboratory: Origin and implications. Ground Water, 1993, 31 (2): 302-310.

Bentley HW; Phillips FM; Davis SN. (1986a) Chlorine-36 in the terrestrial environment. In: P.Fritz and J.Ch. Fontes (eds.), Handbook of Environmental Isotope Geochemistry, Volume 2, The Terrestrial Environment, B. Elsevier, Amsterdam, p. 427-480.

Bentley HW; Phillips FM; Davis SN; Gifford S; Elmore D; Tubbs LE; Gove HE. (1982) Thermonuclear ^{36}Cl pulse in natural water. Nature, 300: 737-740.

Bentley HW; Phillips FM; Davis SN; Hebermehl MA; Airey PL; Calf GE; Elmore D; Gove HE; Torgersen T. (1986b) Chlorine-36 dating of very old groundwater 1. The Great Artesian Basin, Australia. Water Resources Research, 22: 1991-2001.

Cornett RJ; Andrews LA; Chant LA; Davies WG; Greiner BR; Imahori Y; Koslowsky VT; Kotzer T; Milton JCD; Milton GM. (1997) Is ^{36}Cl from weapons test fallout still cycling in the atmosphere? Nucl. Inst. And Meth. In Phys. Res. B, 123: 378-381.

Craig H. (1961) Isotopic variations in meteoric waters. Science, 133: 1702-1703.

Davis SN; Cecil D; Zreda M; Sharma P. (1998) Chlorine-36 and the initial value problem. Hydrogeology Journal, 6: 104-114.

Davisson ML; Smith DK; Kenneally J; Rose TP. (1999) Isotope hydrology of southern Nevada groundwater: stable isotopes and radiocarbon. Water Resources Research, 35: 279-294.

Dettinger MD; Harrill JR; Schmidt DL; Hess JW. (1995) Distribution of carbonate-rock aquifers and the potential for their development, southern Nevada and adjacent parts of California, Arizona and Utah. U.S. Geological Survey, Water-Resources Investigations Report 91-4146, 100 p.

Eakin TE. (1966) A regional interbasin groundwater system in the White River area, southeastern Nevada. Water Resources Research, 2: 251-271.

Fabryka-Martin J; Wightman SJ; Murphy WJ; Wickham MP; Caffee MW; Nimz GJ; Southon JR; Sharma P. (1993) Distribution of chlorine-36 in the unsaturated zone at Yucca Mt.: An indicator of fast transport paths, paper presented at FOCUS '93 Site Characterization and Model Validation, Las Vegas, Nev., Sept.26-29, 1993.

Fehn U; Tullai-fitzpatrick S; Kubik PW; Sharma P; and Others. (1992) I-129 And Cl-36 concentrations in waters of the eastern Clear Lake area, California - Residence times and source ages of hydrothermal fluids. Geochimica et Cosmochimica Acta, 56 (5): 2069-2079.

Hainsworth LJ; Mignerey AC; Helz GR; Sharma P; and Others. (1994) Modern chlorine-36 deposition in southern Maryland, USA. Nuclear Instruments & Methods in Physics Research Section B-Beam Interactions with Materials and Atoms, 92 (1-4): 345-349.

Harrill JR; Gates JS; Thomas JM. (1988) Major ground-water flow systems in the Great Basin region of Nevada, Utah, and adjacent states. U.S. Geological Survey, Hydrologic Investigations Atlas, HA-694-C, scale 1:1,000,000, 2 sheets.

Kenneally J. (1995) Preliminary report evaluating the use of strontium and chloride concentrations and $^{87}Sr/^{86}Sr$ ratios as analogs for the dissolution of inorganic carbon. Lawrence Livermore National Laboratory, unpublished report prepared for the U.S. Department of Energy, Nevada Operations Office, Environmental Restoration Division, April 1995, 14 p.

Knies DL; Elmore D; Sharma P; Vogt S; and others. (1994) Be-7, Be-10, and Cl-36 in precipitation. Nuclear Instruments & Methods in Physics Research Section B-Beam Interactions with Materials and Atoms, 1994, 92 (1-4): 340-344.

Laczniak RJ; Cole JC; Sawyer DA; Trudeau DA. (1996) Summary of hydrogeologic controls on ground-water flow at the Nevada Test Site, Nye County, Nevada. U.S. Geological Survey, Water-Resources Investigation Report 96-4109, 59 p.

Nimz G; Janik C; Goff F; Dunlap C; Huebner M; Counce D; Johnson S. (1999) Regional hydrology of the Dixie Valley geothermal field, Nevada: Preliminary interpretations of chemical and isotopic data. Lawrence Livermore National Laboratory, UCRL-JC-135417, 9 p.

Paul M; Kaufman A; Magaritz M; Fink D; Henning W; Kaim R; Kutschera W; Meirav O. (1986) A new ^{36}Cl hydrologic model and ^{36}Cl systematics in the Jordan River/Dead Sea system. Nature, 321: 511-515.

Phillips FM. (1994) Environmental tracers for water movement in desert soils of the American southwest. Soil Science Society of America Journal, 58 (1): 15-24.

Phillips FM; Mattick JL; Duval TA; Elmore D; Kubik PW. (1988) Chlorine-36 and tritium from weapons fallout as tracer for long-term liquid and vapor movement in desert soils. Water Resources Research, 24: 1877-1891.

Phillips FM; Goff F; Vuataz F; Bentley HW; Elmore D; Gove HE. (1984) ^{36}Cl as a tracer in geothermal systems: Example from Valles caldera, New Mexico. Geophysical Research Letters, 11: 1227-1230.

Rao U; Fehn U; Teng RTD; Goff F. (1996) Sources of chloride in hydrothermal fluids from the Valles Caldera, New Mexico - A Cl-36 study. Journal of Volcanology and Geothermal Research, 72 (1-2): 59-70

Rose TP; Kenneally JM; Smith DK; Davisson ML; Hudson GB; Rego JH. (1997) Chemical and isotopic data for groundwater in southern Nevada. Lawrence Livermore National Laboratory, UCRL-ID-128000, 35 p.

Rose TP; Davisson ML; Criss RE; Smith DK. (1999) Isotopic investigation of recharge to a regional groundwater flow system, Great Basin, Nevada, USA. In: Proceedings, International Symposium on Isotope Techniques in Water Resources Development and Management, Vienna, 10-14 May 1999. International Atomic Energy Agency, IAEA-CSP-2/C, session 2, pp. 63-72.

Rose TP; Davisson ML. (2001) Isotopic and geochemical evidence for Holocene-age groundwater in regional flow systems of south-central Nevada. In: *Late Quaternary Paleohydrology and Paleoenvironments of the Mojave Desert*, Geological Society of America Special Paper, manuscript accepted for publication.

Scanlon BR; Kubik PW; Sharma P; Richter BC; and others. (1990) Bomb chlorine-36 analysis in the characterization of unsaturated flow at a proposed radioactive waste disposal facility, Chihuahuan Desert, Texas. Nuclear Instruments & Methods in Physics Research Section B-Beam Interactions with Materials and Atoms, 52 (3-4):489-492.

Sharma P; Elmore D; Vogt S. (1997) The PRIME Lab external research program. Nuclear Instruments & Methods in Physics Research Section B-Beam Interactions with Materials and Atoms, 123 (1-4): 199-202.

Thomas JM; Welch AH; Dettinger MD. (1996) Geochemistry and isotope hydrology of representative aquifers in the Great Basin region of Nevada, Utah, and adjacent states. U.S. Geological Survey, Professional Paper 1409-C, 100 p.

Torgersen T; Habermehl MA; Phillips FM; Elmore D; Kubik P; Jones BG; Hemmick T; Gove HE. (1991) Chlorine 36 dating of very old groundwater 3. Further studies in the Great Artesian Basin, Australia. Water Resources Research, 27: 3201-3213.

Tyler SW; Chapman JB; Conrad SH; Hammermeister DP; Blout DO; Miller JJ; Sully MJ; Ginanni JM. (1996) Soil-water flux in the southern Great Basin, United States: Temporal and spatial variations over the last 120,000 years. Water Resources Research, 32: 1481-1499.

U.S. Department of Energy. (1997) Regional groundwater flow and tritium transport monitoring and risk assessment of the underground test area, Nevada Test Site, Nevada. U.S. Department of Energy, Nevada Operations Office, Environmental Restoration Division Report DOE/NV-477, 396 p.

Winograd IJ; Friedman I. (1972) Deuterium as a tracer of regional ground-water flow, southern Great Basin, Nevada and California. Geological Society of America Bulletin, 83: 3691-3708.

Winograd IJ; Thordarson W. (1975) Hydrogeologic and hydrochemical framework, south-central Great Basin, Nevada-California, with special reference to the Nevada Test Site. U.S. Geological Survey, Professional Paper 712-C, 126 p.

Winograd IJ; Riggs AC; Coplen TB. (1998) The relative contributions of summer and cool-season precipitation to groundwater recharge, Spring Mountains, Nevada, USA. Hydrogeology Journal, 6: 77-93.

Table 1. Data for Wells and Springs with Environmental $^{36}Cl/Cl$ Values, Southern Great Basin

Sample	Latitude (d m s)	Longitude (d m s)	Surface Elevation (feet)	Water Level Elevation (feet)	Primary HSU	Sample Date	Conductivity (µS/cm)	pH	Temp (°C)	Cl (mg/L)	$^{36}Cl/Cl$ (x 10^{-13})
Ash Meadows											
Big Spring	36 22 30	116 16 25	2240	2240	PzC	9/6/95	670	7.4	27	23.7	3.87
Crystal Pool	36 25 13	116 19 23	2195	2195	PzC	9/6/95	664	7.4	31	22.3	4.37
Fairbanks Spring	36 29 26	116 20 28	2250	2250	PzC	9/6/95	706	7.4	29	20.3	4.22
Mercury Valley											
Army Well #1	36 35 30	116 02 14	3154	2368	PzC	5/12/93	625	7.5	29	24.0	4.23
Jackass Flats / Fortymile Wash											
J-12, NTS, Area 25	36 45 54	116 23 24	3130	2387	Tv	5/13/93	299	7.4	27	8.3	5.03
J-13, NTS, Area 25	36 48 28	116 23 40	3318	2389	Tv	5/13/93	338	7.3	26	7.9	5.02
ER-30-1 #2, NTS, Area 30	37 03 01	116 18 58	4649	4199	Tv	2/1/95	282	9.6	23	6.1	5.38
Frenchman Flat											
Water Well 5c, NTS, Area 5	36 47 20	115 57 49	3081	2387	A	5/20/93	603	8.8	25	12.3	6.96
UE-5c, NTS, Area 5	36 50 11	115 58 47	3216	2410	A, Tv(at)	5/13/93	452	8.0	26	14.1	6.13
UE-5 PW-1, NTS, Area 5	36 51 05	115 56 58	3180	2407	A	5/26/93	377	8.3	23	12.0	8.42
UE-5 PW-2, NTS, Area 5	36 51 52	115 56 57	3248	2406	A	5/26/93	368	8.4	23	15.2	5.27
UE-5 PW-3, NTS, Area 5	36 52 01	115 58 16	3298	2406	Tv	5/26/93	361	8.5	24	10.1	6.78
Yucca Flat											
Water Well 4, NTS, Area 6	36 54 18	116 01 26	3602	2767	Tv	5/20/93	415	7.4	25	15.2	6.16
Water Well C, NTS, Area 6	36 55 08	116 00 35	3921	2381	PzC	5/19/93	1135	6.9	35	43.5	1.76
Water Well C-1, NTS, Area 6	36 55 07	116 00 34	3921	2381	PzC	5/19/93	1131	6.5	33	43.6	1.66
Test Well B, NTS, Area 6	36 58 48	116 00 51	3929	2425	Tv	6/7/93	381	7.5	20	22.6	8.00
ER-6-1, NTS, Area 6	36 59 04	115 59 34	3935	2386 (2461)	PzC (Tv)	11/23/92	514	7.1	39	9.9	3.92
UE-1h, NTS, Area 1	37 00 05	116 04 03	3995	2438	PzC	5/26/93	1029	8.2	25	43.6	1.71
ER-3-1, NTS, Area 3	37 01 33	115 56 13	4413	2397	PzC	10/16/96	1208	6.7	38	43.4	1.32
UE-16f, NTS, Area 16	37 02 09	116 09 25	4652	4285	PzE	7/12/93	1090	8.9	29	18.8	3.12
UE-1c, NTS, Area 1	37 02 53	116 05 52	4206	2908	Tv(at)	9/2/92	479	7.3	26	5.6	7.22

Table 1. Continued

Sample	Latitude (d m s)	Longitude (d m s)	Surface Elevation (feet)	Water Level Elevation (feet)	Primary HSU	Sample Date	Conductivity (µS/cm)	pH	Temp (°C)	Cl (mg/L)	$^{36}Cl/Cl$ (x 10^{-13})
UE-1b, NTS, Area 1	37 02 54	116 06 42	4273	3628	PzE	8/31/92	452	7.5	26	5.9	6.26
UE-1a, NTS, Area 1	37 02 54	116 07 06	4303	3758	A	9/1/92	448	7.4	27	26.3	8.63
U-3cn #5, NTS, Area 3	37 03 34	116 01 20	4012	2391	PzC	1/29/97	512	7.2	42	29.5	4.08
UE-1q, NTS, Area 1	37 03 37	116 03 30	4082	2427	PzC	7/10/92	-	7.8	31	5.3	7.90
UE-16d, NTS, Area 16	37 04 06	116 09 56	4684	3932	PzE	6/2/93	717	-	20	14.3	6.36
Test Well D, NTS, Area 4	37 04 18	116 04 45	4152	2429	PzE	6/8/93	445	7.9	24	6.9	7.24
UE-17a, NTS, Area 17	37 04 19	116 10 17	4697	4062	PzE	6/9/93	803	7.6	24	43.1	3.58
UE-10j (zone 1) 2510-2536' depth	37 11 08	116 04 53	4574	2413	PzC	3/17/97	1087	6.4	33	24.0	2.41
UE-10j (zone 2) 2401-2428' depth	37 11 08	116 04 53	4574	2413	PzC	3/20/97	725	6.7	32	16.0	3.91
UE-10j (zone 3) 2267-2293' depth	37 11 08	116 04 53	4574	2413	PzC	3/24/97	589	7.0	32	12.5	4.45
Pahute Mesa / Rainier Mesa											
UE-18r, NTS, Area 18	37 08 05	116 26 41	5538	4173	Tv	8/11/92	394	8.1	32	6.3	6.36
TW-1, NTS, Area 17	37 09 29	116 13 23	6156	4691	Tv(at)	8/13/92	238	8.7	27	3.2	9.68
Water Well 8, NTS, Area 18	37 09 56	116 17 21	5695	4618	Tv	6/2/93	194	7.3	25	9.2	5.83
UE-20bh-1, NTS, Area 20	37 14 42	116 24 33	6636	4425	Tv	6/20/93	186	8.3	26	3.9	6.45
Water Well 20, NTS, Area 20	37 15 05	116 25 24	6468	4411	Tv	5/31/95	308	8.2	34	12.0	5.67
UE-19c, NTS, Area 19	37 16 08	116 19 10	7033	4695	Tv	8/13/92	174	7.7	37	3.1	6.26
UE-19h, NTS, Area 19	37 20 34	116 22 25	6780	4669	Tv	8/12/92	415	8.3	28	8.5	4.79
Oasis Valley											
Revert Spring	36 55 04	116 44 37	3370	3370	A (Tv)	9/7/95	544	7.9	28	22.4	4.94
Bailey's Hot Spring	36 58 27	116 43 18	3590	3590	Tv	9/7/95	738	7.4	43	35.4	4.85
Goss Spring	36 59 45	116 42 51	3680	3680	Tv	9/7/95	715	7.7	22	45.0	4.88

Table 1. Continued

Sample	Latitude (d m s)	Longitude (d m s)	Surface Elevation (feet)	Water Level Elevation (feet)	Primary HSU	Sample Date	Conductivity (µS/cm)	pH	Temp (°C)	Cl (mg/L)	$^{36}Cl/Cl$ (x 10^{-13})
Emigrant Valley (NE of NTS)											
Watertown 1	37 14 43	115 48 22	4441	3951	Tv	8/16/95	330	7.7	24	6.9	6.53
Watertown 3	37 15 42	115 49 54	4446	4339	A	8/15/95	425	7.9	23	9.5	5.82
Watertown 4	37 15 38	115 50 06	4447	4337	A	8/15/95	1100	6.9	25	12.6	3.62
Pahranagat Valley											
US Fish & Wildlife Well	37 16 23	115 07 06	3310	shallow	A	8/8/95	1297	7.8	14	83.0	7.47
Alamo City Well #7	37 21 44	115 10 06	3480	3450	A	8/8/95	1032	7.6	19	54.6	7.41
Spencer Well	37 23 42	115 10 49	3540	3503	A	8/6/95	1070	7.7	19	45.9	7.04
Little Ash Spring	37 27 49	115 11 30	3615	3615	PzC	8/8/95	468	7.4	37	9.5	6.51
Sixmile Spring, S.Pahroc Range	37 29 32	115 05 17	5325	5325	Tv(p)	8/8/95	779	7.9	22	3.2	7.16
Crystal Springs	37 31 55	115 13 59	3810	3810	PzC	8/7/95	452	7.5	28	9.6	6.43
Hiko Spring	37 35 54	115 12 52	3875	3875	PzC	8/7/95	542	7.4	27	11.0	6.08
Stewart Brothers Well	37 36 53	115 13 32	3900	shallow	A	8/9/95	1582	7.8	-	13.9	7.03

Key to primary hydrostratigraphic units (HSU):

PzC = Lower Carbonate Aquifer
PzE = Upper Clastic Aquitard (Eleana Fm)
Tv = Tertiary Volcanic Aquifer
Tv(at) = Tertiary Volcanic Aquitard
A = Alluvial Basin Fill Deposits
(p) = Perched water table

Sources of data on wells and primary hydrostratigraphic units

- U.S. Dept. of Energy, Nevada Operations Office (1997) Datapkg/Volume 2/App.A
- Raytheon Services Nevada (1991) Redbook
- Covington and Berger (1997)

Table 2. FY 2000 Analytical Results

Sample Location	Cl (mg/L)	$^{36}Cl/Cl$ (10^{-15})	Comments
Precipitation samples			
Austin Summit	1.65	910 +/- 110	Meteoric water 1/99 – 7/99
Currant Summit	7.35	High sulfur	Meteoric water 11/99 – 5/00
Little Antelope Summit	3.05	not determined	Meteoric water 11/99 – 5/00
Spring Water samples			
Cold Creek Spring	1.55	522 +/- 49	
Deer Creek Spring	1.24	590 +/- 62	
Lithologic samples			
Army Well #1 Limestone			Medium and coarse were
Fine	26.6 ppm	102 +/- 68	combined for $^{36}Cl/Cl$ analysis
Medium	76.5 ppm	11 +/- 6	
Coarse	70.4 ppm		
Devil's Gate Limestone	7.2 ppm	not determined	
UE-7f - Volcanic Tuff			Size fractions were combined for
Coarse	0.7 ppm	48 +/- 36	$^{36}Cl/Cl$ analysis
Fine	0.5 ppm		

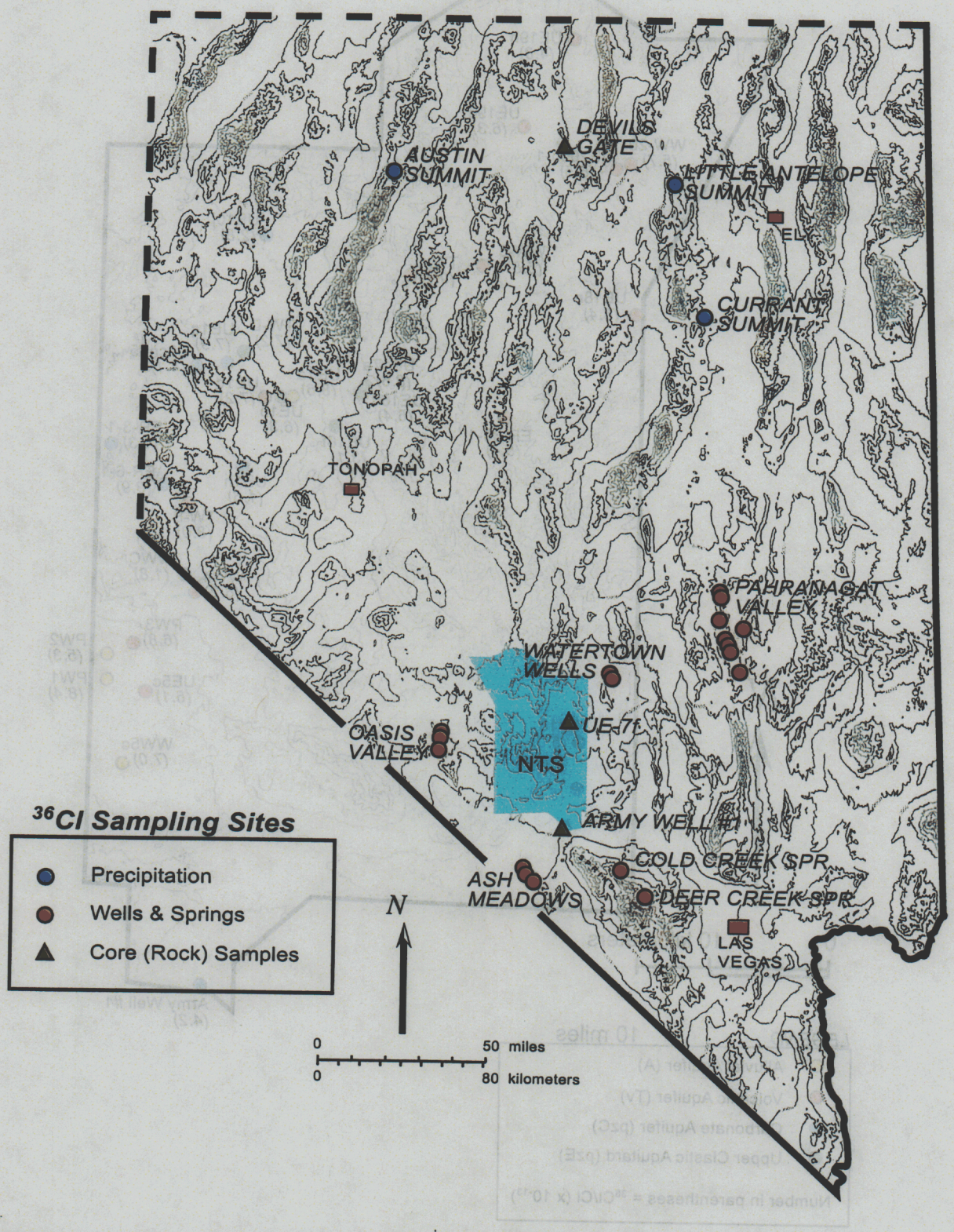

Figure 1. Sample locations for regional ^{36}Cl study (analytical results shown in Tables 1 and 2).

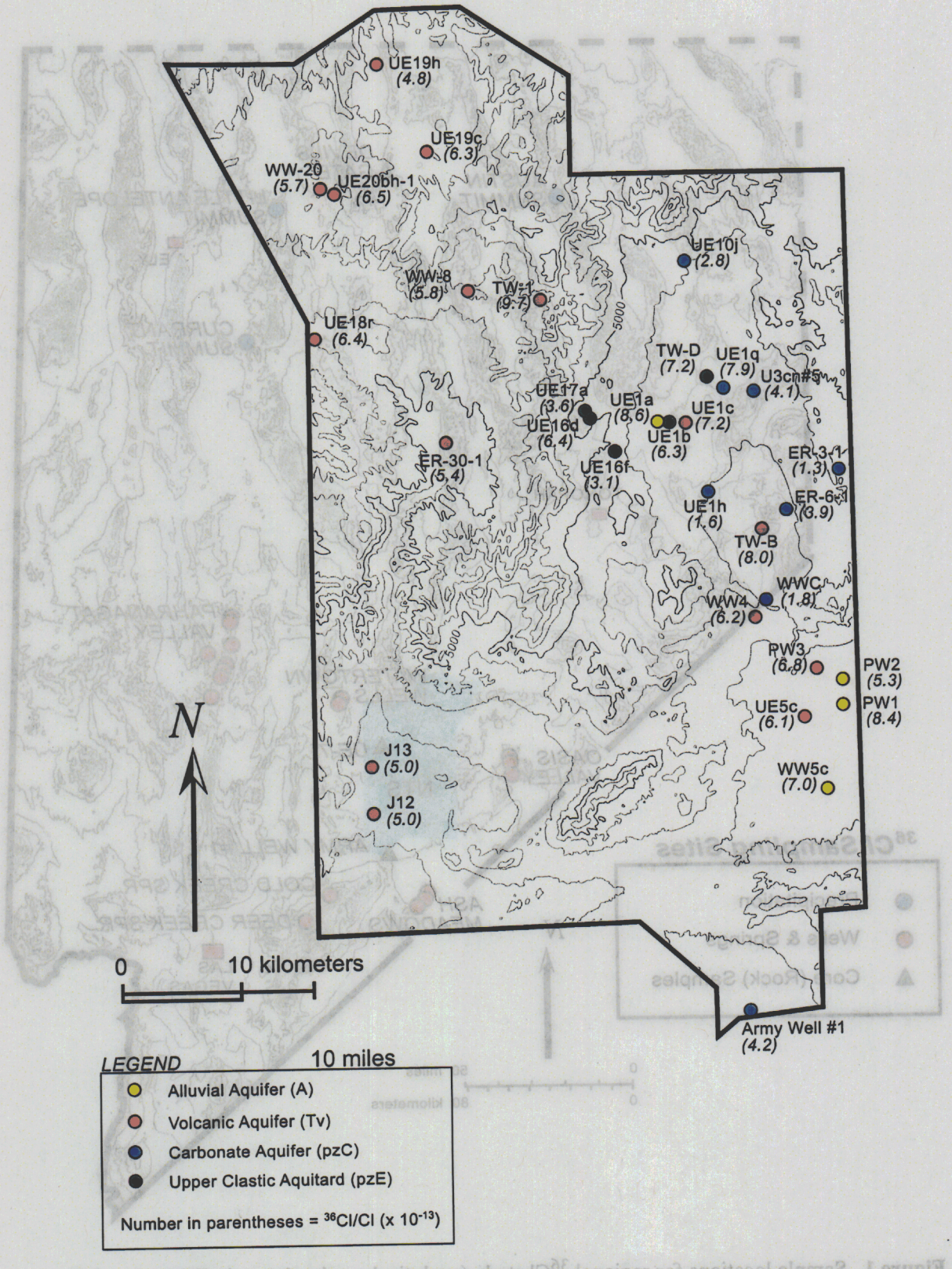

Figure 2. Sample locations for wells on the Nevada Test Site (analytical data shown in Table 1).

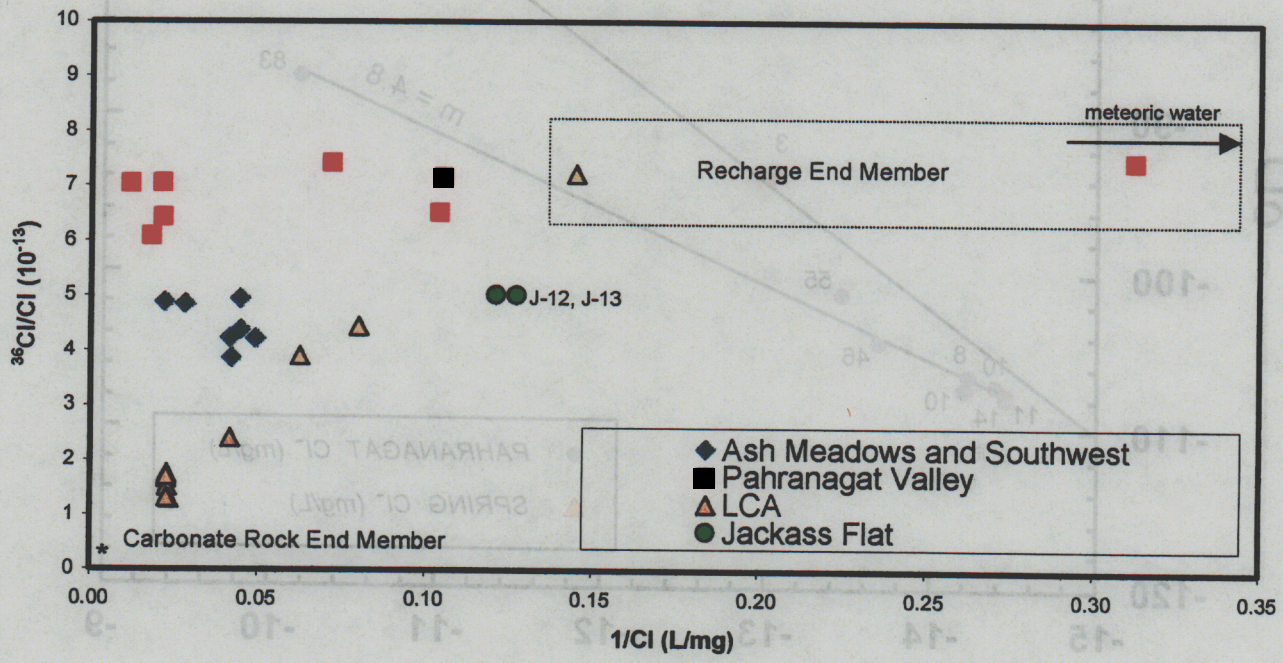

Figure 3. Plot of ^{36}Cl/Cl versus 1/Cl, illustrating mixing processes for the Cl system. Two component mixing is represented by linear trends on this plot. Recharge and rock end members are based on measured and theoretical values. Measured and predicted values for meteoric water are lower in Cl than the range shown here, but increasing Cl by evaporation before recharge is likely.

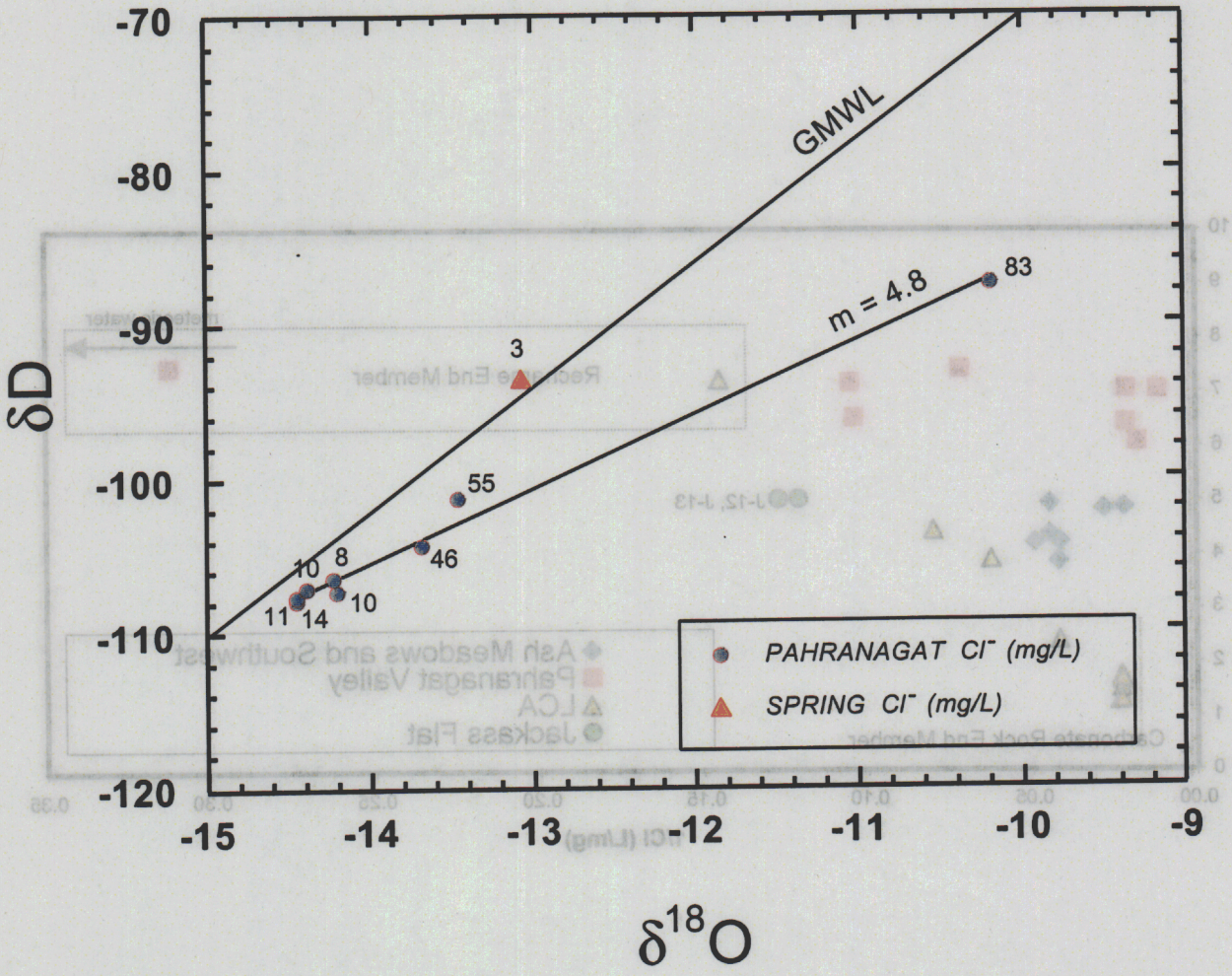

Figure 4. Plot of $\delta^{18}O$ vs. δD values for water samples collected in the Pahranagat Valley. The global meteoric water line (GMWL, $\delta D = 8\delta^{18}O + 10$) is shown for reference. Individual data points are labeled with respect to their Cl concentration. Pahranagat Valley waters fall on an evaporative trend, and show increasing Cl concentrations with increased evaporation. The lowest Cl concentration sample falls on the meteoric water line and represents the probable meteoric chloride input function for this area.

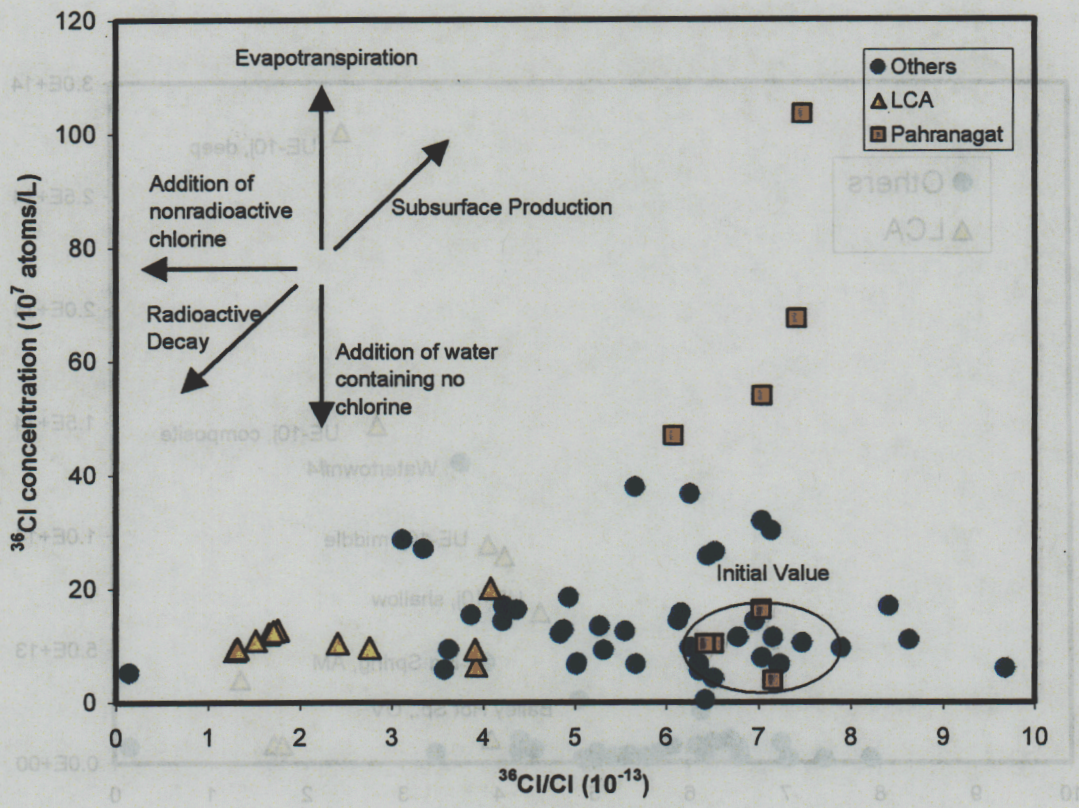

Figure 5. Plot of ^{36}Cl/Cl ratios versus ^{36}Cl concentrations. Data variations on this graph are useful in defining the important processes for the Cl system. The range for the initial value (oval) is based on measured values and theoretical estimates. Pahranagat Valley recharge waters have ^{36}Cl/Cl ratios in the initial value range, although some samples from this area are significantly evaporated. Lower Carbonate Aquifer (LCA) waters fall to the left of the initial value, indicating the importance of water-rock interaction with low ratio material. Subsurface production and radioactive decay are not important processes for these waters.

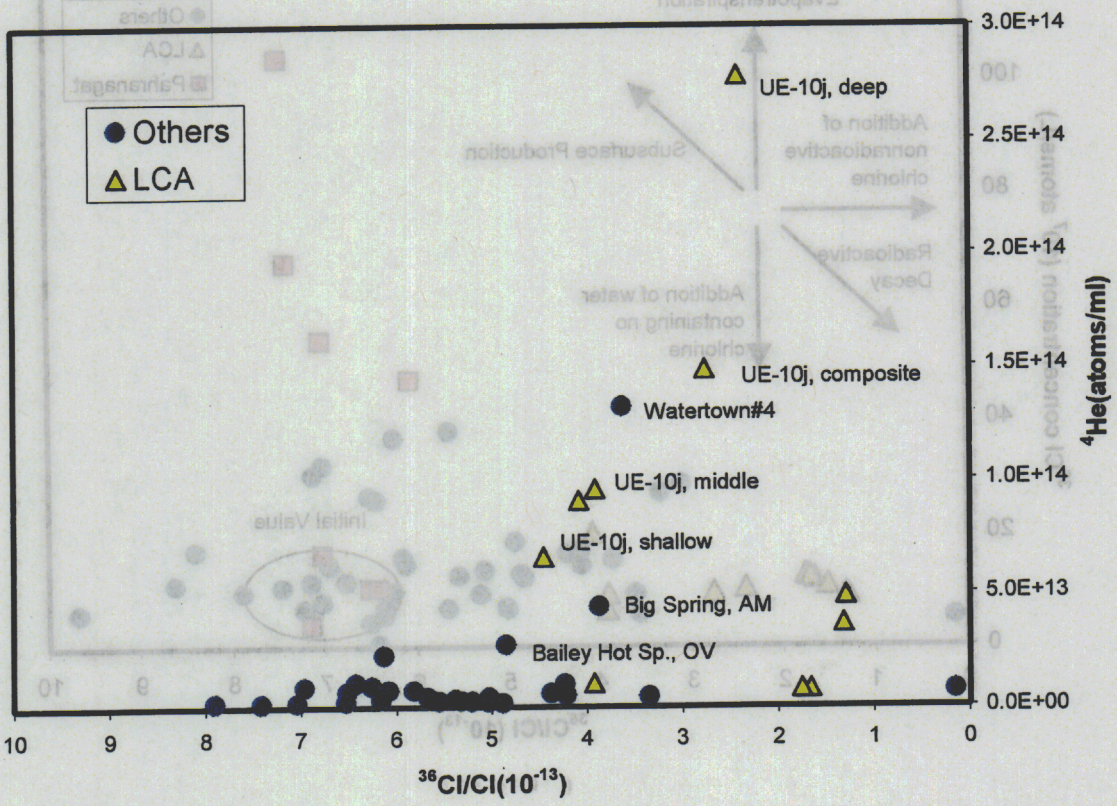

Figure 6. Plot of ^{4}He versus $^{36}Cl/Cl$ ratios for southern Nevada groundwaters. High ^{4}He and low $^{36}Cl/Cl$ values suggest aquifer residence times on the order of thousands to ten thousand years. Samples with notably high ^{4}He values are labeled. Lower Carbonate Aquifer (LCA) samples are shown as yellow triangles.

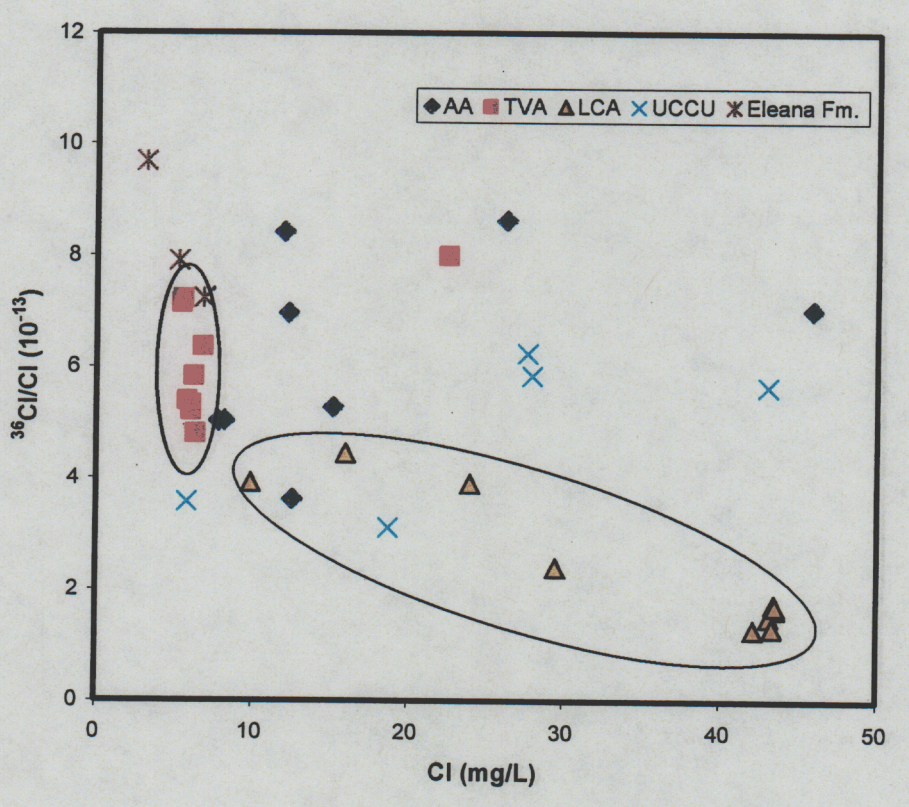

Figure 7. Cl versus $^{36}Cl/Cl$ variations for ground water samples from the NTS. Samples collected from the lower carbonate aquifer clearly plot as a group that is distinct from the Tertiary volcanic aquifer samples. AA = Alluvial Aquifer; TVA = Tertiary Volcanic Aquifer; LCA = Lower Carbonate Aquifer; UCCU = Upper Clastic Confining Unit.

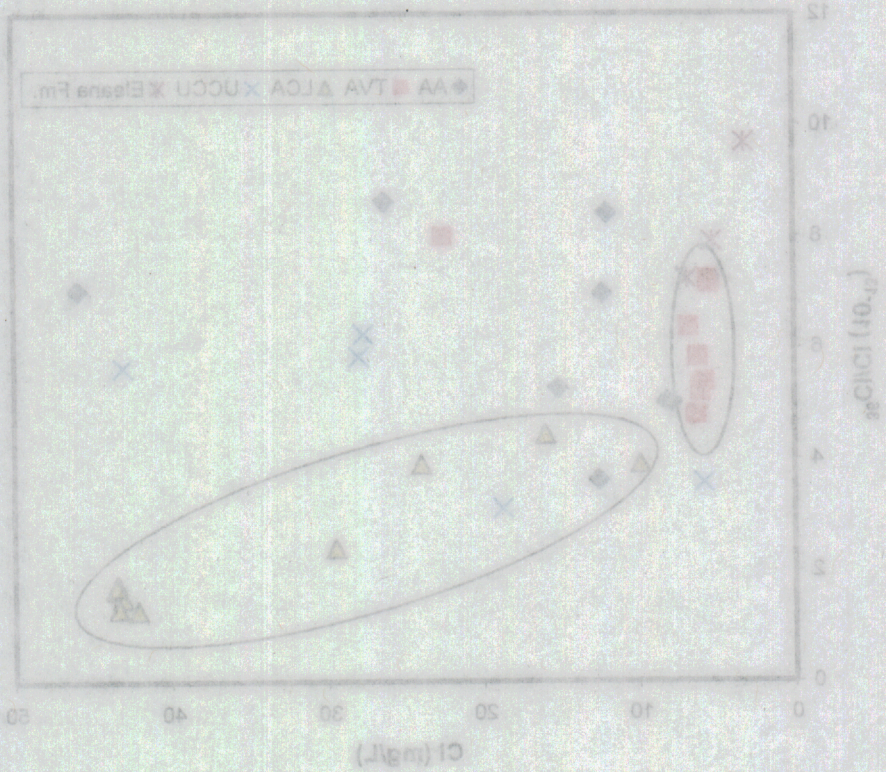

Chapter 8

Isotopic and Geochemical Evidence for Holocene-Age Groundwater in Regional Flow Systems of South-Central Nevada

Timothy P. Rose and M. Lee Davisson

Lawrence Livermore National Laboratory

Abstract

Regional groundwaters in the north-central Death Valley (DV) flow system exhibit $\delta^{18}O$ values that are 1 to 2‰ depleted relative to modern local recharge, and were previously interpreted to have originated from Pleistocene age recharge. New evidence presented in this study is consistent with Holocene ages for these groundwaters. Isotopic, chemical, and hydrogeologic data suggest the DV groundwaters are transported southward up to 300 km through regional carbonate aquifers of the Railroad Valley flow system. Groundwaters in the northern part of the flow system have $\delta^{18}O$ values nearly identical to recharge derived from winter precipitation in central Nevada. Isotopic analyses of snow cores revealed kinetic isotope enrichments in the snowpack *prior to melting* can account for observed isotopic enrichments in groundwaters relative to the global meteoric water line. Geographically consistent trends in $\delta^{18}O$ values, water chemistry, and carbon isotopes are observed along the entire 300 km regional flowpath. Dissolved inorganic carbon quickly reacts with the carbonate aquifer due to elevated subsurface temperatures and cation exchange processes, yielding ^{14}C values <10 pmc within 30 km of the northernmost recharge area. Groundwater mixing along the flowpath maintains uniformly low non-zero ^{14}C values. The complexities of the flow system preclude the application of ^{14}C age correction models. Hydrologic mass balance calculations imply turnover rates are too high to store significant amounts of pluvial recharge in the regional carbonate aquifer. Closed alluvial basins provide more favorable geologic environments for remnant accumulations of Pleistocene groundwater, as indicated by rare, isolated pockets of unusually low $\delta^{18}O$ groundwater.

Introduction

The eastern half of the Great Basin is underlain by an immense carbonate aquifer system that channels regional groundwater flow into southern Nevada from topographically high recharge areas in eastern and central Nevada. Rapid population growth in southern Nevada has motivated a number of studies aimed at determining the feasibility of tapping these vast groundwater reserves (e.g. Mifflin and Hess, 1979; Prudic et al., 1995; Dettinger et al., 1995; Thomas et al., 1996). In southwestern Nevada, similar studies are underway to assess the long-term risk of contaminant transport from underground nuclear test cavities at the Nevada Test Site (e.g. Laczniak et al., 1996; D'Agnese et al., 1997; U.S. Department of Energy, 1997). A key issue in each of these investigations is the rate at which the carbonate aquifers are replenished, and the concomitant rate at which water is transmitted through the system.

Part of the difficulty in assessing recharge and flow rates in this region is a lack of understanding regarding where the groundwater originates, and how disparate basins are interconnected. For example, only one regional flow system is believed to extend all the way from the recharge areas of east-central Nevada into the low desert discharge areas of southern Nevada – the White River flow system in eastern Nevada (Eakin, 1966; Harrill et al., 1988). The possibility that regional flow systems of similar magnitude may transect central Nevada was not previously examined in detail because surface evidence for such flow systems is lacking. In this paper, regional inflow from central Nevada is investigated as a possible means of interpreting environmental isotope data from the northwestern Nevada Test Site (Figure 1).

Environmental isotope studies (e.g. studies using δD, $\delta^{18}O$, $\delta^{13}C$, ^{14}C, ^{3}H data) can help to constrain regional flow systems by providing evidence for the origin and transport rate of groundwater. Many groundwater isotope studies have already been conducted in southern Nevada (e.g. Winograd and Friedman, 1972; Winograd and Pearson, 1976; Claassen, 1986; White and Chuma, 1987; Benson and Kleiforth, 1989; Thomas et al., 1996; Hershey and Acheampong, 1997; Davisson et al., 1999). However, most of these studies focused on the region south of latitude 38°N. Relatively little work has been done to assess the isotope hydrology of the recharge areas in eastern and central Nevada, or to evaluate possible links between these recharge areas and major discharge areas in southern Nevada.

In this paper, we examine the patterns and variations of groundwater chemistry and isotope data in the Railroad Valley flow system (central Nevada), and investigate the possibility that this region is hydraulically connected to the Death Valley regional flow system in southern Nevada (Figure 1). The process of evaluating this flowpath has permitted a more rigorous test of the concepts developed in our previous study of regional flow in Nevada (Davisson et al., 1999). In general, the results presented here validate our earlier conclusions that groundwater mixing and water-rock interaction are the major controls on oxygen and carbon isotope variations, respectively. In addition, we bring new evidence to bear on the stable isotope signatures inherited during recharge, regional variations in groundwater solute chemistry, and the distribution of paleo-groundwater in central and southern Nevada. With regard to the latter, our findings indicate that the paleowater distribution depends on the hydrodynamics of individual flow systems, and that several of the effects that have been widely cited as evidence for pluvial-age recharge can simply be attributed to Holocene-age processes.

Background

Hydrogeologic setting of the Great Basin

The Great Basin province encompasses a 360,000 km^2 area, largely in Nevada and western Utah, characterized by subparallel north-south trending mountain ranges separated by alluvial and fluviolacustrine basins (Harrill et al., 1988). The climate of the region is strongly influenced by the rain shadow effect of the Sierra Nevada and Cascade Ranges, which diminishes the moisture content of prevailing westerly winds originating from the Pacific Ocean (Houghton et al., 1975; Lamb et al., 1976). As a result, Nevada

receives the lowest amount of annual precipitation of the fifty United States. Winter frontal systems deposit >50% of the annual precipitation as snowfall, producing relatively large accumulations in alpine areas. Rapid melting of the mountain snowpack during the spring and early summer probably accounts for most of the annual groundwater recharge budget (Benson and Klieforth, 1989; Winograd et al., 1998; Rose et al., 1999a).

The principal aquifers in the region consist of basin-fill deposits and fractured carbonate rock, although fractured volcanic rocks form locally important aquifers (Winograd and Thordarson, 1975; Thomas et al., 1996). Much of the eastern half of the Great Basin is underlain by Paleozoic carbonate rocks with depositional thicknesses as great as 9,000 m (Stewart, 1980; Dettinger et al., 1995). Within this carbonate province, groundwater is transported along deep regional flowpaths that transcend local topographic boundaries, driven by hydraulic gradients that may be laterally continuous over hundreds of kilometers (Eakin, 1966; Winograd and Thordarson, 1975; Mifflin and Hess, 1979; Harrill et al., 1988; Dettinger et al., 1995). Mesozoic thrust faulting and Cenozoic normal faulting have juxtaposed rocks of different ages and lithologies, locally compartmentalizing the aquifers, and creating hydraulic gradients that tend to be step-like rather than smooth (Winograd and Thordarson, 1975). Hence, several areas of spring discharge may occur along a single regional flowpath, as in the White River flow system (Maxey and Eakin, 1949; Eakin, 1966).

Basin-fill deposits generally consist of unconsolidated or semi-consolidated sediments ranging from 500 to 1,500 m in thickness, with local sediment accumulations sometimes reaching 3,000 m depth (Harrill et al., 1988). The basin-fill aquifers may be hydraulically connected with adjacent and underlying bedrock aquifers, especially where carbonate rock is prevalent (Thomas et al., 1986). The degree of continuity depends in part on the vertical hydraulic conductivity of the deep basin fill (Dettinger et al., 1995). Where low-permeability rocks and sediments surround the basin-fill aquifers, hydrologically closed systems may develop. Closed basins are most common in the western part of the Great Basin, where low-permeability volcanic bedrock is widespread (Thomas et al., 1989; 1996).

Current models for regional groundwater flow in southwestern Nevada

The Death Valley regional flow system covers an area of about 40,000 km^2 in southwestern Nevada and adjacent eastern California (Figure 1), and is characterized by carbonate-hosted interbasin flow associated with large regional springs (Winograd and Thordarson, 1975; Harrill et al., 1988; Laczniak et al., 1996). It is perhaps the best studied of the regional flow systems in the Great Basin because it contains the U.S. Department of Energy's Nevada Test Site and Yucca Mountain project. The Death Valley playa is the terminus of the system, although several subsystems discharge at intermediate points along the flowpath (Harrill et al., 1988; Laczniak et al., 1996). The most prominent of these is the Ash Meadows spring system (Winograd and Thordarson, 1975; Winograd and Pearson, 1976). Recharge to the Death Valley flow system is assumed to be small for three reasons: (1) precipitation rates are generally low; (2) there is a paucity of high elevation catchments; and (3) observed discharge rates and totals are

small. Significant recharge does occur in the Sheep Range and Spring Mountains, the latter being an important source of groundwater for both the Las Vegas Valley (Malmberg, 1965; Morgan and Dettinger, 1996) and the Ash Meadows spring system (Winograd and Friedman, 1972; Winograd and Thordarson, 1975).

For the present study, we will focus on the Pahute Mesa-Oasis Valley subsystem, in the north-central part of the Death Valley flow system (Figure 1), and its possible linkage to regional flow to the north. Pahute Mesa is underlain by a thick sequence of rhyolitic volcanic rocks through which groundwater flow occurs principally along interconnected faults and fractures (Blankennagel and Weir, 1973). This subsystem is of particular interest because Pahute Mesa was the location of nearly 90 underground nuclear tests conducted between 1965 and 1992, the majority of which were detonated below the water table (Laczniak et al., 1996). The underground test area is situated ~40 km NE of Oasis Valley, where approximately 8,000 ac-ft yr^{-1} (27,000 m^3 d^{-1}) of groundwater discharges via evapotranspiration and spring flow (Reiner et al., 1999). Groundwater stable isotope data ($\delta^{18}O$ and δD) is consistent with a direct flowpath between Pahute Mesa and Oasis Valley (White and Chuma, 1987; Rose et al., 1999b). However, the origin of the groundwater underlying Pahute Mesa remains poorly constrained.

Cool season precipitation (October-April) collected at 2145 m elevation on Pahute Mesa has a weighted mean $\delta^{18}O$ value significantly higher (less negative) than groundwater sampled below the Pahute Mesa water table (>600 m depth; see Figure 2; precipitation data from Milne et al., 1987; Benson and Klieforth, 1989). Perched groundwater sampled from nearby Rainier Mesa is also isotopically enriched relative to the deeper groundwater (Figure 2). These data indicate that modern *local* recharge is not the principal source of the deeper groundwater. Two hypotheses have been proposed to explain these observations: (1) groundwater was recharged locally during a cooler climate episode, or (2) recharge is Holocene and occurred in higher elevation regions of central Nevada, and flowed into Pahute Mesa from the north. Each of these hypotheses merit further examination.

Paleoclimate studies

Proxy paleoclimate records are consistent with greater effective moisture in the Great Basin during the late Pleistocene. For example, nearly 100 basins in the northern Great Basin contain evidence of large Pleistocene lakes that oscillated in size in response to changes in climate (Mifflin and Wheat, 1979; Benson et al., 1990). Variations in oxygen isotopes and total organic carbon in cored sediments from these paleolake basins tend to correlate with North Atlantic ice-core and marine paleoclimate records (e.g. Benson, et al., 1996; 1998). In the southern Great Basin, the widespread occurrence of paleospring deposits has been interpreted as evidence for increased recharge and higher water tables during the late Pleistocene (Quade et al., 1995, 1998). However, with few exceptions, the effective moisture was insufficient to support large lakes in the southern Great Basin (Quade et al., 1995), and the full pluvial climate in south-central Nevada may have been similar to the modern climate in extreme northwestern Nevada (Mifflin and Wheat, 1979; Spaulding and Graumlich, 1986).

Increased groundwater recharge rates during the late Pleistocene imply a significant volume of groundwater was added to the regional aquifers at that time. The extent to which this water persists today is largely a function of groundwater flow velocities and turnover rates for individual sub-basins. Pleistocene age groundwater is most likely to be preserved within hydrologically closed or semi-closed alluvial basins. In some cases, this water may mix into the regional flow systems via downward leakage into the underlying carbonate aquifers (e.g. Winograd and Thordarson, 1975). However, this is likely to be a slow process since vertical conductivities are typically 1 to 2 orders of magnitude lower than horizontal conductivities in stratified alluvium (Domenico and Schwartz, 1990).

Previous isotope hydrology studies in the Oasis Valley-Yucca Mountain-Amargosa Desert region (central Death Valley regional flow system) concluded that groundwater in volcanic and alluvial aquifers in south-central Nevada was probably recharged during the last major pluvial cycle (Claassen, 1986; White and Chuma, 1987; Benson and Klieforth, 1989). Cited evidence includes the stable isotope depletions noted above, low deuterium excess values relative to modern precipitation (cf. Dansgaard, 1964; Merlivat and Jouzel, 1979), and unadjusted groundwater ^{14}C ages that yield predominantly late Pleistocene dates (9,000 - 18,000 years b.p.). Whereas paleoclimate models provide one possible interpretation for these data, an alternative hypothesis is developed in the following sections that potentially links the central Death Valley groundwaters to regional inflow from central Nevada.

Revised model for regional groundwater flow into southwestern Nevada

Blankennagel and Weir (1973) inferred that up to 70% of the groundwater underlying Pahute Mesa originates as regional flow from the north, via Kawich Valley and Gold Flat. Precipitation patterns suggest that significant recharge should occur between latitudes 38 and 40°N, where a number of mountain ranges crest well above 3,000 m, and precipitation rates can exceed 50 cm yr^{-1} (e.g. Lamke and Moore, 1965). Although the boundary of the Death Valley flow system, as delineated by Harrill et al. (1988), does not extend into this area, regional groundwater flow southward from central Nevada is a plausible source of the low $\delta^{18}O$ groundwater observed beneath Pahute Mesa.

Davisson et al. (1999) noted that regional groundwater $\delta^{18}O$ values show a systematic increase of nearly 5‰ going from 39° to 36°N latitude in Nevada. This variation is consistent with higher latitude recharge following continuous flow paths along north-south trending graben valleys and progressively mixing with more ^{18}O-enriched recharge at lower latitudes. New isotopic evidence presented in this paper is used to further test this model. These data suggest groundwater in the Pahute Mesa-Oasis Valley area is linked to a regional flow system with recharge areas as far north as 40°N latitude. We infer that much of this groundwater originates from the Railroad Valley regional flow system, located directly north of the central Death Valley flow system (Figure 1).

Hydrogeology of the Railroad Valley region, central Nevada

The 14,500 km^2 Railroad Valley flow system extends north-south almost 200 km from the Newark Valley to the central Railroad Valley playa, and includes the Little Smoky, Hot Creek and Big Sand Springs Valleys (see Figure 3; Rush and Everett, 1966; Van Denburgh and Rush, 1974; Harrill et al., 1988). The flow system is generally considered to terminate at the Railroad Valley playa, which is located within a deep structural depression that hosts a shallow geothermal system associated with productive oil fields (Hulen et al., 1994; Lund et al., 1993). Potentiometric data from deep volcanic aquifers indicate eastward groundwater flow from the northern Hot Creek Valley toward the central Railroad Valley (Dinwiddie and Schroder, 1971). However, water-level data for carbonate and volcanic rock aquifers are lacking for southern Railroad and Hot Creek Valleys, as well as Reveille and Kawich Valleys.

The Railroad Valley flow system approximately coincides with the western extent of the regional carbonate rock province (Dettinger et al., 1995). Carbonate rock exposures occur in many of the ranges that border the flow system (e.g. Stewart and Carlson, 1978) representing potential recharge connections to the carbonate aquifers underlying the alluvial and volcanic deposits in this region. Approximately 15 springs with discharge rates greater than 100 gpm (545 m^3d^{-1}) occur within the Railroad Valley system, nearly all of which are associated with the regional carbonate aquifer. The largest of these (Big Warm Spring, near Duckwater) has an average discharge rate in excess of 6000 gpm (32,700 m^3d^{-1}) (Van Denburgh and Rush, 1974). Little detailed isotope hydrology work has been done in central Nevada, despite the potential significance of this region as a groundwater recharge area. Previous studies that report isotopic data for the Railroad Valley region include Roth and Campana (1989) and Hulen et al. (1994).

Although the Railroad Valley and White River flow systems share a common geographic boundary (Figure 1), they exhibit some notable differences in hydrogeology. The White River flow system displays a continuous north to south water-level gradient in both the basin-fill and carbonate-rock aquifers (Thomas et al., 1986), and is underlain by a thick, laterally continuous carbonate aquifer along the entire flowpath length (Dettinger and Schaefer, 1996). In contrast, basin-fill aquifers in both the Newark and Railroad Valleys contain closed water-level contours in the central part of their basins, rather than a north-south gradient. Moreover, the distribution and lateral continuity of carbonate-rock aquifers is poorly constrained beneath much of the Railroad Valley flow system. Water-level data for the Railroad Valley flow system are examined in more detail later in this paper.

Sampling and Analytical Methods

Water samples were collected from >70 springs, creeks and wells in central Nevada between 1997 and 1999 within an area approximately bounded by latitudes 37°30' to 40°N and longitudes 115° to 117°30'W (Figure 3). Analytical results are presented in Table 1. Most samples collected south of latitude 37°30' are from an earlier data set (Rose et al., 1997), as discussed in Davisson et al. (1999). Water temperature, pH and conductivity values were measured in the field at the time of sample acquisition. Cation

samples were typically passed through a 0.45 μm filter and acidified with HNO_3 in the field; anion samples were untreated. Water chemistry was measured by ICP-AES for cations and ion chromatography for anions.

Carbon isotope samples were collected in glass bottles with teflon-lined septa caps, treated with $HgCl_2$ to prevent biological fractionation effects, and kept refrigerated until analysis. Dissolved inorganic carbon (DIC) was extracted by acidifying the sample under vacuum and cryogenically trapping the evolved CO_2 gas (McNichol et al., 1994). An aliqout of CO_2 is reduced to graphite and analyzed for ^{14}C on an accelerator mass spectrometer; the remaining CO_2 is analyzed for its $^{13}C/^{12}C$ ratio on an isotope ratio mass spectrometer. The ^{14}C results are reported as percent modern carbon (pmc) relative to a NBS oxalic acid standard (Stuiver and Polach, 1977). All data presented in subsequent figures are uncorrected pmc values.

Oxygen and hydrogen stable isotope samples were collected in glass bottles with air tight seals to prevent atmospheric exchange. Water samples were prepared for $^{18}O/^{16}O$ and $^{2}H/^{1}H$ (or D/H) ratio measurements by the CO_2 equilibration (Epstein and Mayeda, 1953) and zinc-reduction (Coleman et al., 1982) methods, followed by analysis on an isotope ratio mass spectrometer. Oxygen, hydrogen and carbon stable isotope ratios are reported in the standard delta (δ) notation as per mil (‰) deviations from V-SMOW (oxygen and hydrogen) or PDB (carbon) reference standards.

Results

Regional distribution of oxygen isotopes in central Nevada groundwater

The geographic distribution of groundwater $\delta^{18}O$ values in central Nevada is shown in Figure 3. Groundwater samples were collected over a broad region that includes the Railroad Valley flow system (the approximate boundaries of which are shown in Figure 3). Individual samples are identified with respect to sample type, and include springs associated with regional flow systems (principally the carbonate aquifer), samples from wells perforating basin fill aquifers, and mountain springs associated with perched aquifers (Figure 3). The latter are especially useful for characterizing the isotopic composition of local groundwater recharge. In general, the term "regional" groundwater will be used to refer to the carbonate aquifer system. However, we recognize that the basin fill and carbonate aquifers are sometimes interconnected, and that some large warm springs related to "regional" flow are not associated with the carbonate aquifer.

Groundwater $\delta^{18}O$ values are generally lower (more negative) at higher latitudes, or in proximity to high elevation recharge areas, in accordance with the strong temperature dependence of the isotope fractionation factor between water and water vapor (see Criss, 1999 for review). The physiography of Nevada tends to accentuate this effect. Relative to southern Nevada, the average surface elevation in central Nevada is ~1 km higher, and the mean annual temperature is 5 to 10°C cooler (Houghton et al., 1975). The $\delta^{18}O$ values of mountain springs clearly reflect these differences, averaging around -15.5‰ near latitude 39°N, and increasing to around -13‰ near latitude 38°N. In contrast, regional groundwaters have $\delta^{18}O$ values that average around -16‰ at latitude 39°N,

decreasing to only about -15‰ at latitude 37°15'N (beneath Pahute Mesa). Two details are worth emphasizing: (1) the $\delta^{18}O$ values of regional groundwaters are similar to those of local mountain springs in the upper part of the regional flow systems; and (2) the $\delta^{18}O$ values of the regional groundwaters increase much more slowly with decreasing latitude compared to local mountain springs.

In the upper part of the Railroad Valley flow system (NE section of Figure 3), local mountain springs have $\delta^{18}O$ values within about 0.5‰ of the regional carbonate springs. One possible interpretation of these data is that modern recharge provides a significant fraction of the regional flow in this area. However, regional springs near latitude 39°N are invariably slightly lower in $\delta^{18}O$ (more negative) than springs in adjacent mountain ranges. This ^{18}O-depletion may suggest that local recharge originates predominantly from the highest elevation parts of the ranges (up to 3500 m altitude), where winter snowfall amounts are greatest, and $\delta^{18}O$ values are the most depleted. Alpine spring samples collected above 2500 m are very poorly represented in the data set.

It should be noted that most of the mountain springs used to delineate recharge areas were sampled only once. The $\delta^{18}O$ values of these springs are generally thought to reflect the mean isotopic value of recharge for a local area, particularly for those with perennial discharge. However, Ingraham et al. (1991) showed that the $\delta^{18}O$ values of small springs in southern Nevada may fluctuate by several per mil in response to large precipitation events with "anomalous" isotopic values. Hence, a multi-year isotopic record for small-volume mountain springs is ultimately needed to constrain $\delta^{18}O$ variations in key recharge areas.

Whereas both regional and local (perched) groundwater $\delta^{18}O$ values generally become more ^{18}O-enriched (less negative) at lower latitudes, the latitudinal ^{18}O gradient in the regional carbonate flow system is quite gradual. For example, carbonate springs discharging along the Railroad Valley system vary from -16.7‰ in Newark Valley to -15.6‰ in the western Railroad Valley – a lateral distance of >150 km. This variation is consistent with a southward moving regional flow system that progressively mixes with local recharge along the length of its flowpath. A convincing argument can be made for this type of process in the White River flow system (cf. Davisson et al., 1999). The continuity in regional groundwater $\delta^{18}O$ values between the western Railroad Valley and Pahute Mesa suggests a possible southward extension of this flow system via Hot Creek, Reveille, and Kawich Valleys, and possibly Gold Flat. This would require additional mixing along the flowpath to increase the regional groundwater to $\delta^{18}O$ values around -15‰ beneath Pahute Mesa. Further evidence for this model is discussed in subsequent sections.

The relationship of the geothermal oil fields in central Railroad Valley to the regional flow system is uncertain, although there is some indication that central Railroad Valley is separated from regional flow to the west. Blue Eagle Spring in eastern Railroad Valley (38°34'N 115°32'W) has a $\delta^{18}O$ value of -15.1‰, and is isotopically similar to thermal waters associated with Railroad Valley oil fields (Hulen et al., 1994). In comparison, the carbonate warm springs emerging along the western side of Railroad Valley are notably

lower (more negative) in their $\delta^{18}O$ and δD values (up to 0.6‰ lower in $\delta^{18}O$ and 8‰ lower in δD).

Rush and Everett (1966) proposed that spring discharge along the western side of Railroad Valley originates from the southwestern part of adjacent Big Sand Springs Valley (see Figure 3). This is in accord with potentiometric data for deep boreholes in northern Hot Creek and Big Sand Springs Valleys (Dinwiddie and Schroder, 1971). The line of springs in western Railroad Valley may therefore indicate the presence of a structural barrier to eastward groundwater flow into central Railroad Valley. In general, these springs have isotopic values that are consistent with a southward continuation of flow from the vicinity of Big Warm Spring (38°57'N 115°46'W; $\delta^{18}O$ = -16‰) and Fish Creek Springs (39°17'N 116°02'W; $\delta^{18}O$ = -15.9‰). Some of this groundwater may also originate in the ranges northwest of Big Sand Springs Valley.

Figure 4 is a map identical to that of Figure 3, except that each sample point is now labeled with respect to water level (in feet above mean sea level). For springs and creeks, the water level is simply the local surface elevation; for wells, it is the static water level in the borehole. Recharge in the mountains bordering the flow system provides the hydrodynamic potential necessary to drive the regional flow system. Arrows show the *inferred* direction of water flow in the carbonate aquifers or deep fractured volcanic aquifers. Note that carbonate aquifer water levels are constrained by only ten carbonate springs in the Railroad Valley flow system. Assuming the entire water budget of the aquifer is not expended at these springs, the difference in the deep potentiometric head between this area and Pahute Mesa may favor continued southward transport. Although water-level data for the carbonate flow system are limited in extent, it does not appear to preclude the interpretations developed on the basis of geochemical evidence.

Finally, it is notable that anomalous pockets of low $\delta^{18}O$ groundwaters are observed in two locations within the study area. Groundwater samples with $\delta^{18}O$ values less than -16‰ were observed from a single well in the central Railroad Valley and a single well in Cactus Flat. The lack of isotopic continuity between these groundwaters and nearby regional carbonate aquifer groundwaters suggests the low-^{18}O waters may represent small, isolated accumulations of pluvial age groundwater "trapped" in basin fill aquifers that are not connected to regional flow systems. The $\delta^{13}C$ and ^{14}C results for these samples generally support this conclusion (see discussion).

Kinetic isotope effects during recharge

Craig (1961) observed that the $\delta^{18}O$ and δD values of worldwide precipitation samples conform to the empirical linear relationship $\delta D = 8\delta^{18}O + 10$, known as the global meteoric water line (GMWL). The y-intercept of the GMWL was subsequently defined as the deuterium excess, or *d*-value, where $d = \delta D - 8\delta^{18}O$ (Dansgaard, 1964). The *d*-value is inherited from the initial isotopic composition of an air mass, as determined by the moisture deficit above the air-sea interface where the air mass originates (Craig and Gordon, 1965; Merlivat and Contiac, 1975). Merlivat and Jouzel (1979) suggested the *d*-value may decrease to values < 10 during maximum glaciation, and that the meteoric

water line described by Pleistocene-age groundwater should reflect this shift. This model has been proposed to account for the conspicuous difference between the *d*-values of regional groundwaters and local precipitation in southern Nevada (e.g. White and Chuma, 1987; Benson and Klieforth, 1989). However, this is not the only process that can result in isotopic enrichments of $\delta^{18}O$ and δD values relative to the GMWL.

Kinetic isotope effects during evaporation also cause heavy isotope enrichments that may not be readily distinguishable from the *d*-value effect in regional groundwater systems. Evaporation effects are well documented in desert environments, and may occur both during the descent of rain droplets, and during runoff and infiltration processes (e.g. Gat and Dansgaard, 1972; Barnes and Allison, 1988; Friedman et al., 1992). In addition, isotope enrichment effects occur during snowpack aging due to mass transport processes within the snowpack (e.g. Stichler et al., 1981; Friedman et al., 1991), and have been widely observed in central Nevada snowpacks (Rose et al., 1999a).

Figure 5 is a plot of $\delta^{18}O$ versus δD values for groundwater samples from the Railroad Valley regional flow system. This plot excludes samples collected in other parts of central Nevada although similar relationships are observed throughout the region. Most samples have isotopic values that plot to the right of the GMWL, with *d*-values for individual samples ranging from +8 to -3, and an average *d*-value near +4. Note that the regional groundwaters exhibit a shift to the right of the GMWL that is comparable to that of the mountain springs in the recharge areas. This is consistent with a link between the regional groundwaters and *modern* recharge in central Nevada, and implies the observed shift off the GMWL is inherited during recharge. Note also that the isotopic values of the different aquifers are indistinguishable from one another, implying no net isotopic effect due to past climate.

A recent study comparing the stable isotope values of spring waters and precipitation in the Spring Mountains near Las Vegas concluded that springtime snowmelt accounts for up to 90% of all groundwater recharge in southern Nevada (Winograd et al., 1998). To test this idea for central Nevada, precipitation gauges were installed at four separate locations at elevations between 2130 and 2280 m, and integrated samples of cool and warm season precipitation were collected during 1999. Evaporation effects were minimized by adding mineral oil to the bottom of the gauges. Small mountain springs located near each of the gauge sites were also sampled at the conclusion of the summer precipitation cycle (end of October). The stable isotope results for these samples are shown on a plot of $\delta^{18}O$ vs. δD (Figure 6). In each case, the local springs have stable isotope values that are similar to the integrated value for winter precipitation, which is dominated by snowfall. Summer rainfall accounts for approximately 10 to 30% of the annual precipitation total, but apparently accounts for a nominal amount of the total recharge budget. However, whereas the winter precipitation samples plot very close to the GMWL, the spring waters are all shifted to the right of the line with *d*-values similar to the regional groundwater. An extended study is underway to determine the long-term variations in precipitation amount and isotopic values at these gauging sites.

Rose et al. (1999a) investigated isotopic variations in the winter snowpack in central Nevada to determine whether the observed enrichments in spring waters are related to processes during snowpack aging and ablation. At the time of peak accumulation (early March), most snowpacks showed physical evidence of snow metamorphism, including the development of depth hoar and grain clusters (Colbeck, 1987). Heat transfer from the ground to the overlying snowpack creates temperature and vapor pressure gradients within the snowpack (Benson and Trabant, 1973). Under these conditions, mass transport and recrystallization processes are accompanied by isotopic fractionation effects (Friedman et al., 1991), and the initial isotopic variability of individual snow layers is strongly attenuated (Judy, 1970).

Figure 7 shows a $\delta^{18}O$-δD plot for 28 bulk snow cores collected throughout central Nevada in March 1998 (Rose et al., 1999a). Many of the data points are shifted to the right of the GMWL, with an average *d*-value near +5. This value is essentially the same as for the groundwaters plotted in Figure 5. These results indicate that kinetic isotope effects related to vapor loss during snow metamorphism cause isotopic enrichments in the snowpack that are not observed when the snowfall is simply accumulated in a precipitation gauge (as shown in Figure 6). Although subsequent processes occurring during late stage melting of the snowpack can further modify the isotopic composition of recharge, this initial vapor loss *prior to melting* is a key factor determining the widely observed isotopic shift off the GMWL in Nevada groundwaters.

Carbon isotope data

The dissolved inorganic carbon (DIC) in groundwater is commonly derived from two main sources: the biochemical production of CO_2 gas in the soil zone, and the chemical dissolution of carbonate minerals. Differences in the $\delta^{13}C$ values of these source materials provide insight into their relative contributions to the total DIC inventory. Biogenic CO_2 has $\delta^{13}C$ values that range from approximately -27 to -12‰, depending on the type of plant material (Deines, 1980; Cerling, 1984), whereas marine carbonate rocks in Nevada have $\delta^{13}C$ values between -2 and +3‰ (Thomas et al., 1996). Deep pedogenic carbonates (>50 cm depth) in southern Nevada vary in $\delta^{13}C$ from about -9 to +4‰ and show a systematic ^{13}C depletion with increasing elevation (Quade et al., 1989).

The application of ^{14}C measurements to dating groundwater requires the careful evaluation of processes influencing the evolution of DIC along a flowpath (see Mook, 1980 for review). A number of different models have been proposed to quantify these processes (e.g. Fontes, 1983). In practice, however, it is difficult to account for *all* the chemical processes in complex regional flow systems. A large amount of ^{14}C dilution (up to 50%) can occur in the recharge zone by the neutralization of dissolved soil CO_2 ($^{14}C \sim 100$ pmc) with ^{14}C-absent carbonate minerals ($^{14}C \sim 0$ pmc). Further reaction with carbonate minerals may occur along the flowpath due to processes such as ion exchange or the addition of deep (magmatic) CO_2 to the system (e.g. Andrews et al., 1994; Rose and Davisson, 1996). Oxidation of organic material can add bicarbonate to the system that contains no ^{14}C but has a $\delta^{13}C$ value similar to the soil gas (Pearson and Hanshaw, 1970). Multiple recharge sources and mixing along the flowpath further complicate ^{14}C

age correction models (Davisson et al., 1999). For the present study, these various processes are not sufficiently well constrained to permit the calculation of meaningful ^{14}C ages. Nevertheless, it is possible to gain insight into some of the more important water-rock processes by examining regional variations in carbon isotopes and water chemistry.

Figure 8 shows a plot of $\delta^{13}C$ vs. ^{14}C data for the Railroad Valley flow system. The results are separated into three groups representing samples from the regional carbonate aquifer, basin fill aquifers, and mountain springs (perched aquifers). The data show a general trend toward decreasing ^{14}C with increasing $\delta^{13}C$ values that is consistent with chemical dissolution or isotopic exchange with carbonate rocks along the flowpath. Mountain spring samples have $\delta^{13}C$ values between about -8 and -12‰, and most have ^{14}C values >75 pmc. We assume most of the mountain spring samples have undergone very little radioactive decay of ^{14}C, and the observed decreases in ^{14}C (to values <100 pmc) mostly reflect dilution from carbonate mineral dissolution during infiltration. One mountain spring (Snowball Ranch Spring) has a rather low ^{14}C value (19 pmc) and Ca-HCO_3 water chemistry that suggest substantial carbonate reaction, but a light $\delta^{13}C$ value (-9.8‰) and relatively low pH value (6.9) that suggest recent infiltration. These data may indicate dissolution/exchange with carbonate under partially open system conditions, although other interpretations are also possible.

Groundwater samples from the basin fill aquifers are generally lower in ^{14}C than the mountain springs, and in some cases have carbon isotope signatures similar to the carbonate aquifer springs (Figure 8). The two basin fill samples with the highest $\delta^{13}C$ values are both from Hot Creek Valley. One is from a deep well in northern Hot Creek Valley (HTH-1, total depth = 1129 m) that perforates tuffaceous sediments (Chapman et al., 1994). The other is from a shallow well in a groundwater discharge area at Twin Springs Ranch, at the southern end of the Pancake Range. The low ^{14}C and high $\delta^{13}C$ values for these samples (see Table 1) suggest a possible hydrologic link to the regional carbonate aquifer.

Groundwater from an artesian well in the central Railroad Valley (total depth = 367 m) has a $\delta^{13}C$ value of -6‰ and a ^{14}C value < 1 pmc (Figure 8). The well perforates alluvium that overlies productive carbonate-hosted oil fields. Borehole temperature vs. depth profiles and mineralogical studies of drill core samples indicate the carbonate aquifer is isolated from the overlying alluvial aquifer in this part of Railroad Valley (Hulen et al., 1994). Compared to other groundwaters in the central Railroad Valley, this sample has an unusually low $\delta^{18}O$ value (-16.6‰) that is similar to groundwater from Newark Valley. However, available evidence suggests the basin fill aquifers are not interconnected between the Newark and Railroad Valleys (Harrill et al., 1988) and this sample may therefore represent "paleowater". Its low ^{14}C value suggests either older Pleistocene recharge, modification of the ^{14}C value by water-rock interaction, or introduction of ^{14}C-depleted CO_2 from the underlying oil field.

Springs associated with the regional carbonate aquifer vary in $\delta^{13}C$ from about -7.1 to -1.5‰ with ^{14}C values between 30 and 2 pmc (Figure 8). The carbonate springs do not show a simple progression toward lower ^{14}C values in a southward direction, probably

because they do not occur along a single flowpath. For example, three carbonate springs located near Duckwater (Figure 3) show a significant variation in ^{14}C (between 3 and 30 pmc), in $\delta^{13}C$ (between -7.1 and -2.9‰) and in temperature (13 to 34°C). These springs occur in an area where Paleozoic carbonate rocks are exposed in low hills along the valley floor, and likely represent groundwater that is forced to the surface by structural barriers. The data variations imply the presence of multiple flowpaths at different depths within the carbonate rocks in this area.

Simonson Warm Spring in Newark Valley is located in the uppermost part of the Railroad Valley flow system, but has a ^{14}C value of 8 pmc, and $\delta^{13}C$ value of -2.5‰. The low $\delta^{18}O$ value for this spring (-16.7‰) may indicate recharge in the southern Ruby Mountains. Even so, it is difficult to envision a flowpath length much greater than 30 or 40 km between the recharge area and the spring. This suggests a significant amount of carbon isotope exchange occurs between the DIC and the carbonate rock along a relatively short path length. Davisson et al. (1999) reached the same conclusion for the springs in the upper part of the White River flow system.

There is a tendency for the carbonate springs with higher $\delta^{13}C$ values to be associated with higher water temperatures. Springs from carbonate aquifers throughout central and southern Nevada show a non-linear increasing trend in $\delta^{13}C$ with temperature (Figure 9; data from this study and Rose et al., 1997). The increasing $\delta^{13}C$ values reflect a shift toward isotopic equilibrium between the DIC and the carbonate rock. At 35°C, dissolved HCO_3 is depleted in ^{13}C by about 1.4‰ relative to $CaCO_3$ under equilibrium conditions (Salomons and Mook, 1986). Thus, many of the warm springs are probably close to equilibrium with the carbonate rock, assuming a $\delta^{13}C$ value near 0‰ for the rock. The springs with high $\delta^{13}C$ values tend to also have higher DIC concentrations, implying greater amounts of carbonate rock dissolution at higher temperatures. This is actually *opposite* to the solubility-temperature relationship for calcite (e.g. Stumm and Morgan, 1981). Water chemistry data (discussed below) suggests that cation exchange with clay minerals may help drive this process. In addition, it is notable that all four springs with water temperatures > 40°C in Figure 9 have pH values < 7, implying high levels of dissolved CO_2.

Discussion

Chemical and isotopic evidence for a Railroad Valley-Pahute Mesa regional flowpath

The isotopic results presented up to this point are generally consistent with a continuous regional flowpath extending from the upper Railroad Valley flow system (Newark Valley) southward into western Railroad Valley and Hot Creek Valley. The regional carbonate springs have $\delta^{18}O$ and δD values that can be reasonably derived from *modern* snowmelt recharge in high elevation areas of central Nevada. These data do not appear to be consistent with pluvial period recharge processes. Carbon isotope data indicates rapid reaction of the DIC in groundwater with the carbonate host rock, and relatively low ^{14}C values (<10 pmc) are found in regional warm springs within the northernmost part of the flow system (Newark Valley). Regional carbonate springs in the western Railroad Valley, 150 km south of Newark Valley, show similarly low ^{14}C values between 2 and 6

pmc. The comparatively small ^{14}C difference over 150 km of regional flow implies mixing with young groundwater recharge along the flowpath in order to maintain a non-zero ^{14}C content (see Davisson et al., 1999). Gradual increases in carbonate spring $\delta^{18}O$ values along the flowpath are consistent with this mixing argument.

If regional groundwater beneath Pahute Mesa originated from the western part of the Railroad Valley flow system, then mixing along the flow path can readily account for the increase in $\delta^{18}O$ values from approximately -15.5‰ in the western Railroad Valley to near -15.0‰ beneath Pahute Mesa. Groundwater discharge at Oasis Valley constrains the approximate volume of water flowing *out* of Pahute Mesa (8,000 ac-ft/yr; Reiner et al., 1999). Regional inflow to Pahute Mesa is ~5,500 ac-ft/yr (Blankennagel and Weir, 1973) implying a "local" recharge amount of ~2,500 ac-ft/yr. For simple two-component mixing:

$$\delta^{18}O_{mix} = \delta_1 X_1 + \delta_2 X_2 \qquad (1)$$

where δ_1 and δ_2 are the isotopic values of the two components, X_1 and X_2 are their fractional mixing proportions, and $X_1 + X_2 = 1$. Assuming the regional inflow has a $\delta^{18}O$ value of -15.5‰, and "local" recharge has a $\delta^{18}O$ value of -13.5‰ (e.g. Figure 2, perched aquifer data), then:

$$\delta^{18}O_{mix} = (-15.5)(5500/8000) + (-13.5)(2500/8000) = -14.88‰.$$

This is similar to $\delta^{18}O$ values observed in wells beneath Pahute Mesa (Figure 3), and in the Oasis Valley discharge area (White and Chuma, 1987; Rose et al., 1999b).

Hydrogeologic and isotopic data that would confirm the proposed regional flowpath is presently unavailable between 38° and 37°15'N latitude. Geologic evidence suggests that carbonate rocks may underlie basin-fill deposits as far south as Kawich Valley (Ekren et al., 1971). However, all of the deep wells on Pahute Mesa are completed in fractured volcanic rocks, and the link to the regional carbonate flow system is by inference. Groundwater beneath Pahute Mesa also has a different chemistry and carbon isotope content than the regional carbonate aquifer to the north. The chemistry of Pahute Mesa groundwater is dominated by Na^+ and HCO_3^- ions (Blankennagel and Weir, 1973), and is lower in Ca^{2+} and HCO_3^- compared to the carbonate aquifer groundwaters. In addition, Pahute Mesa groundwaters have ^{14}C values ranging from 8 to 21 pmc, and $\delta^{13}C$ values between -1.4 and -9.2‰ (Table 1). The increase in ^{14}C values relative to the Railroad Valley carbonate aquifer requires an added component of "younger" water.

Comparison of water chemistry data for the Railroad Valley and Pahute Mesa regional aquifers provides insight into possible processes relating these flow systems. Figure 10 is a plot of HCO_3^- vs. Na^+ ion concentrations for both aquifer systems. In general, the Railroad Valley carbonate springs show a systematic increase in HCO_3^- with Na^+ that is closely related to distance along the proposed regional flowpath. One possible mechanism to account for this variation is a cation exchange process wherein Ca^{2+} is removed from solution by ion exchange on clay minerals, according to the exchange reaction:

$$2NaX + Ca^{2+} = CaX_2 + 2Na^{+} \qquad (2)$$

where X denotes an exchange site on the clay minerals (Pearson and Swarzenki, 1974; Andrews et al., 1994). During this process, HCO_3^- will increase even in calcite-saturated waters, because the removal of Ca^{2+} drives the solution toward calcite undersaturation, allowing further calcite dissolution. This process is therefore consistent with the observed increases in groundwater $\delta^{13}C$ values. It should be noted that while the highest ion concentrations occur in the southernmost carbonate spring (Warm Springs at 38°11'N), the $\delta^{18}O$ value of this spring (-14.4‰) indicates a different origin from all central Railroad Valley samples. The high Na^+ concentration in this sample may imply additional water-rock interaction with volcanic rocks located near the spring.

Repetition of the ion exchange process (equation 2) along a carbonate aquifer flowpath will cause a correlated increase in Na^+ with HCO_3^- (Figure 10), while Ca^{2+} should at most remain constant. However, on a plot of Na^+ vs. Ca^{2+} concentrations (Figure 11), the carbonate springs show an increase in Na^+ with Ca^{2+} along a least-squares regression line of slope 2.18 ($r = 0.90$). This slope is in close agreement with the stoichiometry of the cation exchange reaction. We propose that an independent process may cause additional calcite to dissolve while the exchange reaction controls the observed Na^+ to Ca^{2+} ratio. Some of the carbonate springs, especially those with higher temperatures, exhibit relatively low pH values (< 7). One possible explanation is that CO_2 is added to the system, possibly from a deep source. Low pH values associated with high CO_2 concentrations will enhance calcite dissolution rates, and may account for the increasing Ca^{2+} concentrations in the carbonate groundwaters (Figure 11).

Variations in chemical and isotopic data suggest that two processes may occur during the proposed transition from carbonate to volcanic aquifer lithologies: (1) calcite precipitation, and (2) mixing with local recharge. Groundwater from the Pahute Mesa volcanic aquifer is significantly lower in both HCO_3^- and Ca^{2+} compared to most carbonate springs, suggesting that calcite is precipitated. This process would be driven by the equilibrium state of the reaction $Ca^{2+} + CO_3^{2-} = CaCO_3$. If the groundwater is no longer in contact with a large calcite reservoir, then this reaction will be driven toward the right, according to LeChatelier's principle. Calcite saturation index values indicate that most carbonate aquifer groundwaters are calcite saturated whereas most volcanic aquifer groundwaters are not. Benedict et al. (1999) examined calcite veins and fracture linings from deep boreholes on Pahute Mesa and found the calcite $\delta^{13}C$ and $\delta^{18}O$ values were consistent with deposition from thermal waters originating from the carbonate aquifer.

Groundwater mixing may account for variations in Na^+ vs. Ca^{2+} and HCO_3^- in the volcanic aquifer (Figures 10 and 11) following calcite deposition. Na^+ is conservative during groundwater flow, and is not readily removed once it is in solution. Continuity along a flowpath between the carbonate and volcanic aquifers therefore requires that the Na^+ concentration cannot decrease, except by mixing with a more dilute groundwater. Mixing with chemically dilute recharge may account for the range in Na^+ concentrations in Pahute Mesa groundwater. Observed increases in $\delta^{18}O$ and ^{14}C values between

Railroad Valley and Pahute Mesa are consistent with mixing of local recharge and regional groundwater. While the water chemistry data does not prove a flowpath linkage between the Railroad Valley and Pahute Mesa aquifer systems, the data are generally consistent with the proposed flowpath.

A possible analog for the chemical processes described above is found near Yucca Mountain, ~40 km south of Pahute Mesa. In the Yucca Mountain area, the hydraulic head measured in the deep carbonate aquifer is 20 m higher than the head in the overlying volcanic aquifer, indicating an upward groundwater flow potential (Bredehoeft, 1997). Groundwater temperature anomalies in the volcanic aquifer are consistent with upwelling of warm (57°C) carbonate aquifer water along fault zones (Fridrich et al., 1994). Groundwater from the carbonate aquifer is high in Ca^{2+}, Na^{+} and HCO_3^{-} compared to groundwater in the overlying volcanic aquifer (e.g. Benson and McKinley, 1985). This *may* suggest the occurrence of calcite precipitation and mixing processes similar to those inferred beneath Pahute Mesa, provided the source of groundwater in the volcanic aquifer is from the underlying carbonate aquifer.

Hydrologic mass balance

Estimated groundwater budgets for the Railroad Valley flow system range from approximately 75,000 to 134,000 ac-ft yr^{-1} (Rush and Everett, 1966; Van Denburgh and Rush, 1974; Roth and Campana, 1989; Prudic et al., 1995). A useful summary is provided in Roth and Campana (1989), who estimate an annual hydrologic mass balance of 115,000 ac-ft yr^{-1} (1.4×10^8 m^3yr^{-1}). In general, these models predict that recharge from precipitation and subsurface inflow is balanced by discharge from evapotranspiration and spring flow. It is notable that Van Denburgh and Rush (1974) estimated that only 4 percent of the annual precipitation budget recharges the groundwater system. This value may significantly underestimate the actual recharge rate, given that previous models assumed regional flow did not extend beyond the boundaries of the central Railroad Valley sub-basin. Blankennagel and Weir (1973) estimated that approximately 5,500 ac-ft (6.8×10^6 m^3) of groundwater enters Pahute Mesa annually from the north. Uncertainties in the Railroad Valley mass balance far exceed the amount necessary to account for this underflow.

It is instructive to evaluate the volume of water stored within the carbonate aquifer in Railroad Valley in order to estimate the length of time required for the system to turnover (assuming a well-connected fracture network). The moderately high permeabilities in the carbonate aquifer are the result of fracturing during extensional tectonism and solution enlargement. Effective fracture porosities for the carbonate aquifer are typically ≤0.5%, whereas the effective intercrystalline porosity averages around 1% (Winograd and Thordarson, 1975; U.S. Department of Energy, 1997). The simplest approach is to assume that the entire Railroad Valley flow system is uniformly underlain by a certain thickness of permeable carbonate rock. If we infer that most groundwater flow occurs in the upper 2000 m of the aquifer, and apply an effective porosity of 1%, then the effective volume of water in storage is 14,500 km^2 x 2 km x 0.01 = 290 km^3 (or 2.9×10^{11} m^3).

We will assume a hydrologic mass balance of 1.4 x 10^8 m^3yr^{-1} for the Railroad Valley system (Roth and Campana, 1989). In the process of calibrating a regional-scale conceptual model, Prudic et al. (1995) achieved a reasonable water balance by assuming that ~32% of the total influx enters the carbonate aquifer system, with the remainder going to the alluvial aquifers. Using this value, an annual recharge budget of 4.5 x 10^7 m^3yr^{-1} is obtained for the carbonate aquifer. Dividing this number into the estimated volume of water in storage gives a mean turnover rate of 6,400 years. This suggests the effective volume of water within interconnected fractures could have turned over in Holocene time. This value is consistent with the range of flow rates predicted by permeability and hydraulic gradient data. In reality, groundwater flow is not homogeneously distributed throughout the carbonate rock, but occurs preferentially along a few discrete fractures in more permeable layers (e.g. Mifflin and Hess, 1979). Hence, groundwater turnover rates could be higher than implied by this simple calculation. For example, decreasing the fracture porosity to 0.1% causes a corresponding order-of-magnitude increase in the estimated turnover rate (to 640 years).

Carbonate springs in the Railroad Valley flow system have water temperatures as high as 67°C. Assuming a maximum flow depth of ~3,000 m (e.g. 2,000 m of carbonate rock overlain by ~1,000 m of basin fill) and a geothermal gradient of 30°C/km, groundwater temperatures ≥100°C are expected. The lack of higher spring temperatures may suggest circulation depths <3,000 m, or it may indicate the spring waters are not from the maximum depth, or that they cooled during ascent. Sass et al. (1971) report a relatively wide range in measured vertical temperature gradients in central Nevada, ranging from 7 to 52°C/km. They also note a large region of low heat flow (<1.5 μcal cm^{-2} s^{-1}) in central Nevada (the "Eureka low") which is centered on the Railroad Valley flow system. Sass et al. (1971) propose the Eureka low is related to interbasin groundwater flow "with appreciable vertical velocity components to depths of about 3 km". This suggests that regional flow may advectively transport a sizable fraction of the heat budget in this region.

Implications for pluvial recharge and the distribution of Pleistocene age groundwater

There is good evidence to suggest that the effective moisture in the Great Basin increased during the last glacial-interglacial transition, between approximately 18,000 to 9,000 yr before present time. We could infer that groundwater recharge rates increased in central Nevada during that time. Estimates of the full glacial mean-annual temperature depression in the Great Basin range from ~3 to 8°C (Dohrenwend, 1984; Claassen, 1986; Spaulding and Graumlich, 1986; Benson and Klieforth, 1989). From these estimates, we can calculate the corresponding depletion in the $\delta^{18}O$ value of late Pleistocene recharge. Precipitation $\delta^{18}O$ values vary as a function of mean monthly surface temperature along a line with a slope between approximately 0.52 and 0.57 (Yurtsever, 1975; Van der Straaten and Mook, 1983; Claassen, 1986). Hence, an average temperature decrease of 5°C at full glacial maximum would presumably cause precipitation $\delta^{18}O$ values to decrease by around -2.6 to -2.8‰. This decrease is comparable to that observed in other basins at similar latitudes in the western U.S. (cf. Phillips et al., 1986). If we assume that recharge from winter precipitation currently averages around -15.5‰ at latitude 39°N, we

would predict that similar recharge at glacial maximum would have a $\delta^{18}O$ value < -18‰. Even assuming a conservative temperature shift of only 3°C, we still arrive at a $\delta^{18}O$ value < -17‰. Isotopic depletions of this magnitude are not observed in the carbonate aquifer groundwaters at this latitude, nor is there evidence for similarly depleted groundwater in carbonate aquifers at lower latitudes.

Throughout this paper, we have argued that the observed variations in regional groundwater $\delta^{18}O$ and ^{14}C values can be explained by a combination of Holocene age recharge, groundwater mixing, and water-rock interaction processes. The continuity in regional groundwater $\delta^{18}O$ values over distances up to 300 km (Newark Valley to Pahute Mesa) suggests a well-connected flowpath and relatively rapid transport through the system. In general, the data suggest that pluvial age groundwater either is no longer represented in most regional carbonate and basin-fill aquifers, or it is "lost" in the mixture and difficult to unequivocally identify from existing evidence. Mass balance calculations further indicate that regional groundwater transport rates are too high to store significant amounts of pluvial recharge.

Closed basins are more favorable locations for trapping pluvial age groundwater, particularly in areas that presently receive relatively little recharge. We have noted two locations within the study area where the isotopic data suggest this may have occurred: central Railroad Valley and Cactus Flat. The latter case was briefly discussed in Davisson et al. (1999) who noted the unusually low $\delta^{18}O$ value of groundwater from a well completed in this alluvial basin. Roller Coaster Well in Cactus Flat (37°43'N) has a $\delta^{18}O$ value of -16‰, and a low *d*-value of -1. Springs associated with local perched aquifers in the Kawich and Monitor Ranges have present day $\delta^{18}O$ values near -13.5‰, implying that recharge during the glacial maximum could have been near -16‰, assuming a 5°C paleo-temperature shift. In this case, the stable isotope data fit nicely with the inferred pluvial age climate conditions.

Further illustrations of pluvial age groundwater stored in closed basins are found in the literature. For example, Thomas et al. (1989) studied the geochemical and isotopic evolution of groundwater from a hydrologically closed basin in west central Nevada, and found that less evaporated basinal groundwaters are significantly depeleted in their $\delta^{18}O$-δD values relative to modern recharge. Correcting these data to the GMWL along the observed evaporation trajectory gives an initial $\delta^{18}O$ value near -19‰, which is 3 to 4‰ lighter than modern recharge in this area. In another set of studies, Davisson and Criss (1993, 1996) observed that deep Pleistocene age groundwaters in the closed basin of Sacramento Valley, California have $\delta^{18}O$ values ~2.5‰ depleted relative to shallow, modern recharge. Corrected ^{14}C ages for Sacramento Valley groundwaters suggest turnover rates for this alluvial basin are at least a factor of 2-3 slower than in the Railroad Valley regional carbonate aquifer.

Conclusions

Isotopic and chemical data presented in this study are consistent with the hypothesis that predominantly Holocene-age groundwater enters the north-central Death Valley flow system along regional flowpaths originating from central Nevada. We have proposed that groundwater originates from recharge areas in the Railroad Valley flow system, moves southward along regional carbonate aquifers, and then transitions to fractured volcanic aquifers in the vicinity of the Nevada Test Site (Figure 1). Supporting evidence for this model includes the following:

(1) The Railroad Valley flow system is rimmed by high elevation recharge areas containing significant exposures of carbonate bedrock. These areas receive relatively large amounts of winter snowfall, which is rapidly recharged in the spring. Water-level data for regional carbonate springs in the Railroad Valley flow system and wells on Pahute Mesa (Figure 4) are generally consistent with a continuous regional flowpath.

(2) Groundwater $\delta^{18}O$ values for carbonate springs of the Railroad Valley flow system are similar to $\delta^{18}O$ values of modern precipitation and mountain springs in central Nevada. The regional distribution of $\delta^{18}O$ values defines a continuous north-to-south flowpath that extends into the Pahute Mesa-Oasis Valley region of the Death Valley flow system. Modest increases in $\delta^{18}O$ along this flowpath are inferred to indicate mixing with ^{18}O-enriched "local" recharge at lower latitudes.

(3) Carbon isotope and major ion data indicate extensive water-rock interaction along the carbonate aquifer flowpaths, with higher solute concentrations and greater ^{13}C enrichments generally occurring in warmer springs at lower latitudes. Inferred reaction processes include cation exchange on clay minerals coupled with calcite dissolution. A "deep" CO_2 source may be required to account for relatively low pH values (< 7) observed in some high temperature, chemically evolved carbonate springs. Removal of calcite from chemically evolved carbonate aquifer groundwater can yield a modified groundwater chemistry similar to that observed in volcanic aquifers beneath Pahute Mesa. Subsequent mixing with local recharge may account for variations in the chemistry and carbon isotope content of the Pahute Mesa groundwater.

(4) Hydrologic mass balance considerations suggest that regional groundwater transport rates are too high to store significant amounts of pluvial recharge in the regional carbonate aquifer. Pleistocene age water remaining in the regional flow system is probably highly mixed, and indistinguishable from Holocene age groundwater. Limited evidence for pristine Pleistocene age groundwater is found within two closed alluvial basins located within the study area. In each case, the groundwater $\delta^{18}O$ values are significantly depleted relative to local recharge *and* regional flow.

Although the evidence outlined above is consistent with the proposed regional flow system, we cannot preclude other possible flowpath models. For example, some (or all) of the regional flow entering Pahute Mesa could originate from the region just to the west of the Railroad Valley flow system (via Stone Cabin Valley and Cactus Flat; see Figure

3). However, few of the springs in this area have $\delta^{18}O$ values *less than* the Pahute Mesa groundwaters, suggesting there could be little mixing with isotopically heavier groundwater along this flow path. In addition, the extent to which carbonate rocks underlie the region west of the Railroad Valley flow system is poorly determined. A chemical analysis of the water sampled from a warm spring in Stone Cabin Valley does not suggest interaction with carbonate rocks. Hence, if regional flow does occur in this area, it may be hosted entirely in fractured volcanic aquifers. At this time, there is not a compelling reason to believe that such a flowpath is *more* plausible than the proposed Railroad Valley flowpath, but it clearly warrants further consideration.

In order to more fully test the ideas proposed in this study, a broader range of evidence is required, particularly in terms of hydrogeologic data (e.g. geologic and hydraulic data from boreholes) and geochemical interpretations (e.g. flowpath modeling of chemical data). The development of deep boreholes in the region between the southern Railroad Valley and Pahute Mesa (e.g. Kawich Valley) would be particularly beneficial for obtaining hydraulic, geologic, and geochemical data within the inferred transition zone between carbonate and volcanic aquifers. These evaluations are beyond the scope of this study, although we hope that this paper may provide a framework for developing future studies of regional groundwater flowpaths in central and southern Nevada.

Acknowledgements

This manuscript was significantly improved by thoughtful reviews provided by Jim Thomas, Brent Newman, and one anonymous reviewer. We thank Dave Smith, Ron Hershey, Chris Benedict, and Bob Criss for fruitful discussions regarding this work. Gail Eaton contributed valuable assistance in map preparation, field work and laboratory analyses. Additional field assistance was provided by Jackie Kenneally, Brenda Ekwurzel, and Ross Williams. Funding for this project was provided by the Hydrologic Resources Management Program and Underground Test Area Project of the U.S. Department of Energy, Nevada Operations Office. This work was performed under the auspices of the U.S. Department of Energy by Lawrence Livermore National Laboratory under contract number W-7405-Eng-48.

References

Andrews, J.N., Fontes, J.Ch., Aranyossy, J.F., Dodo, A., Edmunds, W.M., Joseph, A., and Travi, Y., 1994, The evolution of alkaline groundwaters in the continental intercalaire aquifer of the Irhazer Plain, Niger: Water Resources Research, v. 30, p. 45-61.

Barnes, C.J., and Allison, G.B., 1988, Tracing of water movement in the unsaturated zone using stable isotopes of hydrogen and oxygen: Journal of Hydrology, v. 100, p. 143-176.

Benedict, F.C., Rose, T.P., and Eaton, G.F., 1999, Fracture-coating mineral phase characterization in the Pahute Mesa-Oasis Valley flow system [abs.]: Eos (Transactions, American Geophysical Union), v. 80, p. 327.

Benson, C.S., and Trabant, D.C., 1973, Field measurements on the flux of water vapour through dry snow, In Proceedings, Symposia on the Role of Snow and Ice in Hydrology, Banff, September 1972, Vol. 1: Geneva, Unesco-WMO-IAHS Publication no. 107, p. 291-298.

Benson, L.V., and McKinley, P.W., 1985, Chemical composition of ground water in the Yucca Mountain area, Nevada, 1971-1984: U.S. Geological Survey Open-File Report 85-484, 10 p.

Benson, L.V., and Klieforth, H., 1989, Stable isotopes in precipitation and groundwater in the Yucca Mountain region, southern Nevada: paleoclimatic implications, *in* D.H. Peterson, ed., Aspects of Climate Variability in the Pacific and Western Americas: American Geophysical Union, Geophysical Monograph Series, v. 55, p. 41-59.

Benson, L.V., Currey, D.R., Dorn, R.I., Lajoie, K.R., Oviatt, C.G., Robinson, S.W., Smith, G.I., and Stine, S., 1990, Chronology of expansion and contraction of four Great Basin lake systems during the past 35,000 years: Palaeogeography, Palaeoclimatology, Palaeoecology, v. 78, p. 241-286.

Benson, L.V., Burdett, J.W., Kashgarian, M., Lund, S.P., Phillips, F.M., and Rye, R.O., 1996, Climatic and hydrologic oscillations in the Owens Lake Basin and adjacent Sierra Nevada, California: Science, v. 274, p. 746-749.

Benson, L.V., Lund, S.P., Burdett, J.W., Kashgarian, M., Rose, T.P., Smoot, J.P., and Schwartz, M., 1998, Correlation of late-Pleistocene lake-level oscillations in Mono Lake, California, with North Atlantic climate events: Quaternary Research, v. 49, p. 1-10.

Blankennagel, R.K., and Weir, J.E., Jr., 1973, Geohydrology of the eastern part of Pahute Mesa, Nevada Test Site, Nye County, Nevada: U.S. Geological Survey, Professional Paper 712-B, 35 p.

Bredehoeft, J.D., 1997, Fault permeability near Yucca Mountain: Water Resources Research, v. 33, p. 2459-2463.

Cerling, T.E., 1984, The stable isotopic composition of modern soil carbonate and its relationship to climate: Earth and Planetary Science Letters, v. 71, p. 229-240.

Chapman, J.B., Mihevc, T.M., and Lyles, B.F., 1994, The application of borehole logging to characterize the hydrogeology of the Faultless site, Central Nevada Test Area: Desert Research Institute, Water Resources Center Publication No. 45119, 36 p.

Claassen, H.C., 1986, Late-Wisconsin paleohydrology of the west-central Amargosa Desert, Nevada, U.S.A.: Chemical Geology, v. 58, p. 311-323.

Colbeck, S.C., 1987, Snow metamorphism and classification, *in* Jones, H.G., and Orville-Thomas, W.J., eds., Seasonal Snowcovers: Physics, Chemistry, Hydrology: Dordrecht, Reidel Publishing, p. 1-35.

Coleman, M.L., Sheperd, T.J., Durham, J.J., Rouse, J.E., and Moore, G.R., 1982, Reduction of water with zinc for hydrogen isotope analysis: Analytical Chemistry, v. 54, p. 993-995.

Craig, H., 1961, Isotopic variations in meteoric waters: Science, v. 133, p. 1702-1703.

Craig, H., and Gordon, L.I., 1965, Deuterium and oxygen-18 variations in the ocean and the marine atmosphere, *in* Proceedings, Symposium on Marine Geochemistry, Narraganset Marine Laboratory, University of Rhode Island Publication, v. 3, p. 277-374.

Criss, R.E., 1999, Principles of stable isotope distribution: New York, Oxford University Press, 254 p.

D'Agnese, F.A., Faunt, C.C., Turner, A.K., and Hill, M.C., 1997, Hydrogeologic evaluation and numerical simulation of the Death Valley regional ground-water flow system, Nevada and California: U.S. Geological Survey, Water-Resources Investigations Report 96-4300, 124 p.

Dansgaard, W., 1964, Stable isotopes in precipitation: Tellus, v. 16, p. 436-468.

Davisson, M.L., and Criss, R.E., 1993, Stable isotope imaging of a dynamic groundwater system in the southwestern Sacramento Valley, California, USA: Journal of Hydrology, v. 144, p. 213-246.

Davisson, M.L., and Criss, R.E., 1996, Stable isotope and groundwater flow dynamics of agricultural irrigation recharge into groundwater resources of the Central Valley, California, *in* Proceedings, Symposium on Isotopes in Water Resources Management, Vienna, 20-24 March 1995, Volume 1: International Atomic Energy Agency, p. 405-418.

Davisson, M.L., Smith, D.K., Kenneally, J., and Rose, T.P., 1999, Isotope hydrology of southern Nevada groundwater: stable isotopes and radiocarbon: Water Resources Research, v. 35, p. 279-294.

Deines, P., 1980, The isotopic composition of reduced organic carbon, *in* Fritz, P., and Fontes, J.Ch., eds., Handbook of Environmental Isotope Geochemistry, Volume 1, The Terrestrial Environment, A: Amsterdam, Elsevier, p. 329-406.

Dettinger, M.D., Harrill, J.R., Schmidt, D.L., and Hess, J.W., 1995, Distribution of carbonate-rock aquifers and the potential for their development, southern Nevada and adjacent parts of California, Arizona and Utah: U.S. Geological Survey, Water-Resources Investigations Report 91-4146, 100 p.

Dettinger, M.D., and Schaefer, D.H., 1996, Hydrogeology of structurally extended terrain in the eastern Great Basin of Nevada, Utah, and adjacent states from geologic and geophysical models. U.S. Geological Survey, Hydrologic Investigations Atlas, HA-694-D, 1 sheet.

Dinwiddie, G.A., and Schroder, L.J., 1971, Summary of hydraulic testing in and chemical analyses of water samples from deep exploratory holes in Little Fish Lake, Monitor, Hot Creek, and Little Smoky Valleys, Nevada: U.S. Geological Survey Report, USGS-474-90, 70 p.

Dohrenwend, J.C., 1984, Nivation landforms in the western Great Basin and their paleoclimatic significance: Quaternary Research, v. 22, p. 275-288.

Domenico, P.A., and Schwartz, F.W., 1990, Physical and chemical hydrogeology: New York, John Wiley and Sons, 824 p.

Eakin, T.E., 1966, A regional interbasin groundwater system in the White River area, southeastern Nevada: Water Resources Research, v. 2, p. 251-271.

Ekren, E.B., Anderson, R.E., Rogers, C.L., and Noble, D.C., 1971, Geology of northern Nellis Air Force Base bombing and gunnery range, Nye County, Nevada: U.S. Geological Survey, Professional Paper 651, 91 p.

Epstein, S., and Mayeda, T.K., 1953, Variation of O^{18} content of waters from natural sources: Geochimica et Cosmochimica Acta, v. 4, p. 213-224.

Fontes, J.Ch., 1983, Dating of groundwater, *in* Guidebook on Nuclear Techniques in Hydrology: Vienna, International Atomic Energy Agency Technical Reports Series, no. 91, p. 285-317.

Fridrich, C.J., Dudley, W.W., and Stuckless, J.S., 1994, Hydrogeologic analysis of the saturated-zone ground-water system under Yucca Mountain, Nevada: Journal of Hydrology, v. 154, p. 133-168.

Friedman, I., Benson, C., and Gleason, J., 1991, Isotopic changes during snow metamorphism, *in* Taylor, H.P., Jr., O'Neil, J.R., and Kaplan, I.R., eds., Stable Isotope Geochemistry: A Tribute to Samuel Epstein: The Geochemical Society, Special Publication No. 3, p. 211-221.

Friedman, I., Smith, G.I., Gleason, J.D., Warden, A., and Harris, J.M., 1992, Stable isotope composition of waters in southeastern California, 1. Modern precipitation: Journal of Geophysical Research, v. 97, p. 5795-5812.

Garside, L.J., and Schilling, J.H., 1979, Thermal waters of Nevada: Nevada Bureau of Mines and Geology, Bulletin 91, 163 p.

Gat, J.R., and Dansgaard, W., 1972, Stable isotope survey of the fresh water occurrences in Israel and the northern Jordan Rift Valley: Journal of Hydrology, v. 16, p. 177-212.

Harrill, J.R., Gates, J.S., and Thomas, J.M., 1988, Major ground-water flow systems in the Great Basin region of Nevada, Utah, and adjacent states: U.S. Geological Survey, Hydrologic Investigations Atlas, HA-694-C, scale 1:1,000,000, 2 sheets.

Hershey, R.L., and Acheampong, S.Y., 1997, Estimation of groundwater velocities from Yucca Flat to the Amargosa Desert using geochemistry and environmental isotopes: Desert Research Institute, Water Resources Center Publication No. 45157, 49 p.

Houghton, J.G., Sakamoto, C.M., and Gifford, R.O., 1975, Nevada's weather and climate: Nevada Bureau of Mines and Geology, Special Publication 2, 78 p.

Hulen, J.B., Goff, F., Ross, J.R., Bortz, L.C., and Bereskin, S.R., 1994, Geology and geothermal origin of Grant Canyon and Bacon Flat oil fields, Railroad Valley, Nevada: American Association of Petroleum Geologists Bulletin, v. 78, p. 596-623.

Ingraham, N.L., Lyles, B.F., Jacobson, R.L., and Hess, J.W., 1991, Stable isotopic study of precipitation and spring discharge in southern Nevada: Journal of Hydrology, v. 125, p. 243-258.

Judy, C., Meiman, J.R., and Friedman, I., 1970, Deuterium variations in an annual snowpack: Water Resources Research, v. 6, p. 125-129.

Laczniak, R.J., Cole, J.C., Sawyer, D.A., and Trudeau, D.A., 1996, Summary of hydrogeologic controls on ground-water flow at the Nevada Test Site, Nye County, Nevada: U.S. Geological Survey, Water-Resources Investigation Report 96-4109, 59 p.

Lamb, D., Nielsen, K.W., Klieforth, H.E., and Hallett, J., 1976, Measurements of liquid water content in winter cloud systems over the Sierra Nevada: Journal of Applied Meteorology, v. 15, p. 763-775.

Lamke, R.D., and Moore, D.O., 1965, Interim inventory of surface water resources of Nevada: Nevada Department of Conservation and Natural Resources, Water Resources Bulletin 8, 38 p.

Lund, K., Beard, L.S., and Perry, W.J., Jr., 1993, Relation between extensional geometry of the northern Grant Range and oil occurrences in Railroad Valley, east-central Nevada: American Association of Petroleum Geologists Bulletin, v. 77, p. 945-962.

Malmberg, G.T., 1965, Available water supply of the Las Vegas groundwater basin, Nevada: U.S. Geological Survey, Water Supply Paper 1780, 116 p.

Maxey, G.B., and Eakin, T.E., 1949, Groundwater in White River Valley, White Pine, Nye, and Lincoln Counties, Nevada: Nevada Department of Conservation and Natural Resources, Water Resources Bulletin 8, 59 p.

McNichol, A.P., Jones, G.A., Hutton, D.L., Gagnon, A.R., and Key, R.M., 1994, The rapid preparation of seawater ΣCO_2 for radiocarbon analysis at the National Ocean Sciences AMS facility: Radiocarbon, v. 36, p. 237-246.

Merlivat, L., and Contiac, M., 1975, Study of mass transfer at the air-water interface by an isotopic method: Journal of Geophysical Research, v. 80, p. 3455-3464.

Merlivat, L., and Jouzel, J., 1979, Global climatic interpretation of the deuterium-oxygen 18 relationship for precipitation: Journal of Geophysical Research, v. 84, p. 5029-5033.

Mifflin, M.D., and Hess, J.W., 1979, Regional carbonate flow systems in Nevada: Journal of Hydrology, v. 43, p. 217-237.

Mifflin, M.D., and Wheat, M.M., 1979, Pluvial Lakes and estimated pluvial climates of Nevada: Nevada Bureau of Mines and Geology, Bulletin 94, 57 p.

Milne, W.K., Benson, L.V., and McKinley, P.W., 1987, Isotope content and temperature of precipitation in southern Nevada, August 1983-August 1986: U.S. Geological Survey, Open File Report 87-463, 32 p.

Mook, W.G., 1980, Carbon-14 in hydrogeological studies, *in* Fritz, P., and Fontes, J.Ch., eds., Handbook of Environmental Isotope Geochemistry, Volume 1, The Terrestrial Environment, A: Amsterdam, Elsevier, p. 49-74.

Morgan, D.S., and Dettinger, M.D., 1996, Ground-water conditions in Las Vegas Valley, Clark County, Nevada – Part II, Hydrogeology and simulation of ground-water flow: U.S. Geological Survey, Water-Supply Paper 2320-B, 124 p.

Pearson, F.J., and Hanshaw, B.B., 1970, Sources of dissolved carbonate species in groundwater and their effects on carbon-14 dating, *in* Isotope Hydrology: Vienna, International Atomic Energy Agency, p. 271-286.

Pearson, F.J., and Swarzenki, W.V., 1974, ^{14}C evidence for the origin of arid region groundwater, northeastern province, Kenya, *in* Proceedings, Isotope Techniques in Groundwater Hydrology, Volume 2: Vienna, International Atomic Energy Agency, p. 95-109.

Phillips, F.M., Peeters, L.A., Tansey, M.K., and Davis, S.N., 1986, Paleoclimatic inferences from an isotopic investigation of groundwater in the central San Juan Basin, New Mexico: Quaternary Research, v. 26, p. 179-193.

Prudic, D.E., Harrill, J.R., and Burbey, T.J., 1995, Conceptual evaluation of regional ground-water flow in the carbonate-rock province of the Great Basin, Nevada, Utah, and adjacent states: U.S. Geological Survey, Professional Paper 1409-D, 102 p.

Quade, J., Cerling, T.E., and Bowman, J.R., 1989, Systematic variations in the carbon and oxygen isotopic composition of pedogenic carbonate along elevation transects in the southern Great Basin, United States: Geological Society of America Bulletin, v. 101, p. 464-475.

Quade, J., Mifflin, M.D., Pratt, W.L., McCoy, W., and Burckle, L., 1995, Fossil spring deposits in the southern Great Basin and their implications for changes in water-table levels near Yucca Mountain, Nevada, during Quaternary time: Geological Society of America Bulletin, v. 107, p. 213-230.

Quade, J., Forester, R.M., Pratt, W.L., and Carter, C., 1998, Black mats, spring-fed streams, and late-glacial-age recharge in the southern Great Basin: Quaternary Research, v. 49, p. 129-148.

Reiner, S.R., Laczniak, R.J., DeMeo, G.A., Smith, J.L., Nylund, W.E., and Elliott, P.E., 1999, Preliminary estimate of mean annual evapotranspiration, Oasis Valley, Nye County, Nevada [abs.]: Eos (Transactions, American Geophysical Union), v. 80, p. 328.

Rose, T.P., and Davisson, M.L., 1996, Radiocarbon in hydrologic systems containing dissolved magmatic carbon dioxide: Science, v. 273, p. 1367-1370.

Rose, T.P., Kenneally, J.M., Smith, D.K., Davisson, M.L., Hudson, G.B., and Rego, J.H., 1997, Chemical and isotopic data for groundwater in southern Nevada: Lawrence Livermore National Laboratory Report UCRL-ID-128000, 35 p.

Rose, T.P., Davisson, M.L., Criss, R.E., and Smith, D.K., 1999a, Isotopic investigation of recharge to a regional groundwater flow system, Great Basin, Nevada, USA, *in* Proceedings, International Symposium on Isotope Techniques in Water Resources Development and Management, Vienna, 10-14 May 1999: International Atomic Energy Agency, IAEA-CSP-2/C, session 2, p. 63-72.

Rose, T.P., Hershey, R.L., Thomas, J.M., Benedict, F.C., Hudson, G.B., Eaton, G.F., and Kenneally, J.M., 1999b, Environmental isotopes in the Pahute Mesa-Oasis Valley groundwater flow system [abs.]: Eos (Transactions, American Geophysical Union), v. 80, p. 328.

Roth, J.G., and Campana, M.E., 1989, A mixing-cell model of the Railroad Valley regional groundwater flow system, central Nevada: Desert Research Institute, Water Resources Center Publication # 41123, 175 p.

Rush, F.E., and Everett, D.E., 1966, Water-resources appraisal of Little Fish Lake, Hot Creek, and Little Smoky Valleys, Nevada: Nevada Department of Conservation and Natural Resources, Water Resources – Reconnaissance Series Report 38, 38 p.

Salomons, W., and Mook, W.G., 1986, Isotope geochemistry of carbonates in the weathering zone, *in* Fritz, P., and Fontes, J.Ch., eds., Handbook of Environmental Isotope Geochemistry, Volume 2, The Terrestrial Environment, B: Amsterdam, Elsevier, p. 239-269.

Sass, J.H., Lachenbruch, A.H., Munroe, R.J., Greene, G.W., and Moses, T.H., Jr., 1971, Heat flow in the Western United States: Journal of Geophysical Research, v. 76, p. 6376-6413.

Spaulding, G.W., and Graumlich, L.J., 1986, The last pluvial climatic episodes in the deserts of southwestern North America: Nature, v. 320, p. 441-444.

Stewart, J.H., 1980, Geology of Nevada – a discussion to accompany the geologic map of Nevada: Nevada Bureau of Mines and Geology, Special Publication 4, 136 p.

Stewart, J.H., and Carlson, J.E., 1978, Geologic Map of Nevada: U.S. Geological Survey, scale 1:500,000, 2 sheets.

Stichler, W., Rauert, W., and Martinec, J., 1981, Environmental isotope studies of an alpine snowpack: Nordic Hydrology, v. 12, p. 297-308.

Stuiver, M., and Polach, H., 1977, Reporting of ^{14}C data: Radiocarbon, v. 19, p. 355-363.

Stumm, W., and Morgan, J.J., 1981, Aquatic Chemistry, 2nd edition: New York, Wiley, 780 p.

Thomas, J.M., Mason, J.L., and Crabtree, J.D., 1986, Ground-water levels in the Great Basin region of Nevada, Utah, and adjacent states: U.S. Geological Survey, Hydrologic Investigations Atlas, HA-694-B, scale 1:1,000,000, 2 sheets.

Thomas, J.M., Welch, A.H., and Preissler, A.M., 1989, Geochemical evolution of ground water in Smith Creek Valley – a hydrologically closed basin in central Nevada, U.S.A.: Applied Geochemistry, v. 4, p. 493-510.

Thomas, J.M., Welch, A.H., and Dettinger, M.D., 1996, Geochemistry and isotope hydrology of representative aquifers in the Great Basin region of Nevada, Utah, and adjacent states: U.S. Geological Survey, Professional Paper 1409-C, 100 p.

U.S. Department of Energy, 1997, Regional groundwater flow and tritium transport monitoring and risk assessment of the underground test area, Nevada Test Site, Nevada: U.S. Department of Energy, Nevada Operations Office, Environmental Restoration Division Report DOE/NV-477, 396 p.

Van Denburgh, A.S., and Rush, F.E., 1974, Water-resources appraisal of Railroad and Penoyer Valleys, east-central Nevada: Nevada Department of Conservation and Natural Resources, Water Resources – Reconnaissance Series Report 60, 61 p.

Van der Stratten, C.M., and Mook, W.G., 1983, Stable isotopic composition of precipitation and climatic variability, in Proceedings, Symposium on Paleoclimates and Paleowaters, 1980: A Collection of Environmental Isotope Studies: Vienna, International Atomic Energy Agency, p. 53-64.

White, A.F. and Chuma, N.J., 1987, Carbon and isotope mass balance models of Oasis Valley-Fortymile Canyon groundwater basin, southern Nevada: Water Resources Research, v. 23, p. 571-582.

Winograd, I.J., and Friedman, I., 1972, Deuterium as a tracer of regional ground-water flow, southern Great Basin, Nevada and California: Geological Society of America Bulletin, v. 83, p. 3691-3708.

Winograd, I.J., and Pearson, F.J., Jr., 1976, Major carbon 14 anomaly in a regional carbonate aquifer: possible evidence for megascale channeling, south central Great Basin: Water Resources Research, v. 12, p. 1125-1143.

Winograd, I.J., and Thordarson, W., 1975, Hydrogeologic and hydrochemical framework, south-central Great Basin, Nevada-California, with special reference to the Nevada Test Site: U.S. Geological Survey, Professional Paper 712-C, 126 p.

Winograd, I.J., Riggs, A.C., and Coplen, T.B., 1998, The relative contributions of summer and cool-season precipitation to groundwater recharge, Spring Mountains, Nevada, USA: Hydrogeology Journal, v. 6, p. 77-93.

Yurtsever, Y., 1975, Worldwide survey of stable isotopes in precipitation: International Atomic Energy Agency, Isotope Hydrology Section Report, November, 1975, 40 p.

TABLE 1. WATER SAMPLE LOCATIONS, CHEMICAL AND ISOTOPIC DATA

Sample Name	*Geographic Location*	Latitude	Longitude	Temp (°C)	pH	Cond. (µS/cm)	HCO_3^- (mg/L)	F^- (mg/L)	Cl^- (mg/L)	SO_4^{2-} (mg/L)	Na^+ (mg/L)	K^+ (mg/L)	Ca^{2+} (mg/L)	Mg^{2+} (mg/L)	$\delta^{18}O$ (‰ V-SMOW)	δD (‰ V-SMOW)	$\delta^{13}C$ (‰ PDB)	^{14}C (pmc)
UE-18r Well, NTS	Pahute Mesa	37°08'05"	116°26'41"	32	8.1	394	160	3	6.3	23	73	2.0	15.6	0.3	-15.0	-113	-1.4	8.2
ER-20-5 #3 Well, NTS	Pahute Mesa	37°13'13"	116°28'39"	34	8.6	302	105	3.3	17	35	70	3.1	3.2	0.1	-15.1	-114	-5.7	–
ER-20-5 #1 Well, NTS	Pahute Mesa	37°13'14"	116°28'39"	34	8.2	621	178	10.1	23	39	104	4.5	6.6	0.3	-14.9	-114	-2.3	–
Pahute Mesa #3 Well •	Pahute Mesa	37°14'21"	116°33'37"	–	8.3	748	158	2.5	84.2	92	124	12.3	18.9	4.0	-14.8	-115	–	–
UE-20bh #1 Well, NTS •	Pahute Mesa	37°14'42"	116°24'33"	26	8.3	398	214	4.3	4.7	14	88	8.7	3.1	0.6	-14.7	-109	-9.2	21.0
U-20 Water Well, NTS •	Pahute Mesa	37°15'05"	116°25'45"	37	8.2	309	107	2.2	12.1	32	59	1.6	7.8	0.3	-14.7	-113	-6.2	8.6
ER-20-6 #3 Well, NTS	Pahute Mesa	37°15'33"	116°25'16"	28	8.4	310	102	2.5	13.6	32	56	3.6	10.1	0.8	-15.0	-115	-7.2	16.3
ER-20-6 #2 Well, NTS	Pahute Mesa	37°15'35"	116°25'16"	26	8.2	308	105	3.8	11.6	32	61	3.1	8.3	0.7	-15.0	-115	-7.3	–
ER-20-6 #1 Well, NTS	Pahute Mesa	37°15'36"	116°25'15"	32	8.2	318	103	2.5	12.6	32	60	2.1	5.6	0.4	-15.0	-115	-5.8	–
UE-19c Well, NTS	Pahute Mesa	37°16'08"	116°19'10"	37	7.7	174	65	–	3.1	6	36	0.5	1.4	0.2	-15.0	-111	-5.3	8.1
U-20al Well, NTS •	Pahute Mesa	37°16'12"	116°29'51"	–	8.4	675	250	–	32.8	78	117	11.1	23.7	2.1	–	–	–	–
U-19ba #1 Well, NTS •	Pahute Mesa	37°17'46"	116°18'47"	–	8.1	622	189	–	40.9	10	79	5.5	20.8	1.2	–	–	–	–
UE-19gs Well, NTS •	Pahute Mesa	37°18'14"	116°21'53"	42	7.8	508	181	1.2	9.9	100	74	1	43	0.1	–	–	–	–
UE-19h Well, NTS	Pahute Mesa	37°20'34"	116°22'25"	28	8.3	415	144	–	8.5	–	64	4.0	14.9	1.5	-14.8	-112	-3.3	9.4
Roller Coaster Well	Cactus Flat	37°43'16"	116°44'11"	26	7.8	513	116	0.9	38	34	65	8.0	21.3	1.6	-16.0	-129	-6.6	13.2
Rose Spring	Kawich Range	37°44'46"	116°19'56"	18	7.4	668	322	0.3	23	49	44	1.9	82.4	11.2	-12.8	-104	-8.7	66.7
Cedar Creek Pass Well	Cactus Flat	37°44'48"	116°28'58"	28	7.7	288	100	0.5	15.2	25	35	9.4	20.7	0.5	-14.1	-111	-10.1	21.9
Summer Spring	Kawich Range	37°46'23"	116°17'25"	15	7.8	530	234	0.3	23.6	50	41	2.7	62.7	8.7	-13.3	-107	-8.6	79.1
Sandia Well #6	Cactus Flat	37°47'03"	116°44'59"	23	9.1	624	164	1.6	26.6	44	103	5.6	2.1	0.0	-15.4	-123	-6.7	13.5
Georges Water Spring	Kawich Range	37°51'36"	116°20'59"	10	7.1	179	72	0.3	4	9	14	1.6	16.7	2.7	-13.1	-98	-11.6	–
Silverbow Spring	Kawich Range	37°52'04"	116°30'23"	24	7.1	577	229	0.4	22.6	43	47	2.3	49.1	9.1	-13.1	-108	-13.7	110.9
Pyramid Spring	Reveille Range	37°55'55"	116°07'08"	13	7.3	495	226	0.3	11.7	30	46	1.4	53.1	5.6	-13.0	-100	-10.4	107.0
Reveille Spring	Reveille Range	38°01'54"	116°10'05"	11	7.3	404	191	–	–	–	–	–	–	–	-12.5	-95	-11.0	–
Adavan Spring	Quinn Canyon Range	38°08'19"	115°36'05"	10	7.1	500	290	–	–	–	–	–	–	–	-14.1	-108	-10.0	85.0
Warm Springs †	Jct. Hwy 6 and 375	38°11'16"	116°22'21"	59	6.6	1322	813	3.6	36	96	199	23.3	91.5	22.5	-14.4	-109	-2.8	–
Tonopah City Well	Ralston Valley	38°11'28"	117°04'41"	12	7.4	290	175	–	–	–	–	–	–	–	-14.6	-112	-13.6	–
Twin Springs Ranch Well	Pancake Range	38°12'13"	116°10'29"	12	7.6	570	374	0.3	14.5	24	84	11.8	35.6	4.4	-14.7	-121	-2.8	10.9
Saulsbury Ranch Spring	Monitor Range	38°14'16"	116°49'27"	21	7.8	1350	–	–	–	–	–	–	–	–	-13.2	-106	–	–
Sharp Ranch Well (Nyala)	Railroad Valley	38°14'56"	115°43'40"	11	7.2	1200	234	–	132	209	40	3.2	12	60.8	-14.4	-110	-7.1	39.0
Point of Rocks Spring	W. Stone Cabin Valley	38°17'16"	116°40'07"	20	8.4	850	415	–	–	–	–	–	–	–	-14.9	-118	-2.3	–
Base Camp Well, DOD	Hot Creek Valley	38°18'38"	116°16'41"	18	6.5	362	122	–	9	23	25	4.3	34.3	10.0	-14.0	-109	-7.4	19.7
Warm Spring	W. Stone Cabin Valley	38°20'23"	116°39'43"	23	7.6	700	335	10	14.8	39	161	2.3	8.3	0.7	-15.1	-122	-4.3	13.2
Abel Spring	Railroad Valley	38°21'53"	115°52'01"	44	6.6	1114	708	1.7	17.1	46	106	20.9	102	27.3	-15.6	-123	-1.9	1.8
Blue Jay Well	Hot Creek Valley	38°22'12"	116°13'39"	14	7.9	369	168	–	–	–	–	–	–	–	-14.0	-106	-6.9	–
Mule Shoe Spring	Hot Creek Range	38°22'22"	116°25'46"	11	7.5	463	–	–	–	–	–	–	–	–	-13.4	-107	–	–
Hot Creek Spring	White River Valley	38°22'56"	115°09'11"	33	7.2	482	264	1.0	9.5	42	25	5.6	58.4	22.2	-15.7	-122	-3.2	–
Flag Springs (north spr)	White River Valley	38°25'25"	115°01'14"	16	7.7	357	225	0.3	5.3	9	7	3.2	47	20.3	-14.2	-107	-6.8	–
Rattlesnake Spring	Pancake Range	38°26'59"	116°09'32"	17	7.4	300	–	–	–	–	–	–	–	–	-13.4	-107	–	–
Hunts Canyon Spring	Monitor Range	38°27'27"	116°48'57"	9	7.0	221	98	–	–	–	–	–	–	–	-13.7	-104	-14.5	–
Chimney Spring	Railroad Valley	38°27'46"	115°47'35"	67	6.7	663	519	1.3	12	47	72	19.0	98.6	16.7	-15.7	-123	-1.4	6.4

TABLE 1. WATER SAMPLE LOCATIONS, CHEMICAL AND ISOTOPIC DATA

Sample Name	Geographic Location	Latitude	Longitude	Temp (°C)	pH	Cond. (µS/cm)	HCO_3^- (mg/L)	F^- (mg/L)	Cl^- (mg/L)	SO_4^{2-} (mg/L)	Na^+ (mg/L)	K^+ (mg/L)	Ca^{2+} (mg/L)	Mg^{2+} (mg/L)	$\delta^{18}O$ (‰ V-SMOW)	δD (‰ V-SMOW)	$\delta^{13}C$ (‰ PDB)	^{14}C (pmc)
McCann Canyon Spring	Monitor Range	38°28'03"	116°41'01"	7	7.0	485	190	–	–	–	–	–	–	–	-13.5	-105	-14.1	–
Keller Spring	Toquima Range	38°31'26"	116°59'12"	10	7.3	1092	252	–	–	–	–	–	–	–	-13.8	-107	-8.9	–
Upper Warm Spring †	Hot Creek Range	38°31'57"	116°27'52"	35	8.1	201	100	0.4	7	19	38	0.8	4.7	0.1	-14.6	-113	-14.7	–
Lockes Big Spring †	Railroad Valley	38°33'21"	115°46'15"	37	7.7	662	450	1.2	10	59	52	10	66	21	-15.4	-124	-2.5	5.4
Blue Eagle Spring	Railroad Valley	38°33'43"	115°31'41"	27	7.0	640	409	0.4	10.1	30	36	5.3	73.3	23.2	-15.1	-116	-5.0	12.9
The Big Well (artesian)	Railroad Valley	38°34'50"	115°38'15"	22	7.8	443	208	0.6	25	19	63	10	12	9.6	-16.6	-125	-6.0	0.7
Mexican Spring	Toquima Range	38°35'20"	116°52'55"	10	7.2	509	261	–	–	–	–	–	–	–	-14.9	-112	-12.0	–
E.Barley Ck Summit Spr	Monitor Range	38°35'44"	116°39'10"	6	7.0	323	65	–	–	–	–	–	–	–	-13.7	-103	-11.1	–
Moorman Spring	White River Valley	38°35'44"	115°08'20"	36	7.2	495	257	1.3	9.6	42	26	5.9	62.5	20.3	-15.8	-122	-1.9	–
Combination Spring	Toquima Range	38°35'47"	116°51'26"	11	7.2	446	175	–	–	–	–	–	–	–	-14.8	-111	-8.3	–
Peavine Creek	Toiyabe Range	38°36'59"	117°18'07"	12	–	239	–	–	–	–	–	–	–	–	-14.4	-108	-13.6	–
HTH-1 Well (853 m) §	N. Hot Ck. Valley	38°37'34"	116°12'45"	41	8.2	588	261	10	21.4	39	134	2.2	3.0	0.1	-15.5	-118	-2.8	0.8
HTH-2 Well (174 m) §	N. Hot Ck. Valley	38°37'39"	116°12'48"	19	8.0	287	177	–	4.1	0.7	19	1.4	36.9	5.2	-14.1	-107	-10.3	63.7
UC-1-P-1S Well (150 m) §	N. Hot Ck. Valley	38°37'54"	116°12'42"	18	8.2	217	134	–	2.6	0.6	23	1.4	23	1.7	-14.1	-104	-9.2	44.6
Hardy Springs	White River Valley	38°38'12"	115°04'27"	14	7.5	420	286	0.2	2.8	13	7	3.0	58.7	26.2	-14.7	-112	-7.6	–
Needles Spring	Big Sand Sprs Valley	38°39'44"	116°04'10"	15	7.4	565	285	–	–	–	–	–	–	–	-12.1	-98	-11.3	–
N.Sixmile Canyon Spring	Hot Creek Range	38°40'46"	116°18'13"	8	7.1	386	246	0.1	2.3	6	6	1.7	42.6	25.2	-14.4	-113	-11.0	97.6
Meadow Canyon Spring	Toquima Range	38°41'38"	116°55'10"	9	7.5	198	95	0.2	4.4	11	21	4.5	14.3	2.8	-15.7	-119	-13.4	–
Shoshone Creek	Toquima Range	38°42'41"	117°02'45"	9	–	161	–	–	–	–	–	–	–	–	-14.9	-112	–	–
Indian Spring	White River Valley	38°45'19"	115°03'03"	13	7.5	444	278	0.2	3.1	20	6	1.6	60.3	23.6	-15.1	-117	-7.6	–
Martilletti Spring	Pancake Range	38°47'59"	115°49'57"	10	7.3	430	219	–	–	–	–	–	–	–	-12.5	-102	-10.7	–
Darroughs Hot Spring †	Big Smoky Valley	38°49'16"	117°10'48"	92	9.1	496	153	14	12	53	110	2.6	1.3	0.1	-15.5	-121	-10.3	–
Summit Spring	Horse Range	38°49'23"	115°17'59"	13	7.7	381	232	0.4	13.8	15	27	2.7	51.3	11.1	-13.9	-108	-11.5	–
Secret Spring	Horse Range	38°50'24"	115°17'20"	12	7.2	403	192	–	–	–	–	–	–	–	-14.0	-110	-10.8	–
Silver Spring	White Pine Range	38°50'39"	115°29'02"	10	7.8	715	411	0.9	13.3	42	40	2.6	94.6	17.6	-14.6	-112	-9.1	107.5
Logan Spring	Toquima Range	38°52'08"	116°53'05"	8	7.4	487	212	0.4	15.5	44	45	1.8	49.4	6.5	-14.8	-116	-12.6	–
Little Currant Ck Springs	White Pine Range	38°53'12"	115°22'08"	9	8.2	331	265	–	1.4	3	5	0.8	54.0	11.7	-15.5	-119	-10.9	84.6
N.Fork Twin River	Toiyabe Range	38°53'38"	117°15'14"	9	7.9	86	82	–	–	–	–	–	–	–	-16.0	-125	-12.3	–
Arnoldson Spring	White River Valley	38°54'35"	115°03'49"	23	7.7	408	184	0.4	15	37	12	3.4	41.1	19.5	-15.8	-122	-5.2	–
E.Dobbin Summit Spring	Monitor Range	38°55'26"	116°30'35"	–	–	–	–	–	–	–	–	–	–	–	-14.9	-119	–	–
Spring, E. of Duckwater	Railroad Valley	38°55'41"	115°42'12"	19	7.4	665	350	0.3	9	67	30	8.1	62.0	26.1	-15.7	-122	-6.3	29.6
Big Warm Spring	Railroad Valley	38°56'59"	115°42'00"	34	7.1	597	291	0.6	7.5	43	29	7.1	63.6	22.9	-16.0	-125	-2.9	3.0
Williams Hot Spring	W. of White R. Valley	38°57'07"	115°14'01"	52	9.2	295	56	13	8.9	14	64	0.4	1.6	0.0	-15.4	-123	-7.0	–
Saddle Spring	White Pine Range	38°58'36"	115°23'58"	5	7.3	186	81	0.2	5.5	7	12	1.5	18.5	4.2	-15.4	-118	-10.9	106.6
Young Florio Spring	Pancake Range	38°58'46"	115°48'44"	12	7.0	447	186	0.8	12.2	21	46	6.4	39.4	6.8	-14.3	-111	-11.5	89.9
Dianas Hot Spring †	Monitor Valley	39°01'47"	116°40'02"	47	6.9	608	285	2.8	8	59	57	15	47	11	-16.1	-128	-2.8	–
Snowball Ranch Spring	Antelope Range	39°02'23"	116°13'00"	15	6.9	279	157	0.2	4.5	18	10	3.3	32.5	9.3	-15.8	-123	-9.8	19.3
Bull Creek Spring	Railroad Valley	39°03'01"	115°37'35"	13	7.3	361	194	0.1	12	26	17	3.5	33.1	17.7	-15.9	-123	-7.1	15.4
Willow Spring	Antelope Range	39°04'10"	116°10'28"	16	7.6	205	–	–	–	–	–	–	–	–	-15.3	-123	–	–
Tom Plain Spring	White Pine Range	39°05'15"	115°22'33"	6	7.5	364	167	0.2	11.2	15	10	3.1	56.8	4.0	-15.8	-124	-9.3	50.7

TABLE 1. WATER SAMPLE LOCATIONS, CHEMICAL AND ISOTOPIC DATA

Sample Name	Geographic Location	Latitude	Longitude	Temp (°C)	pH	Cond. (µS/cm)	HCO_3^- (mg/L)	F^- (mg/L)	Cl^- (mg/L)	SO_4^{2-} (mg/L)	Na^+ (mg/L)	K^+ (mg/L)	Ca^{2+} (mg/L)	Mg^{2+} (mg/L)	$\delta^{18}O$ (‰ V-SMOW)	δD (‰ V-SMOW)	$\delta^{13}C$ (‰ PDB)	^{14}C (pmc)
Green Springs	Railroad Valley	39°06'57"	115°34'06"	19	7.1	432	–	–	–	–	–	–	–	–	-15.9	-117	–	–
Sams Spring	Toquima Range	39°10'13"	116°46'49"	6	7.1	663	297	–	–	–	–	–	–	–	-15.0	-118	-12.0	–
Spring, SE of Mt. Hamilton	White Pine Range	39°12'41"	115°30'40"	9	7.1	473	301	–	5	5	10	1.4	61.5	22.1	-15.5	-115	-11.4	91.9
Kingston Creek	Toiyabe Range	39°16'17"	117°09'28"	8	6.6	481	208	–	–	–	–	–	–	–	-16.1	-125	-14.5	–
Fish Creek Springs **	*Fish Creek Range*	39°16'37"	116°02'18"	17	8.2	444	267	–	11	37	38	–	28	29	-15.9	-124	–	–
Spencer Hot Spring †	Big Smoky Valley	39°19'37"	116°51'17"	60	7.0	1199	710	5.2	26	47	198	34	51	9.4	-16.1	-135	-2.9	–
Sand Spring	White Pine Range	39°19'52"	115°27'15"	12	7.6	884	–	–	–	–	–	–	–	–	-15.1	-119	–	–
Klobe Hot Spring †	Antelope Valley	39°24'18"	116°20'50"	65	9.0	305	162	4.8	11	16	66	1.0	10.3	0.0	-16.6	-130	-12.7	–
Faulkner Creek	Monitor Range	39°24'41"	116°22'33"	14	6.3	106	–	–	–	–	–	–	–	–	-15.9	-123	–	–
Little Antelope Spring	N. White Pine Range	39°24'57"	115°27'34"	9	7.3	1421	–	–	–	–	–	–	–	–	-15.5	-122	–	–
Sulphur Spring	Pancake Range	39°25'24"	115°40'49"	13	7.0	552	–	–	–	–	–	–	–	–	-15.4	-119	–	–
Lucky Springs	*Diamond Range*	39°27'30"	115°56'29"	9	6.4	341	–	–	–	–	–	–	–	–	-15.8	-122	–	–
Bade Creek	Toiyabe Range	39°28'27"	117°00'05"	6	7.3	195	–	–	–	–	–	–	–	–	-16.0	-121	–	–
Austin Summit Spring	Toiyabe Range	39°28'49"	117°02'36"	9	8.0	239	–	–	–	–	–	–	–	–	-16.0	-121	–	–
DeBernardi Ranch Spr	Newark Valley	39°37'28"	115°45'53"	16	7.6	288	–	–	–	–	–	–	–	–	-16.4	-124	–	–
Cottonwood Spr (runoff)	Buck Mountain	39°46'08"	115°35'45"	–	–	–	–	–	–	–	–	–	–	–	-17.1	-132	–	–
Simonson Warm Spring	Newark Valley	39°48'41"	115°36'30"	25	7.4	543	294	0.7	6.3	30	18	6.3	61.6	23.6	-16.7	-129	-2.5	7.9
Cold Spring	Newark Valley	39°50'23"	115°45'10"	11	7.3	320	154	0.2	3.8	10	8	1.1	44.4	8.2	-16.3	-123	-10.3	79.6

* Water chemistry measured by the Desert Research Institute, University of Nevada (unpublished data)

† Water chemistry data from Garside and Schilling (1979)

§ Water chemistry, d18O, dD data from Chapman et al. (1994)

** Water chemistry data from Rush and Everett (1966)

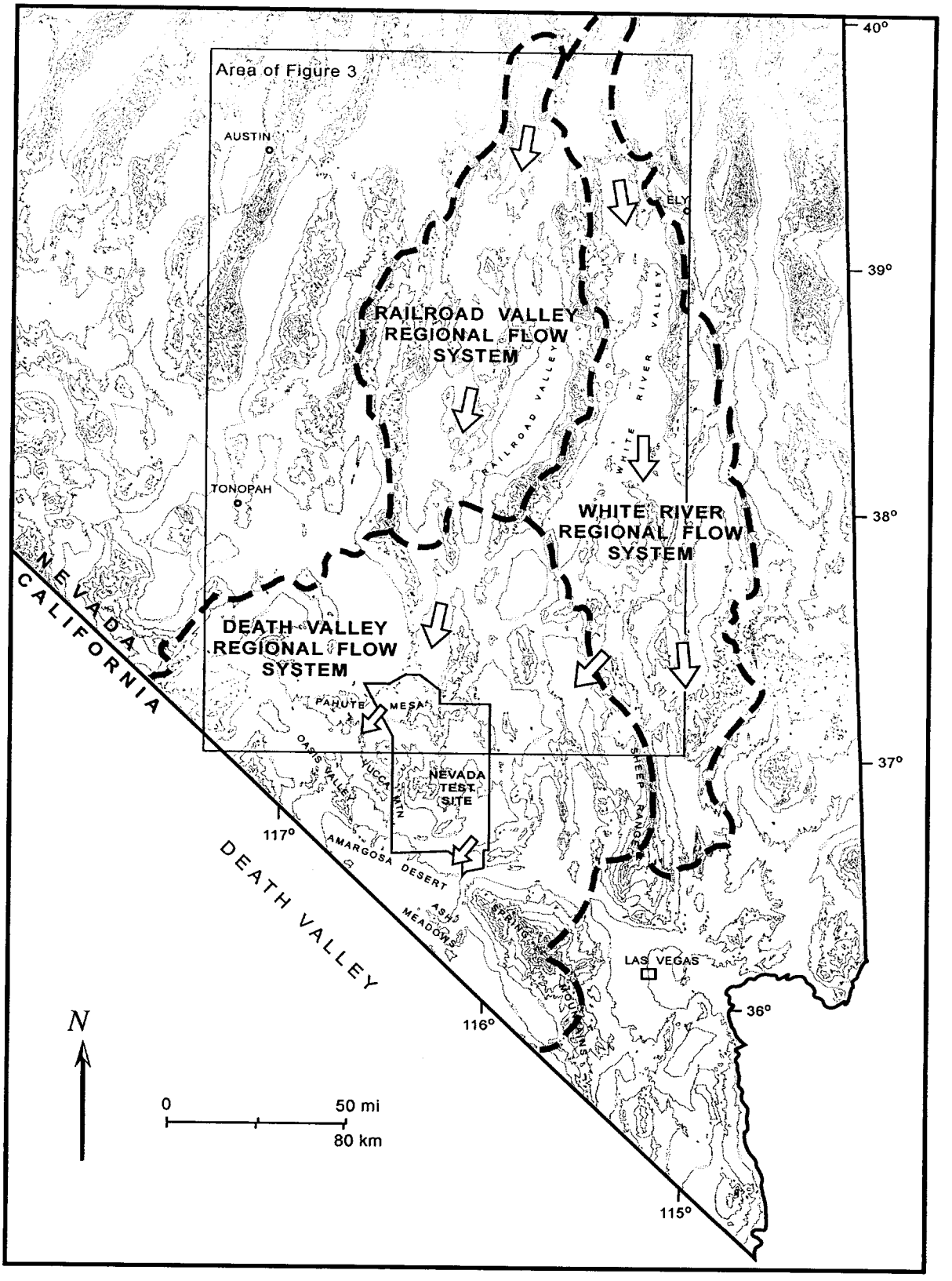

Figure 1. Map of central and southern Nevada showing the approximate boundaries of major regional groundwater flow systems discussed in the text (flow boundaries from Harrill et al., 1988 and Eakin, 1966). Arrows denote the general direction of regional groundwater flow. New evidence presented in this study suggests the Railroad Valley and Death Valley flow systems are linked.

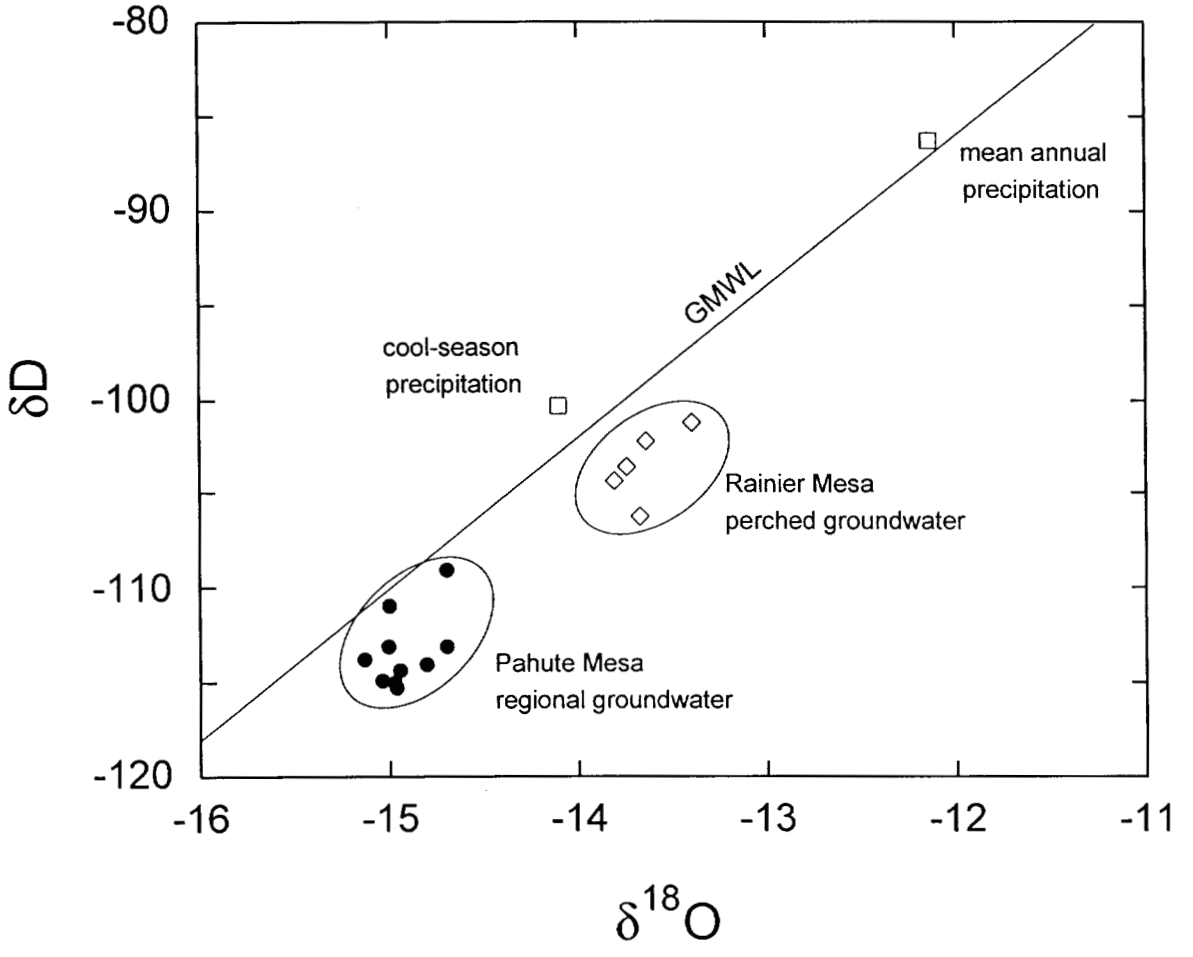

Figure 2. Plot of δD vs. $\delta^{18}O$ values for water samples from the northwestern Nevada Test Site. Regional groundwater flow beneath Pahute Mesa (filled circles) is isotopically depleted relative to both mean annual precipitation on Pahute Mesa (open squares; Milne et al., 1987), and perched groundwater from nearby Rainier Mesa (open diamonds). These data suggest the regional groundwater cannot have a local origin under present climate conditions. GMWL = global meteoric water line (Craig, 1961).

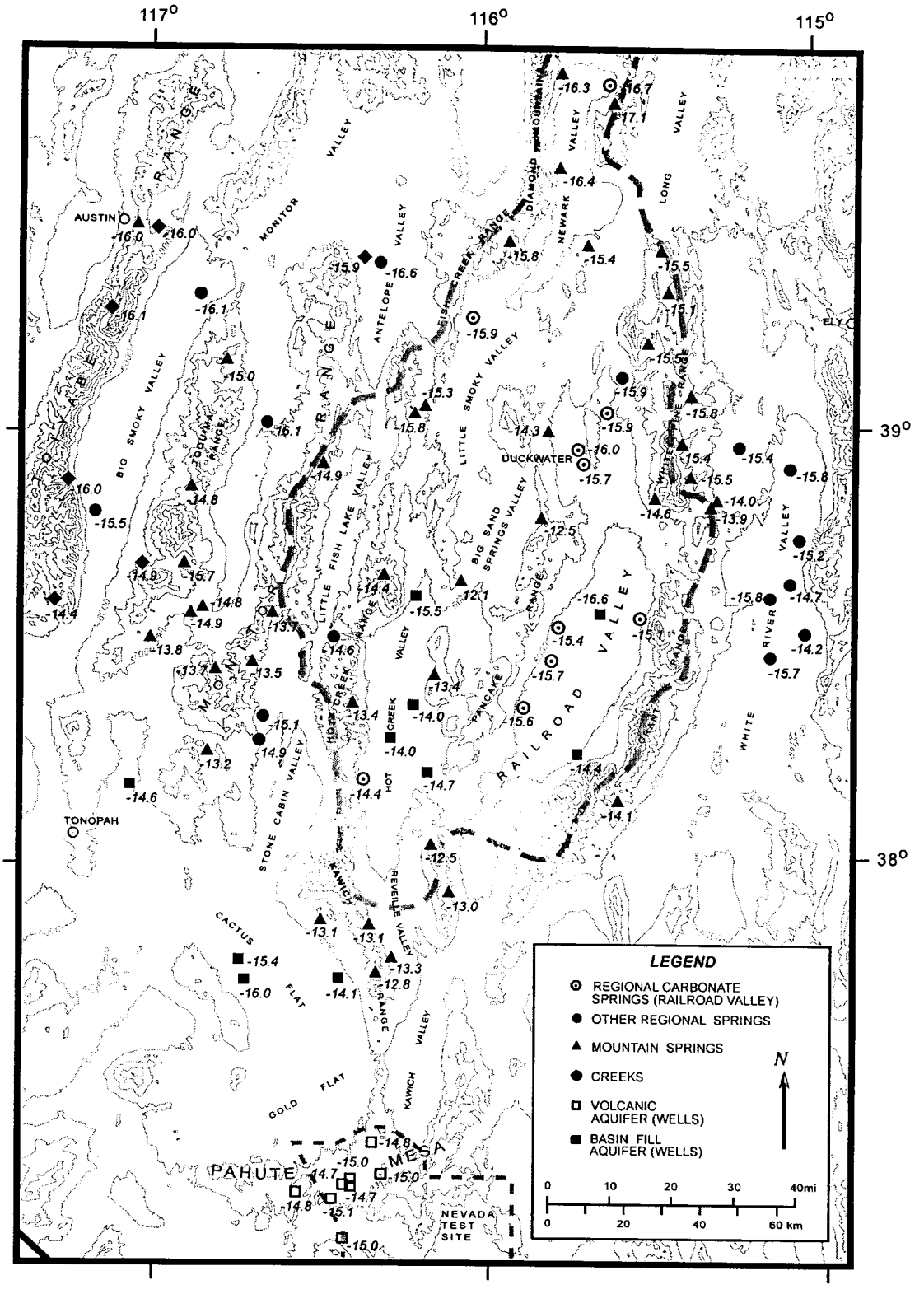

Figure 3. Map of central and southwestern Nevada showing the distribution of samples described in this study, the sample type (see legend), and the corresponding $\delta^{18}O$ values. Geographic locations discussed in the text are also shown. The approximate outline of the Railroad Valley regional flow system is shown as a heavy dashed line (from Harrill et al., 1988).

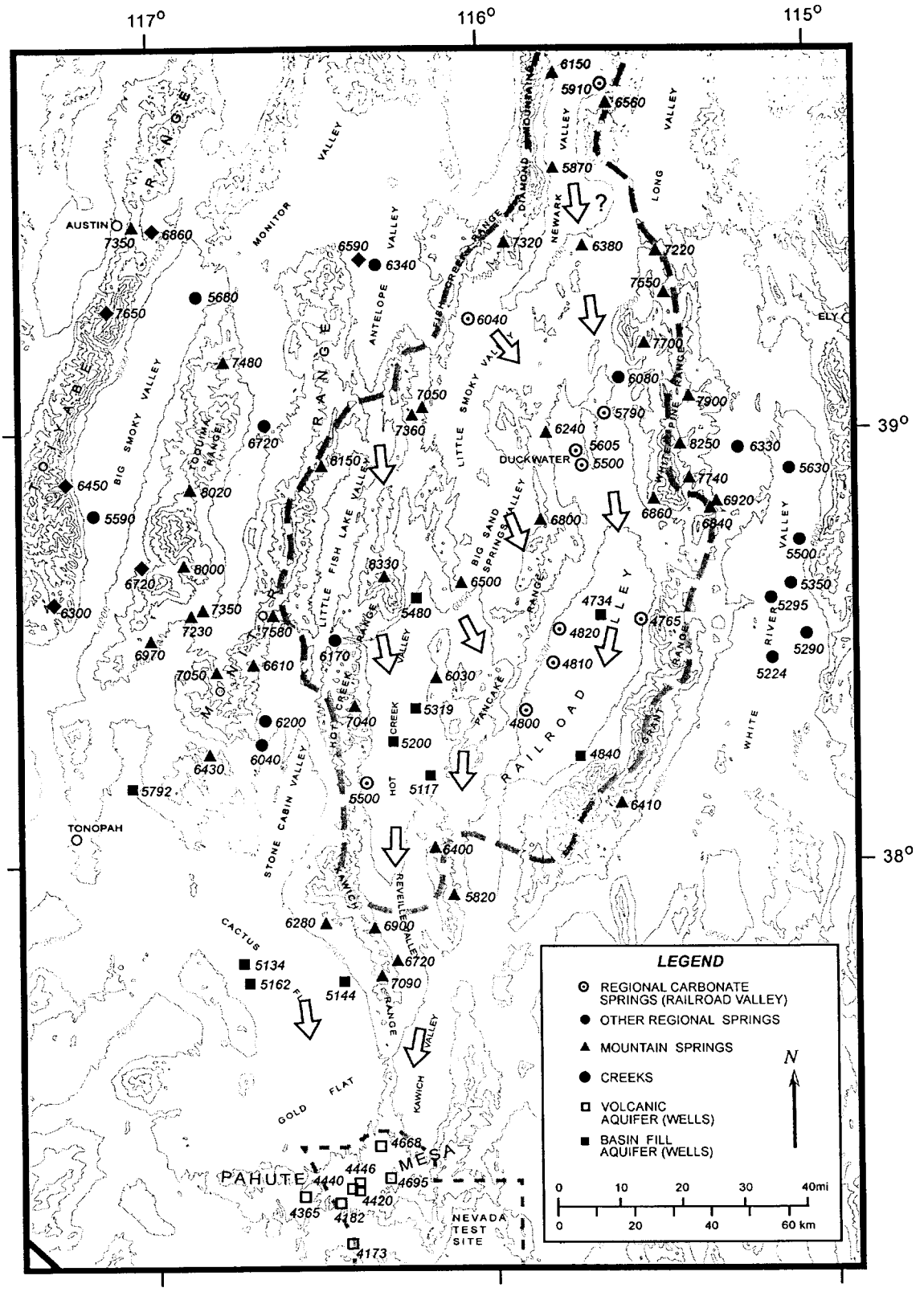

Figure 4. Map of central and southwestern Nevada showing water-level elevations (in feet above mean sea level) for sample locations shown in Figure 3. Arrows indicate the inferred direction of water flow in the carbonate aquifers or deep fractured volcanic aquifers.

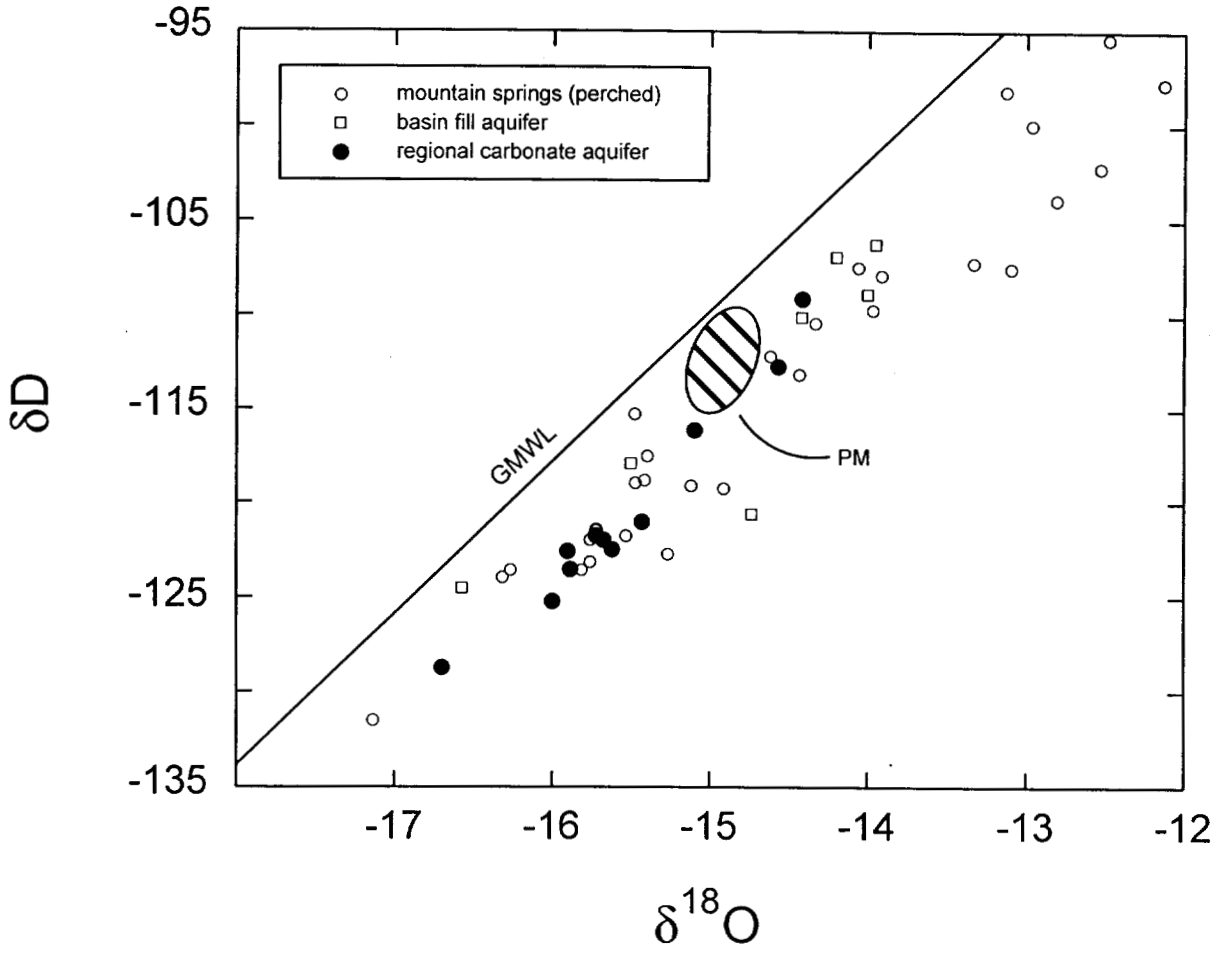

Figure 5. Plot of δD vs. $\delta^{18}O$ values for groundwater samples from the Railroad Valley regional flow system. Groundwater samples are shifted to the right of the global meteoric water line (GMWL) with an average deuterium excess (d-value) near +4. The oval area marked "PM" denotes the Pahute Mesa regional groundwater sample field (from Figure 2).

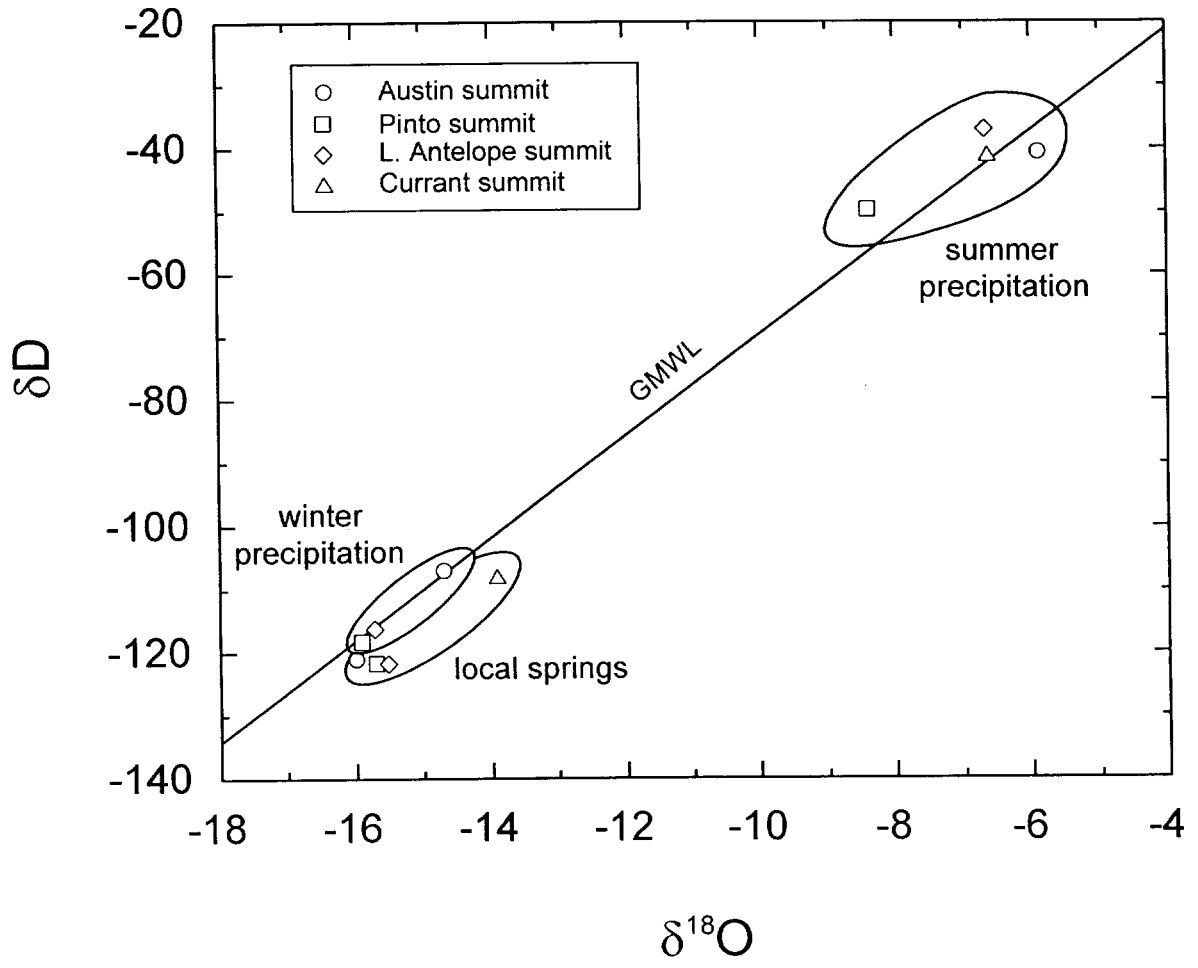

Figure 6. Plot of δD vs $\delta^{18}O$ values for seasonal accumulations of precipitation and small springs collected at four different mountain sites in central Nevada during 1999. Summer precipitation is highly enriched in heavy isotopes relative to winter precipitation. The spring waters are isotopically similar to winter precipitation, implying that most groundwater recharge is derived from snowmelt. Spring samples show a characteristic shift to the right of the global meteoric water line (GMWL).

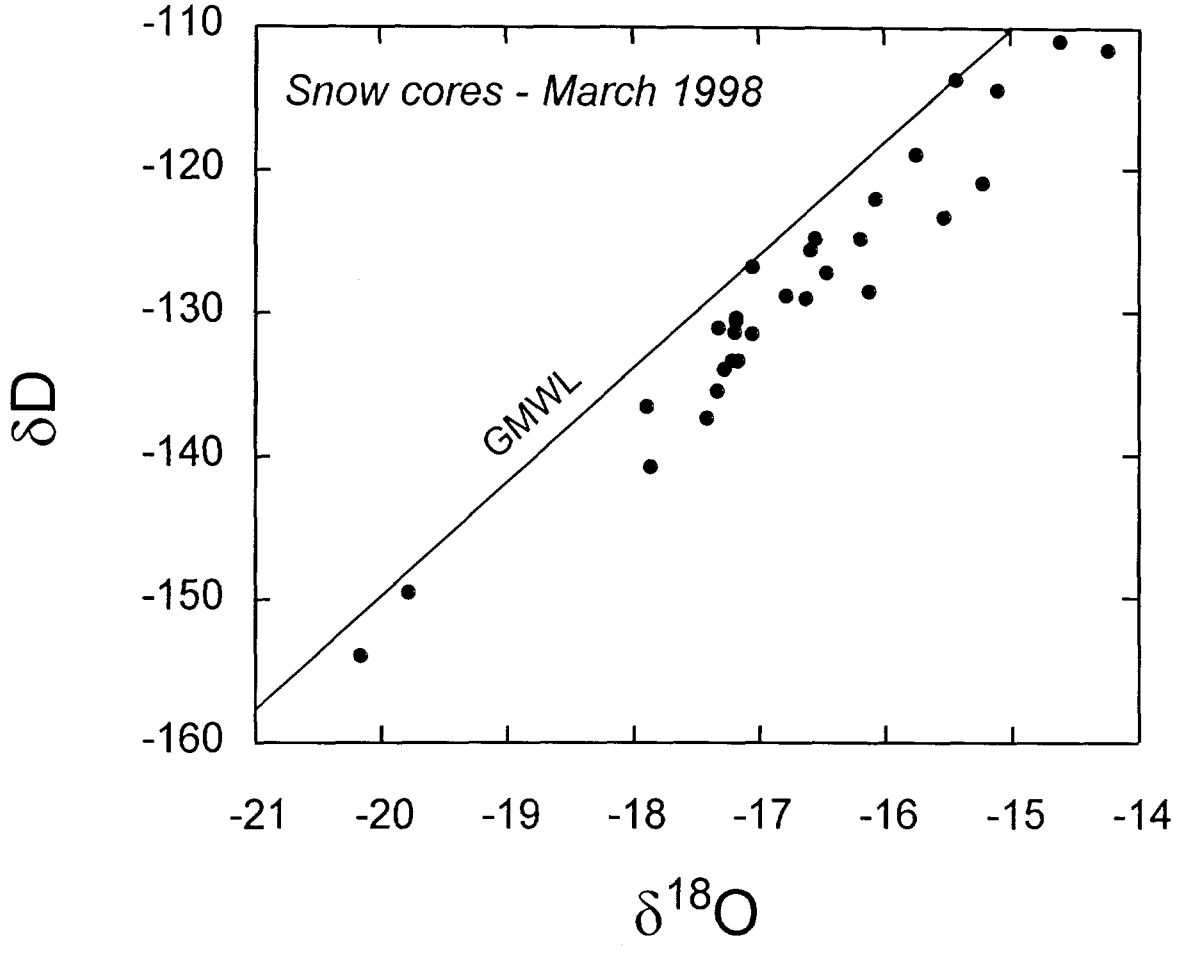

Figure 7. Plot of δD vs. $\delta^{18}O$ values for snow core samples collected throughout central Nevada during March 1998. Many of the data points are shifted to the right of the global meteoric water line (GMWL) due to kinetic isotope fractionation effects that occur during the aging of the snowpack. The average d-value for these samples (+5) is nearly the same as for the groundwaters shown in Figure 5. This comparison suggests the observed isotopic shifts in groundwaters are predominantly inherited from the snowpack.

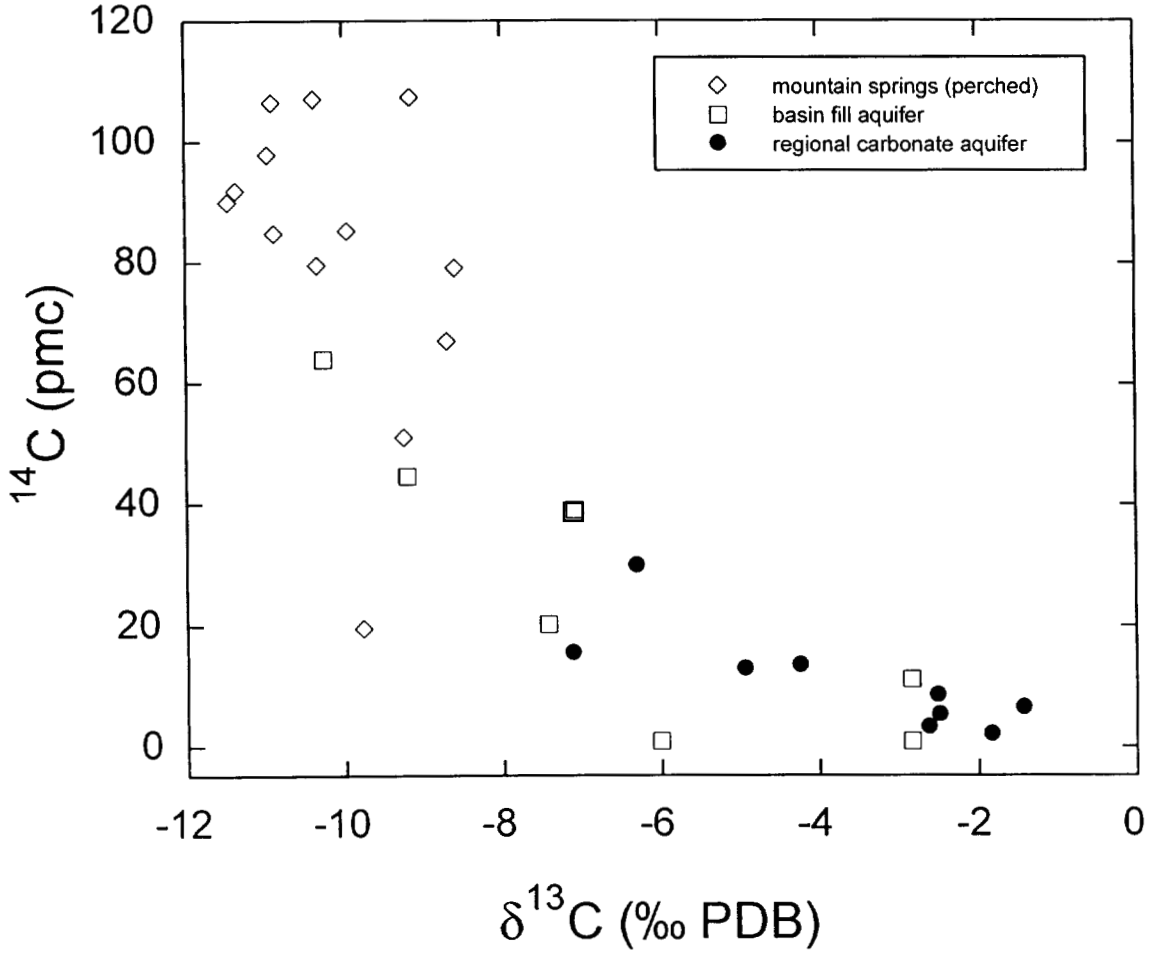

Figure 8. Plot of ^{14}C vs. $\delta^{13}C$ values for dissolved inorganic carbon in groundwater from the Railroad Valley regional flow system. Carbon isotope values for mountain springs are generally consistent with soil CO_2 gas dissolution and reaction with carbonate minerals in the recharge zone. Regional carbonate aquifer groundwaters have relatively high $\delta^{13}C$ and low ^{14}C values that indicate water-rock interaction with the host aquifer.

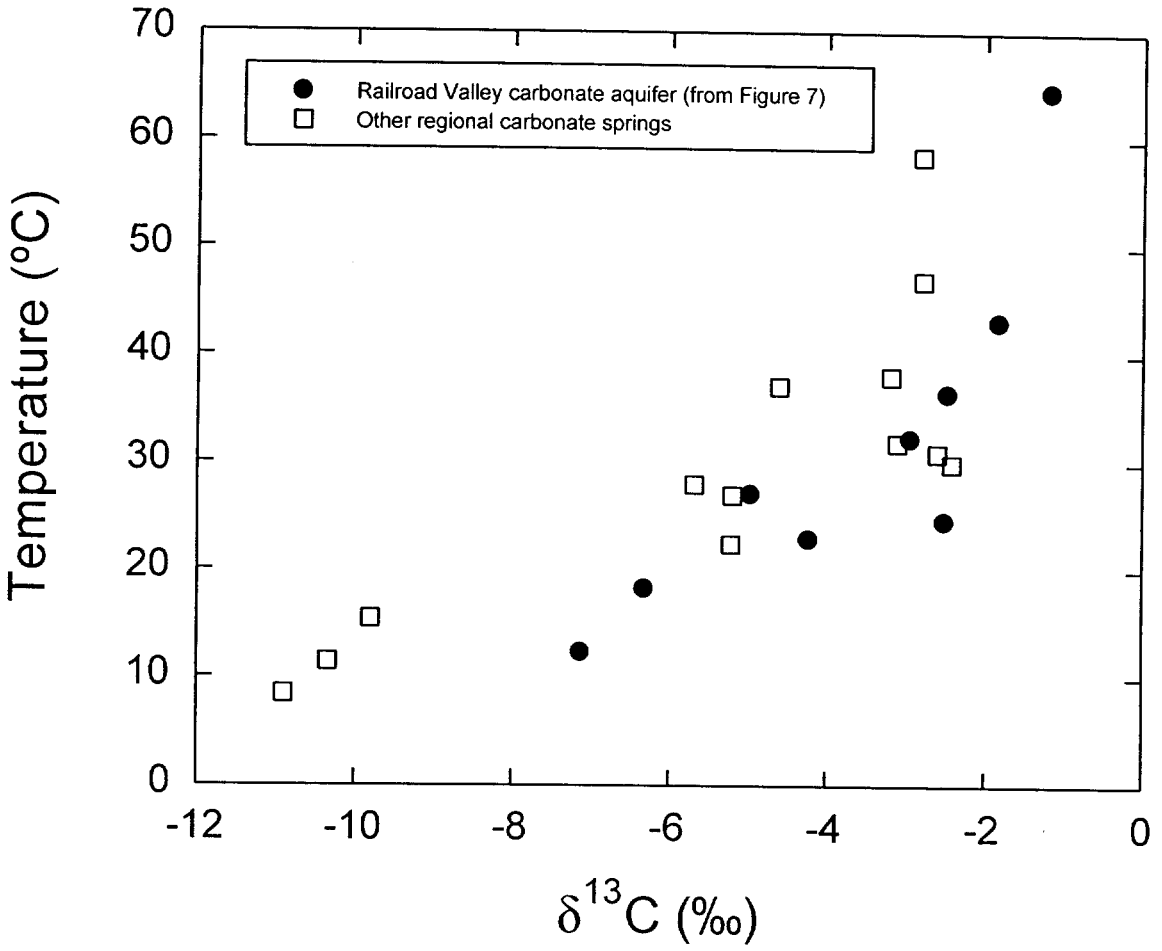

Figure 9. Temperature vs. $\delta^{13}C$ plot for samples collected from regional carbonate aquifer springs throughout central and southern Nevada. The trend toward higher $\delta^{13}C$ values with increasing temperature is interpreted to indicate increasing water-rock interaction, and may be driven in part by cation exchange processes with clay minerals in the aquifer (see discussion in text). Plot includes additional data from Rose et al. (1997).

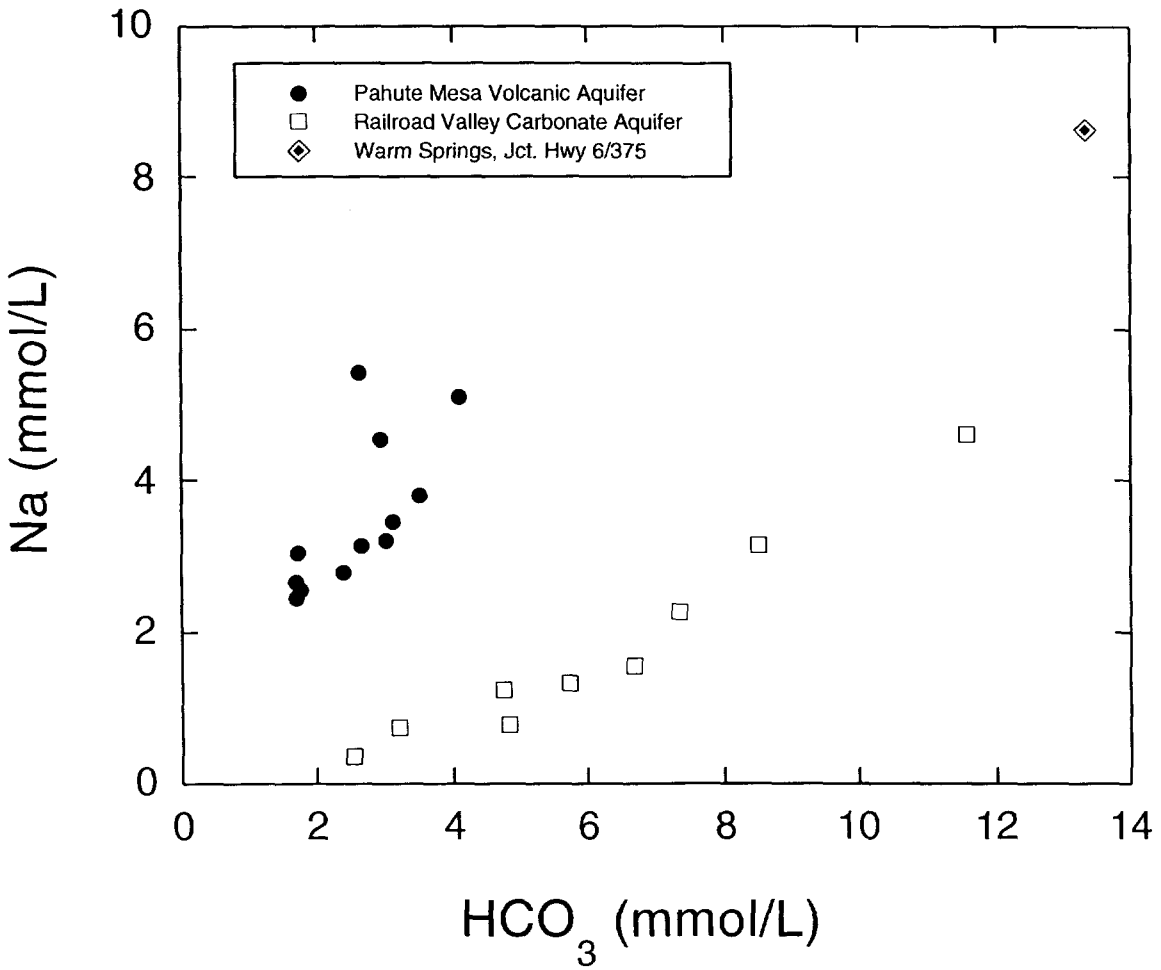

Figure 10. Plot of Na^+ vs. $HCO3^-$ ion concentrations in groundwater samples from the Railroad Valley carbonate and Pahute Mesa volcanic aquifers. The Railroad Valley data show an increase in $HCO3^-$ with Na^+ that may indicate calcium-sodium ion exchange on clay minerals. Ion exchange would drive the solution toward calcite undersaturation, allowing further calcite dissolution, and causing a progressive increase in $HCO3^-$ along the regional flowpath. Pahute Mesa groundwaters have Na^+ ion concentrations similar to chemically evolved carbonate aquifer groundwaters, but significantly lower $HCO3^-$, implying carbonate mineral precipitation (see Figure 11). The Warm Springs sample (Jct. Hwy 6/375) is from a travertine spring in the western Hot Creek Valley, but it has a $\delta^{18}O$ value that is isotopically distinct from all other Railroad Valley carbonate springs.

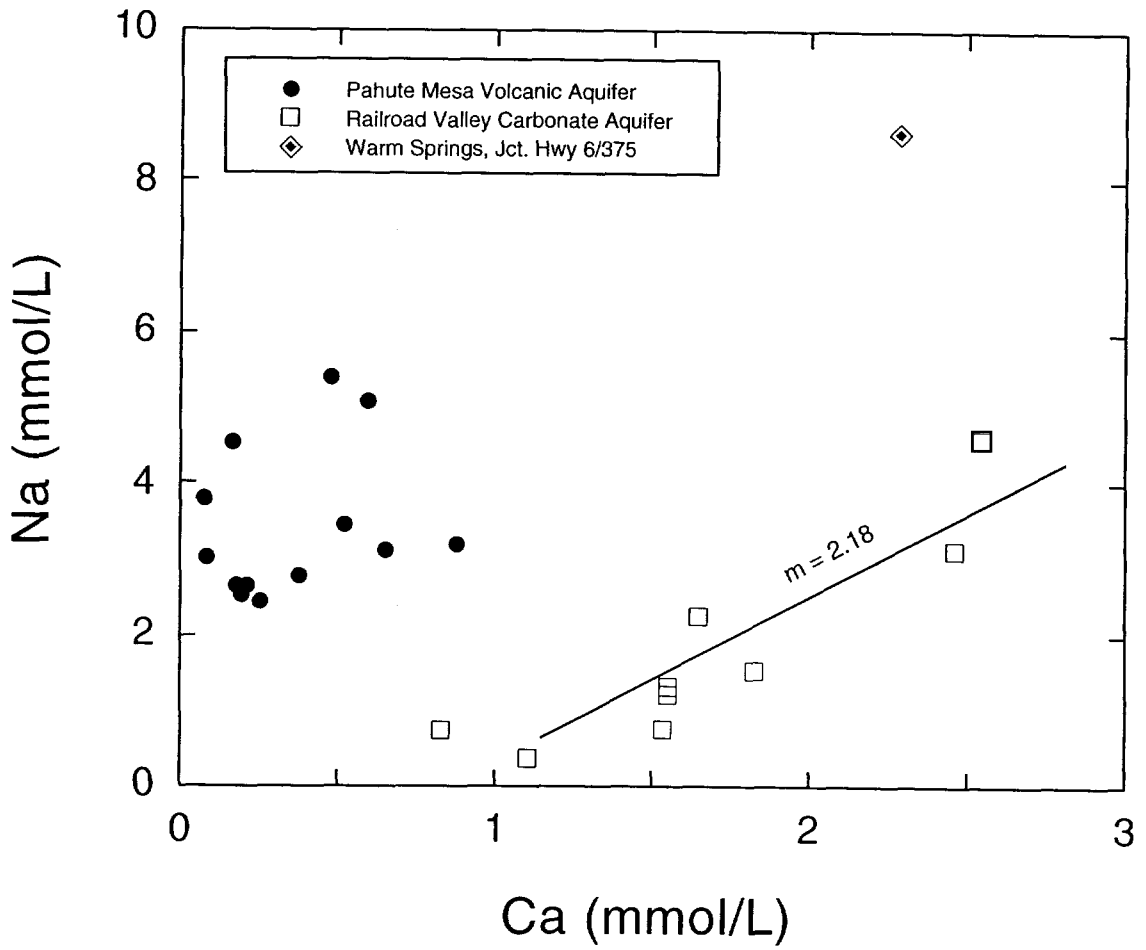

Figure 11. Plot of Na^+ vs. Ca^{2+} ion concentrations for the same samples as shown in Figure 10. The Railroad Valley carbonate groundwaters show a correlated increase in Na^+ with Ca^{2+} along a line with a slope of ~2, in accord with the proposed ion exchange model. The difference in Ca^{2+} concentrations between the two different aquifers likely reflects calcite precipitation. Scatter in the volcanic aquifer data may reflect variable amounts of mixing with dilute local recharge.